ISSN 1949-8470 (online)

World Journal of *Radiology*

Monthly Volume 17 Number 11 November 28, 2025



Published by Baishideng Publishing Group Inc

World Journal of Radiology

Contents

Monthly Volume 17 Number 11 November 28, 2025

REVIEW

Merchant SA, Merchant N, Varghese SL, Shaikh MJS. Large language models and large concept models in radiology: Present challenges, future directions, and critical perspectives. *World J Radiol* 2025; 17(11): 114754 [DOI: 10.4329/wjr.v17.i11.114754]

MINIREVIEWS

Shi JF, Zhou WY, Zhang HX, Shen Y, Zhang H, Li T. Advancements and challenges of ultrasound imaging in the management of thyroid-associated ophthalmopathy. *World J Radiol* 2025; 17(11): 112638 [DOI: 10.4329/wjr.v17.i11.112638]

Tlaiss Y, Tarchichi A, Atallah K, Al Mashtoub E, Zalzali I, Chokor Z, Fassih I, Harb N, Kassas J, Hamze H. Point-of-care ultrasonography for detecting raised intracranial pressure through optic nerve sheath diameter in non-traumatic headache patients. *World J Radiol* 2025; 17(11): 113012 [DOI: 10.4329/wjr.v17.i11.113012]

Perera Molligoda Arachchige AS, Alves GAM, Fedorov D, Ressa G, Cappellini L, Levi R, Savini G, Catapano F, Francone M, Politi LS. Neuroimaging with photon-counting computed tomography: A review of clinical applications. *World J Radiol* 2025; 17(11): 113701 [DOI: 10.4329/wjr.v17.i11.113701]

ORIGINAL ARTICLE

Retrospective Study

Karangeli N, Triantafyllou G, Papadopoulos-Manolarakis P, Arkoudis NA, Velonakis G, Samolis A, Piagkou M. Variations in the spatial relationship between the hyoid bone and the carotid arteries and their clinical significance. *World J Radiol* 2025; 17(11): 113153 [DOI: 10.4329/wjr.v17.i11.113153]

Observational Study

Viceconti N, Paratore M, Del Zompo F, Zocco MA, Ainora ME, Esposto G, Gasbarrini A, Pompili M, Riccardi L, Garcovich M. Shear wave elastography in healthy patients: Pancreatic stiffness is less reliable than liver and spleen measurements. *World J Radiol* 2025; 17(11): 111651 [DOI: 10.4329/wjr.v17.i11.111651]

LETTER TO THE EDITOR

Qi X, Zhao FY. Value of radiomics models in precision diagnosis of dual-phenotype hepatocellular carcinoma and intrahepatic cholangiocarcinoma. *World J Radiol* 2025; 17(11): 114193 [DOI: 10.4329/wjr.v17.i11.114193]

Perera Molligoda Arachchige AS. Magnetic resonance tractography of the cervical spine: Toward routine clinical use. *World J Radiol* 2025; 17(11): 114451 [DOI: 10.4329/wjr.v17.i11.114451]

Contents

ABOUT COVER

Peer Reviewer of *World Journal of Radiology*, Suleman A Merchant, MD, Professor, Lokmanya Tilak Municipal Medical College & Lokmanya Tilak Municipal General Hospital, Mumbai 400022, India.
suleman.merchant@ltmmc.edu.in

AIMS AND SCOPE

The primary aim of *World Journal of Radiology* (*WJR*, *World J Radiol*) is to provide scholars and readers from various fields of radiology with a platform to publish high-quality basic and clinical research articles and communicate their research findings online.

WJR mainly publishes articles reporting research results and findings obtained in the field of radiology and covering a wide range of topics including state of the art information on cardiopulmonary imaging, gastrointestinal imaging, genitourinary imaging, musculoskeletal imaging, neuroradiology/head and neck imaging, nuclear medicine and molecular imaging, pediatric imaging, vascular and interventional radiology, and women's imaging.

INDEXING/ABSTRACTING

The *WJR* is now abstracted and indexed in PubMed, PubMed Central, Emerging Sources Citation Index (Web of Science), Reference Citation Analysis, China Science and Technology Journal Database, and Superstar Journals Database. The 2025 Edition of Journal Citation Reports® cites the 2024 journal impact factor (JIF) for *WJR* as 1.5; JIF without journal self cites: 1.4; 5-year JIF: 1.6; JIF Rank: 137/212 in radiology, nuclear medicine and medical imaging; JIF Quartile: Q3; and 5-year JIF Quartile: Q3.

RESPONSIBLE EDITORS FOR THIS ISSUE

Production Editor: *Yue-Yuan Lei*; **Production Department Director:** *Xiao-Mei Zheng*; **Cover Editor:** *Jia-Ping Yan*.

NAME OF JOURNAL
World Journal of Radiology

ISSN
ISSN 1949-8470 (online)

LAUNCH DATE
January 31, 2009

FREQUENCY
Monthly

EDITORS-IN-CHIEF
Thomas J Vogl

EDITORIAL BOARD MEMBERS
https://www.wjgnet.com/1949-8470/editorialboard.htm

PUBLICATION DATE
November 28, 2025

COPYRIGHT
© 2025 Baishideng Publishing Group Inc

INSTRUCTIONS TO AUTHORS
https://www.wjgnet.com/bpg/gerinfo/204

GUIDELINES FOR ETHICS DOCUMENTS
https://www.wjgnet.com/bpg/GerInfo/287

GUIDELINES FOR NON-NATIVE SPEAKERS OF ENGLISH
https://www.wjgnet.com/bpg/gerinfo/240

PUBLICATION ETHICS
https://www.wjgnet.com/bpg/GerInfo/288

PUBLICATION MISCONDUCT
https://www.wjgnet.com/bpg/gerinfo/208

ARTICLE PROCESSING CHARGE
https://www.wjgnet.com/bpg/gerinfo/242

STEPS FOR SUBMITTING MANUSCRIPTS
https://www.wjgnet.com/bpg/GerInfo/239

ONLINE SUBMISSION
https://www.f6publishing.com

© 2025 Baishideng Publishing Group Inc. All rights reserved. 7041 Koll Center Parkway, Suite 160, Pleasanton, CA 94566, USA
E-mail: office@baishideng.com https://www.wjgnet.com

World Journal of Radiology

Submit a Manuscript: https://www.f6publishing.com

World J Radiol 2025 November 28; 17(11): 114754

DOI: 10.4329/wjr.v17.i11.114754

ISSN 1949-8470 (online)

REVIEW

Large language models and large concept models in radiology: Present challenges, future directions, and critical perspectives

Suleman A Merchant, Neesha Merchant, Shaju L Varghese, Mohd Javed S Shaikh

Specialty type: Radiology, nuclear medicine and medical imaging

Provenance and peer review: Invited article; Externally peer reviewed.

Peer-review model: Single blind

Peer-review report's classification
Scientific Quality: Grade A, Grade A
Novelty: Grade A, Grade A
Creativity or Innovation: Grade A, Grade A
Scientific Significance: Grade A, Grade A

P-Reviewer: Omullo FP, MD, Senior Researcher, Kenya

Received: September 27, 2025
Revised: October 7, 2025
Accepted: November 3, 2025
Published online: November 28, 2025
Processing time: 61 Days and 8.2 Hours

Suleman A Merchant, Department of Radiology, LTM Medical College and LTM General Hospital, Mumbai 400022, Maharashtra, India

Neesha Merchant, Department of Diagnostic Radiology, Medical Imaging, University of Toronto, Toronto M5G2C4, Ontario, Canada

Shaju L Varghese, Department of Imaging, Accura Diagnostic Centre, Mumbai 400014, Maharashtra, India

Mohd Javed S Shaikh, Department of Radiology, Brigham and Women's Hospital and Harvard Medical School, Boston, MA 02115, United States

Corresponding author: Suleman A Merchant, MD, Former Dean, Professor and Head, Department of Radiology, LTM Medical College and LTM General Hospital, Sion, Mumbai 400022, Maharashtra, India. suleman.a.merchant@gmail.com

Abstract

Large language models (LLMs) have emerged as transformative tools in radiology artificial intelligence (AI), offering significant capabilities in areas such as image report generation, clinical decision support, and workflow optimization. The first part of this manuscript presents a comprehensive overview of the current state of LLM applications in radiology, including their historical evolution, technical foundations, and practical uses. Despite notable advances, inherent architectural constraints, such as token-level sequential processing, limit their ability to perform deep abstract reasoning and holistic contextual understanding, which are critical for fine-grained diagnostic interpretation. We provide a critical perspective on current LLMs and discuss key challenges, including model reliability, bias, and explainability, highlighting the pressing need for novel approaches to advance radiology AI. Large concept models (LCMs) represent a nascent and promising paradigm in radiology AI, designed to transcend the limitations of token-level processing by utilizing higher-order conceptual representations and multimodal data integration. The second part of this manuscript introduces the foundational principles and theoretical framework of LCMs, highlighting their potential to facilitate enhanced semantic reasoning, long-range context synthesis, and improved clinical decision-making. Critically, the core of this section is the proposal of a novel theoretical framework for LCMs, formalized and extended from our group's foundational concept-based models - the world's earliest articulation of this paradigm for medical AI. This conceptual shift has since been externally validated and propelled by the recent publication of the LCM architectural pro-

posal by Meta AI, providing a large-scale engineering blueprint for the future development of this technology. We also outline future research directions and the transformative implications of this emerging AI paradigm for radiologic practice, aiming to provide a blueprint for advancing toward human-like conceptual understanding in AI. While challenges persist, we are at the very beginning of a new era, and it is not unreasonable to hope that future advancements will overcome these hurdles, pushing the boundaries of AI in Radiology, far beyond even the most state-of-the-art models of today.

Key Words: Radiology artificial intelligence; Large language models; Large concept models; Medical imaging artificial intelligence; Artificial intelligence in healthcare; Multimodal artificial intelligence models; Explainable artificial intelligence; Artificial intelligence model limitations and challenges; Natural language processing in radiology; Conceptual reasoning in artificial intelligence

©The Author(s) 2025. Published by Baishideng Publishing Group Inc. All rights reserved.

Core Tip: Current capabilities, applications, limitations of large language models (LLMs) in radiology artificial intelligence (AI). LLMs transformed radiology AI, improved textual-analysis, workflow automation, clinical decision support. Challenges: Limited reasoning depth, inaccuracies. Transformative role of LLMs in radiology, their architectural foundations, clinical utility are discussed. LLM limitations, like token-level processing, hallucinations, and challenges in clinical adoption. Exploring new paradigm large concept models, having conceptual reasoning and multimodal integration to enhance clinical accuracy and reliability. Ethical, regulatory, and explainability considerations for AI tools in healthcare also discussed and a balanced and forward-looking view on AI's role in radiology, covering both current innovations and anticipated advances through large concept models.

Citation: Merchant SA, Merchant N, Varghese SL, Shaikh MJS. Large language models and large concept models in radiology: Present challenges, future directions, and critical perspectives. *World J Radiol* 2025; 17(11): 114754
URL: https://www.wjgnet.com/1949-8470/full/v17/i11/114754.htm
DOI: https://dx.doi.org/10.4329/wjr.v17.i11.114754

INTRODUCTION

Part 1

Artificial intelligence (AI) has profoundly influenced radiology practice, particularly through the development of large language models (LLMs) that support textual analysis, report generation, and clinical workflow automation. The impact is felt across the board: For radiology and other clinicians, mainly *via* rapid and accurate image interpretation; for health systems, by major workflow improvements and their immense potential for reducing medical errors; and for patients, by enabling them to better process their own medical data for health advocacy[1]. However, LLMs' token-based architecture inherently limits their reasoning depth and the conceptual robustness necessary for complex diagnostic tasks. By reviewing both achievements and limitations, we lay down the foundational understanding essential for appreciating next-generation AI paradigms in radiology.

Part 2

Building upon the exploration of LLMs in part 1, part 2 introduces large concept models (LCMs) as a conceptual framework for a new paradigm in radiology AI. Specifically, the core contribution of part 2 is the proposal of a novel theoretical framework for LCMs, directly extended and formalized from our foundational concept-based models first articulated in 2022. This approach represents the world's earliest articulation of concept-based models for medical AI, emphasizing a holistic approach and the integration of clinical expertise and multimodal data to enable robust AI reasoning beyond traditional token-level approaches.

While this foundational work has since been validated and extended by other research groups, including Meta AI (who have adopted the term "LCMs" and demonstrated implementations grounded in explicit semantic representations and cross-modal reasoning), our manuscript synthesizes these external advances with novel theoretical extensions rooted in our original conceptual framework. By integrating these strands, part 2 offers a unified, forward-looking framework for LCMs, situating our early vision within the evolving scientific landscape and outlining pathways toward clinical translation. Our contribution is therefore both foundational and progressive, setting scholarly expectations and underscoring the unique role our work plays in advancing AI's conceptual evolution in radiology. It is important to note, however, that these are early beginnings, with significant development still required before LCMs become integrated into everyday clinical use.

The advent of LLMs, epitomized by OpenAI's ChatGPT, marked a transformative leap in natural language processing (NLP). However, despite their impressive capabilities, LLMs face inherent architectural limitations, especially in specialized domains such as Radiology. Their token-level sequential processing constrains their capacity for robust

abstract reasoning and deep conceptual understanding. By predicting one word or sub-word at a time based on preceding tokens, LLMs struggle to capture long-range dependencies and the complex semantic relationships essential for nuanced diagnostic interpretation. For radiology stakeholders, it is crucial to recognize that this token-level processing is fundamentally insufficient for the intricate complexities of diagnostic reasoning, where contextual understanding and abstract inference are paramount. This new paradigm promises to address persistent challenges in diagnostic accuracy, interpretability, and contextual synthesis, signaling a critical advance toward more intelligent and clinically meaningful AI systems in radiology.

PART 1: CURRENT CAPABILITIES AND LIMITATIONS OF LLMS IN RADIOLOGY AI

The capabilities of LLMS in radiology

This is a rapidly expanding field, with new research emerging daily. Results already indicate that LLMs will soon be applied to every aspect of radiology practice[2]. They have proven to be valuable in answering Radiology-related questions, providing clarifications regarding procedures, and offering general information about different types of imaging modalities[3]. LLMs play a significant role in patient triage and workflow optimization, helping in the automated determination of imaging studies and protocols based on radiology request forms[4] and the generation of radiology reports[5]. Algorithms like ChatGPT can improve patient outcomes, increase the efficiency of radiology interpretation, and aid in the overall workflow of radiologists[6,7] and it is reported that Generative Pre-trained Transformer (GPT)-4 was an effective tool for post hoc structured reporting in radiology, with its autonomous ability to select the most appropriate structuring template making it a highly scalable and easily implementable solution that required minimal database restructuring effort. Furthermore, LLMs have been shown to be versatile tools for establishing an accurate differential diagnosis, with the potential to improve clinicians' diagnostic reasoning and accuracy in challenging cases and to empower physicians and widen patients' access to specialist-level expertise[8]. ChatRadioValuer, for example, surpassed state-of-the-art models in disease diagnosis from radiology reports and alleviated the annotation workload of experts[9]. This part of the manuscript explores the evolution and current landscape of LLMs in radiology AI, emphasizing their capabilities and practical applications. Part 2 will cover LCMs.

Historical context and evolution of AI to LCMs: To appreciate the significance of LLMs and LCMs, it is important to trace the historical evolution of AI, from foundational principles established decades ago, to the emergence of LCMs in 2025. This journey represents a continuum of transformative milestones, with many advances still ahead.

Early foundations-symbolic AI: The birth of AI is often marked by the Dartmouth Conference in 1956, where the term "AI" was coined and the initial aspirations for creating thinking machines were discussed. This early era was dominated by symbolic AI, which focused on representing knowledge through symbols, rules, and logical structures. Expert systems, designed to mimic the decision-making of human experts using predefined rules, were a prominent application of this approach[10,11]. While the Dartmouth Conference aimed to bring together researchers from various disciplines with the specific intent of exploring the possibility of creating machines that could exhibit intelligent behavior, and laid the foundation for the field, symbolic AI's reliance on explicitly programmed rules proved to be a significant limitation. Importantly, the term "AI" was adopted at this conference and many of the early AI programs were started after this conference. It also aided in establishing key areas of research that continue to be explored today, as well as fostered collaborations and connections among researchers who would go on to make significant contributions to AI. Thus, this conference marked the beginning of AI as a distinct field of research and set the stage for decades of AI development and innovation. It is worth noting that while the conference was groundbreaking, the early optimism about achieving human-level AI quickly proved to be overly ambitious[12]. The field experienced periods of "AI winters" when funding and interest waned[13]. However, the Dartmouth Conference's legacy remains strong, and its impact on the development of modern AI is undeniable[14]. Turing's question "Can machines think" along with his further fundamental contributions to AI inspired the Dartmouth conference participants to look forward to building the first machines that could pass the Turing test[15]. The conference aimed to explore the possibilities of creating machines that could demonstrate intelligent behavior, a goal emanating from Turing's inquiries[16]. Early AI relied on rule-based systems, which struggled with real-world complexities, particularly in handling uncertainty and learning from data. The manual creation of these rules was time-consuming, brittle, and difficult to scale, ultimately limiting the capabilities of symbolic AI in addressing complex, real-world problems. This inherent limitation paved the way for the rise of data-driven approaches[11,17].

Machine learning, neural networks, and deep learning: Machine learning (ML) involves developing software that learns autonomously from data, identifying patterns to make predictions or decisions without explicit programming[18]. Its main objective is to enable systems to adapt without human intervention. ML methods are broadly divided into supervised learning, which predicts or classifies new data from labeled examples, and unsupervised learning, which discovers hidden patterns without pre-defined outputs[19]. By the 1980s, ML marked a shift from symbolic AI. Decision trees[20], support vector machines[21], and Bayesian networks (which demonstrated success in various tasks, offering a more adaptive and data-driven approach) broadened the AI landscape in healthcare. These algorithms enabled data-driven predictions and classification, offering a more flexible alternative to rigid rule-based systems[11,17]. ML soon radically improved radiology and enabled automated pattern recognition across modalities including X-ray, computed tomography (CT), magnetic resonance imaging (MRI), positron emission tomography; and even radiology reports, supporting diagnosis, reducing errors; and became capable of extracting complex, high-level data, even from unlabeled datasets[18,22]. It also fueled advances in computer-aided diagnosis, which integrated radiology, pathology, and

genomics data to improve workflows and productivity[23].

Neural networks: Basic neural networks were introduced in the 1980s but gained momentum after 2003, when Bengio *et al*[24] developed the first feed-forward neural network language model that predicted words in sequence, overcoming earlier statistical limitations and laying the foundations for modern NLP[24]. While early neural nets showed promise in pattern recognition, they struggled with sequential data and lacked the scale for complex tasks[17]. Recurrent neural networks (RNNs) later improved contextual information retention with long short-term memory networks[25] and gated recurrent units becoming dominant sequence-processing architectures[26]. These networks powered breakthroughs in image recognition and NLP, fueling an AI renaissance[27]. However, RNNs faced challenges: (1) Retaining information across long sequences; and (2) Limited parallelization during training, which constrained scalability. These shortcomings highlighted the need for deeper, more efficient architectures.

Deep learning: Deep learning (DL), a subset of ML, uses multilayered ("deep") artificial neural networks to model complex data patterns[18,19] and proved particularly effective for tasks where manual feature extraction was impractical, especially in large imaging datasets.

Significant limitations remain: DL and ML both require large, diverse, and well-annotated datasets, which are often difficult to obtain due to privacy restrictions, institutional variability, and the high cost of expert labeling. Models are also vulnerable to bias and poor generalizability, as performance often drops when applied to underrepresented demographics, new imaging protocols, or to data from different equipment. Furthermore, their interpretability remains limited: Deep neural networks function as "black boxes," making clinical trust and regulatory approval difficult[28]. Equally pressing are integration and sustainability issues. Clinical adoption requires seamless incorporation into workflows, ongoing retraining to match rapidly evolving imaging techniques, and careful attention to ethical, regulatory, and workforce considerations[19]. Overfitting and narrow task-specific performance further constrain real-world utility, underscoring the gap between research prototypes and practical deployment. In summary, ML laid the groundwork for automated pattern recognition in radiology, neural networks expanded contextual understanding, and DL harnessed depth and scale for tackling complex imaging tasks. Together, these approaches have transformed radiology while still grappling with data scarcity, bias, interpretability, and integration challenges.

Attention breaking mechanism and the Transformers

Dzmitry Bahdanau *et al*[29], introduced the attention mechanism in 2016 addressing challenges faced with traditional architectures that were known to struggle with longer input sentences. This was a significant breakthrough in the context of sequence-to-sequence models, particularly for neural machine translation. The attention mechanism allowed the model to selectively focus on different parts of the input sequence when generating each word of the output sequence and was a huge improvement over previous methods, which struggled with long sentences because they had to compress the entire input into a fixed-length vector. Bahdanau *et al*[29], "attention mechanism" allowed the model to dynamically "pay attention" to the relevant parts of the input. This mechanism therefore allowed models to focus entirely on relevant parts of input sequences dynamically, improving translation quality immensely. This innovation directly addressed a key limitation of earlier neural network architectures in NLP.

Transformers: Subsequently, 8 Google employees, wrote the historic "Transformers Paper" the most consequential technology breakthrough in recent history[27]. The transformer architecture was a revolutionary neural network architecture that relied entirely on the attention mechanism. It eliminated the need for RNNs or convolutional neural networks, which were previously the dominant architectures for sequence-to-sequence tasks. The limitations in handling long sequences effectively before the "Transformer era" were a core motivation for the Transformer's development as highlighted in the "Attention is all you need" paper[30]. The Transformer architecture provided a more effective way to process sequential data, paving the way for significant advancements in NLP. Although the transformer architecture used "attention" it is actually much greater than the original attention mechanism. Bahdanau *et al*[29], introduced the concept of attention, while the Google team built an entire architecture around it. The transformer architecture used a self-attention model, that allowed the model to look at the input, and then look at the input again, in relation to itself and also uses an encoder and decoder system, that greatly enhances the ability of the model. This allowed the model to: (1) Directly access and weigh the importance of different parts of the input sequence when processing each position, which addressed the long-range dependency problem; and (2) Perform parallel processing. Unlike RNNs, the Transformer architecture allows for significant parallelization during training. This made it possible to train much larger models on massive datasets, unlocking unprecedented levels of language understanding and generation. This scalability and improved handling of context were crucial steps towards the development of LLMs and their subsequent evolutions, including the multi-modal LLMs (MLLMs) used in medical imaging[31]. Although Bahdanau *et al*'s work[29] was a crucial steppingstone that paved the way for the transformer architecture, the Google "8 authors team" took that idea and built a much more powerful and versatile system. These authors started with neural networks - and made it into something else: A digital system so powerful that its output can feel like the product of an alien intelligence. Called transformers, this architecture is the not-so-secret sauce behind all those mind-boggling AI products, including ChatGPT, Gemini and the omnipresent mesmerizing graphic generators one interacts with of late[27]. The Transformer innovation was a turning point, enabling more advanced NLP models which provided the impetus for the emergence of sophisticated language models like Llama 2 (developed by Meta AI), GPT-4 (developed by Open AI), and a host of others[32] including the hot out of the oven Llama 4, with a mind boggling 2 trillion parameter model[33]. All of these, underpinned by extensive training data, have elevated NLP to a level of understanding and text generation that closely approximates

human-like language. The success of the Transformer architecture demonstrated the power of scaling and novel architectural designs in overcoming previous limitations in NLP. Earlier, the dominant sequence transduction models were based on convolutional neural networks in an encoder and decoder configuration. Vaswani *et al*[30] proposed a novel, simple network architecture based solely on an attention mechanism, dispensing with recurrence and convolutions entirely. Their model entirely replaced recurrent and convolutional networks with self-attention mechanisms, enabling much greater parallelization and efficiency. Their single model with 165 million parameters, achieved 27.5 Bilingual Evaluation Understudy (BLEU) on English-to-German translation, improving over the then existing best ensemble result by over 1 BLEU. On English-to-French translation, they outperformed the previous single state-of-the-art with model by 0.7 BLEU, achieving a BLEU score of 41.1[30]. This outperformed previous state-of-the-art models significantly and gave an immense boost to AI. Unfortunately, Google was slow to utilize this concept invented by 8 people from their own team. However, a (then) start-up, called Open AI was quick to pounce upon this transformer-based concept[27]; and that is how Open AI and Sam Altman made their names! It's striking how clearly the authors anticipated the broad applicability of Transformer models beyond just text. Their vision for extending it to images, audio, and video has indeed come to fruition in a massive way. Their statement "We are excited about the future of attention-based models"[30] now reads like a profound understatement. It's fascinating to see how a seemingly simple title, inspired by a famous Beatles song (all you need is love), ended up getting attached to such a revolutionary piece of work that has reshaped the entire landscape of AI.

Impact on LLMs: The Transformer architecture was the foundation on which LLMs like GPT[34] and Bidirectional Encoder Representations from Transformers[35] and Google's Bard[36] were established and enabled advancements in tasks such as machine translation, question answering (QA), and multimodal generative AI. For example, Google's Bard sought to combine the breadth of the world's knowledge with the power, intelligence and creativity of their LLMs and drew information from the web to provide fresh, high-quality responses[36]. Pichai explained how AI could deepen our understanding of information and turn it into useful knowledge more efficiently, making it easier for people to get to the heart of what they were looking for. The Transformer's ability to process long sequences and its parallelization capabilities enabled the training of models with an unprecedented number of parameters, leading to the emergence of LLMs with remarkable language capabilities[17,30]. This represented a significant leap in AI's ability to understand and generate human-like text. Yet these models still primarily operated on the statistical relationships between words (tokens). Bard (now known as Gemini) was initially powered by a family of LLMs developed by Google AI called Language Model for Dialogue Applications[37]. Language Model for Dialogue Applications itself was built upon the transformer architecture.

Human-like language approximation: The capabilities demonstrated by models like GPT-4, Gemini and Llama 2, in terms of fluency, coherence, and contextual understanding are evident in their performance on various NLP benchmarks and in real-world applications. While "human-like" is a complex and debated term, the advancements in these models represent a significant leap in text generation quality. These capabilities are often showcased in their respective technical reports and evaluations. However, this impressive linguistic ability often masks a fundamental limitation: LLMs primarily excel at manipulating tokens and identifying statistical patterns in language, rather than possessing a genuine understanding of the underlying concepts and their relationships in the real world. This lack of deep conceptual understanding becomes particularly apparent when faced with tasks requiring abstract reasoning or cross-modal integration, an integral part of current healthcare needs. Thus, limiting their ability to truly understand and reason presented concepts.

Scaling up of LLMs

LLMs like GPT-3 (2020) demonstrated unprecedented capabilities in generating human-like text by scaling up parameters and training on vast datasets. LLMs soon began driving innovations across a vast spectrum of industries. Earliest LLMs were mainly designed as general-purpose chatbots. The deployment of LLMs within the healthcare sector had sparked both enthusiasm and apprehension. These models exhibited the remarkable capability to provide proficient responses to free-text queries, demonstrating a nuanced understanding of professional medical knowledge *etc*[38]. While scaling has led to emergent capabilities, such as improved performance on certain reasoning tasks; it has not fundamentally altered the core mechanism of token prediction. This inherent limitation restricts their ability to perform robust abstract reasoning, integrate information across different modalities (like text and images), and truly grasp the conceptual underpinnings of the data they process, including presented concepts - the very challenges that LCMs aim to address.

Specialized medical domain models and limitations

Subsequently, research focused on developing specialized models for the medical domain, such as Meditron[39], Med-PaLM[40], GMAI[41], BioMistral[42], by medical knowledge enriching of the training data of LLMs. However, this approach required significant computational resources that were not commonly available and the same was also not applicable to closed-source LLMs, which are often the most powerful[43]. While LLMs had achieved state-of-the-art performance on a wide range of subjects, including medical QA tasks, they still faced challenges with hallucinations and outdated knowledge[44]. Hence techniques such as the already widely adopted retrieval-augmented generation (RAG) [45] were introduced in the medical domain, which allowed information to be dynamically retrieved from medical databases during the model generation process. Thus, enriching the output with medical knowledge without any need to train the model[44]. The reliance on external knowledge retrieval mechanisms like RAG highlights the LLMs' inherent limitations in storing and reasoning with vast amounts of information in a conceptually rich and readily accessible

manner[45]. It underscores their dependence on surface-level pattern matching rather than a deep understanding of the underlying medical concepts. Despite their proficiency in language, the lack of deep conceptual understanding can lead to errors in reasoning and the generation of plausible but incorrect medical information (hallucinations), a critical concern in high-stakes domains like healthcare, where accuracy and reliability are paramount. This fundamental limitation underscores the need for AI models that go beyond surface-level language processing and possess a more robust understanding of medical concepts and their interrelationships[31].

Detailed applications of LLMs in clinical workflow

LLMs have been used for other varied purposes in the medical domain which included named entity recognition, extracting other clinical information from electronic health records, document classification, summarizing, structuring, or explaining medical texts, relation extraction to natural language inference, streamlining administrative tasks in clinical practice, and enhancing medical research, multi-modal applications, quality control, education and question-answering[7,38,46,47]. Nazih and Peng[38] provide a comprehensive exploration of the current landscape of LLMs in healthcare, addressing their role in transforming medical applications. By leveraging the capabilities of LLMs in healthcare processes, organizations can provide better patient care, research, and data privacy thanks to LLMs' ability to generate, and summarize text-rich data[48]. In an article titled "Best 10 LLMs in Healthcare in 2025" Dilmegani *et al*[48] have elaborated upon LLMs in healthcare in detail; wherein they have also stated that LLMs have also been used to assist in transcribing and summarizing doctor-patient conversations, drafting patient discharge summaries, generating diagnostic reports and that AI-powered chatbots can handle tasks like symptom triage, providing health information, and translating medical jargon into patient-friendly language. LLMs can also help bridge communication gaps between healthcare providers and patients, especially those who speak different languages, enhancing understanding and care delivery. For literature review/research support too LLMs can assist in extracting key insights from the vast resources of available medical literature, summarizing recent studies, and collating requisite evidence on clinical conditions or treatments. Such LLMs evolved rapidly from a score of 33.3% (GPT-Neo December 2020) to 86.5% in March 2023 (Medical PaLM 2), on Medical Question Answering (United States Medical Licensing Examination style) accuracy[48]. While these applications demonstrate the utility of LLMs in automating and enhancing various aspects of healthcare, they often rely on sophisticated pattern recognition and language manipulation rather than a deep, conceptual understanding of the underlying medical knowledge. This highlights the potential for more robust and reliable AI, through models that can truly understand and reason about medical concepts. An AI model is helping researchers detect disease based on coughs. Google Research introduced health acoustic representations (HeAR), a bio-acoustic foundation model designed to listen to human sounds and flag early signs of disease[49]. HeAR was trained on 300 million pieces of de-identified audio data and used to develop a cough model trained with approximately 100 million cough sounds. This model is now being used by Swaasa to enhance early detection of tuberculosis (TB)[50]. "Every missed case of TB is a tragedy; every late diagnosis, a heartbreak," attributed by Shetty[50], to Kakarmath a product manager at Google Research working on HeAR and "Acoustic biomarkers offer the potential to rewrite this narrative". Having proposed a collaborative global effort to eradicate the scourge of TB, vide our "TB Revisited" plan, amongst others[51], we heartily welcome such accomplishments and feel that they will further the global effort to eradicate TB. This example highlights the potential of AI beyond language and underscores the need for models capable of integrating and reasoning across different data modalities - a hallmark of LCMs.

Radiological perspective[2,19,52-56]: The opportunities to apply LLMs in radiology is diverse, with new research being published every day. These results already indicate that LLMs will soon be applied to every aspect of radiology practice [2]. They have proven to be valuable in answering radiology-related questions, providing clarifications regarding procedures, and offering general information about different types of imaging modalities[3]. They can play a role in patient triage and workflow optimization, by helping in the automated determination of the imaging study and protocol based on radiology request forms[4] and in generation of radiology reports[5]. Algorithms like ChatGPT can improve patient outcomes, increase the efficiency of radiology interpretation, and aid in the overall workflow of radiologists[6]. Adams *et al*[7] reported that GPT-4 was an effective tool for post hoc structured reporting in radiology, with its autonomous ability to select the most appropriate structuring template making it a highly scalable and easily implementable solution that required minimal database restructuring effort. Furthermore, LLMs have been shown to be versatile tools for establishing an accurate differential diagnosis (with the potential to improve clinicians' diagnostic reasoning and accuracy in challenging cases and to empower physicians and widen patients' access to specialist-level expertise[8]. ChatRadio-Valuer, for example surpassed state-of-the-art models in disease diagnosis in radiology reports and reduced the workload of expert annotation[8]. LLMs have also served as prognostic models in medicine, analyzing vast, complex datasets to predict patient outcomes and guide treatment decisions[38,57]. Jiang *et al*[57] approach, for instance, leveraged advances in NLP to train an LLM for medical language and subsequently fine-tuned it across a wide range of clinical and operational predictive tasks. The deployment of these intelligent systems has bolstered decision-making, expedited diagnostic processes, and elevated the quality of patient care. They have been used to grapple with the ever-expanding body of medical knowledge, decipher intricate patient records, and formulate highly tailored treatment plans[38].

Evolution to multimodal models and advanced architectures: More recently, large multimodal models (LMMs) are emerging as powerful tools, particularly in radiology[55,56]. These models, built upon LLMs, including through the use of techniques like context engineering[58] and prompt engineering[55], integrate various imaging types (*e.g.*, CT, MRI, X-ray, endoscopy, digital pathology) alongside textual data such as radiology reports, clinical notes, and structured electronic health record (EHR) data[31]. Their defining feature is the ability to concurrently process and align information across modalities, often mapping them into a shared representational space. This synergy allows for a more compre-

hensive understanding than unimodal approaches permit[55]. This capability enables them to tackle complex cross-modal tasks such as radiology report generation from images and visual QA (VQA) that incorporates both imaging and clinical context[31,55]. Current applications of LMMs span automatic generation of preliminary radiology reports, visual query answering, and interactive diagnostic support. Examples of this evolution include embeddings for language/image-aligned X-rays which leveraged a language-aligned image encoder grafted onto a fixed LLM, PaLM 2, to perform a broad range of chest X-ray tasks[59]. CheX-GPT[60], RadLing[61] are other examples for the chest X-ray domain. Despite these promising capabilities, several significant challenges hinder widespread clinical adoption. For example, LMMs require access to large-scale, high-quality multimodal datasets, which are scarce in the medical domain. Their implementation is further complicated by risks of hallucinated findings, lack of transparency in decision-making processes, and high computational demands, a challenge shared by earlier LLMs as well. Nam *et al*'s review[31] summarizes the current capabilities and limitations of MLLMs in medicine and outlines key directions for future research. They suggested critical areas include incorporating region-grounded reasoning to link model outputs to specific image regions, developing robust foundation models pre-trained on large-scale medical datasets, and establishing strategies for the safe and effective integration of LMMs into clinical practice. Recently, it has been reported that LLMs can now learn without labels, enabling self-evolving Language Models using unlabeled data[62]. A new algorithm called self logits evolution decoding (SLED) has been introduced[63]. Standard LLMs often rely solely on the final layer, potentially leading to incorrect but "popular" answers due to missed contextual cues. SLED improves this by using information from all layers of the LLM, not just the last one. It does this by reusing the final projection matrix in the Transformer architecture on early exit logits to create probability distributions over the same set of possible tokens that the final layer uses. It then takes a weighted average of the distributions from all the layers, giving more importance to some layers than others, thus refining the LLM's predictions by incorporating information from different stages of its processing. However, all these advanced models are still fundamentally built upon LLMs and are therefore vulnerable to similar limitations. Being LLM based models, they still fundamentally process statistical patterns between words rather than abstract concepts, potentially limiting their depth of reasoning and long-range coherence compared to a human physician's diagnostic abilities.

Limitations of AI

ML, DL, and LLMs: While ML, DL, and LLMs have driven major advances in medical imaging, their clinical adoption remains tempered by important limitations. These technologies require large, diverse, and expertly annotated datasets, which are often scarce in healthcare settings. They are susceptible to variability and bias, raising risks of inequitable outcomes across patient groups and imaging protocols. Their decision-making processes often lack interpretability, making it difficult for clinicians to trust or validate outputs in critical diagnostic contexts. In addition, training and deploying advanced models entails substantial computational and environmental costs, challenging sustainability and scalability. Finally, there are unresolved ethical and regulatory concerns, including questions of liability, data privacy, and the absence of robust frameworks for validating non-deterministic outputs[19,52-55]. Collectively, these constraints highlight why AI systems in medicine are best viewed as decision-support tools rather than autonomous replacements for clinicians. Taken together, these limitations illustrate why AI in its current forms - ML, DL, and LLMs, cannot yet serve as fully autonomous clinical decision-makers. They remain valuable adjuncts but not replacements. Although AI has advanced far beyond the rule-based systems of the past, there is still a pressing need for models capable of deeper conceptual reasoning and contextual understanding, thinking more like the human brain does. Further in this manuscript we highlight the continuous efforts undertaken to enhance AI's capabilities in understanding and reasoning about complex information including the birth of LCMs[30], which in reality have been considered by some to represent a potential natural evolutionary step for LLMs[64]. LCMs offer a conceptual leap, moving beyond simple tokenization and enabling models to operate at the level of clinical concepts, sentences, and integrated multi-modal data streams. This architecture allows for the preservation of complex relationships across a patient's medical record - from imaging and pathology to laboratory results and genomic data, driving more robust abstraction, contextual synthesis, and reliable clinical interpretation.

The concept of concept models

In June 2022, Merchant *et al*[51] published their maxim: "AI needs real intelligence to guide it!" They proposed a multimodal, holistic approach to AI in healthcare, emphasizing that to maximize accuracy and utility in diagnosis and treatment, AI must incorporate experiential wisdom accumulated over decades of clinical practice. Key teaching and clinical parameters, including prognostic indicators, should complement big data to enhance algorithmic performance[19,51]. This appears to be among the earliest works to advocate for concept-based processing in AI, particularly in the medical domain. The authors stressed the need to move beyond a purely data-driven approach and to integrate human expertise for more reliable outcomes. As Merchant[65] noted - echoing Alan Kay's quote, "The best way to predict the future is to invent it" - his vision of making "machines think like us, not the other way around"[65] finds a natural extension in the development of LCMs[66].

The birth of LCMs: The first successful implementation of LCMs was from META's FAIR team on December 11, 2024[67,68]. They introduced a concept-based architecture operating on explicit semantic representations that were language and modality-agnostic. Their "LCMs" treated a concept as equivalent to a sentence, relying on SONAR - an embedding space supporting 200 languages in both text and speech. Using models with 1.6B parameters and training on 1.3T tokens, LCMs demonstrated impressive zero-shot generalization across languages, outperforming same-size LLMs. This marked a major step toward human-like reasoning: While LLMs excel at statistical language modeling, LCMs target structured

understanding of concepts and their relationships[67,68]. Although still in their infancy and not yet as widely recognized as LLMs, LCMs are positioned to address the key limitations of LLMs and to enable genuine conceptual reasoning, logical inference, and ethical alignment[66,69].

Understanding LCMs: LLMs process input at the token level, often struggling with coherence over long sequences, a major drawback in domains like healthcare that demand extended, precise reasoning[70]. LCMs, by contrast, process sentences or concepts, enabling richer semantic reasoning and better handling of long contexts[71] Their design mirrors human thought by emphasizing concepts over words, spanning modalities and languages[65,66]. Figure 1 shows the conceptual shift from LLMs (sequential, token-based) to LCMs (relational, conceptual). Since LLMs handle input at the token level, processing one word or sub-word at a time[70], this fine-grained approach can lead to difficulties in maintaining coherence over long sequences, particularly for extended text generation, which is a common requirement of healthcare, including radiology and allied fields. In contrast LCMs process fewer units (sentences instead of tokens), enabling them to handle large contexts more efficiently and produce more structured outputs[71]. This allows them to build "conceptual maps" that mirror how humans think. The key distinctions are summarized in Table 1, which outlines the key methodological differences between LLMs trained primarily on natural language and specialized LCMs that are co-trained on vast repositories of programming code. LCMs thus represent a significant advancement over LLMs, and their creative layout mimics human thought processes by emphasizing concepts over words and span across modalities and languages. For example, when prompted with "The scientist worked late in the …", an LLM predicts "laboratory" without understanding context. An LCM, however, might generate: "The scientist worked late in the laboratory to finalize results for a groundbreaking study", reflecting deeper comprehension of intent[66,72]. Figure 2 displays the architectural contrast between LLMs that use a language-centric flow *vs* LCMs' integrative, multimodal concept integration.

Key abilities of LCMs (prelude) include: (1) Understanding and manipulating abstract concepts: Going beyond statistical patterns in language to grasp the underlying meaning, relationships, and properties of concepts (like "infection", "immunity", "drug resistance", "socioeconomic factors"); (2) Causal reasoning and inference: Understanding cause-and-effect relationships more deeply than correlation patterns often found by LLMs; and (3) Multi-modal concept integration: Connecting concepts across different data types (text, images, structured data, genomic data). This concept-based approach allows LCMs to capture the underlying meaning and relationships between different pieces of information, enabling more sophisticated AI applications, including in healthcare. For example, building and reasoning over knowledge graphs/ontologies: Explicitly modelling the relationships between different concepts relevant to a common disease TB (*e.g.*, mycobacterium TB causes TB, rifampicin treats TB but can cause hepatitis, poverty is a risk factor for exposure). This capability to model complex relationships is crucial for tasks that require deeper understanding and inference. As Ahmed *et al*[71] describe, LCMs identify and embed concepts in semantic space, reasoning across diverse expressions. This "conceptual learning" extends beyond pattern recognition, allowing models to infer meaning and apply it in context[73,74]. Since they are trained on both text data and conceptual data, this allows LCMs to develop a deeper understanding of the meaning of the text that they generate and hence implement concepts too[66].

Key disadvantages of ML/DL and LLMs in radiology and healthcare

While ML, DL, and LLMs have transformed radiology and medical imaging, they remain constrained by several key limitations that must be acknowledged for responsible clinical adoption[2,19,52-56]. Many limitations of LLMs have already been described in general AI discourse, but their impact in radiology and healthcare is especially acute. Key challenges include restricted reasoning, resource intensity, ethical risks, hallucinations, and misplaced trust in model fluency. Together, these issues highlight why current AI models cannot yet function as autonomous clinical decision-makers (Table 2). In their systematic review of 89 LLM studies across 29 specialties, Busch *et al*[43] identified widespread shortcomings including lack of medical domain optimization, poor transparency, non-reproducibility, unsafe outputs, and bias. Their taxonomy distinguished between design limitations (*e.g.*, insufficient domain adaptation, restricted data access, opaque validation) and output limitations (*e.g.*, non-comprehensiveness, incorrectness, unsafety, bias). Alarmingly, nearly half the studies reviewed reported that LLMs were not optimized for the medical domain.

Data requirements: ML/DL/LLM models require vast, diverse, well-annotated datasets, for effective training and validation. These are difficult to obtain in healthcare due to privacy constraints, institutional heterogeneity, and the intensive expert annotation costs.

Variability and bias: Continue to undermine robustness. Differences in protocols, scanners, and patient demographics introduce heterogeneity in image appearance. Validating the information generated by LLMs is essential and requires regular audits, fairness-aware training[75-77]. Providing additional context or paraphrasing a question to an LLM can change the subsequent response[78]. Hence, the validation needs to be not only on scientific rigor but also on the contextual understanding of LLMs. For example, a non-contrast CT's rounded peripheral hyper density - may reflect a contusion (in the context of trauma), a metastatic lesion (in a patient with a known malignant melanoma), a spontaneous hemorrhage (in an older patient with amyloid angiopathy), or a hemorrhagic venous infarct (in a young female on oral contraceptives)[55]. Understanding the clinical context in such cases is critical. Bias in training data leads to underperformance and inequities. LLMs, which rely on massive internet-scale corpora, are especially prone to propagating cultural, gender, or racial biases[79-81]. The inability of LLMs to filter biases properly continues to be a significant drawback.

Table 1 Methodological comparison of standard large language models and large concept models

Feature	LLMs	LCMs
Level of abstraction	Token-level prediction (word/sub word)	Concept-level prediction (sentence/idea)
Input representation	Processes individual tokens, language-specific	Uses sentence embeddings, language-agnostic
Reasoning and planning	Focuses on local predictions, lacks structured reasoning	Explicitly models hierarchical reasoning and structured planning
Zero-shot generalization	Requires fine-tuning for new tasks/Languages	Strong zero-shot learning across languages and modalities
Architectural modularity	Monolithic transformer, hard to modify	Modular design, allows easy extension and updates

LLM: Large language model; LCM: Large concept model.

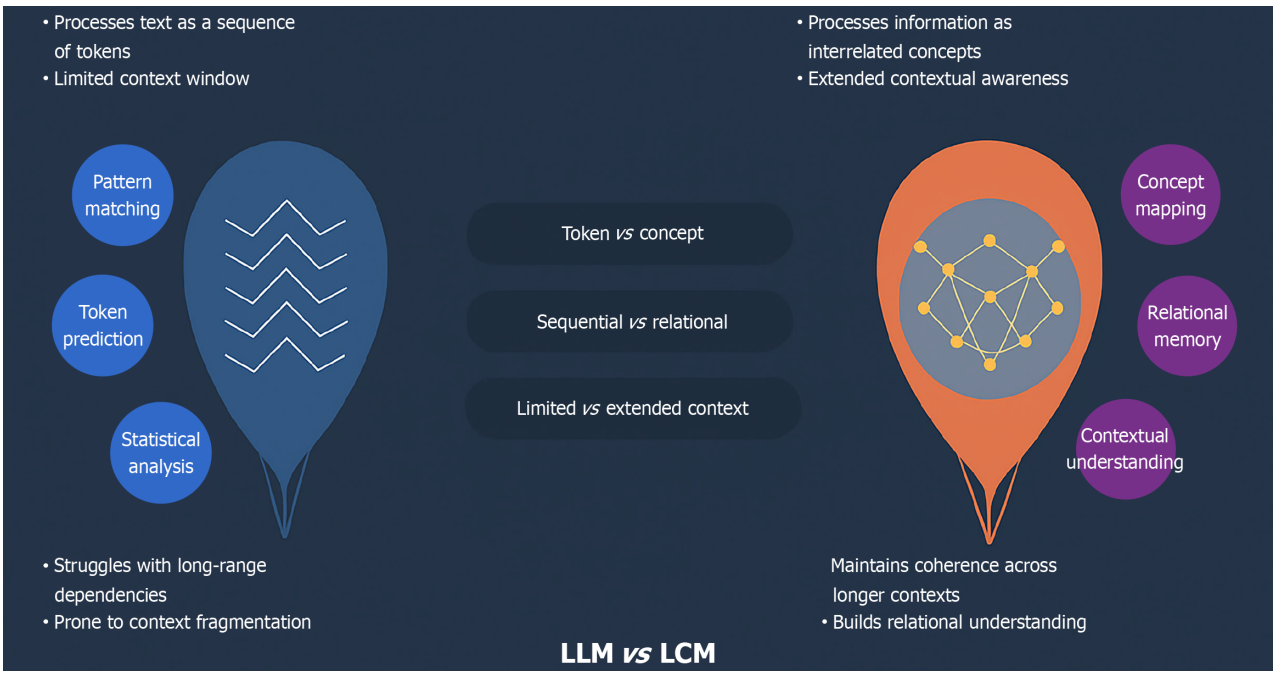


Figure 1 The conceptual shift from large language models to large concept models. This diagram illustrates the fundamental difference in processing. Large language models operate *via* a sequential, token-based analysis, leading to potential context fragmentation and struggles with long-range dependencies. Large concept models operate on a relational, conceptual level, building a deeper relational understanding and maintaining coherence across longer contexts. LLM: Large language model; LCM: Large concept model.

Incorrectness, hallucinations, and related phenomena: Incorrectness was reported in 32.9% of cases (Busch *et al*[43]). Many of these errors stemmed from hallucinations, fabricated or inaccurate outputs without grounding in input or reality. Busch *et al*[43] further categorized these into: (1) Illusion (13.5%): Characterized by the generation of deceptive perceptions or the distortion of information by conflating similar but separate concepts (*e.g.*, suggesting that MRI-type sounds might be experienced during standard nuclear medicine imaging); (2) Delirium (38.2%): Generating significant gaps in vital information, resulting in a fragmented or confused understanding of a subject (*e.g.*, omission of crucial information about caffeine cessation for stress myocardial perfusion scans); (3) Extrapolation (12.4%): Applying general knowledge or patterns to specific situations where they are inapplicable (*e.g.*, advice about injection-site discomfort that is more typical of CT contrast administration); (4) Delusion (15.7%): A fixed, false belief despite contradictory evidence (*e.g.*, inaccurate waiting times for a thyroid scan); and (5) Confabulation (20.2%): Filling in memory or knowledge gaps with plausible but invented information (*e.g.*, "You should drink plenty of fluids to help flush the radioactive material from your body", for a biliary system–excreted radiopharmaceutical)[43]. These errors, ranging from minor inaccuracies to complete fabrications, raise serious concerns about the reliability of LLMs in medical contexts, where even small mistakes can have significant consequences[43].

Hallucination: Rates are not trivial: 15%-20% in ChatGPT alone[6,82]. Factors such as biased training data, source-reference divergence, and token-by-token prediction increase susceptibility[82]. In medicine, where accuracy is critical, hallucinations raise the risk of misinformation, unsafe recommendations, or discriminatory content[55]. A summary of causes and types of Hallucinations and other forms of model incorrectness in LLMs are listed in Figure 3. LLM hallucination may stem from factors such as source-reference divergence, biased training data, and privacy concerns;

Table 2 Key limitations of artificial intelligence in radiology: From machine learning to large language models

Category	Description	Ref.
Data requirements	AI models (ML, DL, LLMs) require vast amounts of high-quality, annotated data, which is scarce in the medical domain. Privacy concerns and the cost of data acquisition and annotation are significant barrier	Nadkarni and Merchant [19], 2022 Hager *et al*[52], 2024
Variability and bias	Differences in imaging protocols, scanner types, and patient demographics can reduce model robustness. Training on biased datasets can perpetuate and even amplify clinical disparities	Marcus *et al*[79], 2023 Chen *et al*[80], 2021 Guo *et al*[81], 2024
Incorrectness and hallucinations	LLMs, in particular, may produce outputs that are factually inaccurate or fabricated. This is a critical issue in high-stakes clinical scenarios where accuracy is paramount	Guo *et al*[81], 2024 Olabiyi *et al*[17], 2025 Floridi *et al*[88], 2018 Bajaj S *et al*[6], 2024
Limited contextual uderstanding	LLMs operate at a token level and struggle with long-range dependencies, abstract reasoning, and integrating non-linguistic data. This leads to outputs that are often superficial and lack the depth of a human physician's diagnostic reasoning	Hendrycks *et al*[86], 2021 Marcus *et al*[79], 2023 Polonski *et al*[96], 2018 Bender *et al*[87], 2021 Najjar *et al*[18], 2023 Jiang *et al*[57], 2023 Nam *et al*[31], 2025 Grandison[64], 2025 Vaswani *et al*[30], 2017
Lack of interpretability and trust	Many AI models function as "black boxes", providing no insight into their decision- making process. This opacity undermines trust among clinicians and poses a significant hurdle to clinical adoption and patient safety	Hendrycks *et al*[86], 2021 Bender *et al*[87], 2021
Performance in rare diseases	AI performance often deteriorates in rare conditions, atypical presentations, and underrep-resented demographics. These "edge cases" demand nuanced reasoning that goes beyond narrow pattern recognition	Busch *et al*[43], 2025 Ouyang *et al*[84], 2025 Atil *et al*[85], 2025
Obsolescence and adaptability	The rapid pace of innovation in radiology means models must continually adapt to new techniques and protocols. Without frequent retraining and validation, AI systems can become obsolete, or their performance can degrade	Najjar *et al*[18], 2023
Clinical integration and medicolegal	Embedding AI into clinical workflows	Nadkarni and Merchant [19], 2022
Liability	Requires extensive infrastructure and training. If an AI error leads to patient harm, the question of legal liability between developers, institutions, and clinicians remains a significant, unresolved barrier	Hager *et al*[52], 2024 Soni *et al*[55], 2025
Computational and environmental costs	Training and running large-scale models like LLMs are resource-intensive, expensive, and have a high carbon footprint, which presents a sustainability challenge	Faiz *et al*[90], 2024 The Institution of Engineering and Technology[92], 2024 Ren *et al*[93], 2024
Delusions of progress	The overestimation of current AI capabilities, often due to misleading metrics, can lead to a "delusion of progress" that results in flawed decision-making and misplaced trust in high-stakes clinical scenarios	Topol[1], 2019

AI: Artificial intelligence; ML: Machine learning; DL: Deep learning; LLMs: Large language models.

leading to potential spread of misinformation, discriminatory content, and privacy violations[82]. The problem of hallucinations is particularly concerning in critical applications like healthcare, where inaccurate or fabricated information can have severe consequences. This highlights a fundamental limitation of LLMs: Their lack of grounding in reality and true understanding makes them prone to generating outputs that are not only incorrect but also potentially harmful.

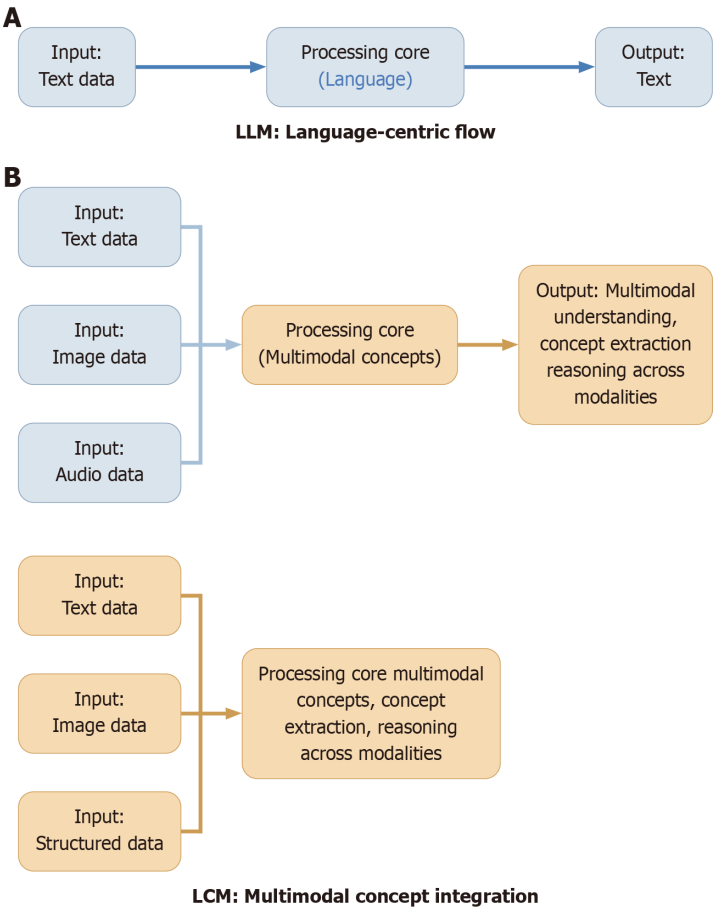


Figure 2 Architectural contrast of data processing in large language models *vs* large concept models. This diagram contrasts the linear, text-focused processing of large language model (LLM) with the integrative, multimodal architecture of large concept models (LCMs). A: LLM - language-centric flow: Text input flows into a centralized language processing core, producing text-based output. This represents LLM' sequential, language-driven pipeline; B: LCM - multimodal concept integration: Multiple input types - text, image, audio, structured data - converge into a more complex processing core capable of extracting and reasoning over abstract, cross-modal concepts. The output is richer and reflects a broader understanding that spans diverse modalities. LLM: Large language model; LCM: Large concept model.

Privacy and safety: Busch *et al*[43] found that 32% of studies judged LLM outputs unsafe (including misleading), 28.2% contained harmful content, and smaller but notable proportions revealed language bias (2.3%), insurance-related bias, or disparities affecting underserved racial groups and underrepresented procedures (1.1% each). These findings raise concerns that LLMs may perpetuate or even exacerbate healthcare inequities. Compounding these risks, LLMs remain vulnerable to "jailbreak" prompts - crafted queries that disguise harmful intent within narratives or instructions. Such attacks exploit token-based prediction and weak safety filters, leading to inappropriate, biased, or unsafe outputs[83]. In healthcare, this could result in unauthorized advice, misinformation, or privacy violations.

Non-comprehensiveness and reliability: Busch *et al*[43] reported that nearly 90% of reviewed studies demonstrated non-comprehensiveness. In clinical settings, incomplete results can have severe consequences, ranging from missed diagnoses to insufficient therapy recommendations that undermine entire treatment plans. For example, an incomplete therapy suggestion could compromise an entire treatment plan and risk patient harm. This pervasive non-comprehensiveness therefore represents a major obstacle to the safe and effective use of LLMs in healthcare decision-making. Additional reports[84,85] emphasize the non-reproducibility of LLM outputs, which obstructs validation and raises serious challenges for clinical trust and safe integration.

Interpretability and trust: DL and LLMs operate as "black boxes," recognizing correlations without causal reasoning. Although LLMs show promise for text-heavy integration, coherence across data types is inconsistent[55]. Their opacity undermines clinicians' trust, particularly when recommendations lack medical interpretability[55,86,87]. Providing identical queries in slightly altered contexts may also produce inconsistent responses, illustrating the fragility of their contextual reasoning[55].

Feedback loops and error propagation: Systematic misinterpretations or clinician overreliance may amplify diagnostic errors. Without active monitoring and retraining, these "model drifts" can compromise patient safety[55].

Ethical risks: Remain unresolved. Prejudices embedded in training datasets can manifest in biased or harmful outputs[17,

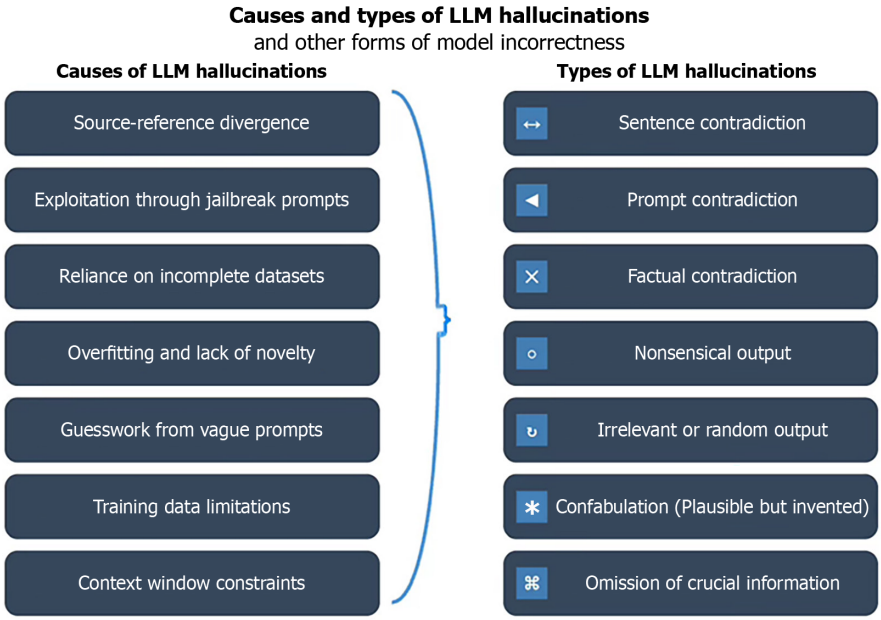


Figure 3 Causes and types of large language models hallucinations and other forms of model incorrectness (such as Illusion, delirium, extrapolation, delusion, confabulation). LLM: Large language model.

81,88]. Some of the ethical concerns can be attributed to "Hallucinations"[82]; and also relate to its potential impact on employment.

Computational resources and environmental costs/resource intensity and sustainability: Training deep models and large LLMs demands advanced graphics processing units/tensor processing units, massive storage, and a high energy consumption[55]. This poses financial and sustainability barriers[69,89], particularly for under-resourced health systems [90,91]. Training ChatGPT-3, for example, consumed energy comparable to millions of hours of video streaming[92]. Although some analyses argue that LLMs may offer efficiency gains compared to human labor[93], the balance between performance and environmental cost remains unresolved. Diffusion models, though powerful, remain computationally prohibitive for many medical applications[94,95].

Clinical integration: Integrating AI into healthcare workflows requires substantial infrastructure, clinician training, and cultural adaptation[19]. Models must also be frequently retrained to reflect new imaging modalities, evolving protocols, and shifting data distributions, creating heavy resource burdens. Overreliance on imperfect systems risks "error propagation", where clinician trust amplifies systematic model errors[55].

Delusions of progress: Excessive trust in AI can create "delusions of progress", where fluency is mistaken for comprehension. This misplaced confidence risks adoption of outputs that lack nuance, clinical grounding and contextual understanding needed for 'high-stakes medicine' decision making[1,55].

Limited contextual understanding and high-level reasoning: ML, DL systems and LLMs, while powerful, have inherent limitations in contextual comprehension and high-level reasoning. LLMs operate primarily at the token level, processing language as patterns rather than interconnected concepts[55]. This often results in superficial outputs that lack depth and nuance, with potential misinterpretation of metaphorical or context-dependent language[79,86,96]. The "stochastic parrots" critique underscores that fluency does not equal comprehension[87].

Limited high-level reasoning: These AI models struggle with high-level reasoning, particularly in tasks requiring abstraction, multi-step problem solving, or integration of domain-specific knowledge[18,79]. In radiology, this can manifest as misinterpretation of complex imaging patterns, incorrect differential diagnoses, or oversights in multi-modal clinical reasoning when subtle relationships across patient history, imaging, and laboratory data must be synthesized[31, 57]. These limitations highlight the need for advanced AI frameworks, such as LCMs, which aim to model concepts and relationships in a manner more akin to human cognition[30,64].

Regulatory, ethical challenges and practical considerations: Include validation, safety, accountability, ethical concerns, data privacy, and algorithmic bias. Radiology is a rapidly evolving field with new imaging techniques and data types emerging frequently. Most models require continuous retraining and updating to keep pace with these advancements, which is resource intensive[55]. Regulatory approval remains limited. The United States Food and Drug Administration (FDA) has so far authorized nearly 1000 AI-enabled medical devices, but none have been based on LLMs. This highlights a regulatory gap between conventional AI systems, which are relatively constrained and validated for specific functions, and LLMs, whose non-deterministic and non-transparent outputs pose unique challenges for clinical validation and

safety monitoring. Their susceptibility to variability, error, and non-reproducibility calls for entirely new regulatory frameworks[97].

Model specific limitations: Include limited scope and overfitting. Many current ML/DL applications in radiology are designed for specific tasks or clinical situations, rather than the broad spectrum of real-world clinical scenarios. DL models can overfit training data, leading to poor performance on unseen datasets if training data are not sufficiently diverse or representative.

Rare diseases and edge cases: AI performance often deteriorates in rare conditions, atypical presentations, and underrepresented demographics. This "long tail" of medicine challenges models trained primarily on common conditions and is particularly relevant in radiology, where edge cases demand nuanced reasoning beyond narrow pattern recognition.

Transparency, reproducibility, and peer review: Lack of transparency in model design, opaque validation, and absence of external reproducibility hinder clinical trust[43,84,85]. Independent peer review and access to external datasets are essential for acceptance.

Dynamic nature of radiology: The field's rapid pace of innovation poses its own challenge. DL models must continually adapt to new imaging techniques, protocols, and disease presentations, requiring frequent retraining and validation[18]. Without such updates, AI systems risk obsolescence or degraded performance.

Medicolegal liability: Remains unresolved: If an AI-generated recommendation leads to harm, liability between developers, institutions, and clinicians remains unclear[55]. This ambiguity represents a significant barrier to clinical deployment of LLM-based systems. Ethical concerns, such as patient data privacy, algorithmic bias, and the potential impact of automation on radiology employment, further complicate adoption.

Moving forward

The advent of LLMs, epitomized by OpenAI's ChatGPT marked a transformative leap in NLP. However, despite their impressive capabilities, LLMs face inherent architectural limitations, especially in specialized domains such as radiology [98-100]. Additionally, the development of LLMs has been led largely by computer scientists and business stakeholders, with little direct input from radiologists and physicians[19,51,101]. Without stronger collaboration, the gap between technical performance and clinical applicability will persist. These constraints underscore that LLMs should be treated as adjuncts, not autonomous decision-makers. Radiology, given its complexity and reliance on contextual integration, demonstrates both their utility as well as exposes their critical shortcomings. Despite the transformative advances through ML and DL in imaging analytics, anomaly detection, and diagnostic support, unresolved challenges remain: Data access, interpretability, bias, workflow integration, sustainability, and especially regulatory and legal oversight. Until these are systematically addressed, AI in radiology will remain powerful but constrained, unable to fully deliver on its full promise. More recently, LMMs are emerging as powerful tools, particularly in radiology[55,56]. These models, built upon LLMs and enhanced by techniques like prompt engineering[55], integrate multiple imaging types (*e.g.*, CT, MRI, X-ray, endoscopy, digital pathology) alongside textual data (radiology reports, clinical notes, and structured EHR data)[31]. Their defining feature is the ability to concurrently process and align information across modalities, mapping them into a shared representational space. This synergy enables more comprehensive understanding than unimodal approaches[55]. This capability enables them to address complex cross-modal tasks such as radiology report generation from images and VQA that incorporates both imaging and clinical context[31,55]. Current applications of MLLMs span automatic generation of preliminary radiology reports, VQA and interactive diagnostic support. Examples include embeddings for language/image-aligned X-rays, which leveraged a language-aligned image encoder grafted onto a fixed LLM, PaLM 2, to perform a broad range of chest X-ray tasks[59]. CheX-GPT[60]) and RadLing[61] are other recent chest X-ray domain models. While these multimodal LLMs show great promise by integrating imaging and clinical data[31], their clinical adoption is limited by data quality, implementation challenges, and insufficient clinician involvement. For example, MLLMs require access to large-scale, high-quality multimodal datasets, which are scarce in the medical domain. Their implementation is further complicated by risks of hallucinated findings, lack of transparency in decision-making processes, and high computational demands - a challenge shared by earlier LLMs as well. Nam *et al*'s review[31] summarizes the current capabilities and limitations of MLLMs in medicine and outlines key directions for future research. They suggested critical areas include incorporating region-grounded reasoning to link model outputs to specific image regions, developing robust foundation models pre-trained on large-scale medical datasets, and establishing strategies for the safe and effective integration of MLLMs into clinical practice. Recently, it has been reported that LLMs can now learn without labels, enabling self-evolving language models using unlabeled data[62]. A new algorithm called SLED has been introduced[63]. Standard LLMs often rely solely on the final layer, potentially leading to incorrect but "popular" answers due to missed contextual cues. SLED improves this by using information from all layers of the LLM, not just the last one. It does this by reusing the final projection matrix in the Transformer architecture on early exit logits to create probability distributions over the same set of possible tokens that the final layer uses. It then takes a weighted average of the distributions from all the layers, giving more importance to some layers than others, thus refining the LLM's predictions by incorporating information from different stages of its processing. However, all of these advanced models are still fundamentally built upon LLMs and are therefore vulnerable to similar limitations. They still fundamentally process statistical patterns between words rather than abstract concepts, potentially limiting their depth of reasoning and long-range coherence, compared to a human physician's diagnostic abilities. LLM/LMM constraints in abstract reasoning and multimodal integration motivate the exploration of new paradigms. Future directions may lie in LCMs, which move

beyond token prediction to represent clinical concepts and multimodal integration in a manner more akin to human reasoning[30,64]. By enabling abstraction and contextual synthesis across complex medical data streams, LCMs represent a potential evolutionary step toward more trustworthy, clinically aligned AI. This discussion will be continued in part 2, which elaborates upon the conceptual framework of LCMs, an emerging paradigm that aims to overcome these limitations by enabling richer semantic understanding and contextual reasoning. We will explore the evolution of these more advanced models that address these limitations and the challenges that lie ahead.

PART 2 - BEYOND LLMS IN RADIOLOGY AI: INTRODUCING LCMS AS THE CONCEPTUAL FRAMEWORK OF A NEW PARADIGM AND FUTURE DIRECTIONS

LCMs

What are LCMs? LCMs represent a transformative shift in AI's evolution beyond traditional LLMs, that rely on token-level sequential processing. Rooted in explicit semantic representations, LCMs operate at the level of clinical concepts and sentences rather than individual tokens, enabling enhanced semantic reasoning, long-range context synthesis, and integration of diverse, multi-modal data types; such as text, images, and structured clinical information. This richer conceptual framework allows LCMs to unlock insights and perform complex clinical decision-making that remains beyond the capabilities of current LLMs[66,69]. As Stephen Hawking suggested, "We are at the very beginning of time for the human race". It is thus reasonable to hope for continued progress extending far beyond even today's state-of-the-art AI models and agents.

Technical details of LCMs

Human cognition operates on concepts, not tokens. LCMs emulate this by leveraging SONAR embeddings, covering 200 languages and 76 speech inputs[102] to represent meaning across modalities[67,68]. Unlike LLMs, which tokenize input and predict sequential tokens, LCMs manipulate higher-order embeddings, enabling reasoning, independent of language boundaries[67,68,70]. Innovations in LCMs include hierarchical architectures for long-form coherence, diffusion-based generation that predicts embeddings instead of tokens, dual-tower models separating context encoding from generation, quant-LCMs for efficiency and scalability, zero-shot generalization across unseen modalities, and SONAR-based decoding that enables simultaneous multilingual outputs while reducing latency[74,103,104]. Figure 4A shows the detailed architecture of LCMs, illustrating language-agnostic, universal, and multimodal concept processing. Figure 4B combines the legends/keys for the visual elements, color coding, and capability categories shown in Figure 4A.

LCMs introduce several innovations: That can also be used to advance language modeling, such as[74,103,104]: (1) Hierarchical architecture which mirrors the human reasoning processes and enhances the coherence of long-form content and allows for local edits without disrupting the broader context; (2) Mean squared error regression - a foundational approach for sentence prediction; (3) Diffusion-based generation - such models predict the next SONAR embedding based on preceding embeddings and may be: Single tower architecture: Wherein a single transformer decoder handles context encoding and denoising (or combined context processing and sentence generation), or dual tower architecture: Which provides dedicated components for each task *i.e.* separates context encoding and denoising (separating context understanding from generation); (4) Quant-LCM for embedding quantization and enhanced robustness ensuring scalability and efficiency. This also addresses the quadratic complexity of standard Transformers, enabling LCMs to handle long contexts more effectively than token-level processing; (5) Zero-shot generalization: LCMs display strong zero-shot generalization capabilities on unseen languages and modalities by leveraging SONAR's extensive multilingual and multimodal support; and (6) Search and stop criteria: The search algorithm based on the distance to the "document end" concept ensures coherent and complete generation without the need for any fine-tuning. Quantized SONAR models: Have been considered as an upcoming enhancement in the LCM ecosystem[104] and thereby should ensure relatively easier upgradation of LLMs to LCMs or hybrid systems.

Overcoming long-range dependencies: By encoding concepts instead of tokens, LCMs manage long-range dependencies more effectively, reducing repetition and hallucinations[73]. Their multimodal design integrates text, images, and audio, supporting more holistic reasoning[66]. This approach reduces computational costs and resembles META's Joint Embedding Predictive Architecture; though Joint Embedding Predictive Architecture emphasized abstract representation learning, while LCMs model reasoning processes directly[105].

Representation and reasoning: LLMs represent text *via* token embeddings, limiting their ability to model complex relationships. With LCMs, the internal representations are closer to the "conceptual maps" that we humans form in our minds. LCMs explicitly encode concepts in high-dimensional space, enabling clustering, analogies, and hierarchical reasoning[73]. An analogy with hierarchical reasoning would be the example of a university professor taking a talk on a particular subject. He will definitely not write down all his words in his presentation, but just mention the key points through which he derives the rest. Every time (he gives the same talk) he may use different words, but his content/key points will remain the same, *i.e.* the essence of the talk remains unchanged despite the change in some/many words. Similarly, LCMs manipulate concepts, ensuring consistency across varied expressions. As LCMs generate output by manipulating whole concepts rather than predicting one token at a time, they maintain consistency over hundreds of words. Sentences are the basic building blocks that represent concepts. Eliot[106] stated that LCMs can devour sentences and adore concepts and has outlined the LCM workflow as a six-step process: (1) User enters a sentence composed of one

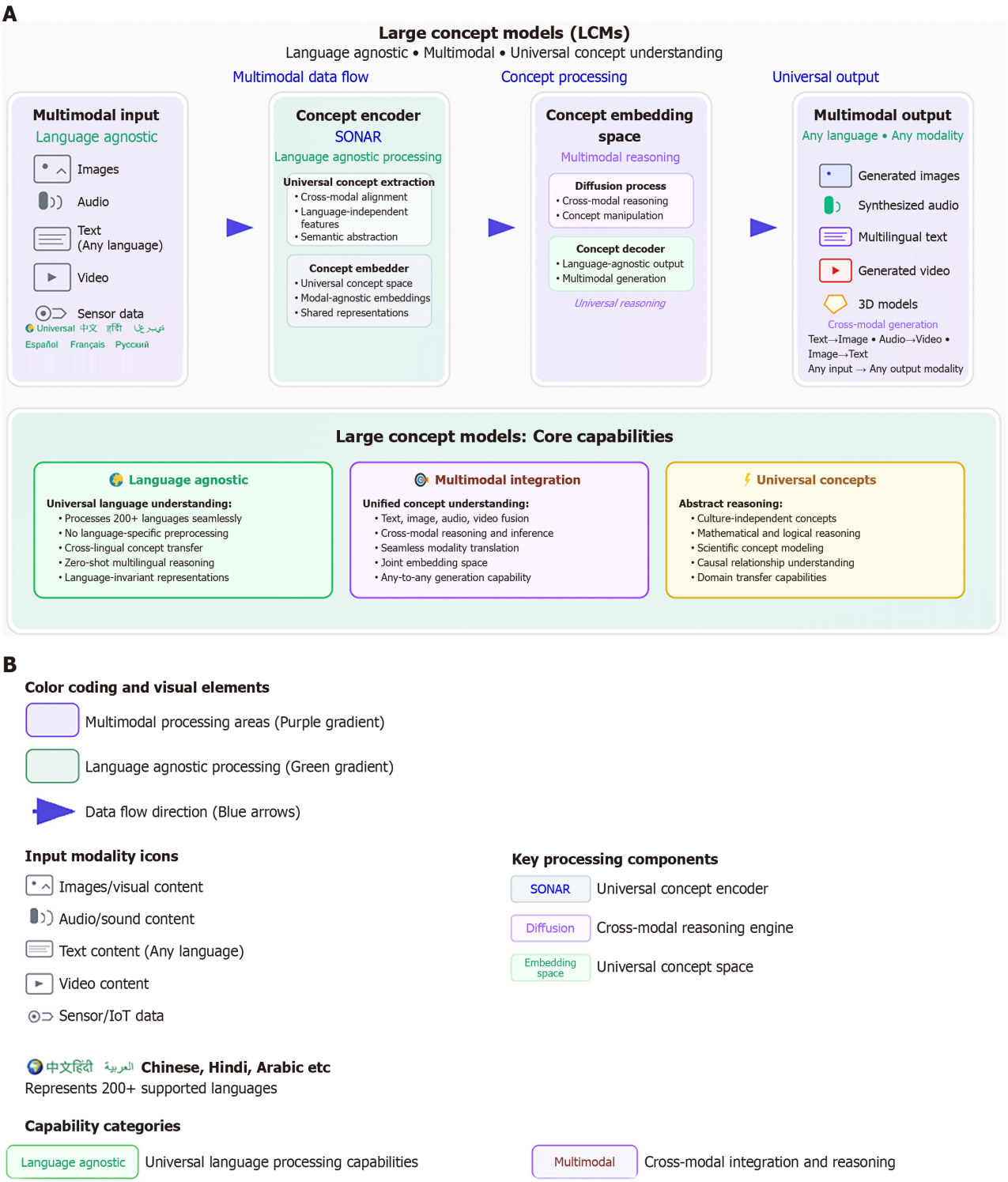


Figure 4 Large concept models. A: Large concept models detailed architecture illustrates language-agnostic, multimodal data flow with universal concept encoding, hierarchical reasoning, and multilingual output capability. This figure details the end-to-end processing pipeline of a large concept model, contrasting it with traditional language-centric artificial intelligence. The architecture is composed of two main sections: Top (multimodal data flow): Illustrates the flow from a Language-Agnostic Multimodal Input (accepting text, images, audio, video, and sensor data) to a Concept Encoder (like SONAR) which performs universal concept extraction. This encoded concept is then processed in a Concept Embedding Space *via* multimodal reasoning and diffusion processes. Finally, a Concept Decoder generates a Multimodal Output in any language or modality, demonstrating a true "any-input-to-any-output" capability. Bottom (core capabilities): Summarizes the three foundational pillars that this architecture enables: (1) Language agnostic universal language understanding across hundreds of languages; (2) Multimodal integration for unified concept understanding and reasoning across diverse data types; and (3) Universal concepts, enabling high-level abstract, logical, and causal reasoning that is independent of culture or domain; B: Reveals the color coding, visual elements, input modality icons, key processing components and capability categories illustrated regarding large concept models shown in Figure 4A. LCM: Large concept model.

or more words; (2) Concept encoder examines the sentence to figure out what concepts might mathematically and computationally underpin the text-based sentence provided in step[1] above; (3) Feed those speculated concepts into a LCM for computational processing; (4) LCM generates responsive concepts, which the LCM produces as internal outputs - a set of concepts; (5) Concept decoder produces text-based answers for the user; and (6) User is shown the generated sentence composed as a result of these steps[106]. This ensures outputs maintain fidelity to original meaning, while allowing flexible multilingual and multimodal decoding without re-running inference[67,68]. The key distinction is that LLMs predict "what to say next", whereas LCMs know what the prompt is about and encode "why and how" to the answer, grounding outputs in reasoning and relationships[69]. What differentiates an LCM from other works is its power to dive deeper into the meaning and interrelation of concepts, that generates a far more accurate response and implementation in the outputs[69].

Strategies for conceptual correctness in LCMs

While LLMs excel at processing and generating language from statistical patterns, LCMs aim for structured understanding of concepts and their non-linguistic relationships[107,108]. This difference enables LCMs to address incorrectness in ways beyond the reach of standard LLMs.

Direct manipulation and verification of conceptual graphs/networks: LCMs represent knowledge in structured forms such as conceptual graphs or semantic networks, allowing for direct analysis and verification[107,109,110] enabling: (1) Identification of contradictions (*e.g.*, "A is a type of B" *vs* "A is not a type of B"); (2) Verification of conceptual distance and relevance between linked concepts; (3) Comparison of conceptual graphs with ontologies or knowledge bases; and (4) Propagation of uncertainty scores. These operations are not feasible in LLMs, where knowledge is embedded in inaccessible neural weights[107,110].

Multi-modal conceptual grounding: While MLLMs align features across modalities, LCMs target modality-agnostic conceptual representations, allowing: (1) Verification of semantic consistency across modalities (*e.g.*, "cat" in image *vs* "cat" in text); (2) Confirmation of conceptual implications across modalities (*e.g.*, an X-ray of a broken leg validating textual implications of limited mobility)[107,108]; (3) Simulative verification and plausibility checks, by modeling causal relationships and rejecting implausible scenarios such as the objects floating upward plausibility[111]; and (4) Meta-conceptual reasoning and self-correction, including identification of low conceptual confidence, refinement of internal knowledge, and explanation of reasoning in terms of conceptual transformations rather than linguistic steps[110]. LLMs, by contrast, lack such meta-cognition.

Complementary strategies for correctness: Knowledge verification systems: LCMs must address factual errors, conceptual drift, and temporal inconsistencies by aligning with established knowledge frameworks[112-114]. Beyond textual retrieval, RAG integrates structured knowledge, ontologies, and multi-modal data to enrich conceptual grounding[45]. Uncertainty Awareness. LCMs should signal ambiguity, avoid false certainty, and request clarification when concepts are unclear[109,113]. Adversarial Training. Strengthens resistance against conceptual manipulation, prompt injection, and misleading inputs[114]. Human feedback loops: Enable alignment with human values, intuition, and expert knowledge across diverse contexts[114]. Transparency Mechanisms. Facilitate user trust by making reasoning pathways and conceptual links auditable. Multi-modal verification: Ensures consistent conceptual grounding across text, images, audio, and other modalities[108]. Provides an overview of strategies designed to address and prevent all forms of incorrectness in LCMs (Figure 5).

Integrated approach

A holistic framework integrates all these strategies[114]: (1) Strong pre-training on fundamental concepts; (2) Verification layers using RAG and knowledge frameworks; (3) Explicit handling of uncertainty; (4) Human feedback for continual conceptual refinement; and (5) Transparency to reveal reasoning and knowledge sources. Together, these strategies address factual inaccuracies, conceptual misunderstandings, and flawed reasoning. The goal is not only accuracy but a reliable, trustworthy, and conceptually sound AI system.

Key advantages of LCMs in healthcare

LCMs offer transformative benefits by emphasizing relationships, causal reasoning, and conceptual frameworks. For example, incorporating lamellar effusion into screening algorithms improved pediatric TB detection[51], while recognition of demographic disease shifts informs public health policy. This conceptual synthesis can significantly improve patient outcomes[19,51]. Merchant *et al*[51] emphasized that "AI needs real intelligence to guide it" underscoring the value of combining imaging with clinical evidence rather than relying on single modalities. This reflects a broader truth that meaningful intelligence, human or artificial, requires flexibility, humility, and willingness to adapt when established views are disproven[115]. As Merchant[65] observed, "we are drowning in information while starving for wisdom" pointing to the need for holistic, concept-based AI that embeds decades of experience and prognostic knowledge into its frameworks[19,51]. Unlike LLMs, which generate outputs token by token, LCMs reason with higher-level concepts, mapping symptoms to diagnoses, integrating comorbidities, and combining imaging, genetic, and lab data into cohesive assessments[19,51.116]. Cross-modal capacity further allows them to integrate narratives, data streams, and images into cohesive outputs[68,103], a critical advantage in clinical practice. A distinguishing strength of LCMs lies in semantic reasoning and context-aware decision-making[116]. By embedding patient-specific variables such as age, lifestyle, and comorbidities, their outputs are more interpretable than the "black box" systems of LLMs, providing explanations

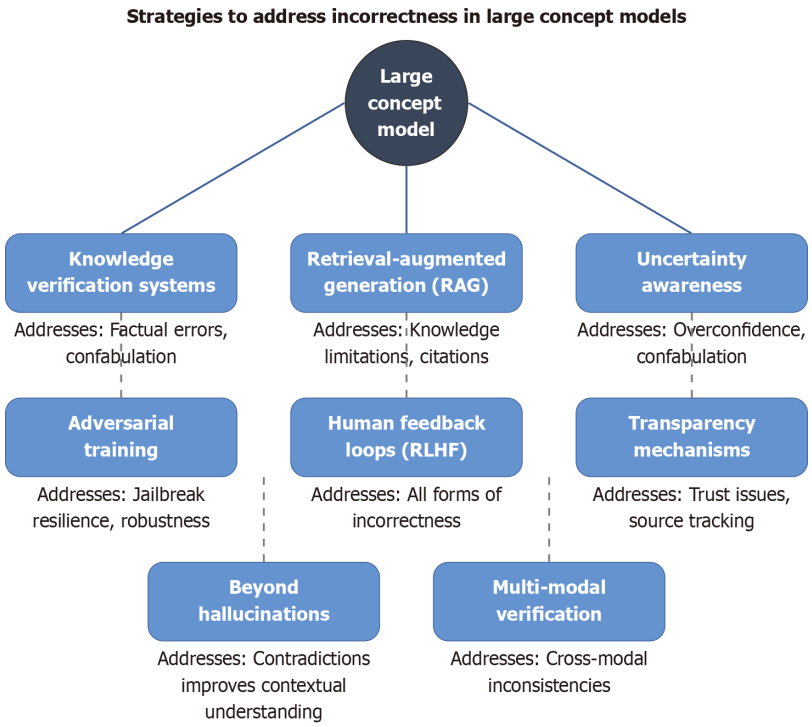


Figure 5 Strategies to address all forms of incorrectness in large concept models. These strategies work together to address the full spectrum of incorrectness issues - from outright hallucinations to subtle misinterpretations, inappropriate confidence, and contextual misunderstandings. The goal isn't just factual accuracy but a more reliable, trustworthy and useful artificial intelligence system overall. RAG: Retrieval-augmented generation; RLHF: Reinforcement learning from human feedback.

clinicians can validate[117,118], thereby building trust and improving adoption.

Efficiency is another advantage: With fewer parameters and lower energy demands, LCMs support "Green AI"[69,119-121]. Meta's prototypes demonstrated that leaner architectures could deliver superior performance while reducing costs and emissions. Moreover, they can be domain-tailored for radiology, oncology, or cardiology offering specialized solutions while retaining their broader reasoning abilities[66,122]. Compared with LLMs like GPT or bidirectional encoder representations from Transformers, which excel primarily at natural language tasks, LCMs' conceptual depth positions them as more suitable for complex, high-stakes healthcare applications where reasoning and interpretability matter most[50,122].

Regulatory outlook: Since LCMs emphasize explainability and transparency, they may face fewer regulatory hurdles. The FDA's assessment framework prioritizes interpretability, clinician trust, and auditability, criteria that LCMs, with clearer decision pathways, are better positioned to meet compared to opaque LLMs.

AI's journey in radiology and the dawn of LCMs

AI has long promised to revolutionize healthcare, with radiology- an early adopter, at the forefront of experimentation and deployment[123,124]. From initial excitement to real-world applications, the field has witnessed a decade of evolution in both expectations and implementation[1]. To appreciate the transformative potential of LCMs, it is helpful to briefly trace this journey. Early reviews[125] and later analyses[126] highlight both enthusiasm and anxiety around AI's disruptive potential. They point to AI's roles in workflow optimization, error reduction, improved imaging efficiency, and precision medicine, all enabling earlier diagnosis and proactive healthcare. By 2024, radiology remained central to healthcare, not only in preserving lives but also in generating significant economic output[126]. The rising demand for diagnostic services, advances in imaging, and AI integration have fueled rapid global growth in radiology. Industry revenues were projected to surpass 45 billion dollars by 2024 and 51 billion dollars by 2032[127,128], driven largely by chronic illness, aging populations, and expanded healthcare access. Similarly, the AI health market, once valued at 6.6 billion dollars in 2021 with a 40% compound annual growth rate, was forecast to grow more than tenfold within five years[129]. These market dynamics underscore radiology's role as a global driver of healthcare innovation[124]. The integration of AI and now LCMs promises to further accelerate diagnostic accuracy, workflow efficiency, and personalized care - unlocking both clinical and economic impact.

The lessons of the past and the crossroads of AI in healthcare

The decline of Kodak serves as a cautionary tale about ignoring innovation[130]. Healthcare faces a similar crossroads: Whether to adopt AI now or wait. Despite rapid uptake of imaging equipment, software adoption, including AI, often lags. Many radiologists remain focused on ML, even as LLMs and LCMs open far greater possibilities[66]. The impending

widespread implementation of large context models casts a long shadow of potential disruption across the healthcare landscape. This powerful new wave of AI promises unprecedented capabilities in diagnosis, treatment planning, drug discovery, and personalized medicine[131]. The journey of AI in radiology, from early excitement to the current transformative potential of LCMs, underscores the critical need for proactive adoption and strategic integration of these advanced models to shape the future of healthcare. Kodak's fate illustrates the danger: (1) Strategic blunder leadership resisted digital photography to protect film profits; (2) Slow adoption investments in digital were half-hearted, designed not to cannibalize film; and (3) Inevitable decline as digital and then smartphone photography surged, Kodak became irrelevant, filing for bankruptcy in 2012[132-134]. For healthcare, the lesson is clear: Protecting the present at the expense of the future risks' obsolescence. Innovate or evaporate[135]. As Darwin observed, "It is not the strongest of the species that survives, nor the most intelligent, but the one most adaptable to change".

The impending revolution - LCMs and the future of healthcare

With LCMs now implementable, the landscape of AI in healthcare could shift dramatically. They promise unprecedented capabilities in diagnosis, treatment planning, drug discovery, and personalized medicine[131]. The transition, however, demands proactive adoption. History is littered with dominant entities that failed to adapt. Economic incentives are strong: Private payers could save 80-110 billion dollars annually in the next five years, and physician groups another 20-60 billion dollars through AI-driven efficiencies[130]. The development of responsible AI ensuring transparency, trust, and safety - is essential for deploying advanced technologies[136]. Yet challenges in data modeling (small sample sizes, noisy data) and algorithmic complexity must be addressed to ensure ethical, sustainable implementation. In diagnostic imaging and interventional radiology, AI and robotics are already enhancing workflows, though many models remain experimental[137-145]. LLM-based models are only beginning to appear in this space, and LCMs remain largely conceptual. Having established the foundational role of multimodal, concept-capable LCMs in healthcare, the discussion now shifts to their broader applications. LCMs and emerging hybrid LLM-LCM frameworks are expected to transform not only clinical care, but also research, education, and system-level decision-making. Their capacity to integrate complex multimodal data aligns closely with radiology's trajectory, where AI has evolved from experimental promise to increasingly sophisticated practice. Positioned at this intersection, LCMs are poised to redefine the application of AI across healthcare domains. The next section outlines these illustrative applications across healthcare, highlighting the breadth of opportunities, before turning to detailed case scenarios.

Illustrative applications across healthcare

By integrating diverse conceptual frameworks, LCMs offer insights beyond conventional LLMs, synthesizing patient symptoms, medical histories, multimodal imaging, and research literature into concept-driven diagnoses[64,69,122]. This capability extends across domains from radiology to Interventional radiology, supporting research, clinical care, and system-level decisions. By enabling earlier diagnoses, personalized planning, improved workflows, and collaborative research, LCMs can enhance healthcare quality, accessibility, and outcomes worldwide. The following sections illustrate these wide-ranging applications.

Diagnostic excellence: LCMs integrate multimodal data - including symptoms, structured histories, imaging, biomarkers, and literature - to generate robust diagnostic insights that surpass LLMs[64,69,122]. This multidimensional synthesis supports early disease detection, identification of subtle radiological markers, and contextual understanding of clinical language, reconciling terminological differences across reports[51,66,74].

Key capabilities include: Early disease detection - detecting faint anomalies or subtle biomarkers by linking multimodal signals, conceptually linking multiple data types beyond simple keyword matching[146]. Multimodal data integration and synthesis - integrating clinical, genomic, and literature evidence to prioritize differential diagnoses, by conducting rapid and deep reviews of thousands of research articles to identify contradictions, knowledge gaps, and emerging hypotheses that support clinical and research decisions. Longitudinal data and clinical context awareness - summarizing prior imaging and tracking disease evolution across records truly encapsulating the patient's entire clinical journey. Tracking progression of multiple conditions: Follow the evolution of symptoms, findings, and treatments across years of patient records, supporting updated diagnosis in complex cases and for follow-up, maintaining longitudinal coherence where standard LLMs struggle with extensive clinical context[74]. Diagnostic support and decision assistance - correlating findings with literature to suggest or rank differentials. Global and multilingual capabilities - analyzing multilingual clinical data at a conceptual level, enabling cross-border collaboration[67].

Longitudinal and personalized care: Radiology and medicine depend heavily on longitudinal interpretation - a challenge LCMs address by maintaining conceptual coherence across extended records. They track lesion progression, edema resolution, or metastasis emergence even when terminology shifts, effectively acting as a longitudinal "concept radar"[66,74]. Integrated with electronic medical records (EMRs), genomics, and lab data, LCMs support personalized treatment, predict therapeutic responses, flag contraindications, and optimize interventions[19,131,147,148].

Advanced imaging and radiology

Radiology's multimodal complexity makes it an ideal test case for LCMs.

Applications include: Concept-aware archive: (*e.g.* Picture Archiving and Communication System) search: Moving beyond keyword-based retrieval, clinicians can perform nuanced conceptual queries such as "progressive bilateral ground-glass opacities" or "sclerotic bone lesions with periosteal reaction", enabling retrieval of clinically meaningful

studies over time[117,124]. For example, this allows radiologists to efficiently track disease progression or treatment response by retrieving and comparing conceptually relevant prior images, reducing diagnostic delays.

Automated and grounded reporting: Drafting radiology reports directly linked to visual findings and conceptual metadata, improving precision and reducing ambiguity. LCMs also assist in populating structured reporting templates (*e.g.*, Breast Imaging Reporting and Data System, Liver Imaging Reporting and Data System) based on conceptual criteria rather than manual input[139,149]. This leads to more standardized reports that enhance communication with referring physicians and streamline clinical decision-making.

Image quality optimization: Enhance imaging by noise reduction and contrast adjustment, facilitating better tissue characterization and differentiation, which is critical for accurate diagnosis and treatment monitoring[141,149]. Improved image quality can reduce repeat scans, decreasing patient exposure to radiation and lowering healthcare costs.

Workflow standardization: Guiding acquisition protocols in real time to improve efficiency, LCMs help ensure acquisition of diagnostically optimal images, accelerating throughput and reducing the need for repeat exams[150].

Research and knowledge discovery: LCMs accelerate scientific discovery and translational medicine by modeling complex relationships between biological, clinical, and imaging data: (1) Literature review acceleration: Uncovering hidden patterns, reconciling conflicting findings and surfacing new hypotheses, through conceptual linkage with medical literature[116,151]; (2) Global knowledge integration: Bridging linguistic/cultural divides in research[64]; (3) Drug development: Predicting molecule efficacy, toxicity, and interactions by integrating molecular, clinical trial, and regulatory datasets[19,152]; (4) Pharmacovigilance: Real-time monitoring of adverse events[149]; (5) Precision medicine: Identifying novel correlations between imaging phenotypes, genomic markers, and clinical outcomes[153]; and (6) Patient engagement and communication: LCMs improve health literacy and shared decision-making by translating complex concepts into accessible language.

Multilingual and concept translation - improved cross-cultural and inter-provider communication: Utilizing a language-agnostic concept (like SONAR), LCMs serve as universal medical translators and preserve the subtlety of medical nuance beyond rote translation, enabling precise cross-cultural communication and remote healthcare coordination[136]. This in turn enables more accurate communication between healthcare providers, patients, and their relatives, helping patients make informed decisions. This capability can prove to be a major game-changer in various nationwide/worldwide 'remote' activities and research coordination where multiple languages/dialects are common.

Simplify medical language: LCMs can make complex reports, trial info, and discharge summaries patient-friendly for enhanced engagement and literacy, supporting better understanding and engagement[154].

Improved patient monitoring: Integrating sensor and EMR data to issue alerts, encouraging proactive care[116,151,155]. This patient-centered approach promotes equity in care and empowers vulnerable populations.

Education and training: Concept-driven platforms support clinicians and students.

Case simulation: Engaging learners in reasoning about clinical concept interrelationships, with real-time feedback and adaptive challenges that emphasize conceptual consistency[19,65].

Immersive augmented reality/virtual reality: Providing AI tutor guidance within virtual patient scenarios, reinforcing visual and conceptual learning grounded in the reasoning behind medical facts[19,66,149,156].

Predictive analytics and system-level decisions: LCMs aid system-level foresight by modeling interdependencies across healthcare data.

Disaster preparedness and outbreak modeling: Simulating pandemics or supply chain disruptions[64,130].

Global data integration: Bridging linguistic and cultural barriers for enriched epidemiologic and policy insights.

Strategic market and operational analysis: Supporting strategic planning, mergers, and product development[68].

Real-world and emerging applications

Though nascent, early implementations highlight LCM potential across medicine and beyond. By moving beyond text-centric LLMs to include visual and conceptual data, they advance diagnosis, treatment, and multi-omics research, revealing novel biological patterns, uncovering hidden relationships *e.g.* protein folding dynamics[64,74,116,151]. Their ability to process multiple data types simultaneously and discover higher-order correlations broadens applicability into logistics, finance, manufacturing, defense, and environmental sciences. LCMs thus need not be confined to a single purpose but may be fine-tuned for diverse industries and use cases[64] Additionally, LCMs show promise in the pharmaceutical and biopharmaceutical analysis of drugs, vitamins, and minerals across biological matrices like whole blood, plasma, serum, and urine, providing nuanced insights that accelerate research pipelines. Finally, some researchers, including our lead author, anticipate that LCMs may represent a step toward artificial general intelligence (AGI) by bridging knowledge domains[67,68].

Bridging to radiology - systemic benefits of LCMs

Beyond their broad applications across healthcare, LCMs also offer systemic advantages particularly relevant to radiology. First, their conceptual reasoning strengthens predictive capabilities, enabling more accurate forecasts of disease progression and treatment outcomes[157]. Second, by lowering technical barriers, LCMs democratize AI use, making advanced tools accessible to radiologists without extensive computational expertise. Third, their integration fosters innovation and cross-disciplinary collaboration, accelerating the development of novel AI applications. Taken together, these systemic benefits provide a strong foundation for radiology-specific adoption. These theoretical advantages become most compelling when examined through real-world clinical applications. We have elaborated upon how concept-based inputs could be incorporated into radiology AI algorithms *via* case scenarios, as detailed below, in scenarios 1-3, demonstrating the practical utility of LCMs in clinical diagnostics and workflow optimization.

Scenario 1

Adding key imaging parameters to AI algorithms: Leveraging lamellar effusion in childhood pulmonary TB (CPTB) screening: Offers several critical advantages[19,51,65]: The urgent need for enhanced algorithms in CPTB screening. CPTB remains a major global health challenge, particularly in high-burden, resource-limited settings, where accurate diagnosis is hampered by clinical complexity and limited expertise[158]. Despite a significant disease burden, children often lack access to antituberculosis treatment, as most control programs still prioritize sputum smear-positive adults[159].

Effective screening is vital for early diagnosis and timely intervention, yet several barriers persist: (1) Non-specific clinical presentation: CPTB often mimics other childhood illnesses, complicating clinical differentiation[160]; (2) Microbiological diagnostic challenges: Paucibacillary disease and difficulties in obtaining samples reduce the yield of microbiological confirmation[160]; (3) Chest radiograph complexity: Chest X-ray interpretation for pediatric TB is difficult[160]. The classic Ghon complex (Ghon focus, lymphangitis, hilar lymphadenopathy) can be subtle and/or mimic normal anatomical variations or other pathologies, demanding specialized expertise[161]. Figure 6 is a radiographic demonstration of the classic findings of the Primary TB complex (Ghon complex) in a pediatric patient. The figure consists of two parts and shows the typical radiographic appearance of the Ghon complex and an annotated version of the chest X-ray clearly demarcating the peripheral Ghon focus and the enlarged, draining lymphatic vessels and hilar lymph nodes that define the complex. Figure 7A is an axial CT image of the chest in a child and demonstrates the complete primary TB complex (Ghon complex). The image clearly shows the parenchymal Ghon focus, prominent hilar lymphadenopathy, and the definitive finding of a continuous chain of connecting lymphatics (lymphangitis) between the focus and the enlarged nodes; (4) Hilar lymphadenopathy: Differentiating pathological lymphadenopathy from prominent pulmonary arteries is particularly difficult in young children[51,162]; (5) Limited radiological expertise: Many high-burden countries, face a severe shortage of pediatric chest imaging experts, resulting in delays and diagnostic bottlenecks[163-166]; (6) Recognizing potentially fatal complications: Childhood TB can also be associated with serious complications such as Hemophagocytic Lymphohistiocytosis (HLH), complicating diagnosis and management further; and (7) Potential for algorithmic assistance: Innovative AI tools offer an opportunity to augment radiological interpretation and improve accessibility[167]. Marais *et al*[160] highlighted foundational concepts in childhood pulmonary TB: (1) Accurate case definitions: Differentiating primary infection from active disease; (2) Risk stratification: Recognizing variable progression risk by age; and (3) Diverse disease pathology: Understanding wide clinical presentations requiring precise classification. Integrating these time-tested principles into modern AI design can merge expert wisdom with large datasets to improve clinical outcomes[19,51,66].

The potential impact of leveraging lamellar effusion in algorithms: Integrating lamellar effusion detection into AI-powered algorithms for pediatric chest X-ray analysis offers several critical advantages: (1) Improved accuracy: The high specificity of this sign could significantly enhance the accuracy of TB screening, reducing false positives and negatives; (2) Overcoming expertise gaps: Algorithms trained to identify lamellar effusion can function as reliable first-line screening tools in settings without pediatric radiology specialists; (3) Empowering imaging technicians: Clear guidelines on lamellar effusion visualization, supported by algorithmic assistance, can equip technicians to play a stronger role at the point of care.; (4) Enhance early case detection: By focusing on a distinctive radiological marker - lamellar effusion detection supports prompt diagnosis and treatment initiation; and (5) Feasibility and scalability: AI integration leverages existing X-ray infrastructure, enabling cost-effective expansion in underserved populations.

AI-powered lamellar effusion detection: Translating clinical insights into AI involves designing LCMs trained on expert-annotated pediatric chest X-rays to accurately detect lamellar effusions, distinguishing TB from other thoracic conditions: (1) Concept: LCMs trained on expert-annotated pediatric chest X-rays - including confirmed CPTB cases and non-TB controls - can learn subtle imaging patterns associated with lamellar effusion; and (2) Benefit: Such models would enable highly sensitive and accessible first-line screening. Early identification of lamellar effusion could trigger timely diagnostic workups, reduce missed cases, and enhance confidence in treatment decisions, particularly where microbiological confirmation is not feasible. Importantly, this targeted marker allows non-expert healthcare workers to flag high-probability cases for further expert review, strengthening TB suspicion in otherwise ambiguous presentations. Furthermore, the presence of lamellar effusion can strengthen TB suspicion in cases where treatment is based on strong clinical and other radiological findings.

Conclusion: Screening for childhood pulmonary TB is fraught with clinical and radiological challenges, compounded by limited expert availability in high-burden regions. Incorporating highly specific signs such as lamellar effusion into AI algorithms, particularly within LCM frameworks - offers a promising approach to enhance accuracy, accessibility, and scalability of CPTB screening. This integration has the potential to improve case detection, accelerate treatment, and

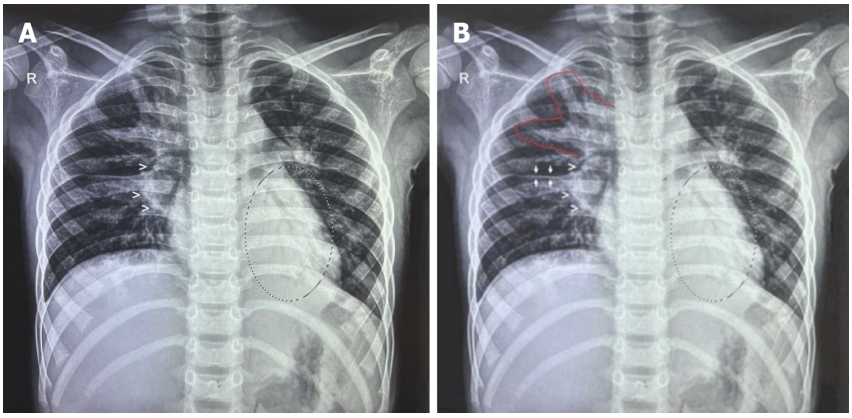


Figure 6 Tuberculosis primary complex - the classic Ghon complex. A: As seen in in a 5-year-old child: (1) Multiple: Ghon foci in the right upper lobe; (2) Draining lymphatics heading towards; (3) Right hilar lymphadenopathy (white open arrowheads); and (4) Minimal (lamellar) effusion in right horizontal fissure with minimal blunting of the right costo-phrenic angle. Additionally, a retrocardiac air bronchogram indicates tuberculosis (TB) broncho pneumonia (circled area) and hepatomegaly are noted. (Image courtesy Dr. Prakash V Vaidya, Child Health Clinic, Mumbai and Sr. Consultant Pediatrician, Fortis Hospital, Mumbai 400080); B: TB primary complex in a 5-year-old child: The classic Ghon Complex: (1) Multiple: Ghon foci in the rt. upper lobe; (2) Draining lymphatics [(1) and (2) are the areas marked with a red outline]; (3) Heading towards right. hilar lymphadenopathy (large white open arrowheads); and (4) Minimal (lamellar) effusion in right horizontal fissure (white arrows) with minimal blunting of the right costo-phrenic angle. Additionally, a retrocardiac air bronchogram indicates TB broncho pneumonia (circled area), and hepatomegaly are noted. (Image courtesy Dr. Prakash V Vaidya, Child Health Clinic, Mumbai and Sr. Consultant Pediatrician, Fortis Hospital, Mumbai 400080).

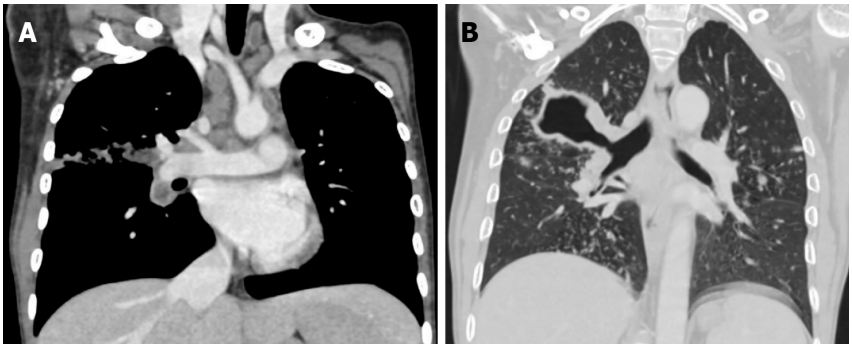


Figure 7 Computed tomography image. A: Childhood tuberculosis primary Ghons' complex computed tomography appearance: Laterally positioned Ghon foci with sub-pleural involvement, with their draining lymphatics heading all the way up to right hilar lymphadenopathy. Additionally note mediastinal lymphadenopathy (many lymph nodes reveal necrotic areas); B: Computed tomography image: Large thick-walled tuberculosis cavity communicating with the right main bronchus in a multidrug-resistant patient. (Image courtesy Dr. Anagha Joshi, Prof and HOD, Radiology, LTMMC and LTMGH, Mumbai 400022).

ultimately reduce morbidity, mortality, and transmission in vulnerable pediatric populations[19,51].

Scenario 2

The concept of screening for pulmonary cavities in TB patients: (*i.e.*, open TB) is crucial for isolating infectious individuals and preventing further spread[51]. TB remains a major global health threat[168] and pulmonary cavities remain a central feature of adult PTB. Parenchymal cavities occur in 40%-45% of post-primary PTB cases and are strongly associated with reactivation of disease[169-171]. Multiple cavities are seen more frequently in patients with MDR TB[169-172] and (> 3 cavities) were observed only in patients with MDR TB[173]. In resource-limited settings, anti-TB treatment (ATT) often starts on strong clinical and radiological suspicion despite negative microbiological tests, underscoring the critical need for accurate radiological interpretation. Studies demonstrate that thick-walled cavities (> 5 mm) are frequently seen in patients with early active TB and represent necrotizing consolidation in the early stage. The presence of lung cavities is a significant indicator of active, often infectious, disease[51,174]. Patients with cavitary TB often have higher sputum bacterial counts, delayed culture conversion, prolonged therapy, and increased relapse risk[168,175,176]. Kim *et al*[177] demonstrated that cavity wall thickness is a reliable marker of active disease, with thinner walls (mean 3.4 mm, range 1.4-10.2 mm) indicating chronic inactive disease and thicker walls (> 5 mm, mean 6.6 mm, range 1.3-14.7 mm) reflecting necrotizing, transmissible disease. Figure 7B is a CT image of a large, thick-walled TB cavity communicating with the bronchus in a multidrug-resistant (MDR) patient. Imaging also distinguishes active cavities, often with irregular thick walls or air-fluid levels, from healed, fibrotic cavities with smooth, non-enhancing walls[169,178]. Figure 8 reveals a comparison of axial CT images showing a TB cavity before and after 4 months of ATT. Patients with cavitary TB had more acid-fast bacillus culture-positive results at 2 months, longer treatment duration, treatment relapses/higher

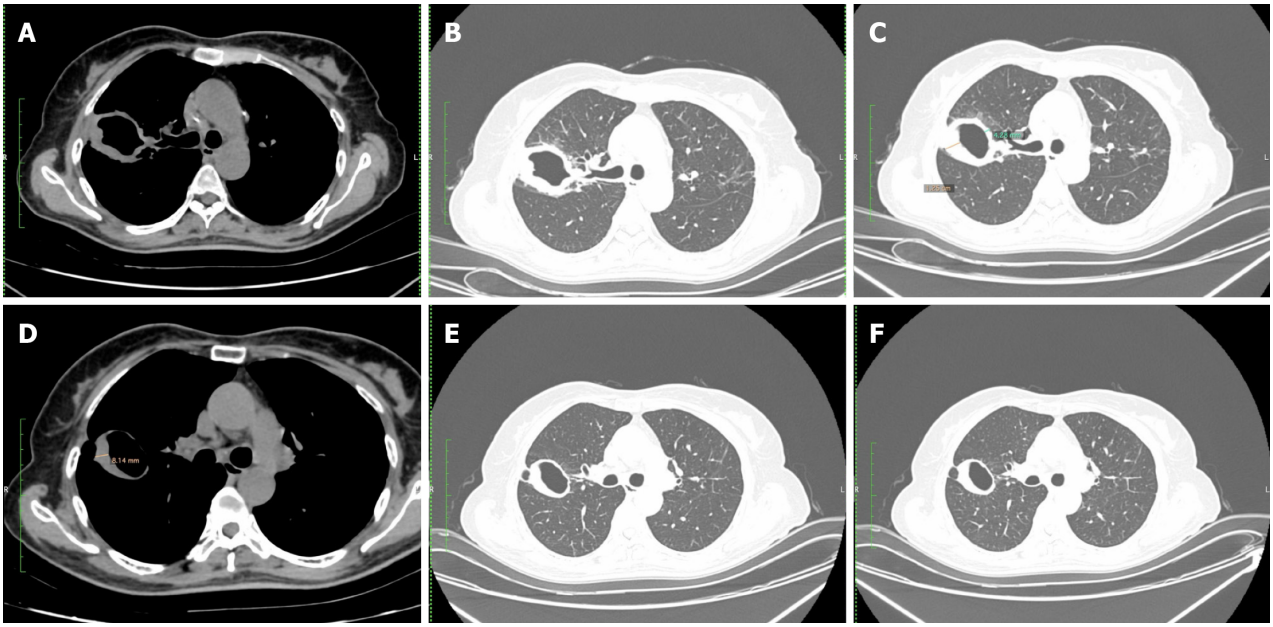


Figure 8 Axial computed tomography images in soft tissue window and lung window in a 59-year-old female, with sputum culture positive for mycobacterium tuberculosis. A-C: Demonstrates a thick-walled cavity in the right upper lobe. After 4 months of anti-tuberculosis treatment; D-F: Reduced wall thickness of the right upper lobe cavity is noted (from 12.5 mm to 8.14 mm) and the cavity appears much smoother. (Image courtesy Dr. Anagha Joshi, Prof and HOD, Radiology, LTMMC and LTMGH, Mumbai 400022).

recurrence rates than those with non-cavitary TB[168,175]. This is particularly concerning in the context of drug-resistant TB, including MDR-TB and extensively drug-resistant (XDR) TB, given that these strains are increasingly difficult and costly to treat, and are associated with poorer patient outcomes[168,176]. It is pertinent to note that most cases of MDR and XDR TB have cavities[176]. TB cavities are dynamic physical and biochemical structures that interface the host response with a unique mycobacterial niche to drive TB-associated morbidity and transmission; and advances in non-invasive imaging can provide valuable insights into the drivers of cavitation, which in turn will guide the development of tailored pharmacological interventions to prevent cavitation in individuals with TB[168]. Saeed[176] emphasized three critical aspects of cavitary TB: (1) Immune hyperactivation in response to high bacillary load causes largely irreversible lung damage. Once the bacillary growth in a cavity has increased manifold, it triggers a putative architectural distorting cascade with very little reversibility possible, including post-treatment; (2) Once mycobacterium tuberculosis achieves a load of a billion plus bacilli/gram, the population gradually slows down its activity, underpinning persistence and relapse risk, finally becoming dormant, which is the root of the cause of persistence and relapse; and (3) At this load there is a real, though small, threat of emergence of resistant mutants and a substantially bigger threat of secondary resistance in chronic cavities, the holy grail of MDR and XDR-TB development[179]. Timely identification of cavitary TB is pivotal for isolation and infection control, enabling tailored treatment and reducing transmission risk[160,168,175].

Challenges of clinical and radiological detection: Traditional methods - clinical symptoms, sputum microscopy, or bronchoscopy - are insufficient for reliably detecting cavities[180-182]. Bronchoscopy, though useful in smear-negative cases, is invasive and offers limited scope[180]. Despite their essential role in diagnosing pulmonary TB and detecting cavities. Chest X-rays present challenges in interpreting cavitary lesions. These challenges arise from subtle findings, potential obscuration by lung opacities, and the presence of multiple or small cavities[183-185]. Figure 9A is a frontal chest radiograph of a 14-year-old male presenting with cough and fever, demonstrating a thin-walled tuberculous cavity in the right upper lobe. The situation is further compounded in high-prevalence areas due to the scarcity of skilled radiologists[186,187]. This diagnostic gap underscores the need for automated, scalable solutions.

The need for AI-assisted detection: Traditional techniques to increase early detection, lower misdiagnosis, and strengthen international TB control initiatives can be supported by AI[188]. The increasing burden of drug-resistant TB underscores the urgency of rapid and accurate identification of infectious individuals[189]. Delayed detection of cavitary disease in these patients can have significant public health implications, contributing to the amplification and dissemination of drug-resistant strains[189]. Figure 9B is a frontal chest radiograph of a child with MDR TB showing a miliary pattern in the lungs and multiple air-fluid levels in the abdomen, signs of TB intestinal obstruction. Thus, there is an urgent need for automated, reliable, widely deployable tools capable of accurate pulmonary cavity detection on chest X-rays in suspected or confirmed TB patients[190]. Such tools offer: (1) Enhanced infection control: Early isolation of infectious patients to prevent spread of drug-susceptible and resistant TB strains; (2) Improved treatment strategies: Tailored therapy based on cavity presence and characteristics; (3) Enhanced workflow: Rapid assessments reduce radiologist backlog in high-volume settings; (4) Wider accessibility: Usable in resource-poor areas with limited expert radiology; and (5) Proactive MDR/XDR TB identification: Timely detection supports targeted interventions.

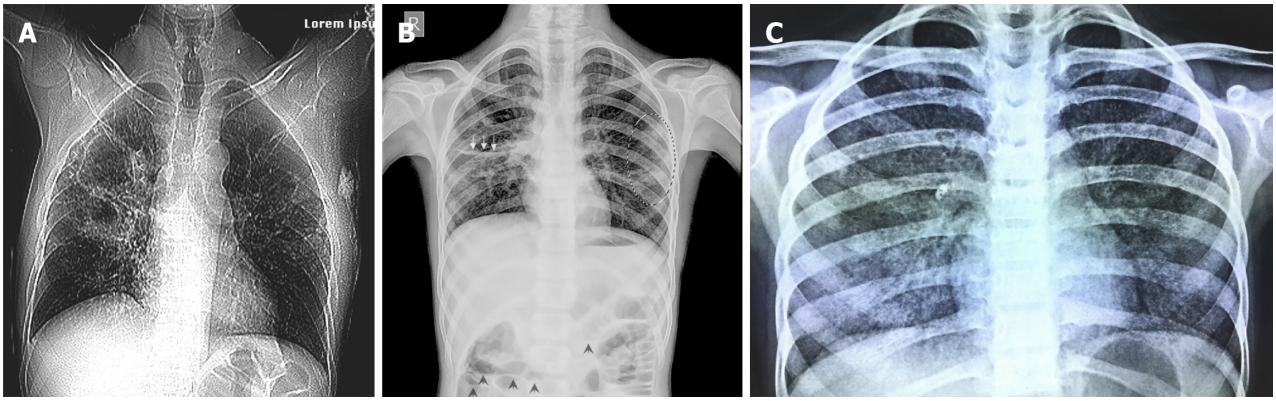


Figure 9 Frontal chest radiograph. A: Frontal chest radiograph of a 14-year-old male presenting with cough and fever. Radiography demonstrates a thin-walled tuberculous cavity in the right upper lobe (white open arrowheads); B: Frontal chest radiograph of 9-year-old male with vomiting and abdominal pain, subsequently diagnosed with MDR tuberculosis (TB). Miliary pattern seen throughout both lung fields along with multiple larger lesions indicating multiple developing cavities (circled area), minimal effusion in the right horizontal fissure (white arrows) and hepatomegaly. Multiple air-fluid levels are seen in the visualized abdomen, signifying intestinal obstruction due to TB adhesions (short black arrows). (Figure 9A and B courtesy Dr. Jairaj Nair. Prof and HOD, Chest Medicine, LTMMC and LTMGH, Mumbai 400022); C: Frontal chest radiograph of 12-year-old boy with secondary hemophagocytic lymphohistiocytosis as a result of disseminated TB. Numerous miliary nodules are noted in both lungs (extensively) with additional patchy airspace opacities noted in the medial aspect of right lower lobe (note air-bronchogram). Calcified right hilar lymph nodes are also noted. He recovered well post treatment for same (including anti-TB treatment). (Image courtesy Dr. Prakash V Vaidya, Child Health Clinic, Mumbai and Sr. Consultant Pediatrician, Fortis Hospital, Mumbai 400080).

AI-powered thick-walled cavity identification: Concept: Train LCMs on a vast and diverse global dataset of adult chest X-rays. This dataset will include: (1) Images of patients with microbiologically confirmed pulmonary TB, with detailed annotations of lung cavities, specifically focusing on those characterized by thick walls. Annotations should include location, size, shape, wall thickness, and presence/absence of air-fluid levels. This should also include chest X-rays of patients who started treatment based on clinic-radiological findings (even if initially smear-negative) and documentation of any cavities present; (2) Images of patients with other lung diseases that can present with cystic or cavitary lesions (*e.g.*, lung abscess, fungal infections, malignancy, pneumatoceles), with detailed annotations of these lesions to enable the LCM to differentiate them from TB cavities; and (3) Images of healthy adult lungs and those with other non-cavitary lung findings to establish a baseline and identify potential false positives.

Learning focus: The LCM will be trained to learn the specific visual characteristics of thick-walled lung cavities associated with active TB, across various imaging modalities, patient demographics, and disease stages. It will also learn to differentiate these from other lung lesions based on subtle visual cues and contextual information within the chest X-ray.

Benefit: This initiative aims to develop a universally applicable AI tool capable of automatically detecting and localizing thick-walled lung cavities on standard adult chest X-rays, with high sensitivity and specificity. Such a tool would be a crucial screening mechanism for identifying potentially infectious TB patients, including those with MDR/XDR TB, who may require isolation. Early identification of cavitary lesions can facilitate the timely implementation of appropriate infection control measures, optimize treatment strategies, and help restrict disease spread, especially for drug-resistant forms. This automated screening is particularly valuable in high-burden settings and for rapid initial assessment[19,51].

Scenario 3

Leveraging known (and rare) TB associations to improve outcomes.

HLH: HLH is a severe and often fatal hematological disorder, increasingly recognized in TB, particularly during paradoxical worsening on ATT[191,192]. Active TB accounts for 9%-25% of infection-associated HLH cases across all ages (14 days-83 years; median 40 years). HLH is driven by immune dysregulation with excessive macrophage and lymphocyte activation, systemic inflammation, and tissue destruction, often progressing to organ failure and death. Clinical features include fever, organomegaly, cytopenias, hyperferritinemia, hypertriglyceridemia, hypofibrinogenemia, hemophagocytosis, low NK-cell activity, and elevated soluble interleukin-2 receptor[192]. Ferritin > 10000 μg/L is highly specific for HLH in children[193]. HLH can be familial (infancy/early childhood) or sporadic (all ages), with infections as common triggers. TB-HLH is diagnostically challenging due to overlap with disseminated TB. Awareness is critical: Combined anti-TB and immunomodulatory therapy improves survival to 66%, compared with 56% for anti-TB drugs alone and 0% with immunomodulators alone[192]. Timely recognition of hyperferritinemia and cytopenias can guide diagnosis and save lives[191].

Why TB - HLH matters for AI integration: Untreated TB-HLH carries 100% mortality, underscoring the urgency of early detection. Key clinical dynamics: (1) TB as a trigger for HLH: Disseminated TB, especially miliary forms, can provoke secondary HLH, causing cytokine storm and hemophagocytosis. Active TB is implicated in a significant proportion (9%-25%) of infection-associated HLH cases[192]. Figure 9C is a frontal chest radiograph showing numerous miliary nodules

and patchy opacities in a boy with disseminated TB leading to HLH; (2) HLH exacerbating TB: HLH can mimic or exacerbate paradoxical worsening during ATT, making it challenging to distinguish between an expected inflammatory response to effective TB treatment and the life-threatening condition of HLH. The uncontrolled inflammation in HLH can cause severe systemic inflammation, multi-organ failure and death, independent of the TB infection itself; (3) Diagnostic overlap: Fever, cytopenias, and organomegaly mimic disseminated TB. Immune dysregulation can render tests (tuberculin skin test, interferon gamma release assay) unreliable; and (4) The "*vice versa*": While less direct, HLH predisposes to TB, masks TB signs with systemic inflammation, and complicates treatment due to immunosuppression, potentially increasing the risk of TB reactivation, or make it harder to control the TB infection. Careful consideration and often a combination of anti-TB and immunomodulatory therapies are required, without which the survival rate drops to an abysmal zero.

The critical importance of timely treatment - (100% mortality without it): Without prompt dual therapy (anti-TB drugs and immunomodulatory agents), TB-HLH is almost universally fatal. (1) Untreated HLH: Cytokine storm drives rapid multi-organ failure; (2) TB as the underlying driver: If the underlying TB infection driving the HLH is not addressed with effective anti-TB drugs, the inflammatory trigger persists, further fueling the HLH; and (3) Synergistic lethality: The combination of active, potentially disseminated TB with the systemic devastation of HLH creates a highly lethal scenario.

Enhancing recognition of TB-associated HLH using LCMs: Concept: Trained on multimodal datasets LCMs could transform detection of TB-HLH. Datasets should include: (1) Clinical data: Longitudinal TB records, paradoxical worsening, HLH features (fever, organomegaly, cytopenias), serial ferritin and inflammatory markers, comorbidities, and treatment regimens. In addition, guidelines suggest empirical treatment of TB when clinic-radiological suspicion is high, despite negative microbiological tests[193], a commonly practiced approach in developing countries, should be included in the dataset; (2) Imaging data: Chest X-rays/CTs, particularly miliary TB, annotated for disease evolution and paradoxical reactions. Annotations should focus on the evolution of TB-related findings alongside any imaging features potentially suggestive of HLH (though these may be non-specific); (3) Hematological data: Bone marrow findings, hemophagocytosis, differential counts; (4) Genetic data (where available): Predispositions to familial HLH in pediatric cases; and (5) Literature and expert knowledge: Incorporate relevant medical literature, guidelines and annotated diagnostic/management patterns. This will help the LCM understand the complex interplay between the two conditions.

Learning objectives: (1) Detect patterns linking TB treatment, paradoxical worsening, and HLH, while distinguishing these from drug-resistant TB; (2) Recognize HLH-specific cues (persistent fever, organomegaly, cytopenias, hyperferritinemia, hypofibrinogenemia and specific laboratory findings such as markedly elevated ferritin, hypertriglyceridemia, hypofibrinogenemia, hemophagocytosis, low natural killer-cell activity, and high levels of soluble interleukin-2 receptor; (3) Stratify HLH risk in TB patients, especially during paradoxical worsening, by integrating information across clinical, imaging, and hematological data and imaging, while considering the temporal dynamics that help differentiate it from drug resistance; (4) Differentiate HLH from drug resistance, emphasizing the role of drug susceptibility testing; (5) Correlate dual-treatment regimens with outcomes in TB-HLH cases, and contrast these with outcomes in drug-resistant TB; and (6) Understand paradoxical worsening as often self-limiting (with continued ATT) *vs* HLH, which requires urgent intervention.

Benefits: (1) Raise clinician awareness by flagging HLH patterns in TB patients; (2) Enable earlier HLH diagnosis and treatment initiation, while guiding drug resistance investigations; (3) Improve survival by reducing delays in dual therapy; (4) Support monitoring of paradoxical reactions and highlight when to suspect resistance; and (5) Advance medical knowledge and potential for personalized medicine by identifying novel TB-HLH associations. By embedding HLH recognition into AI-driven systems, LCMs can enable earlier, more accurate detection of this devastating TB complication, transforming outcomes where delayed diagnosis currently means near-certain mortality.

Additional novel integrations

TB and diabetes mellitus: The bidirectional relationship between TB and diabetes mellitus is well established[194,195]. Diabetes increases susceptibility to active TB and worsens treatment outcomes due to immune suppression, while TB impairs glycemic control. World Health Organization (WHO) recommends screening TB patients for diabetes mellitus and vice versa, making this a natural fit for algorithmic integration to enable earlier detection and management[195].

TB and papillary thyroid carcinoma: Though far rarer, a possible association has been proposed[196]. While causality and mechanisms remain unproven, LCMs could flag subsets of TB patients for thyroid evaluation where clinically indicated, promoting hypothesis generation and vigilance in complex presentations. Incorporating these and similar comorbidities would enable LCMs to support more holistic TB care, addressing both common complications such as diabetes and rarer, exploratory links like TB-papillary thyroid carcinoma.

Final thought

Whereas LLMs excel at pattern recognition, detecting imaging features such as opacities, nodules, and cavities[197,198], LCMs advance toward conceptual reasoning, modeling causal and mechanistic relationships. By synergizing with existing AI methods rather than replacing them, LCMs could transform TB imaging and management: Moving from recognition of patterns to understanding of disease mechanisms, and ultimately to more timely, personalized, and life-saving interventions. An LCM would not replace these methods, but rather work synergistically to add deeper layers of conceptual understanding and reasoning.

Federated learning

Enabling collaborative AI while preserving privacy. Despite its potential, LCMs face persistent privacy, security, and regulatory challenges, especially with sensitive medical data, including imaging. Federated learning (FL) addresses these challenges by training models across decentralized institutions or devices holding local datasets, without centralizing patient data[199]. Instead, only encrypted model updates are exchanged, with a central server maintaining the global model and local models retained at each site. Contributions are quality-checked before aggregation to prevent malicious or biased updates. Unlike centralized learning, FL iteratively refines the global model *via* secure exchanges to deliver solutions suited for clinical environments[19,51,200-202]. Beyond privacy, FL offers systemic benefits: It trains on diverse, heterogeneous datasets, reduces algorithmic bias, enhances generalizability, and accelerates clinical adoption. For example, FL has been successfully applied to train diagnostic models for TB chest X-rays across multiple centers, including resource-limited settings, achieving high accuracy while safeguarding patient privacy[203].

Potential applications in healthcare[19,136]: (1) Privacy-preserving medical image analysis (*e.g.*, FL-based TB chest X-ray models outperforming local models in heterogeneous African datasets); (2) Development of personalized treatment models by leveraging distributed clinical data; (3) Decentralized outbreak prediction using federated disease surveillance; (4) Collaborative drug discovery and real-world evidence generation while maintaining data sovereignty; and (5) Equipment manufacturers can address the digital imaging and communications in medicine issues faced by radiologists with modern ultrasound machines.

Integrating FL with LCMs can unite multimodal data streams: Text, imaging, genomics, and sensors - across institutions, producing more robust, globally relevant models without recurring data transfer and regulatory hurdles. Together, LCMs and FL form complementary pillars of next-generation radiology AI, enabling unbiased, scalable, and ethically sound solutions for TB, oncology, rare diseases, and beyond.

The hype cycle and challenges of LCMs in radiology AI

As with many emerging technologies, LCMs in radiology AI are also likely to face the classic "hype cycle" characterized by initial enthusiasm followed by a phase of realistic assessment of the significant challenges ahead[51,66,67]. While LCMs offer great promise to go beyond token-based models by enabling conceptual reasoning, multimodal integration, and long-range context synthesis, they remain early-stage technologies confronting formidable hurdles. A major barrier is the immense difficulty of creating large-scale, expertly annotated datasets for concepts, which is substantially more complex than annotating tokens. This requires capturing rich clinical knowledge, context, and multimodal correspondences at scale, a task necessitating intensive radiologist expertise and standardized annotation protocols[19,66]. This challenge was one of the core motivations behind our original concept-based framework[19,51]. While large-scale collaborations are mandated to ensure quality LCM development, earlier implementation challenges might be mitigated by the growing adoption of FL, which facilitates multi-institutional collaboration while preserving patient privacy and data security[19,51,199]. This collaborative approach holds promise in overcoming barriers related to data heterogeneity, regulatory compliance, and annotation costs. The innovative architectures underpinning LCMs, such as hierarchical and dual-tower models, introduce significant computational demands and require advanced infrastructure[67,73]. However, despite their computational intensity, these models are expected to be relatively more environmentally sustainable ("green") compared to traditional LLMs, due to optimization techniques like embedding quantization and efficient diffusion mechanisms; offering potential energy savings without compromising performance[67,66]. This environmental consideration is critical for scaling LCMs in resource-constrained clinical settings. The path to clinical adoption hinges on a rigorous, multi-stage validation process involving prospective trials that assess diagnostic accuracy, safety, and generalizability across diverse patient populations. Encouragingly, LCMs' enhanced transparency, explainability, and ethical alignment may expedite regulatory approvals, including from the FDA, overcoming challenges faced by earlier opaque AI models[19,51,66,67]. It is notable that although over 1000 AI-enabled medical devices have received FDA clearance, none to date involve LLM-based methodologies, underscoring the hurdles faced by black-box, token-based AI systems in clinical validation[97]. LCMs represent a meaningful advance toward AI systems that emulate human clinical reasoning and deliver actionable insights in radiology. A nuanced understanding of the hype cycle and attendant challenges promotes a balanced perspective, tempering undue optimism with cautious realism. The successful translation of LCMs from concept to clinical reality will require sustained interdisciplinary collaboration, adherence to robust standards for data and evaluation, ethical governance, and ongoing technical innovation.

Future directions and regulatory landscape

The future of LCMs in healthcare is vibrant and multi-faceted. Essential priorities include: (1) Developing hybrid LCM architectures combining symbolic and DL for optimal reasoning, interpretability, and clinical relevance; (2) Optimizing architectures to process the unique characteristics of medical data, such as high dimensionality and class imbalance; (3) Pioneering multimodal fusion techniques to align imaging, structured EHR, text, genomics, and sensor data for a holistic picture of patient health; (4) Integrating genomic data with imaging and clinical notes to enable personalized diagnostic and treatment strategies; (5) Advancing explainable AI methods, with clinician-in-the-loop development to provide actionable rationale and transparency; (6) Leveraging clinician expertise during model development to improve trust, transparency, and intuitive explanations; (7) Conducting large-scale, prospective, multi-center validation studies measuring clinical impact, workflow integration, cost-effectiveness, and outcomes compared to standard practice; and (8) Proactively addressing data privacy, robustness, regulatory compliance, and socio-technical challenges, including lifelong learning and real-time updates.

Regulatory considerations: Healthcare demands exceptionally high levels of accuracy and safety. Rigorous clinical validation is essential before deployment, particularly in radiology, where subtle visual details are crucial. Linking abstract concepts to specific anatomical and imaging findings remains non-trivial. Key considerations include: (1) Data privacy and safety: Compliance with Health Insurance Portability and Accountability Act (United States)[204] General Data Protection Regulation (Europe)[205], Digital Personal Data Protection Act, 2023 (India)[206]. FL can address these concerns while enabling collaborative research; (2) Data quality and bias: FDA[207,208], European Medicines Agency [209], Central Drugs Standard Control Organization of India[210] require careful curation of diverse datasets, bias detection, and mitigation strategies. Collaboration with clinicians from varied backgrounds is essential; (3) Transparency, explainability, ethical considerations and interoperability and standards (Health Level Seven International-The Standard, 2024) are also critical considerations that will effectively require regulatory approval[211]. Tools must provide interpretable outputs for clinical use; and (4) WHO guidance: WHO provides guidance on governance, ethics, and regulation to ensure AI use in healthcare is safe, effective, and trustworthy[212]. Chauhan *et al*[213] reviewed regulatory strategies across European Union, FDA, and Central Drugs Standard Control Organization of India, emphasizing adaptive approaches, pre-certification programs, and compliance advice. FDA guidance for AI-enabled medical devices highlights best practices in ML development, version control, patient safety, and lifecycle management data[209]. The European Commission's broader AI regulations address societal implications, requiring careful ethical oversight[214]. The ethical implications of using LCMs for diagnosis and treatment decisions, including issues of accountability and patient autonomy, will require careful consideration and the development of ethical guidelines specific to this technology in healthcare.

Current status of AI approvals: As of early 2025, the FDA has cleared over 1000 AI models for clinical use, mainly in radiology and cardiology[97]. These models assist in image analysis, diagnostic support, and treatment planning. However, no LLMs have yet received FDA approval. Contributing factors include their black-box nature, regulatory frameworks not designed for generative models, and challenges in clinical validation. Despite these hurdles, LCMs are expected to achieve faster regulatory approval when developed. Their structured conceptual reasoning, transparency, ethical design, and alignment with clinical workflows can directly address the concerns limiting LLM approval. Interpretable outputs and validated reasoning pathways make LCMs more amenable to regulatory scrutiny, potentially accelerating their safe adoption in healthcare.

Summary

The evolution of AI, from its early symbolic roots championed by McCarthy *et al*[10] to the current era of LLMs and the emerging LCMs, represents a transformative leap in technological capability[58,102,215-217]. As William Gibson observed, "The future is already here - it's just not evenly distributed" a sentiment particularly resonant with the nascent yet immensely promising stage of LCM development[67,68]. LCMs offer a path forward beyond the hallucinations and ambiguities of current AI models, providing robustness, deeper understanding, and trustworthiness, qualities critical in complex fields such as medicine[216,217]; and thus represent a significant addition to our AI armamentarium.

Clinical integration and medical relevance: LCMs facilitate the integration of diverse data sources - including imaging, clinical parameters, and patient history, while incorporating expert knowledge and explainable AI techniques. This synergy of "wisdom combined with knowledge" directly addresses limitations in current medical AI, particularly in radiology, where decisions demand a holistic understanding of the patient's clinical context. Historically, the breadth and complexity of clinical knowledge posed encoding challenges[19]. LCMs overcome these hurdles by representing nuanced clinical concepts, combining accumulated knowledge and meta-knowledge (problem-solving strategies) with AI's computational versatility. This enables a shift from reactive diagnostics to predictive, personalized patient management. Explainable AI also mitigates the "black box" problem[28], fostering trust among clinicians and ensuring the responsible and ethical deployment of AI[88]. This aligns with the growing recognition of the need for multi-modal AI in healthcare, where seamless integration and reasoning across diverse data sources are paramount. Active involvement of radiologists and other clinicians ensures clinical relevance, supporting adoption and maximizing the utility of LCMs in practice.

From intelligence to general intelligence: LCMs unlock a new realm of possibility, where the canvas of imagination becomes the blueprint for AI reality. They are capable of learning from experience and adapting to novel scenarios without explicit programming and bring us closer to AGI; incorporating reasoning, problem-solving, and creativity[65,66]. This progression toward AGI in healthcare emphasizes augmenting, not replacing, human expertise. Multi-modal reasoning, cross-domain knowledge integration, and coherence across extended contexts make LCMs revolutionary for radiology and allied fields, providing a roadmap toward cognitive AI, AGI, and beyond[65,66]. The emphasis remains on leveraging AI to empower human clinicians, leading to more informed decisions and ultimately superior patient care. Rigorous validation remains crucial. LCMs are still research concepts, and their real-world performance, scalability, and reliability in high-stakes domains must be empirically proven[72,147]. Investment in proof-of-concept studies and robust validation will solidify their clinical role.

Synergistic horizons - quantum computing

Quantum computing (QC) promises unprecedented computational power, accelerating the capabilities of AI in healthcare [19,51]. Advances such as 256-qubit superconducting quantum computers and topological qubits in 2D materials[218-220] provide stable, robust quantum states essential for practical AI applications. These advancements are crucial for addressing the current limitations of QC and paving the way for practical applications in healthcare[156,221]. QC is poised to revolutionize healthcare, including radiology and its allied fields with its ability to process complex biological

data, simulate molecular interactions, and optimize drug discovery, at scales previously unimaginable, presenting unprecedented opportunities for personalized medicine and disease modeling[221].

LCM-quantum synergy: The combination of LCMs with quantum computational power could enable: (1) Enable complex simulations of molecular interactions and disease processes, advancing drug discovery and personalized medicine; (2) Accelerate data analysis across genomics, medical imaging, and patient records, improving diagnostic speed and accuracy; and (3) Reveal novel insights in medical data, identifying biomarkers, therapeutic targets, and disease mechanisms, advancing toward artificial super intelligence[65,66,221].

Beyond quantum - towards artificial super intelligence and the infraspace

Future horizons include quantum-enhanced artificial super intelligence, potentially surpassing human cognition and operating near physical limits[222-225]. The profound implication is that "with quantum-enhanced AI, recursive self-improvement, a scenario where an AI system refines its own algorithms in a continuous loop, could occur at a pace and scale unimaginable with classical hardware". This leap in computational power might allow AI systems to achieve levels of understanding and creativity surpassing human capabilities, while raising critical questions about control, ethics, and the very definition of intelligence[224-227]. The development of such advanced AI must be accompanied by robust ethical guidelines and control mechanisms to ensure beneficial outcomes.

Speculative manifestations include: (1) Quantum sovereign intelligence: Autonomous quantum entities capable of mastery at the quantum scale; (2) The omega sentience: Conceptual unified consciousness addressing fundamental scientific and philosophical questions; and (3) Post-quantum frontier (infraspace): Intelligence operating below the quantum level, manipulating the informational substrate of reality[228]. Additionally, bio-inspired computation, such as quantum super-radiance in human cells[229,230] may guide future AI paradigms, merging biological and quantum processing for unprecedented efficiency. Imagine an AI that mimics the quantum super-radiance of biological cells to achieve unprecedented processing power. Such bio-quantum AI could revolutionize not only healthcare but also our understanding of consciousness and biological intelligence itself.

CONCLUSION

The future of AI in radiology and healthcare stands at the exhilarating crossroads of QC, biological inspiration, and ever-advancing conceptual intelligence. As researchers probe the mysteries of the quantum realm and the untapped computational capacity of living cells, possibilities for medical imaging, both diagnostic and interventional, are rapidly expanding. Upcoming breakthroughs could make "even Sherlock Holmes's legendary deductive powers seem quaint", not because they are diminished, but because the tools at our disposal will be far more powerful, holistic, and accessible. Imagine an AI system that continuously ingests cross-continental radiology studies, EMRs, multiomics, and real-time biosensor data, alongside global epidemic alerts, then notifies city imaging departments, hospitals, rural health centers, and other stakeholders about emerging complications, outbreaks, or subclinical trends before clinical suspicion arises - what was once fiction now stands on the precipice of feasibility. The climb from the symbolic "logic" of early AI, through ML, to LCMs' growing "intuition", is akin to a symphony expanding from a solo performance to a collaborative orchestra: Accessible, rich, and multidimensional. Truly, the "song" of modern AI is composed by entire ensembles, each player contributing wisdom from their own tradition. The time for bold, responsible innovation is now. For radiologists, LCMs and quantum-powered AI promise breathtaking acceleration in clinical, research, and workflow advances previously inconceivable. No longer do AI's strengths lie solely in linear logic or brute-force computation; LCMs herald a leap into imaginative, multi-modal reasoning - integrating imaging, text, sensor streams, and molecular profiles for a richer diagnostic canvas. As Dickstein[230] has been attributed to have observed, "Prediction is very difficult, especially about the future", yet the momentum in this space suggests we are barreling toward previously unimaginable advances. As Albert Einstein wisely stated, "Imagination is more important than knowledge". This burgeoning field invites us to move beyond the known limitations of traditional AI and conceptualize applications previously confined to science fiction.

Democratization of radiology and healthcare: Radiology will not only benefit from AI democratization but also serve as a central force driving it. Future-facing systems could allow a radiologist in Mumbai, an imaging technician in rural Africa, a trauma specialist in New York, a primary care doctor in rural Brazil, and even an astronaut on a Mars mission to collaborate through an LCM-powered imaging assistant or "holographic doctor"[231] - a virtual colleague capable of synthesizing literature, images, patient histories, biosensor feeds, research insights, and expert wisdom, translating findings into any language or context. Imagine a patient's smartwatch detecting subtle heart irregularities, cross-referencing their medical history, and triggering proactive, understandable alerts, empowering personalized, preventative care at scale and extending AI's benefits to a broader range of users without requiring deep technical expertise. This democratization is crucial for fostering widespread innovation and ensuring LCM benefits are broadly accessible. LCMs encourage us to "think left and think right and think low and think high"[232]. While cautious optimism and responsible development are vital, the foundation of LCMs lies in human creativity to envision and implement complex, transformative concepts. "Creativity is intelligence having fun" (Albert Einstein). Concept-based, multi-modal AI is here; humans need not learn coding, as machines handle that. Let human intelligence have fun. This vision holds immense potential for empowering individuals and driving innovation across all sectors.

Accelerated validation and responsible deployment: Historically, the validation of groundbreaking scientific technologies has often taken decades or even centuries, as exemplified by foundational theories in physics. For instance, Newton's laws of motion were formulated in the late 1600s, but their full implications took years to unfold; Maxwell's

equations in the 1860s unified electricity and magnetism long before they found widespread experimental confirmation. Most notably, Einstein's field equations proposed in 1915 laid the foundation for general relativity, but precise experimental validations, including gravitational waves, occurred many decades later[233,234]. These examples illustrate how the realm of theoretical physics is widely respected for its foundational concepts, often preceding empirical proof by significant time spans. Similarly, concept-based AI models like LCMs represent an analogous leap in theoretical computer science. With accelerated computational innovations and with pioneering independent validation by leaders such as Meta AI, whose recent publications mirror our core propositions and terminology concerning LCMs[67]. LCMs are poised to rapidly transition from theory to practice. This means we can have clinically relevant, multi-institutionally validated tools reaching our domains within a much shorter cycle. While radiologists have traditionally been swift adopters of new imaging hardware (ultrasound, CT, MRI), they have shown more caution in embracing advanced AI software, seeking clinically validated and transparent tools that support rather than replace their expertise[235,236]. The field continues to rigorously evaluate ML and DL models, often focusing narrowly on these paradigms. Yet, more advanced AI paradigms like LLMs and especially LCMs offer substantially greater potential, enabling deeper semantic understanding, holistic data integration, and improved clinical decision-making. It is therefore imperative to overcome this inertia and adopt these transformative AI frameworks to catalyze the next massive leap in clinical radiology and patient care. The journey from theory to clinical impact will require the collaboration of experts from AI, linguistics, cognitive science, clinicians, and patients, as well as those from specific application domains like radiology and other allied healthcare fields[67,68]. This must be accompanied by the establishment of clear ethical guidelines for their deployment in critical applications [221]. The shift from token-based, single-task models to concept-based, multi-modal systems is the next major frontier in medical AI. It promises to transform the role of the radiologist from an image interpreter to a holistic patient diagnostician, working in a powerful human-AI partnership. Key hurdles remain: Ensuring robustness against bias, developing ethical norms, and sustaining transparent, explainable decision-making to maintain professional and patient trust. Progress in FL, radiologist-in-the-loop annotation, and alignment with regulatory expectations for clinical-grade AI will help mitigate development costs and accelerate reliable deployment. Robustness against imaging bias, clinically actionable explainability, and collaboration amongst radiologists, data scientists, and end-users are essential for safe translation into clinical workflows. Radiologist input remains crucial for curating datasets, evaluating model relevance, and assessing the utility of concept-based reasoning in nuanced imaging scenarios such as rare disease detection, or subtle lesion follow-up. As Thomas Edison aptly said, "The value of an idea lies in the using of it", the challenge is now to translate LCM theory into safe, real-world systems that deliver on the promise of improved patient care.

Overcoming challenges for a holistic future: A holistic approach - combining diverse data, expert knowledge, and explainable AI, promises more accurate diagnoses, personalized treatments, and effective disease management. LCMs offer richer differential diagnoses, deeper pattern recognition across imaging and non-imaging data, and patient-specific longitudinal analysis spanning years of prior images and contextual reports. While current AI faces difficulties in complex reasoning, context-aware decision-making, and cross-modality integration, LCMs synthesize CT, MR, ultrasound, and molecular data, drawing not just from pixels but from clinical and biological context, raising both, expectations and standards for radiology AI performance. Given the critical need for trust and transparency, enhancing explainability remains paramount for clinician adoption and regulatory compliance[136]. Demonstrating AI functionality clearly to professionals unfamiliar with the technology is crucial, and annotation costs can be mitigated with semi-supervised and active learning techniques. It's also important to acknowledge that the annotation and labeling required for training, especially when demanding human expertise, can be costly[136]. However, advances in semi-supervised learning and active learning techniques may help mitigate these costs and accelerate the development of robust LCMs. Radiology stands to benefit from FL, human-in-the-loop expert feedback, and interpretability methods highlighting why findings were flagged. These advancements are essential for building trust, calibrating clinical utility, and streamlining deployment in reading rooms. Emerging paradigms such as QC and advanced interpretability will further bridge the gap toward precision outcome modeling, including radiotherapy[136]. Imagine LCMs, powered by quantum breakthroughs, instantly analyzing a patient's complete imaging archive, genomics, and real-time biosensor data to forecast pathology evolution, recommend tailored scan protocols, link imaging findings to prospective outcomes, or even optimize individualized treatment for complex conditions. AI systems could proactively suggest lifestyle interventions, optimize surgical plans with millimeter precision, or design novel drug molecules tailored to an individual's biology. By embracing a creative, collaborative spirit and centering radiologist leadership in development and validation, LCMs can accelerate the arrival of patient-centered, precision imaging, tackling global challenges in cancer screening, infectious disease monitoring, and chronic illness management, while broadening access to world-class imaging expertise. As we walk this path, let Einstein's insight guide us: "Logic will get you from A to B. Imagination will take you everywhere". By fostering collaboration, addressing ethical considerations proactively, and investing in rigorous research, we can usher in a new era of intelligent systems that truly augment human capabilities. For radiology, this evolution means smarter, more insightful, and ultimately more human-centered patient care. The journey from early AI to LCMs and beyond is a testament to human ingenuity. This ongoing evolution, driven by both scientific curiosity and practical necessity, ensures AI will continue to play an increasingly vital role in shaping the future of medicine and human well-being. LCMs represent not merely a technological transition but a profound exercise in humanity's drive to heal, empower, and imagine a healthier tomorrow. With foresight, rigor, and open-mindedness, the "possible" in healthcare stands ready to be redefined. As Clarke[237] famously posited: "Any sufficiently advanced technology is indistinguishable from magic". With large conceptual models, radiologists and allied professionals are not merely building tools, they are crafting the next generation of "magic" for radiology and healthcare, transforming the seemingly impossible into clinical reality and elevating the impact of radiology at the heart of precision healthcare.

ACKNOWLEDGEMENTS

The authors wish to acknowledge Dr. Mohammed Mulla Jafarali Mamjiwala for his dedicated interest in the topic, passion for academic pursuits, and his help with the bibliography section. The author sincerely hopes this encouragement and exposure inspires Dr. Mohammed Mulla Jafarali Mamjiwala toward future academic endeavors.

FOOTNOTES

Author contributions: Merchant SA was responsible for the conceptualization of the critical perspective, defining the scope and structure, conducting the primary literature searches and synthesis, and drafting the initial and final versions of the manuscript; Merchant N, Varghese SL, and Shaikh MJS performed supplementary literature searches, provided critical intellectual content throughout the analysis, and critically reviewed and revised the manuscript for scientific accuracy; and all authors have read and approved the final manuscript.

Conflict-of-interest statement: All the authors report no relevant conflicts of interest for this article.

Open Access: This article is an open-access article that was selected by an in-house editor and fully peer-reviewed by external reviewers. It is distributed in accordance with the Creative Commons Attribution NonCommercial (CC BY-NC 4.0) license, which permits others to distribute, remix, adapt, build upon this work non-commercially, and license their derivative works on different terms, provided the original work is properly cited and the use is non-commercial. See: https://creativecommons.org/Licenses/by-nc/4.0/

Country of origin: India

ORCID number: Suleman A Merchant 0000-0001-6513-450X; Neesha Merchant 0009-0008-1505-9095; Shaju L Varghese 0009-0004-2902-1419; Mohd Javed S Shaikh 0000-0002-5615-4813.

S-Editor: Bai Y
L-Editor: A
P-Editor: Lei YY

REFERENCES

1 **Topol EJ**. High-performance medicine: the convergence of human and artificial intelligence. *Nat Med* 2019; **25**: 44-56 [*RCA*] [PMID: 30617339 DOI: 10.1038/s41591-018-0300-7] [FullText]
2 **Akinci D'Antonoli T**, Stanzione A, Bluethgen C, Vernuccio F, Ugga L, Klontzas ME, Cuocolo R, Cannella R, Koçak B. Large language models in radiology: fundamentals, applications, ethical considerations, risks, and future directions. *Diagn Interv Radiol* 2024; **30**: 80-90 [*RCA*] [PMID: 37789676 DOI: 10.4274/dir.2023.232417] [FullText] [Full Text(PDF)]
3 **Bhayana R**, Bleakney RR, Krishna S. GPT-4 in Radiology: Improvements in Advanced Reasoning. *Radiology* 2023; **307**: e230987 [*RCA*] [PMID: 37191491 DOI: 10.1148/radiol.230987] [FullText]
4 **Gertz RJ**, Bunck AC, Lennartz S, Dratsch T, Iuga AI, Maintz D, Kottlors J. GPT-4 for Automated Determination of Radiological Study and Protocol based on Radiology Request Forms: A Feasibility Study. *Radiology* 2023; **307**: e230877 [*RCA*] [PMID: 37310247 DOI: 10.1148/radiol.230877] [FullText]
5 **Sun Z**, Ong H, Kennedy P, Tang L, Chen S, Elias J, Lucas E, Shih G, Peng Y. Evaluating GPT4 on Impressions Generation in Radiology Reports. *Radiology* 2023; **307**: e231259 [*RCA*] [PMID: 37367439 DOI: 10.1148/radiol.231259] [FullText]
6 **Bajaj S**, Gandhi D, Nayar D. Potential Applications and Impact of ChatGPT in Radiology. *Acad Radiol* 2024; **31**: 1256-1261 [*RCA*] [PMID: 37802673 DOI: 10.1016/j.acra.2023.08.039] [FullText]
7 **Adams LC**, Truhn D, Busch F, Kader A, Niehues SM, Makowski MR, Bressem KK. Leveraging GPT-4 for Post Hoc Transformation of Free-text Radiology Reports into Structured Reporting: A Multilingual Feasibility Study. *Radiology* 2023; **307**: e230725 [*RCA*] [PMID: 37014240 DOI: 10.1148/radiol.230725] [FullText]
8 **McDuff D**, Schaekermann M, Tu T, Palepu A, Wang A, Garrison J, Singhal K, Sharma Y, Azizi S, Kulkarni K, Hou L, Cheng Y, Liu Y, Mahdavi SS, Prakash S, Pathak A, Semturs C, Patel S, Webster DR, Dominowska E, Gottweis J, Barral J, Chou K, Corrado GS, Matias Y, Sunshine J, Karthikesalingam A, Natarajan V. Towards accurate differential diagnosis with large language models. *Nature* 2025; **642**: 451-457 [*RCA*] [PMID: 40205049 DOI: 10.1038/s41586-025-08869-4] [FullText]
9 **Zhong T**, Zhao W, Zhang Y, Pan Y, Dong P, Jiang Z, Jiang H, Zhou Y, Kui X, Shang Y, Zhao L, Yang L, Wei Y, Li Z, Zhang J, Yang L, Chen H, Zhao H, Liu Y, Zhu N, Li Y, Wang Y, Yao J, Wang J, Zeng Y, He L, Zheng C, Zhang Z, Li M, Liu Z, Dai H, Wu Z, Zhang L, Zhang S, Cai X, Hu X, Zhao S, Jiang X, Zhang X, Liu W, Li X, Zhu D, Guo L, Shen D, Han J, Liu T, Liu J, Zhang T. ChatRadio-Valuer: A Chat Large Language Model for Generalizable Radiology Impression Generation on Multi-institution and Multi-system Data. *IEEE Trans Biomed Eng* 2025; **PP** [PMID: 40788800 DOI: 10.1109/TBME.2025.3597325] [FullText]
10 **McCarthy J**, Minsky ML, Rochester N, Shannon CE. A Proposal for the Dartmouth Summer Research Project on Artificial Intelligence, August 31, 1955. *AI Magazine* 2006; **27**: 12 [DOI: 10.1609/aimag.v27i4.1904] [FullText]
11 **Wood R**. Historical Context and Evolution of AI/ML: A Journey Through Time. In: Wood R. Business Applications of Artificial Intelligence and Machine Learning. Oklahoma: Oklahoma State Regents for Higher Education, 2024
12 **Ivezic M**. The 1956 Dartmouth Workshop: The Birthplace of Artificial Intelligence (AI). Mar 3, 2017. [cited 3 September 2025]. Available from: https://securing.ai/ai/dartmouth-birth-ai/
13 **Sahota N**. AI Winter: A Cool Down for Overheated Expectations. Sept 30, 2024. [cited 3 September 2025]. Available from: https://www.

neilsahota.com/ai-winter-a-cool-down-for-overheated-expectations/#:~:text=Funding%20decline%3A%20As%20enthusiasm%20fades,development%20tends%20to%20dry%20up

14 **Mitchell R**. History of AI: Key Milestones and Impact on Technology. Mar 26, 2025. [cited 3 September 2025]. Available from: https://www.electropages.com/blog/1970/01/history-ai-key-milestones-impact-technology

15 **Peralta R**. Alan Turing's Everlasting Contributions to Computing, AI and Cryptography. Jun 23, 2022. [cited 3 September 2025]. Available from: https://www.nist.gov/blogs/taking-measure/alan-turings-everlasting-contributions-computing-ai-and-cryptography

16 **Trustees of Dartmouth College**. Artificial Intelligence Coined at Dartmouth. [cited 3 September 2025]. Available from: https://home.dartmouth.edu/about/artificial-intelligence-ai-coined-dartmouth

17 **Olabiyi W**, Akinyele D, Joel E. The Evolution of AI: From Rule-Based Systems to Data-Driven Intelligence. Jan, 2025. [cited 3 September 2025]. Available from: https://www.researchgate.net/publication/388035967_The_Evolution_of_AI_From_Rule-Based_Systems_to_Data-Driven_Intelligence

18 **Najjar R**. Redefining Radiology: A Review of Artificial Intelligence Integration in Medical Imaging. *Diagnostics (Basel)* 2023; **13**: 2760 [*RCA*] [PMID: 37685300 DOI: 10.3390/diagnostics13172760] [FullText] [Full Text(PDF)]

19 **Nadkarni P**, Merchant SA. Enhancing medical-imaging artificial intelligence through holistic use of time-tested key imaging and clinical parameters: Future insights. *Artif Intell Med Imaging* 2022; **3**: 55-69 [*RCA*] [DOI: 10.35711/aimi.v3.i3.55] [FullText] [Full Text(PDF)]

20 **Quinlan JR**. Induction of decision trees. *Mach Learn* 1986; **1**: 81-106 [*RCA*] [DOI: 10.1007/bf00116251] [FullText]

21 **Cortes C**, Vapnik V. Support-vector networks. *Mach Learn* 1995; **20**: 273-297 [*RCA*] [DOI: 10.1007/bf00994018] [FullText]

22 **Wang S**, Summers RM. Machine learning and radiology. *Med Image Anal* 2012; **16**: 933-951 [*RCA*] [PMID: 22465077 DOI: 10.1016/j.media.2012.02.005] [FullText]

23 **Mun SK**, Wong KH, Lo SB, Li Y, Bayarsaikhan S. Artificial Intelligence for the Future Radiology Diagnostic Service. *Front Mol Biosci* 2020; **7**: 614258 [*RCA*] [PMID: 33585563 DOI: 10.3389/fmolb.2020.614258] [FullText] [Full Text(PDF)]

24 **Bengio Y**, Ducharme R, Vincent P, Jauvin C. A neural probabilistic language model. *J Mach Learn Res* 2003; **3**: 1137-1155

25 **Hochreiter S**, Schmidhuber J. Long short-term memory. *Neural Comput* 1997; **9**: 1735-1780 [*RCA*] [PMID: 9377276 DOI: 10.1162/neco.1997.9.8.1735] [FullText]

26 **Cho K**, van Merrienboer B, Bahdanau D, Bengio Y. On the Properties of Neural Machine Translation: Encoder–Decoder Approaches. Proceedings of SSST-8, Eighth Workshop on Syntax, Semantics and Structure in Statistical Translation; 2014 Oct, Doha, Qatar. Pennsylvania: Association for Computational Linguistics, 2014: 103-111

27 **Levy S**. 8 Google Employees Invented Modern AI. Here's the Inside Story. Mar 20, 2024. [cited 3 September 2025]. Available from: https://www.wired.com/story/eight-google-employees-invented-modern-ai-transformers-paper/

28 **Guidotti R**, Monreale A, Ruggieri S, Turini F, Giannotti F, Pedreschi D. A Survey of Methods for Explaining Black Box Models. *ACM Comput Surv* 2019; **51**: 1-42 [DOI: 10.1145/3236009] [FullText]

29 **Bahdanau D**, Cho K, Bengio Y. Neural Machine Translation by Jointly Learning to Align and Translate. 2016 Preprint. Available from: arXiv: 1409.0473 [DOI: 10.48550/arXiv.1409.0473] [FullText]

30 **Vaswani A**, Shazeer N, Parmar N, Uszkoreit J, Jones L, Gomez AN, Kaiser L, Polosukhin I. Attention is All you Need. Part of Advances in Neural Information Processing Systems 30 (NIPS 2017). 2017. [cited 3 September 2025]. Available from: https://papers.nips.cc/paper_files/paper/2017/hash/3f5ee243547dee91fbd053c1c4a845aa-Abstract.html

31 **Nam Y**, Kim DY, Kyung S, Seo J, Song JM, Kwon J, Kim J, Jo W, Park H, Sung J, Park S, Kwon H, Kwon T, Kim K, Kim N. Multimodal Large Language Models in Medical Imaging: Current State and Future Directions. *Korean J Radiol* 2025; **26**: 900-923 [*RCA*] [PMID: 41015856 DOI: 10.3348/kjr.2025.0599] [FullText]

32 **Maksi Y**. The Evolution of Transformers and LLM (Large Language Models): Roadmap, Impact, and Future Prospects. [cited 3 September 2025]. Available from: https://www.kaggle.com/discussions/general/458973

33 **Pacheco M**. The Llama 4 herd: The beginning of a new era of natively multimodal AI innovation. April 6, 2025. [cited 3 September 2025]. Available from: https: https://www.skool.com/data-alchemy/the-llama-4-herd-the-beginning-of-a-new-era-of-natively-multimodal-ai-innovation

34 **Radford A**, Narasimhan K, Salimans T, Sutskever I. Improving Language Understanding by Generative Pre-Training. [cited 3 September 2025]. Available from: https://cdn.openai.com/research-covers/language-unsupervised/language_understanding_paper.pdf

35 **Devlin J**, Chang MW, Lee K, Toutanova K. 2019. BERT: Pre-training of deep bidirectional transformers for language understanding. Proceedings of the 2019 Conference of the North American Chapter of the Association for Computational Linguistics: Human Language Technologies, Volume 1 (Long and Short Papers); 2019 Jun; Minneapolis, Minnesota. Pennsylvania: Association for Computational Linguistics, 2019: 4171-4186

36 **Pichai S**. An important next step on our AI journey. Sundar Pichai. Feb 6, 2023. [cited 3 September 2025]. Available from: https://blog.google/technology/ai/bard-google-ai-search-updates/

37 **Thoppilan R**, De Freitas D, Hall J, Shazeer N, Kulshreshtha A, Cheng H, Jin A, Bos T, Baker L, Du Y, Li YG, Lee H, Zheng HS, Ghafouri A, Menegali M, Huang Y, Krikun M, Lepikhin D, Qin J, Chen D, Xu Y, Chen Z, Roberts A, Bosma M, Zhao V, Zhou Y, Chang CC, Krivokon I, Rusch W, Pickett M, Srinivasan P, Man L, Meier-Hellstern K, Morris MR, Doshi T, Delos Santos R, Duke T, Soraker J, Zevenbergen B, Prabhakaran V, Diaz M, Hutchinson B, Olson K, Molina A, Hoffman-John E, Lee J, Aroyo L, Rajakumar R, Butryna A, Lamm M, Kuzmina V, Fenton J, Cohen A, Bernstein R, Kurzweil R, Aguera-Arcas B, Cui C, Croak M, Chi E, Le Q. LaMDA: Language Models for Dialog Applications. 2022 Preprint. Available from: arXiv: 2201.08239 [DOI: 10.48550/arXiv.2201.08239] [FullText]

38 **Nazi ZA**, Peng W. Large Language Models in Healthcare and Medical Domain: A Review. 2024 Preprint. Available from: arXiv: 2401.06775 [DOI: 10.48550/arXiv.2401.06775] [FullText]

39 **Chen ZM**, Hernández Cano AH, Romanou A, Bonnet A, Matoba K, Salvi F, Pagliardini M, Fan S, Köpf A, Mohtashami A, Sallinen A, Sakhaeirad A, Swamy V, Krawczuk I, Bayazit D, Marmet A, Montariol S, Hartley MA, Jaggi M, Bosselut A. 2023. MEDITRON-70B: Scaling Medical Pretraining for Large Language Models. 2023 Preprint. Available from: arXiv: 2311.16079 [DOI: 10.48550/arXiv.2311.16079] [FullText]

40 **Singhal K**, Azizi S, Tu T, Mahdavi SS, Wei J, Chung HW, Scales N, Tanwani A, Cole-Lewis H, Pfohl S, Payne P, Seneviratne M, Gamble P, Kelly C, Babiker A, Schärli N, Chowdhery A, Mansfield P, Demner-Fushman D, Agüera Y Arcas B, Webster D, Corrado GS, Matias Y, Chou K, Gottweis J, Tomasev N, Liu Y, Rajkomar A, Barral J, Semturs C, Karthikesalingam A, Natarajan V. Large language models encode clinical knowledge. *Nature* 2023; **620**: 172-180 [*RCA*] [PMID: 37438534 DOI: 10.1038/s41586-023-06291-2] [FullText] [Full Text(PDF)]

41 **Moor M**, Banerjee O, Abad ZSH, Krumholz HM, Leskovec J, Topol EJ, Rajpurkar P. Foundation models for generalist medical artificial intelligence. *Nature* 2023; **616**: 259-265 [*RCA*] [PMID: 37045921 DOI: 10.1038/s41586-023-05881-4] [FullText]

42 **Labrak Y**, Bazoge A, Morin E, Gourraud P, Rouvier M, Dufour R. BioMistral: A Collection of Open-Source Pretrained Large Language Models for Medical Domains. Findings of the Association for Computational Linguistics ACL 2024; 2024 Aug; Bangkok, Thailand. PA, United States: Association for Computational Linguistics, 2024: 5848-5864

43 **Busch F**, Hoffmann L, Rueger C, van Dijk EH, Kader R, Ortiz-Prado E, Makowski MR, Saba L, Hadamitzky M, Kather JN, Truhn D, Cuocolo R, Adams LC, Bressem KK. Current applications and challenges in large language models for patient care: a systematic review. *Commun Med (Lond)* 2025; **5**: 26 [*RCA*] [PMID: 39838160 DOI: 10.1038/s43856-024-00717-2] [FullText] [Full Text(PDF)]

44 **Xiong GZ**, Jin Q, Lu ZY, Zhang AD. Benchmarking Retrieval-Augmented Generation for Medicine. Findings of the Association for Computational Linguistics ACL 2024; 2024 Aug 11-16; Bangkok, Thailand. PA, United States: Association for Computational Linguistics, 2024: 6233-6251

45 **Lewis P**, Perez E, Piktus A, Petroni F, Karpukhin V, Goyal N, Küttler H, Lewis M, Yih W, Rocktäschel T, Riedel S, Kiela D. Retrieval-Augmented Generation for Knowledge-Intensive NLP Tasks. 2021 Preprint. Available from: arXiv: 2005.11401 [DOI: 10.48550/arXiv.2005.11401] [FullText]

46 **Yang X**, Chen A, PourNejatian N, Shin HC, Smith KE, Parisien C, Compas C, Martin C, Costa AB, Flores MG, Zhang Y, Magoc T, Harle CA, Lipori G, Mitchell DA, Hogan WR, Shenkman EA, Bian J, Wu Y. A large language model for electronic health records. *NPJ Digit Med* 2022; **5**: 194 [*RCA*] [PMID: 36572766 DOI: 10.1038/s41746-022-00742-2] [FullText] [Full Text(PDF)]

47 **Tian S**, Jin Q, Yeganova L, Lai PT, Zhu Q, Chen X, Yang Y, Chen Q, Kim W, Comeau DC, Islamaj R, Kapoor A, Gao X, Lu Z. Opportunities and challenges for ChatGPT and large language models in biomedicine and health. *Brief Bioinform* 2023; **25**: bbad493 [*RCA*] [PMID: 38168838 DOI: 10.1093/bib/bbad493] [FullText] [Full Text(PDF)]

48 **Dilmegani C**, Palazoğlu M. Compare 10+ LLMs in Healthcare. Oct 16, 2025. [cited 3 September 2025]. Available from: https://research.aimultiple.com/large-language-models-in-healthcare/?utm_source=chatgpt.com

49 **Baur S**, Nabulsi Z, Weng WH, Garrison J, Blankemeier L, Fishman S, Chen C, Kakarmath S, Maimbolwa M, Sanjase N, Shuma B, Matias Y, Corrado GS, Patel S, Shetty S, Prabhakara S, Muyoyeta M, Ardila D. 2024. HeAR -- Health Acoustic Representations. 2024 Preprint. Available from: arXiv: 2403.02522 [DOI: 10.48550/arXiv.2403.02522] [FullText]

50 **Shetty S**. This AI model is helping researchers detect disease based on coughs. google.com. Aug 19, 2024. [cited 3 September 2025]. Available from: https://blog.google/technology/health/ai-model-cough-disease-detection/

51 **Merchant SA**, Shaikh MJS, Nadkarni P. Tuberculosis conundrum - current and future scenarios: A proposed comprehensive approach combining laboratory, imaging, and computing advances. *World J Radiol* 2022; **14**: 114-136 [*RCA*] [PMID: 35978978 DOI: 10.4329/wjr.v14.i6.114] [FullText] [Full Text(PDF)]

52 **Hager P**, Jungmann F, Holland R, Bhagat K, Hubrecht I, Knauer M, Vielhauer J, Makowski M, Braren R, Kaissis G, Rueckert D. Evaluation and mitigation of the limitations of large language models in clinical decision-making. *Nat Med* 2024; **30**: 2613-2622 [*RCA*] [PMID: 38965432 DOI: 10.1038/s41591-024-03097-1] [FullText] [Full Text(PDF)]

53 **Henderson M**. Understanding the capabilities and limitations of LLMs in radiology: Large language models in radiology are promising yet face barriers to their wider adoption. RSNA. Jul 31, 2025. [cited 3 September 2025]. Available from: https://www.rsna.org/news/2025/july/using-llms-in-radiology?utm_source=chatgpt.com

54 **Kim TT**, Makutonin M, Sirous R, Javan R. Optimizing Large Language Models in Radiology and Mitigating Pitfalls: Prompt Engineering and Fine-tuning. *Radiographics* 2025; **45**: e240073 [*RCA*] [PMID: 40048389 DOI: 10.1148/rg.240073] [FullText]

55 **Soni N**, Ora M, Agarwal A, Yang T, Bathla G. A Review of the Opportunities and Challenges with Large Language Models in Radiology: The Road Ahead. *AJNR Am J Neuroradiol* 2025; **46**: 1292-1299 [*RCA*] [PMID: 39572201 DOI: 10.3174/ajnr.A8589] [FullText] [Full Text(PDF)]

56 **Pan LR**, Zhao ZY, Lu Y, Tang KW, Fu LY, Liang QC, Peng SL. Opportunities and challenges in the application of large artificial intelligence models in radiology. *Meta Radiol* 2024; **2**: 100080 [DOI: 10.1016/j.metrad.2024.100080] [FullText]

57 **Jiang LY**, Liu XC, Nejatian NP, Nasir-Moin M, Wang D, Abidin A, Eaton K, Riina HA, Laufer I, Punjabi P, Miceli M, Kim NC, Orillac C, Schnurman Z, Livia C, Weiss H, Kurland D, Neifert S, Dastagirzada Y, Kondziolka D, Cheung ATM, Yang G, Cao M, Flores M, Costa AB, Aphinyanaphongs Y, Cho K, Oermann EK. Health system-scale language models are all-purpose prediction engines. *Nature* 2023; **619**: 357-362 [*RCA*] [PMID: 37286606 DOI: 10.1038/s41586-023-06160-y] [FullText] [Full Text(PDF)]

58 **Mei LR**, Yao JY, Ge YY, Wang YW, Bi BL, Cai YJ, Liu JZ, Li MY, Li ZZ, Zhang DZ, Zhou CL, Mao JY, Xia TZ, Guo JF, Liu SH. A Survey of Context Engineering for Large Language Models. 2025 Preprint. Available from: arXiv: 2507.13334 [DOI: 10.48550/arXiv.2507.13334] [FullText]

59 **Xu S**, Yang L, Kelly C, Sieniek M, Kohlberger T, Ma M, Weng WH, Kiraly A, Kazemzadeh S, Melamed Z, Park J, Strachan P, Liu Y, Lau C, Singh P, Chen C, Etemadi M, Kalidindi SR, Matias Y, Chou K, Corrado GS, Shetty S, Tse D, Prabhakara S, Golden D, Pilgrim R, Eswaran K, Sellergren A. 2023. Elixr: Towards a general purpose x-ray artificial intelligence system through alignment of large language models and radiology vision encoders. 2023 Preprint. Available from: arXiv: 2308.01317 [DOI: 10.48550/arXiv.2308.01317] [FullText]

60 **Gu J**, Cho HC, Kim J, You K, Hong EK, Roh B. CheX-GPT: Harnessing large language models for enhanced chest x-ray report labeling. 2024 Preprint. Available from: arXiv: 2401.11505 [DOI: 10.48550/arXiv.2401.11505] [FullText]

61 **Dhanaliwala AH**, Ghosh R, Karn SK, Ullaskrishnan P, Farri O, Comaniciu D, Kahn CE. 2023. General-purpose vs. domain-adapted large language models for extraction of data from thoracic radiology reports. 2024 Preprint. Available from: arXiv: 2311.17213 [DOI: 10.48550/arXiv.2311.17213] [FullText]

62 **Hassan S**. LLMs Can Now Learn without Labels: Researchers from Tsinghua University and Shanghai AI Lab Introduce Test-Time Reinforcement Learning (TTRL) to Enable Self-Evolving Language Models Using Unlabeled Data. April 23, 2025. [cited 3 September 2025]. Available from: https://metaailabs.com/llms-can-now-learn-without-labels-researchers-from-tsinghua-university-and-shanghai-ai-lab-introduce-test-time-reinforcement-learning-ttrl-to-enable-self-evolving-language-models-using-unlabeled-da/#:~:text=TTRL%20is%20a%20training%20framework%20that%20applies%20RL,estimate%20pseudo-rewards%20through%20majority%20voting%20across%20sampled%20outputs

63 **Rashtchian C**, Juan DC. Making LLMs more accurate by using all of their layers. Sep 17, 2025. [cited 3 September 2025]. Available from: https://research.google/blog/making-llms-more-accurate-by-using-all-of-their-layers/

64 **Grandison T**. Large Language Models vs Large Concept Models: What's going on? Apr 17, 2025. [cited 3 September 2025]. Available from: https://www.linkedin.com/pulse/large-language-models-vs-concept-whats-going-tyrone-grandison-dautc/

65 **Merchant S**. AI in GUTB: The concept of a holistic multi-modal approach. Feb 13, 2025. [cited 3 September 2025]. Available from: https://www.expresshealthcare.in/news/ai-in-gutb-the-concept-of-a-holistic-multi-modal-approach/448041/

66 **PA TIMES Online**. The Evolution of AI: From John McCarthy to DALL-E. [cited 3 September 2025]. Available from: https://patimes.org/the-evolution-of-ai-from-john-mccarthy-to-dall-e/

67 **Meta AI**. Large Concept Models: Language Modeling in a Sentence Representation Space. Dec 11, 2024. [cited 3 September 2025]. Available from: https://ai.meta.com/research/publications/large-concept-models-language-modeling-in-a-sentence-representation-space/

68 **Barrault L**, Duquenne PA, Elbayad M, Kozhevnikov A, Alastruey B, Andrews P, Coria M, Couairon G, Costa-jussà MR, Dale D, Elsahar H, Heffernan K, Janeiro JM, Tran T, Ropers C, Sánchez E, Roman RS, Mourachko A, Saleem S, Schwenk H. Large Concept Models: Language Modeling in a Sentence Representation Space. 2024 Preprint. Available from: arXiv: 2412.08821 [DOI: 10.48550/arXiv.2412.08821] [Full Text]

69 **Sil S**. Why Large Concept Models are the Future: Unveiling the Shift from LLMs to LCMs. [cited 3 September 2025]. Available from: https://www.coforge.com/what-we-know/blog/why-large-concept-models-lcms-are-the-future-unveiling-the-shift-from-llms-to-lcms

70 **Synced**. From Token to Conceptual: Meta introduces Large Concept Models in Multilingual AI. December 17, 2024. [cited 3 September 2025]. Available from: https://medium.com/syncedreview/from-token-to-conceptual-the-rise-of-metas-large-concept-models-in-multilingual-ai-b32acbfeb792

71 **Ahmed H**, Goel D. The Future of AI: Exploring the Potential of Large Concept Models. 2025 Preprint. Available from: arXiv: 2501.05487 [DOI: 10.48550/arXiv.2501.05487] [FullText]

72 **Nazar T**. Large Concept Models (LCMs): The Future of AI Beyond Token Prediction. Medium.com > Towards AI. March 12, 2025. [cited 3 September 2025]. Available from: https://pub.towardsai.net/large-concept-models-lcms-the-future-of-ai-beyond-token-prediction-11e0a50d055d

73 **Pranja AA**. LCMs vs. LLMs: Why Concept-Based AI May Be the Key to AGI. Mar 18, 2025. [cited 3 September 2025]. Available from: https://prajnaaiwisdom.medium.com/lcms-vs-llms-why-concept-based-ai-may-be-the-key-to-agi-bc11e1aac2a6

74 **Pruseth D**. LCMs: Large Concept Models – The Path to AGI (Artificial General Intelligence) & The Future of AI Thinking. [cited 3 September 2025]. Available from: https://debabratapruseth.com/lcms-large-concept-models-the-path-to-agi-the-future-of-ai-thinking/

75 **Ullah E**, Parwani A, Baig MM, Singh R. Challenges and barriers of using large language models (LLM) such as ChatGPT for diagnostic medicine with a focus on digital pathology - a recent scoping review. *Diagn Pathol* 2024; **19**: 43 [*RCA*] [PMID: 38414074 DOI: 10.1186/s13000-024-01464-7] [FullText] [Full Text(PDF)]

76 **Bhayana R**. Chatbots and Large Language Models in Radiology: A Practical Primer for Clinical and Research Applications. *Radiology* 2024; **310**: e232756 [*RCA*] [PMID: 38226883 DOI: 10.1148/radiol.232756] [FullText]

77 **Esmradi A**, Yip DW, Chan CF. A Comprehensive Survey of Attack Techniques, Implementation, and Mitigation Strategies in Large Language Models. Communications in Computer and Information Science. Springer: Singapore, 2024: 76-95

78 **Van de Plassche-Boers EM**, Drexhage HA, Kokjé-Kleingeld M. The use of somatic antigen of Haemophilus influenzae for the monitoring of T cell-mediated skin test reactivity in man. *J Immunol Methods* 1985; **83**: 353-361 [*RCA*] [PMID: 3877118 DOI: 10.1016/0022-1759(85)90257-1] [FullText]

79 **Marcus E**, Davis G. How Not to Test GPT-3. Fab 21, 2023. [cited 3 September 2025]. Available from: https://garymarcus.substack.com/p/how-not-to-test-gpt-3

80 **Chen M**, Tworek J, Jun H, Yuan Q, de Oliveira Pinto HP, Kaplan J, Edwards H, Burda Y, Joseph N, Brockman G, Ray A, Puri R, Krueger G, Petrov M, Khlaaf H, Sastry G, Mishkin P, Chan B, Gray S, Ryder N, Pavlov M, Power A, Kaiser L, Bavarian M, Winter C, Tillet P, Petroski Such FP, Cummings D, Plappert M, Chantzis F, Barnes E, Herbert-Voss A, Guss WH, Nichol A, Paino A, Tezak N, Tang J, Babuschkin I, Balaji S, Jain S, Saunders W, Hesse C, Carr AN, Leike J, Achiam J, Misra V, Morikawa E, Radford A, Knight M, Brundage M, Murati M, Mayer K, Welinder P, McGrew B, Amodei D, McCandlish S, Sutskever I, Zaremba W. Evaluating Large Language Models Trained on Code. 2021 Preprint. Available from: arXiv: 2107.03374 [DOI: 10.48550/arXiv.2107.03374] [FullText]

81 **Guo Y**, Guo M, Su J, Yang Z, Zhu M, Li H, Qiu M, Liu SS. 2024. Bias in Large Language Models: Origin, Evaluation, and Mitigation. 2024 Preprint. Available from: arXiv: 2411.10915 [DOI: 10.48550/arXiv.2411.10915] [FullText]

82 **Huang L**, Yu W, Ma W, Zhong W, Feng Z, Wang H, Chen Q, Peng W, Feng X, Qin B, Liu T. A Survey on Hallucination in Large Language Models: Principles, Taxonomy, Challenges, and Open Questions. *ACM Trans Inf Syst* 2025; **43**: 1-55 [DOI: 10.1145/3703155] [FullText]

83 **Mozes M**, He XL, Kleinberg B, Griffin LD. Use of LLMs for Illicit Purposes: Threats, Prevention Measures, and Vulnerabilities. 2023 Preprint. Available from: arXiv: 2411. 2308.12833 [DOI: 10.48550/arXiv.2308.12833] [FullText]

84 **Ouyang S**, Zhang JM, Harman M, Wang M. An Empirical Study of the Non-Determinism of ChatGPT in Code Generation. *ACM Trans Softw Eng Methodol* 2025; **34**: 1-28 [DOI: 10.1145/3697010] [FullText]

85 **Atil B**, Chittams A, Fu L, Ture F, Xu L, Baldwin B. LLM Stability: A detailed analysis with some surprises. 2025 Preprint. Available from: arXiv: 2408.04667 [DOI: 10.48550/arXiv.2408.04667] [FullText]

86 **Hendrycks D**, Burns C, Basart S, Zou A, Mazeika M, Song D, Steinhardt J. Measuring Massive Multitask Language Understanding. 2021 Preprint. Available from: arXiv: 2009.03300 [DOI: 10.48550/arXiv.2009.03300] [FullText]

87 **Bender EM**, Gebru T, Mcmillan-Major A, Shmitchell S. On the Dangers of Stochastic Parrots: Can Language Models Be Too Big? Proceedings of the 2021 ACM Conference on Fairness, Accountability, and Transparency. 2021 Mar 3-10; Canada. New York: Association for Computing Machinery, 2021: 610-623

88 **Floridi L**, Cowls J, Beltrametti M, Chatila R, Chazerand P, Dignum V, Luetge C, Madelin R, Pagallo U, Rossi F, Schafer B, Valcke P, Vayena E. AI4People-An Ethical Framework for a Good AI Society: Opportunities, Risks, Principles, and Recommendations. *Minds Mach (Dordr)* 2018; **28**: 689-707 [*RCA*] [PMID: 30930541 DOI: 10.1007/s11023-018-9482-5] [FullText] [Full Text(PDF)]

89 **Buchholz K**. The Extreme Cost of Training AI Models. Sep 23, 2024. [cited 3 September 2025]. Available from: https://www.statista.com/chart/33114/estimated-cost-of-training-selected-ai-models/

90 **Faiz A**, Kaneda S, Wang R, Osi R, Sharma P, Chen F, Jiang L. LLM Carbon: Modeling the End-To-End Carbon Footprint of Large Language Models. 2024 Preprint. Available from: arXiv: 2309.14393 [DOI: 10.48550/arXiv.2309.14393] [FullText]

91 **Wahl B**, Cossy-Gantner A, Germann S, Schwalbe NR. Artificial intelligence (AI) and global health: how can AI contribute to health in resource-poor settings? *BMJ Global Health* 2018; **3**: e000798 [*RCA*] [DOI: 10.1136/bmjgh-2018-000798] [FullText] [Full Text(PDF)]

92 **The Institution of Engineering and Technology**. Simplistic searches on Large Language Models bad for the environment. The Institute of Engineering and Technology. Nov 29, 2024. [cited 3 September 2025]. Available from: https://www.theiet.org/media/press-releases/press-

releases-2024/press-releases-2024-october-december/29-november-2024-simplistic-searches-on-large-language-models-bad-for-the-environment

93 **Ren S**, Tomlinson B, Black RW, Torrance AW. Reconciling the contrasting narratives on the environmental impact of large language models. *Sci Rep* 2024; **14**: 26310 [*RCA*] [PMID: 39487230 DOI: 10.1038/s41598-024-76682-6] [FullText]

94 **Wu JD**, Ji W, Fu HZ, Xu M, Jin YM, Xu YW. MedSegDiff-V2: Diffusion-Based Medical Image Segmentation with Transformer. *Proc AAAI Conf Artif Intell* 2024; **38**: 6030-6038 [DOI: 10.1609/aaai.v38i6.28418] [FullText]

95 **Tong R**, Xu T, Ju XX, Wang. LR. Progress in Medical AI: Reviewing Large Language Models and Multimodal Systems for Diagonosis. *AI Med* 2025; **1**: 5 [DOI: 10.71423/aimed.20250105] [FullText]

96 **Polonski V**. AI has huge potential – but it won't solve all our problems. World Economic Forum. June 14, 2018. [cited 3 September 2025]. Available from: https://www.weforum.org/stories/2018/06/ai-cannot-solve-all-our-problems/

97 **Warraich HJ**, Tazbaz T, Califf RM. FDA Perspective on the Regulation of Artificial Intelligence in Health Care and Biomedicine. *JAMA* 2025; **333**: 241-247 [*RCA*] [PMID: 39405330 DOI: 10.1001/jama.2024.21451] [FullText]

98 **Thubron R**. ChatGPT adds 100 million users in two months, making it the fastest-growing "app" ever. Feb 3, 2023. [cited 3 September 2025]. Available from: https://www.techspot.com/news/97486-chatgpt-adds-100-million-users-two-months-making.html

99 **Open AI**, Achiam J, Adler S, Agarwal S, Ahmad L, Akkaya I, Aleman FL, Almeida D, Altenschmidt J, Altman S, Anadkat S, Avila R, Babuschkin I, Balaji S, Balcom V, Baltescu P, Bao H, Bavarian M, Belgum J, Bello I, Berdine J, Bernadett-Shapiro G, Berner C, Bogdonoff L, Boiko O, Boyd M, Brakman AL, Brockman G, Brooks T, Brundage M, Button K, Cai T, Campbell R, Cann A, Carey B, Carlson C, Carmichael R, Chan B, Chang C, Chantzis F, Chen D, Chen S, Chen R, Chen J, Chen M, Chess B, Cho C, Chu C, Chung HW, Cummings D, Currier J, Dai Y, Decareaux C, Degry T, Deutsch N, Deville D, Dhar A, Dohan D, Dowling S, Dunning S, Ecoffet A, Eleti A, Eloundou T, Farhi D, Fedus L, Felix N, Fishman SP, Forte J, Fulford I, Gao L, Georges E, Gibson C, Goel V, Gogineni T, Goh G, Gontijo-Lopes R, Gordon J, Grafstein M, Gray S, Greene R, Gross J, Gu SS, Guo Y, Hallacy C, Han J, Harris J, He Y, Heaton M, Heidecke J, Hesse C, Hickey A, Hickey W, Hoeschele P, Houghton B, Hsu K, Hu S, Hu X, Huizinga J, Jain S, Jain S, Jang J, Jiang A, Jiang R, Jin H, Jin D, Jomoto S, Jonn B, Jun H, Kaftan T, Kaiser Ł, Kamali A, Kanitscheider I, Keskar NS, Khan T, Kilpatrick L, Kim JW, Kim C, Kim Y, Kirchner JH, Kiros J, Knight M, Kokotajlo D, Kondraciuk Ł, Kondrich A, Konstantinidis A, Kosic K, Krueger G, Kuo V, Lampe M, Lan I, Lee T, Leike J, Leung J, Levy D, Li CM, Lim R, Lin M, Lin S, Litwin M, Lopez T, Lowe R, Lue P, Makanju A, Malfacini K, Manning S, Markov T, Markovski Y, Martin B, Mayer K, Mayne A, McGrew B, McKinney SM, McLeavey C, McMillan P, McNeil J, Medina D, Mehta A, Menick J, Metz L, Mishchenko A, Mishkin P, Monaco V, Morikawa E, Mossing D, Mu T, Murati M, Murk O, Mély D, Nair A, Nakano R, Nayak R, Neelakantan A, Ngo R, Noh H, Ouyang L, O'Keefe C, Pachocki J, Paino A, Palermo J, Pantuliano A, Parascandolo G, Parish J, Parparita E, Passos A, Pavlov M, Peng A, Perelman A, de Avila Belbute P, Petrov M, de Oliveira Pinto HP, Michael, Pokorny, Pokrass M, Pong VH, Powell T, Power A, Power B, Proehl E, Puri R, Radford A, Rae J, Ramesh A, Raymond C, Real F, Rimbach K, Ross C, Rotsted B, Roussez H, Ryder N, Saltarelli M, Sanders T, Santurkar S, Sastry G, Schmidt H, Schnurr D, Schulman J, Selsam D, Sheppard K, Sherbakov T, Shieh J, Shoker S, Shyam P, Sidor S, Sigler E, Simens M, Sitkin J, Slama K, Sohl I, Sokolowsky B, Song Y, Staudacher N, Such FP, Summers N, Sutskever I, Tang J, Tezak N, Thompson MB, Tillet P, Tootoonchian A, Tseng E, Tuggle P, Turley N, Tworek J, Uribe J FC, Vallone A, Vijayvergiya A, Voss C, Wainwright C, Wang JJ, Wang A, Wang B, Ward J, Wei J, Weinmann CJ, Welihinda A, Welinder P, Weng J, Weng L, Wiethoff M, Willner D, Winter C, Wolrich S, Wong H, Workman L, Wu S, Wu J, Wu M, Xiao K, Xu T, Yoo S, Yu K, Yuan Q, Zaremba W, Zellers R, Zhang C, Zhang M, Zhao S, Zheng T, Zhuang J, Zhuk W, Zoph B. GPT-4 Technical Report. March. 2024 Preprint. Available from: arXiv: 2303.08774 [DOI: 10.48550/arXiv.2303.08774] [FullText]

100 **Zhao WX**, Zhou K, Li J, Tang T, Wang X, Hou Y, Min Y, Zhang B, Zhang J, Dong Z, Du Y, Yang C, Chen Y, Chen Z, Jiang J, Ren R, Li Y, Tang X, Liu Z, Liu P, Nie JY, Wen JR. 2023. A Survey of Large Language Models. 2025 Preprint. Available from: arXiv: 2303.18223 [DOI: 10.48550/arXiv.2303.18223] [FullText]

101 **Rubin DL**. Artificial Intelligence in Imaging: The Radiologist's Role. *J Am Coll Radiol* 2019; **16**: 1309-1317 [*RCA*] [PMID: 31492409 DOI: 10.1016/j.jacr.2019.05.036] [FullText]

102 **Duquenne PA**, Schwenk H, Sagot B. SONAR: Sentence-Level Multimodal and Language-Agnostic Representations. 2023 Preprint. Available from: arXiv: 2308.11466 [DOI: 10.48550/arXiv.2308.11466] [FullText]

103 **AIbase**. Meta Launches 'Large Concept Models' (LCMs)! Breaking Through LLM Limitations and Leading a New Direction in AI Language Understanding. Dec 16, 2024. [cited 3 September 2025]. Available from: https://www.aibase.com/news/13985

104 **Kulshrestha U**. Reimagining AI: METAs Large Concept Models (LCMs) vs Large Language Models (LLMs). Jan 3, 2025. [cited 3 September 2025]. Available from: https://www.linkedin.com/pulse/reimagining-ai-metas-large-concept-models-lcms-vs-llms-kulshrestha-hcatc/

105 **Gottumukkala S**. Large Concept Models (LCMs): From Tokens to Concepts. [cited 3 September 2025]. Available from: https://www.linkedin.com/pulse/large-concept-models-lcms-from-tokens-concepts-sateesh-gottumukkala-jx9uc/

106 **Eliot L**. AI Is Breaking Free Of Token-Based LLMs By Upping The Ante To Large Concept Models That Devour Sentences And Adore Concepts. Jan 06, 2025. [cited 3 September 2025]. Available from: https://nycalive.com/lander/nycalive.com/index.php?_=%2Fsites%2Flanceeliot%2F2025%2F01%2F06%2Fai-is-breaking-free-of-token-based-llms-by-upping-the-ante-to-large-concept-models-that-devour-sentences-and-adore-concepts%2F%236bZ7zjvhmhT0JYiEBX1G%2BEMA6rB3Rw%3D%3D

107 **Jain R**, Professor. What are Conceptual Graphs? [Video]; 2025. YouTube. [cited 3 September 2025]. Available from: https://www.youtube.com/watch?v=u7uNw31Cg7E.

108 **Li ZW**, Xu Q, Zhang D, Song H, Cai YQ, Qi Q, Zhou R, Pan JT, Li ZF, Vu VT, Huang ZD, Wang T. Grounding GPT: Language enhanced multi-modal grounding model. 2024 Preprint. Available from: arXiv: 2401.06071 [DOI: 10.48550/arXiv.2401.06071] [FullText]

109 **Wiczew D**. Uncertainty Aware AI: Embracing the Power of Doubt in Smart Decision-Making. Jan 8, 2024. [cited 3 September 2025]. Available from: https://www.linkedin.com/pulse/uncertainty-aware-ai-embracing-power-doubt-smart-daniel-wiczew-bw87e/

110 **Zhang Z**, Wang Y, Yao Q. Searching meta reasoning skeleton to guide LLM reasoning. 2025 Preprint. Available from: arXiv: 2510.04116 [DOI: 10.48550/arXiv.2510.04116] [FullText]

111 **Hand DJ**, Khan S. Validating and Verifying AI Systems. *Patterns (N Y)* 2020; **1**: 100037 [*RCA*] [PMID: 33205105 DOI: 10.1016/j.patter.2020.100037] [FullText] [Full Text(PDF)]

112 **Wang HR**, Shu K. Explainable Claim Verification via Knowledge-Grounded Reasoning with Large Language Models. Findings of the Association for Computational Linguistics: EMNLP; 2023 Dec 2023; Singapore. Pennsylvania: Association for Computational Linguistics, 2023: 6288-6304

113 **Cao JJ**, Kwon DH, Ghaziani TT, Kwo P, Tse G, Kesselman A, Kamaya A, Tse JR. Accuracy of Information Provided by ChatGPT Regarding Liver Cancer Surveillance and Diagnosis. *AJR Am J Roentgenol* 2023; **221**: 556-559 [*RCA*] [PMID: 37222278 DOI: 10.2214/AJR.23.29493] [FullText]

114 **Death D**. Understanding and Addressing Inaccurate or Misleading Outputs in AI Systems. Feb 21, 2025. [cited 3 September 2025]. Available from: https://www.linkedin.com/pulse/understanding-addressing-inaccurate-misleading-outputs-death-zyure/

115 **Robson D**. The Intellect Trap. Vols. New York: W.W. Norton & Company, 2019

116 **Norelus E**. Large Concept Models (LCMs) — Rethinking the Future of AI. Mar 25, 2025. [cited 3 September 2025]. Available from: https://ernesenorelus.medium.com/large-concept-models-lcms-rethinking-the-future-of-ai-8bb5b268c78d

117 **Moltisanti D**. Large Concept Models: Meta's Next Frontier in AI. Dec 25, 2024. [cited 3 September 2025]. Available from: https://staituned.com/learn/expert/large-concept-model-meta

118 **Zhan Y**, Hao Y, Wang X, Guo D. Advances of artificial intelligence in clinical application and scientific research of neuro-oncology: Current knowledge and future perspectives. *Crit Rev Oncol Hematol* 2025; **209**: 104682 [*RCA*] [PMID: 40032186 DOI: 10.1016/j.critrevonc.2025.104682] [FullText]

119 **Schwartz R**, Dodge J, Smith NA, Etzioni O. Green AI. *Commun ACM* 2020; **63**: 54-63 [DOI: 10.1145/3381831] [FullText]

120 **Doo FX**, Vosshenrich J, Cook TS, Moy L, Almeida EPRP, Woolen SA, Gichoya JW, Heye T, Hanneman K. Environmental Sustainability and AI in Radiology: A Double-Edged Sword. *Radiology* 2024; **310**: e232030 [*RCA*] [PMID: 38411520 DOI: 10.1148/radiol.232030] [FullText]

121 **Bolón-canedo V**, Morán-fernández L, Cancela B, Alonso-betanzos A. A review of green artificial intelligence: Towards a more sustainable future. *Neurocomputing* 2024; **599**: 128096 [DOI: 10.1016/j.neucom.2024.128096] [FullText]

122 **Danda R**. Large Concept Models: The Next Revolutionary Frontier In AI. January 23, 2025. [cited 3 September 2025]. Available from: https://www.forbes.com/councils/forbestechcouncil/2025/01/23/large-concept-models-the-next-revolutionary-frontier-in-ai/

123 **Brady AP**, Neri E. Artificial Intelligence in Radiology-Ethical Considerations. *Diagnostics (Basel)* 2020; **10**: 231 [*RCA*] [PMID: 32316503 DOI: 10.3390/diagnostics10040231] [FullText] [Full Text(PDF)]

124 **European Society of Radiology (ESR)**. The role of radiologist in the changing world of healthcare: a White Paper of the European Society of Radiology (ESR). *Insights Imaging* 2022; **13**: 100 [*RCA*] [PMID: 35662384 DOI: 10.1186/s13244-022-01241-4] [FullText] [Full Text(PDF)]

125 **Syed AB**, Zoga AC. Artificial Intelligence in Radiology: Current Technology and Future Directions. *Semin Musculoskelet Radiol* 2018; **22**: 540-545 [*RCA*] [PMID: 30399618 DOI: 10.1055/s-0038-1673383] [FullText]

126 **Abimbola A**. A Review of the Historical Development and Future Significance of Artificial Intelligence in Radiology. *medtigo J Med* 2024; **2**: e3062253 [DOI: 10.63096/medtigo3062253] [FullText]

127 **Databridge Market Research**. Global radiology market size, share, and trends analysis report-Industry Overview and Forecast to 2032. [cited 3 September 2025]. Available from: https://www.databridgemarketresearch.com/reports/global-radiology-market

128 **Databridge Market Research**. Global Radiology Market Size, Share, and Trends Analysis Report – Industry Overview and Forecast to 2032. [cited 3 September 2025]. Available from: https://www.databridgemarketresearch.com/reports/global-radiology-market?srsltid=AfmBOoplGI74hRp99wnYGMNB9I4ruURHrmR-Vbi5SJNamzv7H0CHyPuo

129 **Accenture**. Artificial Intelligence: Healthcare's new nervous system. [cited 3 September 2025]. Available from: https://www.accenture.com/content/dam/accenture/final/a-com-migration/manual/r3/pdf/pdf-49/Accenture-health-artificial-intelligence-j.pdf

130 **Kasyanau A**. Balancing The Cost Of AI In Healthcare: Future Savings Vs. Current Spending. 2024. [cited 3 September 2025]. Available from: https://www.forbes.com/councils/forbestechcouncil/2024/04/17/balancing-the-cost-of-ai-in-healthcare-future-savings-vs-current-spending/

131 **Su J**, Yang L, Sun Z, Zhan X. Personalized Drug Therapy: Innovative Concept Guided With Proteoformics. *Mol Cell Proteomics* 2024; **23**: 100737 [*RCA*] [PMID: 38354979 DOI: 10.1016/j.mcpro.2024.100737] [FullText] [Full Text(PDF)]

132 **Stanwick PA**, Stanwick SD. The Rise and Fall of Eastman Kodak: Looking Through Kodachrome Colored Glasses. *Am J Hum Soc Sci Res* 2020; **4**: 219-224

133 **Bazerman MH**, Tenbrunsel AE. Blind Spots. 2011 Princeton: Princeton University Press, 2011

134 **Christensen CM**. The Innovator's Dilemma: When New Technologies Cause Great Firms to Fail. Harvard Business School. Boston: Harvard Business, 1997

135 **Higgins JM**. Innovate or Evaporate: Test and Improve Your Organization's Innovation Quotient. New York: New Management Publishing Company, 1995

136 **Niraula D**, Cui S, Pakela J, Wei L, Luo Y, Ten Haken RK, El Naqa I. Current status and future developments in predicting outcomes in radiation oncology. *Br J Radiol* 2022; **95**: 20220239 [*RCA*] [PMID: 35867841 DOI: 10.1259/bjr.20220239] [FullText] [Full Text(PDF)]

137 **Zhao H**, Zhou Z, Wu F, Xiang D, Zhao H, Zhang W, Li L, Li Z, Huang J, Hu H, Liu C, Wang T, Liu W, Ma J, Yang F, Wang X, Zheng C. Self-supervised learning enables 3D digital subtraction angiography reconstruction from ultra-sparse 2D projection views: A multicenter study. *Cell Rep Med* 2022; **3**: 100775 [*RCA*] [PMID: 36208630 DOI: 10.1016/j.xcrm.2022.100775] [FullText] [Full Text(PDF)]

138 **Gao Y**, Song Y, Yin X, Wu W, Zhang L, Chen Y, Shi W. Deep learning-based digital subtraction angiography image generation. *Int J Comput Assist Radiol Surg* 2019; **14**: 1775-1784 [*RCA*] [PMID: 31367806 DOI: 10.1007/s11548-019-02040-x] [FullText]

139 **Ueda D**, Katayama Y, Yamamoto A, Ichinose T, Arima H, Watanabe Y, Walston SL, Tatekawa H, Takita H, Honjo T, Shimazaki A, Kabata D, Ichida T, Goto T, Miki Y. Deep Learning-based Angiogram Generation Model for Cerebral Angiography without Misregistration Artifacts. *Radiology* 2021; **299**: 675-681 [*RCA*] [PMID: 33787336 DOI: 10.1148/radiol.2021203692] [FullText]

140 **Zeng Y**, Liu X, Xiao N, Li Y, Jiang Y, Feng J, Guo S. Automatic Diagnosis Based on Spatial Information Fusion Feature for Intracranial Aneurysm. *IEEE Trans Med Imaging* 2020; **39**: 1448-1458 [*RCA*] [PMID: 31689186 DOI: 10.1109/TMI.2019.2951439] [FullText]

141 **Wisniewski AG**, Shiraz Bhurwani MM, Sommer KN, Monteiro A, Baig A, Davies J, Siddiqui A, Ionita CN. Quantitative angiography prognosis of intracranial aneurysm treatment failure using parametric imaging and distal vessel analysis. *Proc SPIE Int Soc Opt Eng* 2022; **12036**: 120360D [*RCA*] [PMID: 35983494 DOI: 10.1117/12.2611550] [FullText]

142 **Amigo N**, Valencia A, Wu W, Patnaik S, Finol E. Cerebral aneurysm rupture status classification using statistical and machine learning methods. *Proc Inst Mech Eng H* 2021; **235**: 655-662 [*RCA*] [PMID: 33685288 DOI: 10.1177/09544119211000477] [FullText]

143 **Fujimura S**, Koshiba T, Kudo G, Takeshita K, Kazama M, Karagiozov K, Fukudome K, Takao H, Ohwada H, Murayama Y, Yamamoto M, Ishibashi T, Otani K. Development of Machine Learning Model for Selecting the 1st Coil in the Treatment of Cerebral Aneurysms by Coil Embolization. *Annu Int Conf IEEE Eng Med Biol Soc* 2023; **2023**: 1-4 [*RCA*] [PMID: 38082640 DOI: 10.1109/EMBC40787.2023.10341191] [FullText]

144 **Bagcilar O**, Alis D, Alis C, Seker ME, Yergin M, Ustundag A, Hikmet E, Tezcan A, Polat G, Akkus AT, Alper F, Velioglu M, Yildiz O, Selcuk HH, Oksuz I, Kizilkilic O, Karaarslan E. Automated LVO detection and collateral scoring on CTA using a 3D self-configuring object detection network: a multi-center study. *Sci Rep* 2023; **13**: 8834 [*RCA*] [PMID: 37258516 DOI: 10.1038/s41598-023-33723-w] [FullText]

145 **Mittmann BJ**, Braun M, Runck F, Schmitz B, Tran TN, Yamlahi A, Maier-Hein L, Franz AM. Deep learning-based classification of DSA image sequences of patients with acute ischemic stroke. *Int J Comput Assist Radiol Surg* 2022; **17**: 1633-1641 [*RCA*] [PMID: 35604489 DOI: 10.1007/s11548-022-02654-8] [FullText] [Full Text(PDF)]

146 **Tang Z**, Tang Z, Wu J. Anomaly detection in medical *via* multimodal foundation models. *Front Bioeng Biotechnol* 2025; **13**: 1644697 [*RCA*] [PMID: 40873433 DOI: 10.3389/fbioe.2025.1644697] [FullText] [Full Text(PDF)]

147 **Focaloid Technologies Private Limited**. Understanding Large Concept Models: The Future of AI and Natural Language Processing. 2025. [cited 3 September 2025]. Available from: https://www.focaloid.com/blog/understanding-large-concept-models-the-future-of-ai-and-natural-language-processing/

148 **Shirole DB**. Optimizing Healthcare Management Systems with AI and Machine Learning. United States: Uphills Publishers LLC, 2025

149 **Zhang J**, Fang J, Xu Y, Si G. How AI and Robotics Will Advance Interventional Radiology: Narrative Review and Future Perspectives. *Diagnostics (Basel)* 2024; **14**: 1393 [*RCA*] [PMID: 39001283 DOI: 10.3390/diagnostics14131393] [FullText]

150 **Tejani AS**, Cook TS, Hussain M, Sippel Schmidt T, O'Donnell KP. Integrating and Adopting AI in the Radiology Workflow: A Primer for Standards and Integrating the Healthcare Enterprise (IHE) Profiles. *Radiology* 2024; **311**: e232653 [*RCA*] [PMID: 38888474 DOI: 10.1148/radiol.232653] [FullText]

151 **Banafa A**. The Learning Concept Model (LCM) in AI: A New Paradigm for Intelligent Systems. Mar 21, 2025. [cited 3 September 2025]. Available from: https://www.linkedin.com/pulse/learning-concept-model-lcm-ai-new-paradigm-systems-prof-ahmed-banafa-zgtoc

152 **Gangwal A**, Lavecchia A. AI-Driven Drug Discovery for Rare Diseases. *J Chem Inf Model* 2025; **65**: 2214-2231 [*RCA*] [PMID: 39689164 DOI: 10.1021/acs.jcim.4c01966] [FullText]

153 **Chen YM**, Hsiao TH, Lin CH, Fann YC. Unlocking precision medicine: clinical applications of integrating health records, genetics, and immunology through artificial intelligence. *J Biomed Sci* 2025; **32**: 16 [*RCA*] [PMID: 39915780 DOI: 10.1186/s12929-024-01110-w] [Full Text] [Full Text(PDF)]

154 **Zaretsky J**, Kim JM, Baskharoun S, Zhao Y, Austrian J, Aphinyanaphongs Y, Gupta R, Blecker SB, Feldman J. Generative Artificial Intelligence to Transform Inpatient Discharge Summaries to Patient-Friendly Language and Format. *JAMA Netw Open* 2024; **7**: e240357 [*RCA*] [PMID: 38466307 DOI: 10.1001/jamanetworkopen.2024.0357] [FullText] [Full Text(PDF)]

155 **Park D**, So K, Prabhakar SK, Kim C, Lee JJ, Sohn JH, Kim JH, Lee SH, Won DO. Early warning score and feasible complementary approach using artificial intelligence-based bio-signal monitoring system: a review. *Biomed Eng Lett* 2025; **15**: 717-734 [*RCA*] [PMID: 40621610 DOI: 10.1007/s13534-025-00486-4] [FullText] [Full Text(PDF)]

156 **Tripathi P**. Will 2025 mark the beginning of practically useful quantum computers? Feb 10, 2025. [cited 3 September 2025]. Available from: https://www.orfonline.org/expert-speak/will-2025-mark-the-beginning-of-practically-useful-quantum-computers

157 **McKee A**. Large Concept Models: A Guide With Examples. Feb 21, 2025. [cited 3 September 2025]. Available from: https://www.datacamp.com/blog/large-concept-models

158 **Chintu C**, Mudenda V, Lucas S, Nunn A, Lishimpi K, Maswahu D, Kasolo F, Mwaba P, Bhat G, Terunuma H, Zumla A; UNZA-UCLMS Project Paediatric Post-mortem Study Group. Lung diseases at necropsy in African children dying from respiratory illnesses: a descriptive necropsy study. *Lancet* 2002; **360**: 985-990 [*RCA*] [PMID: 12383668 DOI: 10.1016/S0140-6736(02)11082-8] [FullText]

159 **Starke JR**. Childhood tuberculosis: ending the neglect. *Int J Tuberc Lung Dis* 2002; **6**: 373-374 [*RCA*] [PMID: 12019911] [FullText]

160 **Marais BJ**, Gie RP, Schaaf HS, Beyers N, Donald PR, Starke JR. Childhood pulmonary tuberculosis: old wisdom and new challenges. *Am J Respir Crit Care Med* 2006; **173**: 1078-1090 [*RCA*] [PMID: 16484674 DOI: 10.1164/rccm.200511-1809SO] [FullText]

161 **Moore BK**, Graham SM, Nandakumar S, Doyle J, Maloney SA. Pediatric Tuberculosis: A Review of Evidence-Based Best Practices for Clinicians and Health Care Providers. *Pathogens* 2024; **13**: 467 [*RCA*] [PMID: 38921765 DOI: 10.3390/pathogens13060467] [FullText]

162 **George A**, Andronikou S, Pillay T, Goussard P, Zar HJ. Intrathoracic tuberculous lymphadenopathy in children: a guide to chest radiography. *Pediatr Radiol* 2017; **47**: 1277-1282 [*RCA*] [PMID: 29052774 DOI: 10.1007/s00247-017-3890-1] [FullText] [Full Text(PDF)]

163 **Ugas-Charcape CF**, Naidoo J, Sodhi KS. Pediatric Radiology in Resource-Limited Settings. In: Otero HJ, Kaplan SL, Medina LS, Blackmore CC, Applegate KE, editors. Evidence-Based Imaging in Pediatrics. Evidence-Based Imaging. New York: Springer, 2022: 1-12

164 **Karera A**, Davidson F, Engel-Hills P. Operational challenges and collaborative solutions in radiology image interpretation: perspectives from imaging departments in a low-resource setting. *J Med Radiat Sci* 2024; **71**: 564-572 [*RCA*] [PMID: 39087494 DOI: 10.1002/jmrs.815] [Full Text]

165 **Kragsterman P**. How Many Radiologists Are There in the World? Nov 2, 2024. [cited 3 September 2025]. Available from: https://about.cmrad.com/articles/how-many-radiologists-are-there-in-the-world

166 **Coulborn RM**, Panunzi I, Spijker S, Brant WE, Duran LT, Kosack CS, Murowa MM. Feasibility of using teleradiology to improve tuberculosis screening and case management in a district hospital in Malawi. *Bull World Health Organ* 2012; **90**: 705-711 [*RCA*] [PMID: 22984316 DOI: 10.2471/BLT.11.099473] [FullText]

167 **Hwang EJ**, Jeong WG, David PM, Arentz M, Ruhwald M, Yoon SH. AI for Detection of Tuberculosis: Implications for Global Health. *Radiol Artif Intell* 2024; **6**: e230327 [*RCA*] [PMID: 38197795 DOI: 10.1148/ryai.230327] [FullText]

168 **Urbanowski ME**, Ordonez AA, Ruiz-Bedoya CA, Jain SK, Bishai WR. Cavitary tuberculosis: the gateway of disease transmission. *Lancet Infect Dis* 2020; **20**: e117-e128 [*RCA*] [PMID: 32482293 DOI: 10.1016/S1473-3099(20)30148-1] [FullText]

169 **Deshpande SS**, Joshi AR, Shah A. Aftermath of pulmonary tuberculosis: computed tomography assessment. *Pol J Radiol* 2020; **85**: e144-e154 [*RCA*] [PMID: 32322321 DOI: 10.5114/pjr.2020.93714] [FullText] [Full Text(PDF)]

170 **Woodring JH**, Vandiviere HM, Fried AM, Dillon ML, Williams TD, Melvin IG. Update: the radiographic features of pulmonary tuberculosis. *AJR Am J Roentgenol* 1986; **146**: 497-506 [*RCA*] [PMID: 3484866 DOI: 10.2214/ajr.146.3.497] [FullText]

171 **Miller WT**, Miller WT Jr. Tuberculosis in the normal host: radiological findings. *Semin Roentgenol* 1993; **28**: 109-118 [*RCA*] [PMID: 8516687 DOI: 10.1016/s0037-198x(05)80100-2] [FullText]

172 **Chung MJ**, Lee KS, Koh WJ, Kim TS, Kang EY, Kim SM, Kwon OJ, Kim S. Drug-sensitive tuberculosis, multidrug-resistant tuberculosis, and nontuberculous mycobacterial pulmonary disease in nonAIDS adults: comparisons of thin-section CT findings. *Eur Radiol* 2006; **16**: 1934-1941 [*RCA*] [PMID: 16508766 DOI: 10.1007/s00330-006-0174-9] [FullText]

173 **Kim HC**, Goo JM, Lee HJ, Park SH, Park CM, Kim TJ, Im JG. Multidrug-resistant tuberculosis versus drug-sensitive tuberculosis in human

immunodeficiency virus-negative patients: computed tomography features. *J Comput Assist Tomogr* 2004; **28**: 366-371 [*RCA*] [PMID: 15100542 DOI: 10.1097/00004728-200405000-00011] [FullText]

174 **Bhalla AS**, Goyal A, Guleria R, Gupta AK. Chest tuberculosis: Radiological review and imaging recommendations. *Indian J Radiol Imaging* 2015; **25**: 213-225 [*RCA*] [PMID: 26288514 DOI: 10.4103/0971-3026.161431] [FullText] [Full Text(PDF)]

175 **Kim SH**, Shin YM, Yoo JY, Cho JY, Kang H, Lee H, Choe KH, Lee KM, Yang B. Clinical Factors Associated with Cavitary Tuberculosis and Its Treatment Outcomes. *J Pers Med* 2021; **11**: 1081 [*RCA*] [PMID: 34834433 DOI: 10.3390/jpm11111081] [FullText] [Full Text(PDF)]

176 **Saeed W**. Cavitating pulmonary tuberculosis: a global challenge. *Clin Med (Lond)* 2012; **12**: 40-41 [*RCA*] [PMID: 22372219 DOI: 10.7861/clinmedicine.12-1-40] [FullText]

177 **Kim SH**, Min JH, Lee JY. How to Differentiate Inactive from Active Disease in Patients of Primary Multidrug-resistant Tuberculosis with Persistent Cavity after Anti-tuberculous Therapy. *Hong Kong J Radiol* 2014; **17**: 240-246 [*RCA*] [DOI: 10.12809/hkjr1413228] [FullText]

178 **Hermel MB**, Gershon-Cohen J. Healing mechanisms of tuberculous cavities. *Radiology* 1954; **63**: 544-549 [*RCA*] [PMID: 13204615 DOI: 10.1148/63.4.544] [FullText]

179 **Flynn JL**, Chan J. Immunology of tuberculosis. *Annu Rev Immunol* 2001; **19**: 93-129 [*RCA*] [PMID: 11244032 DOI: 10.1146/annurev.immunol.19.1.93] [FullText]

180 **Jayasundera CI**, Attapattu M, Kumarasinghe MP. Atypical presentations of pulmonary tuberculosis diagnosed by fibreoptic bronchoscopy. *Postgrad Med J* 1993; **69**: 621-623 [*RCA*] [PMID: 8234105 DOI: 10.1136/pgmj.69.814.621] [FullText]

181 **Pai M**, Nicol MP, Boehme CC. Tuberculosis Diagnostics: State of the Art and Future Directions. *Microbiol Spectr* 2016; **4** [*RCA*] [PMID: 27763258 DOI: 10.1128/microbiolspec.TBTB2-0019-2016] [FullText]

182 **Saurborn DP**, Fishman JE, Boiselle PM. The imaging spectrum of pulmonary tuberculosis in AIDS. *J Thorac Imaging* 2002; **17**: 28-33 [*RCA*] [PMID: 11828209 DOI: 10.1097/00005382-200201000-00003] [FullText]

183 **Pattamapaspong N**, Kanthawang T, Peh WCG, Hammami N, Bouaziz MC, Ladeb MF. Imaging of thoracic tuberculosis: pulmonary and extrapulmonary. *BJR Open* 2024; **6**: tzae031 [*RCA*] [PMID: 39363908 DOI: 10.1093/bjro/tzae031] [FullText]

184 **Wetscherek MTA**, Sadler TJ, Lee JYJ, Karia S, Babar JL. Active pulmonary tuberculosis: something old, something new, something borrowed, something blue. *Insights Imaging* 2022; **13**: 3 [*RCA*] [PMID: 35001143 DOI: 10.1186/s13244-021-01138-8] [FullText] [Full Text (PDF)]

185 **McAdams HP**, Erasmus J, Winter JA. Radiologic manifestations of pulmonary tuberculosis. *Radiol Clin North Am* 1995; **33**: 655-678 [*RCA*] [PMID: 7610237 DOI: 10.1016/S0033-8389(22)00611-X] [FullText]

186 **Frija G**, Blažić I, Frush DP, Hierath M, Kawooya M, Donoso-Bach L, Brkljačić B. How to improve access to medical imaging in low- and middle-income countries ? *EClinicalMedicine* 2021; **38**: 101034 [*RCA*] [PMID: 34337368 DOI: 10.1016/j.eclinm.2021.101034] [FullText] [Full Text(PDF)]

187 **Arora VK**, Chopra KK. Journey of tuberculosis control in India. *Indian J Tuberc* 2019; **66**: 178-183 [*RCA*] [PMID: 30878065 DOI: 10.1016/j.ijtb.2019.02.002] [FullText]

188 **Memon S**, Bibi S, He G. Integration of AI and ML in Tuberculosis (TB) Management: From Diagnosis to Drug Discovery. *Diseases* 2025; **13**: 184 [*RCA*] [PMID: 40558595 DOI: 10.3390/diseases13060184] [FullText] [Full Text(PDF)]

189 **Liebenberg D**, Gordhan BG, Kana BD. Drug resistant tuberculosis: Implications for transmission, diagnosis, and disease management. *Front Cell Infect Microbiol* 2022; **12**: 943545 [*RCA*] [PMID: 36211964 DOI: 10.3389/fcimb.2022.943545] [FullText] [Full Text(PDF)]

190 **World Health Organization**. Chest radiography in tuberculosis detection – summary of current WHO recommendations and guidance on programmatic approaches. [cited 3 September 2025]. Available from: https://iris.who.int/bitstream/handle/10665/252424/9789241511506-eng.pdf

191 **Ducci F**, Mariotti F, Mencarini J, Fabbri C, Manunta AF, Messeri D, Parronchi P, Blanc P, Bartoloni A. Hemophagocytic Lymphohistiocytosis and Miliary Tuberculosis in an Apparently Immunocompetent Patient: A Case Report. *Infect Dis Rep* 2024; **16**: 763-769 [*RCA*] [PMID: 39195009 DOI: 10.3390/idr16040058] [FullText]

192 **Fauchald T**, Blomberg B, Reikvam H. Tuberculosis-Associated Hemophagocytic Lymphohistiocytosis: A Review of Current Literature. *J Clin Med* 2023; **12**: 5366 [*RCA*] [PMID: 37629407 DOI: 10.3390/jcm12165366] [FullText]

193 **Allen CE**, Yu X, Kozinetz CA, McClain KL. Highly elevated ferritin levels and the diagnosis of hemophagocytic lymphohistiocytosis. *Pediatr Blood Cancer* 2008; **50**: 1227-1235 [*RCA*] [PMID: 18085676 DOI: 10.1002/pbc.21423] [FullText]

194 **Jeon CY**, Murray MB. Diabetes mellitus increases the risk of active tuberculosis: a systematic review of 13 observational studies. *PLoS Med* 2008; **5**: e152 [*RCA*] [PMID: 18630984 DOI: 10.1371/journal.pmed.0050152] [FullText] [Full Text(PDF)]

195 **World Health Organization**. TB and Diabetes. 2021. [cited 3 September 2025]. Available from: https://www.who.int/publications/digital/global-tuberculosis-report-2021/featured-topics/tb-diabetes#

196 **Elkrimi Z**, Rsaissi C, Bijou W, Oukessou Y, Rouadi S, Abada R, Roubal M, Mahtar M. Thyroid tuberculosis associated with papillary microcarcinoma: case report and review of literature. *Ann Med Surg (Lond)* 2023; **85**: 6141-6143 [*RCA*] [PMID: 38098586 DOI: 10.1097/MS9.0000000000001163] [FullText] [Full Text(PDF)]

197 **de Camargo TFO**, Ribeiro GAS, da Silva MCB, da Silva LO, Torres PPTES, Rodrigues DDSDS, de Santos MON, Filho WS, Rosa MEE, Novaes MA, Massarutto TA, Junior OL, Yanata E, Reis MRDC, Szarf G, Netto PVS, de Paiva JPQ. Clinical validation of an artificial intelligence algorithm for classifying tuberculosis and pulmonary findings in chest radiographs. *Front Artif Intell* 2025; **8**: 1512910 [*RCA*] [PMID: 39991462 DOI: 10.3389/frai.2025.1512910] [FullText] [Full Text(PDF)]

198 **Nijiati M**, Ma J, Hu C, Tuersun A, Abulizi A, Kelimu A, Zhang D, Li G, Zou X. Artificial Intelligence Assisting the Early Detection of Active Pulmonary Tuberculosis From Chest X-Rays: A Population-Based Study. *Front Mol Biosci* 2022; **9**: 874475 [*RCA*] [PMID: 35463963 DOI: 10.3389/fmolb.2022.874475] [FullText] [Full Text(PDF)]

199 **Sheller MJ**, Edwards B, Reina GA, Martin J, Pati S, Kotrotsou A, Milchenko M, Xu W, Marcus D, Colen RR, Bakas S. Federated learning in medicine: facilitating multi-institutional collaborations without sharing patient data. *Sci Rep* 2020; **10**: 12598 [*RCA*] [PMID: 32724046 DOI: 10.1038/s41598-020-69250-1] [FullText] [Full Text(PDF)]

200 **Rehman MHU**, Hugo Lopez Pinaya W, Nachev P, Teo JT, Ourselin S, Cardoso MJ. Federated learning for medical imaging radiology. *Br J Radiol* 2023; **96**: 20220890 [*RCA*] [PMID: 38011227 DOI: 10.1259/bjr.20220890] [FullText] [Full Text(PDF)]

201 **Gupta S**, Kumar S, Chang K, Lu C, Singh P, Kalpathy-Cramer J. Collaborative Privacy-preserving Approaches for Distributed Deep Learning Using Multi-Institutional Data. *Radiographics* 2023; **43**: e220107 [*RCA*] [PMID: 36862082 DOI: 10.1148/rg.220107] [FullText]

202 **Kwak L**, Bai H. The Role of Federated Learning Models in Medical Imaging. *Radiol Artif Intell* 2023; **5**: e230136 [*RCA*] [PMID: 37293343

DOI: 10.1148/ryai.230136] [FullText]
203 **Fabila J**, Garrucho L, Campello VM, Martín-Isla C, Lekadir K. Federated learning in low-resource settings: A chest imaging study in Africa -- Challenges and lessons learned. 2025 Preprint. Available from: arXiv: 2505.14217
204 **United States Department of Health and Human Services**. Health Information Privacy – HIPAA for Professionals. July 19, 2024. [cited 3 September 2025]. Available from: https://www.hhs.gov/hipaa/for-professionals/index.html
205 **The European Data Protection Regulation**. General Data Protection Regulation – GDPR. 2018. [cited 3 September 2025]. Available from: https://gdpr-info.eu
206 **Ministry of Law And Justice**. The Digital Personal Data Protection Act, 2023. Aug 11, 2023. [cited 3 September 2025]. Available from: https://www.meity.gov.in/static/uploads/2024/06/2bf1f0e9f04e6fb4f8fef35e82c42aa5.pdf
207 **United States Food and Drug Administration**. Artificial Intelligence-Enabled Device Software Functions: Lifecycle Management and Marketing Submission Recommendations. Jan 7, 2025. [cited 3 September 2025]. Available from: https://www.fda.gov/regulatory-information/search-fda-guidance-documents/artificial-intelligence-enabled-device-software-functions-lifecycle-management-and-marketing
208 **United States Food and Drug Administration**. Artificial Intelligence and Machine Learning in Software as a Medical Device. Mar 25, 2025. [cited 3 September 2025]. Available from: https://www.fda.gov/medical-devices/software-medical-device-samd/artificial-intelligence-and-machine-learning-software-medical-device
209 **European Medicines Agency**. Artificial intelligence workplan to guide use of AI in medicines regulation. Dec 18, 2023. [cited 3 September 2025]. Available from: https://www.ema.europa.eu/en/news/artificial-intelligence-workplan-guide-use-ai-medicines-regulation
210 **Ministry of Health and Family Welfare**. Directorate General of Health Services. [cited 3 September 2025]. Available from: https://www.mohfw.gov.in/?q=en/about-us/directorate-general-health-services/directorate-general-health-services-
211 **Health Level Seven International**. HL7 FHIR in Action: Advancing Interoperability at Civitas 2024. Oct 21, 2024. [cited 3 September 2025]. Available from: https://blog.hl7.org/hl7-fhir-in-action-advancing-interoperability-at-civitas-2024
212 **World Health Organization**. Artificial Intelligence for Health. May 27, 2024. [cited 3 September 2025]. Available from: https://www.who.int/publications/m/item/artificial-intelligence-for-health
213 **Chauhan SB**, Gaur R, Akram A, Singh I. Artificial Intelligence Driven insights for Regulatory Intelligence in Medical Devices: Evaluating EMA, FDA and CDSCO Frameworks. *GlobalCE* 2025; **7**: 11-24 [DOI: 10.31354/globalce.v7i2.210] [FullText]
214 **European Commission**. Laying Down Harmonised Rules On Artificial Intelligence (Artificial Intelligence Act) And Amending Certain Union Legislative Acts. Apr 4, 2021. [cited 3 September 2025]. Available from: https://eur-lex.europa.eu/legal-content/EN/TXT/?uri=CELEX%3A52021PC0206
215 **Mityung**. Large Concept Models: The Future Beyond LLMs. March 17, 2025. [cited 3 September 2025]. Available from: https://www.mityung.com/blog/large-concept-models-the-future-beyond-llms
216 **Singh A**. Insights of Meta's Architecture Large Concept Models (LCM) for Elevation of AI Capabilities [DOI: 10.2139/ssrn.5178251] [FullText]
217 **Bhatnagar A**. LCMs: a Paradigm Shift in AI Reasoning. May 14, 2025. [cited 3 September 2025]. Available from: https://www.infoq.com/articles/lcm-paradigm-shift-ai-reasoning/
218 **Amiri A**. Japan Reveals New Quantum Monster Shattering Limits With 4X the Power. April 27, 2025. [cited 3 September 2025]. Available from: https://dailygalaxy.com/2025/04/japan-reveals-new-quantum-computer-shattering-limits-4x-power/
219 **Dinoo H**. Quantum Physics Shaken as Researchers Reveal Hidden Exotic States in Never-Before-Seen Twisted Materials. Apr 25, 2025. [cited 3 September 2025]. Available from: https://www.sustainability-times.com/in-depth/quantum-physics-shaken-as-researchers-reveal-hidden-exotic-states-in-never-before-seen-twisted-materials/
220 **Fitchard K**. Topological quantum computing: The quest for a quality qubit. Feb 4, 2025. [cited 3 September 2025]. Available from: https://www.nokia.com/blog/topological-quantum-computing-the-quest-for-a-quality-qubit/
221 **Suvvari TK**, Konakanchi VSBP, Muppavarapu RS, Arigapudi N. The Potential Role of Quantum Computing in Biomedicine and Healthcare: The Next Frontier Beyond Artificial Intelligence. *Cureus* 2025; **17**: e82759 [*RCA*] [PMID: 40406784 DOI: 10.7759/cureus.82759] [FullText] [Full Text(PDF)]
222 **Rafalski K**. AGI vs ASI: Understanding the fundamental differences between artificial general intelligence and artificial superintelligence. Sep 9, 2025. [cited 10 September 2025]. Available from: https://www.netguru.com/blog/agi-vs-asi
223 **Viva Technology**. How Quantum Computing Will Impact AI in the Next 10 Years. Aug 1, 2025. [cited 3 September 2025]. Available from: https://vivatechnology.com/news/how-quantum-computing-will-impact-ai-in-the-next-10-years
224 **Quantum Zeitgeist**. Artificial General Intelligence and Quantum Computing. June 14, 2024. [cited 3 September 2025]. Available from: https://quantumzeitgeist.com/agi-and-mainstream-quantum-computing/
225 **Wins Solutions**. 7 Ways Artificial Superintelligence Could Transform Sustainability. [cited 3 September 2025]. Available from: https://www.winssolutions.org/artificial-superintelligence-sustainability/#:~:text=With%20unmatched%20data-processing%20capabilities%2C%20Artificial%20Superintelligence%20can%20optimize,change%2C%20preserve%20ecosystems%2C%20and%20build%20more%20efficient%20economies
226 **Kokotajlo D**, Alexander S, Larsen T, Lifland E, Dean R. AI 2027: Predictive scenario and analysis of superhuman artificial intelligence development and its global impact over the next decade. [cited 3 September 2025]. Available from: https://ai-2027.com/
227 **Lee CM**, Vlamis K. The godfather of AI has a tip for surviving the age of AI: Train it to act like your mom. [cited 3 September 2025]. Available from: https://www.businessinsider.com/godfather-of-ai-maternal-instincts-humanity-survival-geoffrey-hinton-2025-8
228 **Prabhakar AV**. Large Concept Models and Advanced AI Frontiers: Conceptualizing Infraspace and Beyond. Jan 5, 2025. [cited 3 September 2025]. Available from: https://ajithp.com/2025/01/05/large-concept-model-lcm-redefining-language-understanding-with-multilingual-and-modality-agnostic-ai/
229 **Laura M**. Neither Artificial Intelligence nor Computers – Scientists Discover Human Brain Outperforms Technology in Quantum Processing. April 3, 2025. [cited 3 September 2025]. Available from: https://unionrayo.com/en/human-body-outperforms-quantum-computers/
230 **Dickstein DP**. Editorial: It's Difficult To Make Predictions, Especially About the Future: Risk Calculators Come of Age in Child Psychiatry. *J Am Acad Child Adolesc Psychiatry* 2021; **60**: 950-951 [*RCA*] [PMID: 33383160 DOI: 10.1016/j.jaac.2020.12.029] [FullText]
231 **Gohd C**. Hologram doctors beamed to space station to visit astronauts. April 19, 2022. [cited 3 September 2025]. Available from: https://www.space.com/hologram-doctor-space-station-nasa-astronauts.
232 **Seuss G**. Oh, the Thinks You Can Think! New York: Random House Books for Young Readers, 1975

233 **Janssen M**, Renn J. Arch and scaffold: How Einstein found his field equations. *Phys Today* 2015; **68**: 30-36 [DOI: 10.1063/pt.3.2979] [Full Text]
234 **Walters S**. How Einstein got his field equations. 2016 Preprint. Available from: arXiv: 1608.05752 [DOI: 10.48550/arXiv.1608.05752] [Full Text]
235 **Mudgal KS**, Das N. The ethical adoption of artificial intelligence in radiology. *BJR Open* 2020; **2**: 20190020 [*RCA*] [PMID: 33178959 DOI: 10.1259/bjro.20190020] [FullText] [Full Text(PDF)]
236 **RamSoft**. Radiologists and AI: Evolving roles in modern healthcare. June 30, 2025. [cited 3 September 2025]. Available from: https://www.ramsoft.com/blog/radiology-opinion-on-ai
237 **Clarke AC**. Profiles of the Future: An Inquiry into the Limits of the Possible. New York: Harper and Row, 1973

World Journal of Radiology

Submit a Manuscript: https://www.f6publishing.com

World J Radiol 2025 November 28; 17(11): 112638

DOI: 10.4329/wjr.v17.i11.112638

ISSN 1949-8470 (online)

MINIREVIEWS

Advancements and challenges of ultrasound imaging in the management of thyroid-associated ophthalmopathy

Ju-Feng Shi, Wei-Yi Zhou, Hong-Xi Zhang, Ya Shen, Hang Zhang, Tuo Li

Specialty type: Radiology, nuclear medicine and medical imaging

Provenance and peer review: Unsolicited article; Externally peer reviewed.

Peer-review model: Single blind

Peer-review report's classification

Scientific Quality: Grade C, Grade C

Novelty: Grade C, Grade C

Creativity or Innovation: Grade C, Grade C

Scientific Significance: Grade C, Grade C

P-Reviewer: Ding Y, PhD, China

Received: August 4, 2025

Revised: August 29, 2025

Accepted: October 31, 2025

Published online: November 28, 2025

Processing time: 116 Days and 23.1 Hours

Ju-Feng Shi, Wei-Yi Zhou, Hong-Xi Zhang, Tuo Li, Department of Endocrinology, Shanghai Changzheng Hospital, Shanghai 200433, China

Ya Shen, Department of Ophthalmology, Shanghai Changzheng Hospital, Shanghai 200433, China

Hang Zhang, Department of Ultrasound Medicine, Shanghai Changzheng Hospital, Shanghai 200433, China

Co-first authors: Ju-Feng Shi and Wei-Yi Zhou.

Co-corresponding authors: Hang Zhang and Tuo Li.

Corresponding author: Tuo Li, MD, Professor, Department of Endocrinology, Shanghai Changzheng Hospital, No. 415 Fengyang Road, Shanghai 200433, China.
dr.lituo@smmu.edu.cn

Abstract

Thyroid-associated ophthalmopathy (TAO), an autoimmune disorder closely associated with thyroid dysfunction, requires timely diagnosis and ongoing accurate evaluation to improve patient outcomes. With the global incidence of TAO increasing and significantly affecting the quality of life of patients, there is an urgent need for effective diagnostic tools. As a noninvasive imaging technique, ultrasound plays a pivotal role in diagnosing and managing TAO, particularly in the early detection of and monitoring of disease progression. Despite its advantages, ultrasound faces challenges such as limited resolution for deep orbital structures and a lack of standardized protocols, which can lead to diagnostic inaccuracies. This paper reviews the current status of ultrasound applications in TAO, including diagnostic utility, recent technological advances, and key challenges. It proposes strategies for future research and improvement, emphasizing analysis of ultrasound imaging data to develop biomarker stratification models. We propose an integrated multimodal framework that combines ultrasound elastography with deep learning to improve diagnostic precision.

Key Words: Thyroid; Ophthalmopathy; Ultrasound imaging; Imaging; Diagnostics

©The Author(s) 2025. Published by Baishideng Publishing Group Inc. All rights reserved.

Core Tip: Thyroid-associated ophthalmopathy, an autoimmune disorder linked to thyroid dysfunction, needs timely diagnosis. Ultrasound, a noninvasive tool, aids thyroid-associated ophthalmopathy diagnosis/management but has limitations. This minireview proposes future research strategies that emphasize analysis of ultrasound data to develop biomarker models. We propose an integrated multimodal framework combining ultrasound elastography with deep learning to enhance diagnostic precision.

Citation: Shi JF, Zhou WY, Zhang HX, Shen Y, Zhang H, Li T. Advancements and challenges of ultrasound imaging in the management of thyroid-associated ophthalmopathy. *World J Radiol* 2025; 17(11): 112638
URL: https://www.wjgnet.com/1949-8470/full/v17/i11/112638.htm
DOI: https://dx.doi.org/10.4329/wjr.v17.i11.112638

INTRODUCTION

Thyroid-associated ophthalmopathy (TAO), a condition closely linked to Graves' disease, presents significant diagnostic and management challenges. With rising incidence rates and substantial impact on quality of life, early and accurate diagnosis is critical. Current diagnostic approaches rely on clinical evaluation and imaging modalities such as computed tomography (CT) and magnetic resonance imaging (MRI), which have limitations, including radiation exposure and high cost. Ultrasound has emerged as a preferred alternative because of its accessibility, noninvasiveness, and real-time monitoring capabilities. However, its utility in TAO is constrained by limited resolution for deep orbital structures, a lack of standardized protocols that introduce inter-center variability, and operator dependence. In this manuscript, we examine how emerging technologies, including ultrasound elastography and artificial intelligence (AI)-driven analysis, can address these limitations. We highlight the unique advantages of ultrasound in assessing disease activity and severity, and propose strategies to standardize protocols and enhance diagnostic precision for personalized TAO management. These strategies form the basis of the diagnostic framework detailed in subsequent sections.

HIERARCHICAL ULTRASONOGRAPHY IN DIAGNOSIS AND STRATIFIED MANAGEMENT OF TAO

Standardization of morphometric evaluation protocols

Ultrasound imaging is essential for the morphological evaluation of TAO, chiefly by measuring standardized parameters such as extraocular muscle thickness, the anteroposterior diameter of the lacrimal gland, and optic nerve sheath diameter (ONSD). Research has shown that extraocular muscle thickness is significantly increased in individuals diagnosed with TAO and strongly correlates with disease activity[1-3]. During the active phase of TAO, enlargement and thickening of the ocular muscles are primarily driven by inflammatory processes, particularly affecting the extraocular muscles[4]. This thickening, together with the proliferation of retro-orbital adipose tissue, is a major contributor to proptosis observed in TAO patients[4]. Evidence indicates that extraocular muscle thickness is markedly greater during the active phase, with the inferior rectus muscle exhibiting particularly pronounced thickening compared with the inactive phase[3]. Consequently, regular assessment of inferior rectus muscle thickness is crucial for monitoring disease progression and evaluating treatment effectiveness. Ultrasound, a noninvasive imaging modality, can accurately quantify inferior rectus muscle thickness, and its results correlate positively with MRI, thereby aiding early diagnosis and ongoing treatment assessment[5].

Furthermore, the establishment of standardized measurement protocols and consistent ultrasound techniques is essential to ensure comparability of findings across medical facilities. Integrating ultrasound with other imaging techniques, such as MRI, can yield a more comprehensive assessment of extraocular muscle condition in patients with TAO[6-8]. In patients with TAO, the condition of the optic nerve is crucial for preserving visual function[9-11]. Measurement of ONSD is an effective method for evaluating optic nerve compression, particularly in TAO, where compression is often caused by inflammation or orbital swelling, leading to enlargement of the extraocular muscles[4,12]. An increase in ONSD may indicate potential compression. Increased ONSD is associated with pathological changes of the orbit, and ultrasound measurement of ONSD is noninvasive and cost-effective, enabling physicians to determine whether the optic nerve is compressed and to correlate this finding with clinical symptoms[13]. In patients presenting with vision loss or blindness, ultrasound can be used to assess the extent of optic nerve damage.

Lacrimal gland volume is a key indicator for assessing tear-secretion function. In patients with TAO, increased volume may indicate an active disease phase[14]. Lacrimal gland function is affected by fluctuations in thyroid hormone levels, and swelling or dysfunction can exacerbate dry eye symptoms. Both ultrasonography and MRI are effective for quantifying lacrimal gland volume. Changes in volume correlate closely with TAO activity; patients with active disease typically have larger volumes[14-16]. Incorporating lacrimal gland volume with other clinical parameters can provide a comprehensive assessment of tear-secretion function in TAO and support timely intervention.

Three-dimensional ultrasound reconstruction is a promising advance in medical imaging. This technique collects multi-angle data from two-dimensional ultrasound images and uses computational algorithms to reconstruct three-dimensional anatomical structures, thereby improving the precision of volume measurements. The technology provides

comprehensive anatomical insights that clarify lesion spatial relationships. Its noninvasive nature and real-time capability are particularly valuable for evaluating ocular diseases[17]. Compared with conventional imaging modalities, three-dimensional ultrasound offers detailed structural information without tissue damage, which is essential for early diagnosis and for recurrent preoperative evaluation of gallbladder disorders, uterine pathologies, and ocular conditions [18-20]. Moreover, this technology can facilitate foreign-body extraction from favorable positions and support decompression surgery in patients with TAO[21]. The real-time imaging feature enables clinicians to monitor dynamic lesion changes instantaneously, thereby improving diagnostic accuracy and supporting timely treatment decisions. With ongoing technological progress, three-dimensional ultrasound is expected to open new avenues for early diagnosis and management of TAO.

Functional ultrasound biomarkers in TAO

In functional imaging, combining the Doppler blood flow grading system with elastography stiffness thresholds provides new insights for early detection of TAO. Notably, the Adler scoring Doppler blood flow grading system, originally developed for assessing blood flow in breast cancer[22], is now widely applied across conditions, including liver cancer, cervical cancer, renal cancer, rheumatoid arthritis, white matter lesions in sickle cell disease, and carpal tunnel syndrome [23-32]. It can also evaluate microcirculatory effects in patients with coronary artery disease and chronic heart failure after surgery and endovascular myocardial revascularization[33].

Consequently, this system may effectively assess blood flow in extraocular muscles. Studies report significantly increased blood flow in extraocular muscles in patients with TAO, closely correlating with inflammatory activity[34]. Elastography stiffness thresholds also offer new opportunities for early diagnosis of TAO. Elastography is a noninvasive imaging technique that evaluates lesions by measuring tissue stiffness, with results closely linked to pathological conditions such as fibrosis and tumors[35-37]. This technique is broadly divided into two types: Strain elastography, which provides qualitative stiffness assessments[35], and shear wave elastography, which provides quantitative stiffness values[38]. Research indicates that ultrasound shear wave elastography and perfusion measurements can serve as biomarkers for tumor response[39]. For conditions requiring long-term follow-up, such as tumors, fatty liver disease, and liver cirrhosis, this technology confers notable advantages[36,39-44]. Studies show that ultrasound findings in patients with TAO may correlate positively with fibrosis, providing important evidence for assessing the degree of fibrosis in this population[45]. The primary multidisciplinary clinical applications of the Adler-Doppler blood flow grading system are detailed in Table 1.

How to overcome he challenges faced by ultrasound

More recently, advances in high-frequency probes have improved resolution, enabling measurement of extraocular muscle thickness and detection of orbital changes in real time[46]. Ultrasound is increasingly recognized for its clinical utility in monitoring disease activity and guiding management decisions. Nevertheless, broader adoption of ultrasound in TAO remains limited by several intrinsic factors, including inadequate resolution for deep orbital structures[47], a lack of standardized acquisition protocols that lead to between-center variability[48], and high operator dependence that reduces reproducibility[49].

Recent technological progress offers opportunities to address these shortcomings. Ultrasound elastography enables quantitative assessment of tissue stiffness, potentially distinguishing active inflammatory changes from chronic fibrosis [35,38]. Moreover, advances in AI and machine learning have opened new avenues for automated image analysis, reducing operator dependence and improving diagnostic consistency[50-52]. These developments may expand the role of ultrasound from a supplementary tool to a central modality for diagnosis, staging, and longitudinal monitoring of TAO.

ULTRASOUND IN TAO PATHOMECHANISMS: KEY CONTRIBUTIONS

Dynamic monitoring of inflammatory activity

The inflammatory reaction in TAO is a core component of the pathogenic mechanism. Initially, abnormal thyroid hormone levels and autoimmune responses lead to infiltration of inflammatory cells in the orbit, consisting primarily of CD4+ T cells and monocytes/macrophages. Subsequently, thyroid-stimulating hormone receptor and insulin-like growth factor-1 synergistically promote fibroblast proliferation and differentiation into adipocytes, resulting in expansion of adipose tissue within extraocular muscles and other orbital fat and connective tissues. In addition, the ability of orbital fibroblasts to synthesize hydrophilic glycosaminoglycans, predominantly hyaluronic acid, increases, contributing to edema and further expansion of orbital tissues[53,54]. Research indicates that severe active TAO is significantly associated with infiltration of CD4+ T cells and monocytes/macrophages[55,56]. The Clinical Activity Score correlates positively with the degree of lymphocyte infiltration (including total lymphocytes, T cells, and B cells) and macrophages [57-59]. Monitoring inflammatory activity can be facilitated by imaging modalities such as ultrasound, which helps determine whether the disease is in an active phase[47]. Furthermore, ultrasound plays a crucial role in evaluating inflammatory biomarkers. Vascular endothelial growth factor (VEGF) is critical for maintaining physiological vascular homeostasis across diverse cell types and tissues. It has been implicated in the molecular mechanisms underlying tumor growth and metastasis, as well as in retinal disorders linked to several blinding conditions, such as age-related macular degeneration and diabetic and hypertensive retinopathy. Pathogenic effects associated with VEGF are primarily due to its role in modulating vascular permeability and promoting neovascularization[60]. Research indicates increased vascular density in acute TAO compared with chronic TAO and control orbital fat, suggesting an angiogenic response. This pro-angiogenic and pro-lymphangiogenic microenvironment may result from heightened expression of VEGF receptors,

Table 1 Multidisciplinary clinical applications of the Adler-Doppler blood flow grading system[1]

Classification	Application	Implications in TAO
Origin research	Evaluating tumor vascularity in breast cancer[43]	Basis for grading orbital inflammation
Cross-disease validation	Hemodynamic assessment in oncology (liver, cervical, renal cancers)[44-53]	Adapted for TAO microcirculation monitoring
Cardiovascular surgery	Microcirculation evaluation in CVD post-revascularization[54]	Potential for assessing TAO-related ischemia
TAO specific validation	Detection of inflammatory-driven blood flow changes in extraocular muscles[69]	Correlates with disease activity and fibrosis

[1]The Adler-Doppler blood flow grading system demonstrates extensive clinical utility across multiple disciplines. Originally developed for evaluating tumor vascularity in breast cancer, this imaging modality has been validated in hemodynamic assessments of hepatic, cervical, cardiovascular interventions and renal malignancies. Recent thyroid-associated ophthalmopathy-specific investigations reveal its capability to detect inflammatory-driven blood flow augmentation in extraocular muscles.
TAO: Thyroid-associated ophthalmopathy; CVD: Cardiovascular disease.

including VEGFR-2, VEGF-A, VEGF-C, and VEGF-D. These observations suggest that periorbital edema in acute TAO may be partially driven by immature blood vessels and lymphatic capillaries with insufficient functional capacity to adequately drain the stroma[61]. Numerous studies also indicate that ultrasound can be used to evaluate abnormal blood flow. Using techniques such as color Doppler imaging and pulsed Doppler mode, together with advances in nanoparticle technology, ultrasound can quantitatively assess hemodynamic alterations in ocular tissues, thereby providing insights into VEGF expression levels and facilitating evaluation of the inflammatory response[61-63].

The advantages of ultrasound for evaluating inflammation and associated biomarkers derive from its noninvasive nature, real-time capability, and cost-effectiveness. In monitoring patients with Crohn's disease, ultrasound can assess structural alterations within the intestine while simultaneously evaluating disease activity and treatment effectiveness by comparing dynamic changes in inflammatory markers[62]. This multifaceted approach establishes ultrasound as a valuable tool that offers immediate feedback in the management of inflammatory conditions such as TAO. Dynamic monitoring is also a major application of ultrasound in assessing inflammatory response. By performing routine ultrasound examinations alongside biomarker assessments, clinicians can achieve a comprehensive evaluation of fluctuations in the inflammatory status of the patient, facilitating timely treatment modifications. This dynamic monitoring enhances the efficiency of disease management and markedly improves patient outcomes. For example, in the management of inflammatory bowel disease, ultrasound can provide objective data on disease activity even in the absence of clinical symptoms, thereby reducing unnecessary invasive procedures[63]. The clinical importance of dynamic monitoring is evident in evaluating treatment response. During active treatment, hormone therapies and monoclonal antibodies are frequently used. Ultrasound offers real-time feedback on the patient's response to these medications, aiding clinicians in assessing treatment efficacy. In patients receiving biologic agents for Crohn's disease, ultrasound can track changes in intestinal wall thickness and blood flow, enabling prompt assessment of treatment outcomes and guiding subsequent therapeutic decisions[64]. These real-time feedback capabilities position ultrasound as an essential tool for managing inflammatory diseases.

Assessment of fibrosis progression

During the inactive phase of TAO, common pathological alterations include adipose tissue hyperplasia, increased synthesis of hyaluronic acid, and conversion of fibroblasts into myofibroblasts, which ultimately leads to tissue fibrosis. These changes are primarily driven by interactions among T cells, B cells, and orbital fibroblasts[53,54,65]. The fibrotic stage is characterized by irreversible structural damage, with symptoms frequently associated with mechanical compression and increased tissue stiffness. Timely identification of the transition from the active to the fibrotic phase is essential for mitigating long-term complications, enhancing prognosis, and improving quality of life for patients. Research indicates that applying color Doppler to assess blood flow parameters in the ophthalmic artery, superior ophthalmic vein, and central retinal artery may aid in differentiating between the active and inactive phases of TAO. Patients with a Clinical Activity Score of 3 or higher (indicative of the active phase) demonstrate significantly elevated arterial Doppler parameters, including peak systolic velocity and end diastolic velocity of the ophthalmic artery, as well as peak systolic velocity of the central retinal artery, whereas the maximum velocity of the superior ophthalmic vein shows a significant decrease, suggesting ongoing inflammatory activity within the orbit[66]. However, the observed increase in arterial blood flow velocity may also reflect a secondary response to intraorbital inflammation from diverse etiologies[67]. As noted above, strain elastography qualitatively assesses tissue stiffness[35], whereas shear wave elastography quantitatively evaluates fibrosis status[38]. In patients with chronic liver disease, routine ultrasound examinations facilitate monitoring of liver fibrosis progression and treatment efficacy[68]. Evidence suggests that regular ultrasound assessments significantly improve early detection of liver fibrosis progression and inform treatment decisions. Clinicians can more thoroughly evaluate hepatic changes by combining elastography (for stiffness) with B-mode ultrasound (for anatomy)[69]. At the molecular level, transforming growth factor beta 1 (TGF-β1) is a key biomarker related to fibrosis. It plays a critical role in its development[70,71].

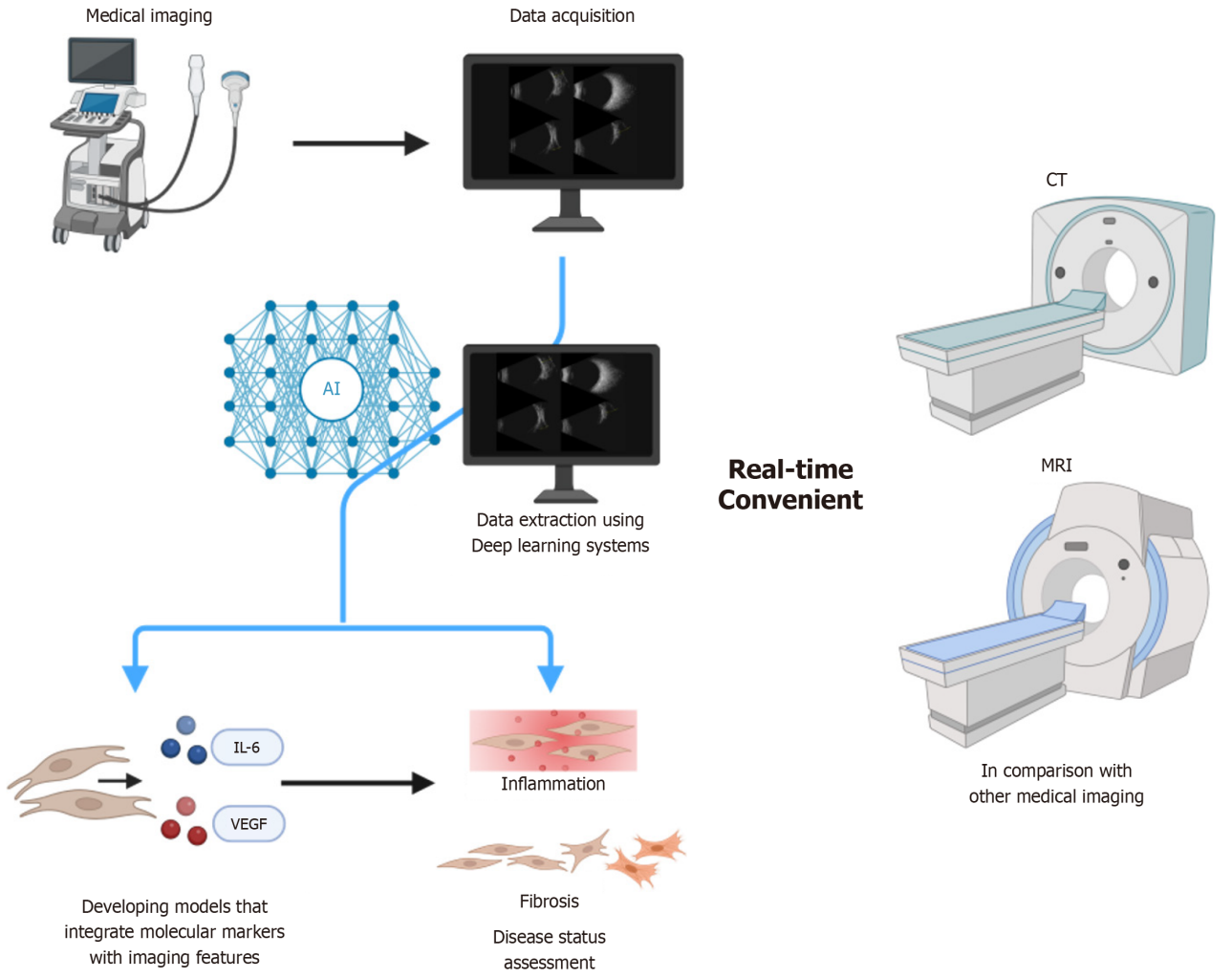


Figure 1 Artificial intelligence-assisted ultrasound diagnostic schematic diagram. Ocular ultrasound combined with deep learning and other artificial intelligence technologies can extract a large amount of imaging data, and construct predictive models by integrating molecular markers such as vascular endothelial growth factor and interleukin-6 to assess the disease status of thyroid-associated ophthalmopathy. Deep learning processes ultrasound data alongside vascular endothelial growth factor/interleukin-6 levels to predict disease severity. This is more real-time and convenient compared to other imaging methods such as computed tomography and magnetic resonance imaging. AI: Artificial Intelligence; VEGF: Vascular endothelial growth factor; IL: Interleukin; CT: Computed tomography; MRI: Magnetic resonance imaging.

Numerous studies have established a significant correlation between elevated serum TGF-β1 levels and fibrosis severity, indicating its potential utility in fibrosis assessment[72,73]. Therefore, combining elastography with TGF-β1 detection may provide more precise information for early diagnosis and evaluation of TAO-related fibrosis. In addition, long-term follow-up should incorporate clinical manifestations of patients and biochemical indicators to formulate personalized management plans, thereby improving outcomes and enhancing quality of life for patients. Establishing a multidisciplinary collaborative team that integrates ultrasound technology with other imaging modalities, such as MRI, can facilitate dynamic monitoring and assessment of fibrosis progression, ensuring optimal treatment and care[74].

INNOVATIONS IN CLINICAL TRANSLATION GUIDED BY ULTRASOUND

Ultrasound imaging provides real-time guidance for muscle monitoring, injections, and treatment assessment. However, challenges remain in visualizing deep orbital structures and in standardizing protocols, which limit diagnostic consistency. Future progress will require enhanced resolution, unified criteria, and integration of nanotechnology and AI to transform ultrasound into a dynamic platform for stratified therapies. This evolution will bridge precision medicine with the complexity of TAO, paving the way for personalized management and improved outcomes. This roadmap (Figure 1) positions ultrasound as a central platform for precision management of TAO and may reduce healthcare costs by 30%-40% compared with current imaging paradigms.

Comparison of clinical applications of ultrasound and CT/MRI in the diagnosis of TAO

Current diagnostic approaches rely primarily on clinical evaluation and radiologic imaging. CT was widely adopted for delineating extraocular muscle enlargement and bony anatomy; however, concerns about radiation exposure limit

repeated use[75]. MRI subsequently emerged as a superior tool for soft-tissue assessment, enabling visualization of orbital inflammation and disease activity[76-78]. Despite these advantages, CT and MRI are costly, less accessible for routine follow-up, involve radiation exposure (for CT), and are impractical for dynamic monitoring. Drawing on research evidence for imaging techniques in TAO, this article analyzes key characteristics of three modalities, ultrasound, CT, and MRI, from the perspectives of technical parameters and comparative medicine. Evidence derived from nine core papers (data as of 2023) focuses on six dimensions: Spatial resolution, hemodynamic evaluation, disease activity staging, bone structure evaluation, cost and accessibility, and safety. Key comparisons are outlined in Table 2.

Ultrasound-guided precision interventions

In the future, ultrasound-guided orbital decompression surgery may reduce surgical complications and shorten recovery times. Ultrasound for real-time monitoring of localized drug injections also enhances procedural precision and effectiveness[79-81]. This monitoring increases treatment safety and yields data to inform personalized strategies, thereby improving overall therapeutic efficacy. As a cost-effective and efficient imaging modality, ultrasound provides real-time imaging and is suitable for repeated use to support ongoing assessment of the condition[82]. Weekly ultrasound evaluations can monitor changes in extraocular muscle thickness, guiding adjustments to hormone dosages and ensuring the safety and effectiveness of treatment regimens. This approach promotes greater personalization and accuracy in treatment and contributes to improved patient outcomes.

Convergent innovation: Ultrasound and nanotechnology

In ultrasound medicine, the integration of targeted therapy and nanotechnology is a pivotal research focus, offering innovative strategies for precise management of TAO. Sonodynamic therapy, a leading technology in this field, activates chemical agents (sonosensitizers) through nonthermal ultrasound effects, enabling superior tissue penetration and spatial selectivity. This noninvasive modality has shown significant advantages in oncology[83-85]. Advances in multifunctional nanoparticles have further expanded the potential applications of this technology. These nanoparticles have been designed as targeted drug carriers for tumors, long-acting ultrasound contrast agents, and enhancers of ultrasound-mediated drug delivery, warranting further investigation as potential anticancer agents[86]. In the future, such nanoparticles may serve as targeted carriers for TAO-related inflammatory factors, such as insulin-like growth factor-1R and interleukin-6, facilitate real-time visualization and monitoring of treatment processes as long-acting ultrasound contrast agents, and improve drug permeation across biological barriers through ultrasound-mediated cavitation. Although research on localized nanoparticle drug delivery systems for TAO remains nascent, ongoing advances in ultrasound molecular imaging and responsive nanomaterials offer promising opportunities for developing an ultrasound-guided, nanoparticle-targeted therapy paradigm for TAO.

AI-driven revolution in ultrasound imaging

Intelligent technologies have markedly improved the quality and efficiency of medical care for the diagnosis and treatment of TAO[50-52]. The integration of AI, particularly in imaging, is progressively reshaping conventional medical paradigms. Research demonstrates that deep learning systems can distinguish papilledema, normal optic discs, and various disc abnormalities by analyzing fundus photographs obtained with pharmacological mydriasis. One system achieved an area under the curve of 0.96 [95% confidence interval (CI): 0.95-0.97], with a sensitivity of 96.4% (95%CI: 93.9-98.3) and a specificity of 84.7% (95%CI: 82.3-87.1)[87]. By harnessing deep learning and big data analytics, AI can extract relevant information from extensive imaging datasets, thereby aiding healthcare professionals in making more precise diagnoses of conditions such as coronavirus disease 2019 and solid cancers, as well as in evaluating coronary artery disease[88-94]. The incorporation of AI into ultrasound imaging analysis has significantly enhanced diagnostic accuracy, enabling the detection of subtle lesions with greater precision than traditional methods and thereby reducing risks of misdiagnosis and missed diagnoses. However, variability among models may lead to errors, and a high false-positive rate could necessitate substantial changes in clinical applications[94]. AI also supports the development of personalized treatment plans through data mining, which can improve treatment outcomes and enhance quality of life for patients. Nonetheless, implementation faces challenges related to data quality and quantity; limited case numbers may adversely affect model performance, and difficulties persist in the architectural design of deep learning algorithms for medical imaging. In addition, the "black box" nature of AI reduces transparency in the decision-making process, potentially fostering skepticism among patients and healthcare providers regarding the results. Consequently, improving the interpretability of AI models represents a critical direction for future research[95,96].

CONCLUSION

Ultrasound offers advantages for TAO assessment, but key limitations remain, including resolution, operator dependence, and protocol variability. Recent technological progress offers opportunities to address these shortcomings. Ultrasound elastography enables quantitative assessment of tissue stiffness, potentially distinguishing active inflammatory changes from chronic fibrosis. Advances in AI and machine learning have opened avenues for automated image analysis, reducing operator dependence and improving diagnostic consistency. These developments may expand the role of ultrasound from a supplementary tool to a central modality for the diagnosis, staging, and longitudinal monitoring of TAO. To advance the field, combining 3D ultrasound with shear-wave elastography and microvascular Doppler, developing validated algorithms using multicenter datasets, and establishing imaging-VEGF/interleukin-6 stratification models are essential and promising steps. This tripartite approach positions ultrasound as a cost-effective, radiation-free

Table 2 Comparison of clinical applications of ultrasound and computed tomography/magnetic resonance imaging in the diagnosis of thyroid-associated orbitopathy

Technical dimension	Ultrasound	CT/MRI	Ref.
Spatial resolution	Moderate (can distinguish muscle/fat layers)	High (MRI provides superior muscle texture detail)	[1,76]
Hemodynamic assessment	Superior (real-time Doppler quantification)	Limited (requires contrast-enhanced scanning)	[46,77]
Disease activity staging	Based on hemodynamic + structural dynamics	MRI T2 signal indicates edema	[1]
Bony structure assessment	Cannot visualize bony walls	Essential (preoperative surgical decompression planning)	[76]
Cost and accessibility	Superior (portable equipment)	Higher (especially MRI)	[46,76]
Safety	Superior (non-ionizing, repeatable)	CT radiation risk; MRI metallic contraindications	[46,76]

CT: Computed tomography; MRI: Magnetic resonance imaging.

cornerstone for TAO management, with the potential to reduce healthcare costs in future medicine.

FOOTNOTES

Author contributions: Shi JF and Zhou WY contributed equally as co-first authors; Li T did conceptualization; Shi JF wrote the original draft; Zhou WY and Zhang HX did review and editing; Zhang H and Shen Y did visualization; Zhang H and Li T did supervision and made equal contributions as co-corresponding authors. All authors have read and agreed to the published version of the manuscript.

Supported by National Natural Science Foundation of China, No. 82170858 and No. 82470935.

Conflict-of-interest statement: All the authors report no relevant conflicts of interest for this article.

Open Access: This article is an open-access article that was selected by an in-house editor and fully peer-reviewed by external reviewers. It is distributed in accordance with the Creative Commons Attribution NonCommercial (CC BY-NC 4.0) license, which permits others to distribute, remix, adapt, build upon this work non-commercially, and license their derivative works on different terms, provided the original work is properly cited and the use is non-commercial. See: https://creativecommons.org/Licenses/by-nc/4.0/

Country of origin: China

ORCID number: Tuo Li 0000-0002-6691-7423.

S-Editor: Wu S
L-Editor: A
P-Editor: Lei YY

REFERENCES

1 **Lennerstrand G**, Tian S, Isberg B, Landau Högbeck I, Bolzani R, Tallstedt L, Schworm H. Magnetic resonance imaging and ultrasound measurements of extraocular muscles in thyroid-associated ophthalmopathy at different stages of the disease. *Acta Ophthalmol Scand* 2007; **85**: 192-201 [*RCA*] [PMID: 17305734 DOI: 10.1111/j.1600-0420.2006.00807.x] [FullText]

2 **Han JS**, Seo HS, Lee YH, Lee H, Suh SI, Jeong EK, Sapkota N, Kim KJ. Fractional anisotropy and diffusivity changes in thyroid-associated orbitopathy. *Neuroradiology* 2016; **58**: 1189-1196 [*RCA*] [PMID: 27844093 DOI: 10.1007/s00234-016-1764-0] [FullText]

3 **Stoyanova NS**, Konareva-Kostianeva M, Mitkova-Hristova V, Angelova I. Correlation between Intraocular Pressure and Thickness of Extraocular Muscles, the Severity and Activity of Thyroid-associated Orbitopathy. *Folia Med (Plovdiv)* 2019; **61**: 90-96 [*RCA*] [PMID: 31237847 DOI: 10.2478/folmed-2018-0050] [FullText]

4 **Yang M**, Du BX, Wang YJ, He WM. [Clinical Analysis of 2 170 Cases of Thyroid-Associated Ophthalmopathy Involving Extraocular Muscles]. *Sichuan Da Xue Xue Bao Yi Xue Ban* 2021; **52**: 510-515 [*RCA*] [PMID: 34018373 DOI: 10.12182/20210560507] [FullText]

5 **Karhanova M**, Kovar R, Frysak Z, Sin M, Zapletalova J, Rehak J, Herman M. Correlation between magnetic resonance imaging and ultrasound measurements of eye muscle thickness in thyroid-associated orbitopathy. *Biomed Pap Med Fac Univ Palacky Olomouc Czech Repub* 2015; **159**: 307-312 [*RCA*] [PMID: 24510024 DOI: 10.5507/bp.2014.001] [FullText]

6 **Rodríguez-González N**, Pérez-Rico C, López-Para Giménez R, Arévalo-Serrano J, Del Amo García B, Calzada Domingo L, Flores Ruiz L, Blanco R. [Short-tau inversion-recovery (STIR) sequence magnetic resonance imaging evaluation of orbital structures in Graves' orbitopathy]. *Arch Soc Esp Oftalmol* 2011; **86**: 351-357 [*RCA*] [PMID: 22040641 DOI: 10.1016/j.oftal.2011.06.010] [FullText]

7 **Nagy EV**, Toth J, Kaldi I, Damjanovich J, Mezosi E, Lenkey A, Toth L, Szabo J, Karanyi Z, Leovey A. Graves' ophthalmopathy: eye muscle involvement in patients with diplopia. *Eur J Endocrinol* 2000; **142**: 591-597 [*RCA*] [PMID: 10832104 DOI: 10.1530/eje.0.1420591] [FullText]

8 **Kilicarslan R**, Alkan A, Ilhan MM, Yetis H, Aralasmak A, Tasan E. Graves' ophthalmopathy: the role of diffusion-weighted imaging in detecting involvement of extraocular muscles in early period of disease. *Br J Radiol* 2015; **88**: 20140677 [*RCA*] [PMID: 25525866 DOI: 10.1259/bjr.20140677] [FullText]

9 **Zhang T**, Xiao W, Ye H, Chen R, Mao Y, Yang H. Peripapillary and Macular Vessel Density in Dysthyroid Optic Neuropathy: An Optical Coherence Tomography Angiography Study. *Invest Ophthalmol Vis Sci* 2019; **60**: 1863-1869 [*RCA*] [PMID: 31042792 DOI: 10.1167/iovs.18-25941] [FullText]

10 **Fan X**, Zha X, Wang N, Han Y. Preliminary Study on the Correlation Between Episcleral Venous Pressure and Intraocular Pressure in TAO Patients and Its Clinical Value. *Altern Ther Health Med* 2024; **30**: 522-527 [*RCA*] [PMID: 38401100] [FullText]

11 **Zeng P**, Wang J, Tian P, Peng YY, Liang JQ, Wang M, Zhou SY. Macular and peripapillary optical coherence tomography angiography metrics in thyroid-associated ophthalmopathy with chorioretinal folds. *Photodiagnosis Photodyn Ther* 2023; **42**: 103146 [*RCA*] [PMID: 36210040 DOI: 10.1016/j.pdpdt.2022.103146] [FullText]

12 **Elkady ZIR**, Elwan S, Said AMA, Farweez YAT, Mahdy MMM. Optical Coherence TomographyStudy of peripapillary Nerve Fiber layer ThicknessinThyroid Associated Ophthalmopathy. *QJM, Int J Med* 2020; **113**: hcaa058.007 [DOI: 10.1093/qjmed/hcaa058.007] [FullText]

13 **Sallam A**, Abdelaal Ahmed Mahmoud M Alkhatip A, Kamel MG, Hamza MK, Yassin HM, Hosny H, Younis MI, Ramadan E, Algameel HZ, Abdelhaq M, Abdelkader M, Mills KE, Mohamed H. The Diagnostic Accuracy of Noninvasive Methods to Measure the Intracranial Pressure: A Systematic Review and Meta-analysis. *Anesth Analg* 2021; **132**: 686-695 [*RCA*] [PMID: 32991330 DOI: 10.1213/ANE.0000000000005189] [FullText]

14 **Byun JS**, Moon NJ, Lee JK. Quantitative analysis of orbital soft tissues on computed tomography to assess the activity of thyroid-associated orbitopathy. *Graefes Arch Clin Exp Ophthalmol* 2017; **255**: 413-420 [*RCA*] [PMID: 27838736 DOI: 10.1007/s00417-016-3538-0] [FullText]

15 **Caltabiano C**, Rana K, Beecher MB, Selva D. Radiological measurements of lacrimal gland in thyroid eye disease. *Int Ophthalmol* 2024; **44**: 11 [*RCA*] [PMID: 38319433 DOI: 10.1007/s10792-024-02991-4] [FullText]

16 **Zhao RX**, Shi TT, Luo S, Liu YF, Xin Z, Yang JK. The value of SPECT/CT imaging of lacrimal glands as a means of assessing the activity of Graves' orbitopathy. *Endocr Connect* 2022; **11**: e210590 [*RCA*] [PMID: 35015696 DOI: 10.1530/EC-21-0590] [FullText] [Full Text(PDF)]

17 **Kharlap SI**. [Modern ultrasound methods of examination in clinical ophthalmology. Background problems and future prospects]. *Vestn Ross Akad Med Nauk* 2003; 32-38 [*RCA*] [PMID: 12698887] [FullText]

18 **Pacheco GHAS**, Castro PT, Tonni G, Werner H, Araujo Júnior E. Prenatal diagnosis of duplicated gallbladder: two-dimensional and three-dimensional ultrasound imaging and reconstruction. *Ultrasound Obstet Gynecol* 2025; **66**: 116-119 [*RCA*] [PMID: 39894938 DOI: 10.1002/uog.29173] [FullText]

19 **Alonso L**, Carugno J. Chronic Endometritis: Three-dimensional Ultrasound and Hysteroscopy Correlation. *J Minim Invasive Gynecol* 2020; **27**: 993-994 [*RCA*] [PMID: 31491509 DOI: 10.1016/j.jmig.2019.08.028] [FullText]

20 **Behrendt S**, Rochels R. [Perspectives in diagnosis and therapy of orbital diseases]. *Klin Monbl Augenheilkd* 1994; **204**: 207-210 [*RCA*] [PMID: 8022148 DOI: 10.1055/s-2008-1035518] [FullText]

21 **Li Y**, Wei XL, Pang KK, Ni PJ, Wu M, Xiao J, Zhang LL, Zhang FX. A comparative study on the features of breast sclerosing adenosis and invasive ductal carcinoma *via* ultrasound and establishment of a predictive nomogram. *Front Oncol* 2023; **13**: 1276524 [*RCA*] [PMID: 37936612 DOI: 10.3389/fonc.2023.1276524] [FullText]

22 **Ferreira De Matos C**, Cougoul P, Zaharie OM, Kermorgant M, Pavy-Le Traon A, Gales C, Senard JM, Strumia M, Bonneville F, Nasr N. Cerebrovascular and cardiovascular autonomic regulation in sickle cell patients with white matter lesions. *Eur J Neurol* 2024; **31**: e16183 [*RCA*] [PMID: 38165013 DOI: 10.1111/ene.16183] [FullText]

23 **Kuang X**, Wang H, Chai W, Yuan H, He T, Shi M, Jiang T. Clinical diagnostic value of contrast-enhanced ultrasound combined with microflow imaging in benign and malignant renal tumors: A retrospective cohort study. *Biomol Biomed* 2024; **24**: 1370-1379 [*RCA*] [PMID: 38613844 DOI: 10.17305/bb.2024.10236] [FullText]

24 **Zhang D**, Wang Y, Yang F, Mao Y, Mu J, Zhao L, Xu W. Diagnostic Value of Multi-Mode Ultrasonic Flow Imaging Examination in Solid Renal Tumors of Different Sizes. *J Clin Med* 2023; **12**: 566 [*RCA*] [PMID: 36675494 DOI: 10.3390/jcm12020566] [FullText]

25 **Chen M**, Fu X, Shen Y. Evaluation of Multimode Color Doppler Flow Imaging in the Diagnosis of Solid Renal Tumor. *Contrast Media Mol Imaging* 2021; **2021**: 6656877 [*RCA*] [PMID: 33880110 DOI: 10.1155/2021/6656877] [FullText] [Full Text(PDF)]

26 **Anand AC**, Nandi B, Acharya SK, Arora A, Babu S, Batra Y, Chawla YK, Chowdhury A, Chaoudhuri A, Eapen EC, Devarbhavi H, Dhiman R, Datta Gupta S, Duseja A, Jothimani D, Kapoor D, Kar P, Khuroo MS, Kumar A, Madan K, Mallick B, Maiwall R, Mohan N, Nagral A, Nath P, Panigrahi SC, Pawar A, Philips CA, Prahraj D, Puri P, Rastogi A, Saraswat VA, Saigal S, Shalimar, Shukla A, Singh SP, Verghese T, Wadhawan M; INASL Task-Force on Acute Liver Failure. Indian National Association for the Study of the Liver Consensus Statement on Acute Liver Failure (Part 1): Epidemiology, Pathogenesis, Presentation and Prognosis. *J Clin Exp Hepatol* 2020; **10**: 339-376 [*RCA*] [PMID: 32655238 DOI: 10.1016/j.jceh.2020.04.012] [FullText]

27 **Han H**, Ding H, Ji Z, Zhang W, Wang Q, Wang W. Primary Application of Micro-Flow Imaging Technology in the Diagnosis of Hepatic Tumors. *Ultrasound Med Biol* 2019; **45**: 395-401 [*RCA*] [PMID: 30409471 DOI: 10.1016/j.ultrasmedbio.2018.09.025] [FullText]

28 **Karahan AY**, Arslan S, Ordahan B, Bakdik S, Ekiz T. Superb Microvascular Imaging of the Median Nerve in Carpal Tunnel Syndrome: An Electrodiagnostic and Ultrasonographic Study. *J Ultrasound Med* 2018; **37**: 2855-2861 [*RCA*] [PMID: 29663478 DOI: 10.1002/jum.14645] [FullText]

29 **Yang F**, Zhao J, Liu C, Mao Y, Mu J, Wei X, Jia J, Zhang S, Xin X, Tan J. Superb microvascular imaging technique in depicting vascularity in focal liver lesions: more hypervascular supply patterns were depicted in hepatocellular carcinoma. *Cancer Imaging* 2019; **19**: 92 [*RCA*] [PMID: 31888768 DOI: 10.1186/s40644-019-0277-6] [FullText] [Full Text(PDF)]

30 **Che D**, Yang Z, Wei H, Wang X, Gao J. The Adler grade by Doppler ultrasound is associated with clinical pathology of cervical cancer: Implication for clinical management. *PLoS One* 2020; **15**: e0236725 [*RCA*] [PMID: 32777812 DOI: 10.1371/journal.pone.0236725] [FullText] [Full Text(PDF)]

31 **Kurtulus Ozturk E**, Ozturk S, Kelesoglu Dincer AB. The reliability and validity of superb microvascular imaging as a potential disease activity marker in rheumatoid arthritis. *Ultraschall Med* 2025; **46**: 388-395 [*RCA*] [PMID: 39510536 DOI: 10.1055/a-2463-8297] [FullText]

32 **Kulchitskaya DB**, Shovkun TV, Yarnykh EV, Konchugova TV, Knyazeva TA, Gushchina NV, Chernyakhovsky OB, Kolbakhova SN. [Impact of external counterpulsation on microcirculation in patients with coronary heart disease complicated by chronic heart failure after surgical and endovascular myocardial revascularization]. *Vopr Kurortol Fizioter Lech Fiz Kult* 2019; **96**: 5-10 [*RCA*] [PMID: 31626154 DOI: 10.17116/kurort2019960515] [FullText]

33 **Kurioka Y**, Inaba M, Kawagishi T, Emoto M, Kumeda Y, Inoue Y, Morii H, Nishizawa Y. Increased retinal blood flow in patients with Graves' disease: influence of thyroid function and ophthalmopathy. *Eur J Endocrinol* 2001; **144**: 99-107 [*RCA*] [PMID: 11182745 DOI: 10.1530/eje.0.1440099] [FullText]

34 **Balleyguier C**, Canale S, Ben Hassen W, Vielh P, Bayou EH, Mathieu MC, Uzan C, Bourgier C, Dromain C. Breast elasticity: principles, technique, results: an update and overview of commercially available software. *Eur J Radiol* 2013; **82**: 427-434 [*RCA*] [PMID: 22445593 DOI: 10.1016/j.ejrad.2012.03.001] [FullText]

35 **Yu JH**, Lee HA, Kim SU. Noninvasive imaging biomarkers for liver fibrosis in nonalcoholic fatty liver disease: current and future. *Clin Mol Hepatol* 2023; **29**: S136-S149 [*RCA*] [PMID: 36503205 DOI: 10.3350/cmh.2022.0436] [FullText] [Full Text(PDF)]

36 **Tang A**, Cloutier G, Szeverenyi NM, Sirlin CB. Ultrasound Elastography and MR Elastography for Assessing Liver Fibrosis: Part 1, Principles and Techniques. *AJR Am J Roentgenol* 2015; **205**: 22-32 [*RCA*] [PMID: 25905647 DOI: 10.2214/AJR.15.14552] [FullText] [Full Text(PDF)]

37 **Sarvazyan AP**, Rudenko OV, Swanson SD, Fowlkes JB, Emelianov SY. Shear wave elasticity imaging: a new ultrasonic technology of medical diagnostics. *Ultrasound Med Biol* 1998; **24**: 1419-1435 [*RCA*] [PMID: 10385964 DOI: 10.1016/s0301-5629(98)00110-0] [FullText]

38 **Voutouri C**, Mpekris F, Panagi M, Krolak C, Michael C, Martin JD, Averkiou MA, Stylianopoulos T. Ultrasound stiffness and perfusion markers correlate with tumor volume responses to immunotherapy. *Acta Biomater* 2023; **167**: 121-134 [*RCA*] [PMID: 37321529 DOI: 10.1016/j.actbio.2023.06.007] [FullText]

39 **Huang JX**, Liu FT, Sun L, Ma C, Fu J, Wang XY, Huang GL, Zhang YT, Pei XQ. Comparing shear wave elastography of breast tumors and axillary nodes in the axillary assessment after neoadjuvant chemotherapy in patients with node-positive breast cancer. *Radiol Med* 2024; **129**: 1143-1155 [*RCA*] [PMID: 39060887 DOI: 10.1007/s11547-024-01848-1] [FullText]

40 **Taiji R**, Cortes AC, Zaske AM, Williams M, Dupuis C, Tanaka T, Nishiofuku H, Chintalapani G, Peterson CB, Avritscher R. Liver Cancer Vascularity Driven by Extracellular Matrix Stiffness: Implications for Imaging Research. *Invest Radiol* 2023; **58**: 894-902 [*RCA*] [PMID: 37403975 DOI: 10.1097/RLI.0000000000001001] [FullText]

41 **Ozturk A**, Kumar V, Pierce TT, Li Q, Baikpour M, Rosado-Mendez I, Wang M, Guo P, Schoen S Jr, Gu Y, Dayavansha S, Grajo JR, Samir AE. The Future Is Beyond Bright: The Evolving Role of Quantitative US for Fatty Liver Disease. *Radiology* 2023; **309**: e223146 [*RCA*] [PMID: 37934095 DOI: 10.1148/radiol.223146] [FullText]

42 **Chen CM**, Tang YC, Huang SH, Pan KT, Lui KW, Lai YH, Tsui PH. Ultrasound tissue scatterer distribution imaging: An adjunctive diagnostic tool for shear wave elastography in characterizing focal liver lesions. *Ultrason Sonochem* 2023; **101**: 106716 [*RCA*] [PMID: 38071854 DOI: 10.1016/j.ultsonch.2023.106716] [FullText]

43 **Ferraioli G**, Soares Monteiro LB. Ultrasound-based techniques for the diagnosis of liver steatosis. *World J Gastroenterol* 2019; **25**: 6053-6062 [*RCA*] [PMID: 31686762 DOI: 10.3748/wjg.v25.i40.6053] [FullText] [Full Text(PDF)]

44 **Rajabi MT**, Papageorgiou K, Taban M, Hwang CJ, Hosseini SS, Rajabi MB, Goldberg RA. Ultrasonographic motion analysis of lower eyelid compartments in patients with chronic thyroid associated ophthalmopathy. *J Curr Ophthalmol* 2017; **29**: 310-317 [*RCA*] [PMID: 29270480 DOI: 10.1016/j.joco.2017.07.002] [FullText] [Full Text(PDF)]

45 **Kim MG**, Yoon C, Lim HG. Recent Advancements in High-Frequency Ultrasound Applications from Imaging to Microbeam Stimulation. *Sensors (Basel)* 2024; **24**: 6471 [*RCA*] [PMID: 39409511 DOI: 10.3390/s24196471] [FullText]

46 **Karhanová M**, Čivrný J, Kalitová J, Schovánek J, Malušková M, Hrevuš M, Schreiberová Z. [Ultrasound Examination of the Orbit in Patients With Thyroid- Associated Orbitopathy – Examination Guide and Recommendations for Everyday Practice. A Review]. *Cesk Slov Oftalmol* 2024; **80**: 3-9 [DOI: 10.31348/2023/11] [FullText]

47 **Stegemann E**, Larbig J, Portig I, Weiske N, Bürger T, Stegemann B. Reliability of a Standardized Ultrasound Protocol for the Diagnosis of Thoracic Outlet Syndrome. *Ultraschall Med* 2025 [*RCA*] [PMID: 39993409 DOI: 10.1055/a-2532-4823] [FullText]

48 **Alyami J**, Almutairi FF, Aldoassary S, Albeshry A, Almontashri A, Abounassif M, Alamri M. Interobserver variability in ultrasound assessment of thyroid nodules. *Medicine (Baltimore)* 2022; **101**: e31106 [*RCA*] [PMID: 36254067 DOI: 10.1097/MD.0000000000031106] [FullText] [Full Text(PDF)]

49 **Liu Z**, Tan K, Zhang H, Sun J, Li Y, Fang S, Li J, Song X, Zhou H, Zhai G. CT-based artificial intelligence prediction model for ocular motility score of thyroid eye disease. *Endocrine* 2024; **86**: 1055-1064 [*RCA*] [PMID: 39046593 DOI: 10.1007/s12020-024-03906-0] [FullText]

50 **Lin LY**, Zhou P, Shi M, Lu JE, Jeon S, Kim D, Liu JM, Wang M, Do S, Lee NG. A Deep Learning Model for Screening Computed Tomography Imaging for Thyroid Eye Disease and Compressive Optic Neuropathy. *Ophthalmol Sci* 2024; **4**: 100412 [*RCA*] [PMID: 38046559 DOI: 10.1016/j.xops.2023.100412] [FullText] [Full Text(PDF)]

51 **Ji Y**, Chen N, Liu S, Yan Z, Qian H, Zhu S, Zhang J, Wang M, Jiang Q, Yang W. Research Progress of Artificial Intelligence Image Analysis in Systemic Disease-Related Ophthalmopathy. *Dis Markers* 2022; **2022**: 3406890 [*RCA*] [PMID: 35783011 DOI: 10.1155/2022/3406890] [Full Text] [Full Text(PDF)]

52 **Bahn RS**. Graves' ophthalmopathy. *N Engl J Med* 2010; **362**: 726-738 [*RCA*] [PMID: 20181974 DOI: 10.1056/NEJMra0905750] [FullText]

53 **Lee ACH**, Kahaly GJ. Pathophysiology of thyroid-associated orbitopathy. *Best Pract Res Clin Endocrinol Metab* 2023; **37**: 101620 [*RCA*] [PMID: 35181241 DOI: 10.1016/j.beem.2022.101620] [FullText]

54 **Eckstein AK**, Quadbeck B, Tews S, Mann K, Krüger C, Mohr CH, Steuhl KP, Esser J, Gieseler RK. Thyroid associated ophthalmopathy: evidence for CD4(+) gammadelta T cells; de novo differentiation of RFD7(+) macrophages, but not of RFD1(+) dendritic cells; and loss of gammadelta and alphabeta T cell receptor expression. *Br J Ophthalmol* 2004; **88**: 803-808 [*RCA*] [PMID: 15148216 DOI: 10.1136/bjo.2003.035915] [FullText]

55 **Pawlowski P**, Wawrusiewicz-Kurylonek N, Eckstein A, Reszec J, Luczynski W, Johnson K, Kretowski A, Bakunowicz-Lazarczyk A, Gorska M, Szamatowicz J, Chyczewski L, Mysliwiec J. Disturbances of modulating molecules (FOXP3, CTLA-4/CD28/B7, and CD40/CD40L) mRNA expressions in the orbital tissue from patients with severe graves' ophthalmopathy. *Mediators Inflamm* 2015; **2015**: 340934 [*RCA*] [PMID: 25653477 DOI: 10.1155/2015/340934] [FullText] [Full Text(PDF)]

56 **Rotondo Dottore G**, Torregrossa L, Caturegli P, Ionni I, Sframeli A, Sabini E, Menconi F, Piaggi P, Sellari-Franceschini S, Nardi M, Latrofa F, Vitti P, Marcocci C, Basolo F, Marinò M. Association of T and B Cells Infiltrating Orbital Tissues With Clinical Features of Graves Orbitopathy. *JAMA Ophthalmol* 2018; **136**: 613-619 [*RCA*] [PMID: 29710102 DOI: 10.1001/jamaophthalmol.2018.0806] [FullText]

57 **Rotondo Dottore G**, Torregrossa L, Lanzolla G, Mariotti S, Menconi F, Piaggi P, Cristofani Mencacci L, Posarelli C, Maglionico MN, Dallan I, Figus M, Nardi M, Marcocci C, Basolo F, Marinò M. Role of the mononuclear cell infiltrate in Graves' orbitopathy (GO): results of a large cohort study. *J Endocrinol Invest* 2022; **45**: 563-572 [*RCA*] [PMID: 34671950 DOI: 10.1007/s40618-021-01692-4] [FullText]

58 **Pawlowski P**, Reszec J, Eckstein A, Johnson K, Grzybowski A, Chyczewski L, Mysliwiec J. Markers of inflammation and fibrosis in the

orbital fat/connective tissue of patients with Graves' orbitopathy: clinical implications. *Mediators Inflamm* 2014; **2014**: 412158 [*RCA*] [PMID: 25309050 DOI: 10.1155/2014/412158] [FullText] [Full Text(PDF)]

59 **Apte RS**, Chen DS, Ferrara N. VEGF in Signaling and Disease: Beyond Discovery and Development. *Cell* 2019; **176**: 1248-1264 [*RCA*] [PMID: 30849371 DOI: 10.1016/j.cell.2019.01.021] [FullText]

60 **Wong LL**, Lee NG, Amarnani D, Choi CJ, Bielenberg DR, Freitag SK, D'Amore PA, Kim LA. Orbital Angiogenesis and Lymphangiogenesis in Thyroid Eye Disease: An Analysis of Vascular Growth Factors with Clinical Correlation. *Ophthalmology* 2016; **123**: 2028-2036 [*RCA*] [PMID: 27423310 DOI: 10.1016/j.ophtha.2016.05.052] [FullText]

61 **Barchi A**, Dal Buono A, D'Amico F, Furfaro F, Zilli A, Fiorino G, Parigi TL, Peyrin-Biroulet L, Danese S, Allocca M. Leaving behind the Mucosa: Advances and Future Directions of Intestinal Ultrasound in Ulcerative Colitis. *J Clin Med* 2023; **12**: 7569 [*RCA*] [PMID: 38137644 DOI: 10.3390/jcm12247569] [FullText] [Full Text(PDF)]

62 **Allocca M**, Furfaro F, Fiorino G, Peyrin-Biroulet L, Danese S. Point-of-Care Ultrasound in Inflammatory Bowel Disease. *J Crohns Colitis* 2021; **15**: 143-151 [*RCA*] [PMID: 32674146 DOI: 10.1093/ecco-jcc/jjaa151] [FullText]

63 **Randhawa A**, Guzowski T. Intestinal Ultrasound: Envisioning a New Future for Crohn's Disease Management. *ACG Case Rep J* 2024; **11**: e01511 [*RCA*] [PMID: 39301462 DOI: 10.14309/crj.0000000000001511] [FullText] [Full Text(PDF)]

64 **Buonfiglio F**, Ponto KA, Pfeiffer N, Kahaly GJ, Gericke A. Redox mechanisms in autoimmune thyroid eye disease. *Autoimmun Rev* 2024; **23**: 103534 [*RCA*] [PMID: 38527685 DOI: 10.1016/j.autrev.2024.103534] [FullText]

65 **Yanik B**, Conkbayir I, Acaroglu G, Hekimoglu B. Graves' ophthalmopathy: comparison of the Doppler sonography parameters with the clinical activity score. *J Clin Ultrasound* 2005; **33**: 375-380 [*RCA*] [PMID: 16240428 DOI: 10.1002/jcu.20154] [FullText]

66 **Jianu DC**, Jianu SN, Petrica L, Motoc AG, Dan TF, Lăzureanu DC, Munteanu M. Clinical and color Doppler imaging features of one patient with occult giant cell arteritis presenting arteritic anterior ischemic optic neuropathy. *Rom J Morphol Embryol* 2016; **57**: 579-583 [*RCA*] [PMID: 27516038] [FullText]

67 **Poon C**, Pellow C, Hynynen K. Neutrophil recruitment and leukocyte response following focused ultrasound and microbubble mediated blood-brain barrier treatments. *Theranostics* 2021; **11**: 1655-1671 [*RCA*] [PMID: 33408773 DOI: 10.7150/thno.52710] [FullText] [Full Text(PDF)]

68 **Choi HJ**, Han M, Seo H, Park CY, Lee EH, Park J. The new insight into the inflammatory response following focused ultrasound-mediated blood-brain barrier disruption. *Fluids Barriers CNS* 2022; **19**: 103 [*RCA*] [PMID: 36564820 DOI: 10.1186/s12987-022-00402-3] [FullText] [Full Text(PDF)]

69 **Hess A**, Gentile SD, Ben Saad A, Rahman RU, Habboub T, Pratt DS, Mullen AC. Single-cell transcriptomics stratifies organoid models of metabolic dysfunction-associated steatotic liver disease. *EMBO J* 2023; **42**: e113898 [*RCA*] [PMID: 37962490 DOI: 10.15252/embj.2023113898] [FullText] [Full Text(PDF)]

70 **Moreau JM**, Velegraki M, Bolyard C, Rosenblum MD, Li Z. Transforming growth factor-β1 in regulatory T cell biology. *Sci Immunol* 2022; **7**: eabi4613 [*RCA*] [PMID: 35302863 DOI: 10.1126/sciimmunol.abi4613] [FullText]

71 **Xu MY**, Hu JJ, Shen J, Wang ML, Zhang QQ, Qu Y, Lu LG. Stat3 signaling activation crosslinking of TGF-β1 in hepatic stellate cell exacerbates liver injury and fibrosis. *Biochim Biophys Acta* 2014; **1842**: 2237-2245 [*RCA*] [PMID: 25092172 DOI: 10.1016/j.bbadis.2014.07.025] [FullText]

72 **Song X**, Shi J, Liu J, Liu Y, Yu Y, Qiu Y, Cao Z, Pan Y, Yuan X, Chu Y, Wu D. Recombinant truncated latency-associated peptide alleviates liver fibrosis in vitro and in vivo *via* inhibition of TGF-β/Smad pathway. *Mol Med* 2022; **28**: 80 [*RCA*] [PMID: 35842576 DOI: 10.1186/s10020-022-00508-2] [FullText] [Full Text(PDF)]

73 **Biris AI**, Karamatzanis I, Biri D, Biris IA, Maravegias N. Non-Invasive Ultrasound Diagnostic Techniques for Steatotic Liver Disease and Focal Liver Lesions: 2D, Colour Doppler, 3D, Two-Dimensional Shear Wave Elastography (2D-SWE), and Ultrasound-Guided Attenuation Parameter (UGAP). *Cureus* 2024; **16**: e72087 [*RCA*] [PMID: 39440161 DOI: 10.7759/cureus.72087] [FullText]

74 **Lee KH**, Jang SY, Lee SY, Yoon JS. Graded decompression of orbital fat and wall in patients with Graves' orbitopathy. *Korean J Ophthalmol* 2014; **28**: 1-11 [*RCA*] [PMID: 24505195 DOI: 10.3341/kjo.2014.28.1.1] [FullText] [Full Text(PDF)]

75 **Song Y**, Li T, Tang W, Lv Q, Zhang XX, Zhou WY, Shi YQ. Application progress of magnetic resonance imaging in thyroid associated ophthalmopathy. *Front Endocrinol (Lausanne)* 2025; **16**: 1537957 [*RCA*] [PMID: 40642513 DOI: 10.3389/fendo.2025.1537957] [FullText] [Full Text(PDF)]

76 **Karhanová M**, Čivrný J, Kalitová J, Schovánek J, Pašková B, Schreiberová Z, Hübnerová P. Computed tomography and magnetic resonance imaging of the orbit in the diagnosis and treatment of thyroid-associated orbitopathy - experience from practice. A Review. *Cesk Slov Oftalmol* 2023; **79**: 283-292 [*RCA*] [PMID: 38086700 DOI: 10.31348/2023/10] [FullText]

77 **Yu Y**, Feng T, Qiu H, Gu Y, Chen Q, Zuo C, Ma H. Simultaneous photoacoustic and ultrasound imaging: A review. *Ultrasonics* 2024; **139**: 107277 [*RCA*] [PMID: 38460216 DOI: 10.1016/j.ultras.2024.107277] [FullText]

78 **Cai L**, Hu M, Lin L, Zheng T, Liu J, Li Z. Evaluation of the efficacy of triamcinolone acetonide in the treatment of keloids by high-frequency ultrasound. *Skin Res Technol* 2020; **26**: 489-493 [*RCA*] [PMID: 31793709 DOI: 10.1111/srt.12820] [FullText]

79 **Cool SK**, Geers B, Roels S, Stremersch S, Vanderperren K, Saunders JH, De Smedt SC, Demeester J, Sanders NN. Coupling of drug containing liposomes to microbubbles improves ultrasound triggered drug delivery in mice. *J Control Release* 2013; **172**: 885-893 [*RCA*] [PMID: 24075924 DOI: 10.1016/j.jconrel.2013.09.014] [FullText]

80 **Mlosek RK**, Malinowska S, Woźniak W. Lipoma removal using a high-frequency ultrasound-guided injection of a Class III CE-marked device-Empirical findings. *J Cosmet Dermatol* 2019; **18**: 469-473 [*RCA*] [PMID: 30027646 DOI: 10.1111/jocd.12681] [FullText]

81 **Chee C**, Hibbert EJ, Lam P, Nanan R, Liu A. Sonographic and other nonglycemic factors can predict large-for-gestational-age infants in diet-managed gestational diabetes mellitus: A retrospective cohort study. *J Diabetes* 2020; **12**: 562-572 [*RCA*] [PMID: 32250016 DOI: 10.1111/1753-0407.13042] [FullText]

82 **Bernal A**, Calcagno C, Mulder WJM, Pérez-Medina C. Imaging-guided nanomedicine development. *Curr Opin Chem Biol* 2021; **63**: 78-85 [*RCA*] [PMID: 33735814 DOI: 10.1016/j.cbpa.2021.01.014] [FullText]

83 **Canaparo R**, Foglietta F, Barbero N, Serpe L. The promising interplay between sonodynamic therapy and nanomedicine. *Adv Drug Deliv Rev* 2022; **189**: 114495 [*RCA*] [PMID: 35985374 DOI: 10.1016/j.addr.2022.114495] [FullText]

84 **Ovais M**, Mukherjee S, Pramanik A, Das D, Mukherjee A, Raza A, Chen C. Designing Stimuli-Responsive Upconversion Nanoparticles that Exploit the Tumor Microenvironment. *Adv Mater* 2020; **32**: e2000055 [*RCA*] [PMID: 32227413 DOI: 10.1002/adma.202000055] [FullText]

85 **Rapoport N**, Gao Z, Kennedy A. Multifunctional nanoparticles for combining ultrasonic tumor imaging and targeted chemotherapy. *J Natl Cancer Inst* 2007; **99**: 1095-1106 [*RCA*] [PMID: 17623798 DOI: 10.1093/jnci/djm043] [FullText]

86 **Milea D**, Najjar RP, Zhubo J, Ting D, Vasseneix C, Xu X, Aghsaei Fard M, Fonseca P, Vanikieti K, Lagrèze WA, La Morgia C, Cheung CY, Hamann S, Chiquet C, Sanda N, Yang H, Mejico LJ, Rougier M-B, Kho R, Thi Ha Chau T, Singhal S, Gohier P, Clermont-Vignal C, Cheng C-Y, Jonas JB, Yu-Wai-Man P, Fraser CL, Chen JJ, Ambika S, Miller NR, Liu Y, Newman NJ, Wong TY, Biousse V; BONSAI Group. Artificial Intelligence to Detect Papilledema from Ocular Fundus Photographs. *N Engl J Med* 2020; **382**: 1687-1695 [*RCA*] [PMID: 32286748 DOI: 10.1056/NEJMoa1917130] [FullText]

87 **Rajpurkar P**, Lungren MP. The Current and Future State of AI Interpretation of Medical Images. *N Engl J Med* 2023; **388**: 1981-1990 [*RCA*] [PMID: 37224199 DOI: 10.1056/NEJMra2301725] [FullText]

88 **Freeman K**, Geppert J, Stinton C, Todkill D, Johnson S, Clarke A, Taylor-Phillips S. Use of artificial intelligence for image analysis in breast cancer screening programmes: systematic review of test accuracy. *BMJ* 2021; **374**: n1872 [*RCA*] [PMID: 34470740 DOI: 10.1136/bmj.n1872] [FullText] [Full Text(PDF)]

89 **Forrest IS**, Petrazzini BO, Duffy Á, Park JK, Marquez-Luna C, Jordan DM, Rocheleau G, Cho JH, Rosenson RS, Narula J, Nadkarni GN, Do R. Machine learning-based marker for coronary artery disease: derivation and validation in two longitudinal cohorts. *Lancet* 2023; **401**: 215-225 [*RCA*] [PMID: 36563696 DOI: 10.1016/S0140-6736(22)02079-7] [FullText]

90 **Batra P**, Khera AV. Machine learning to assess coronary artery disease status-is it helpful? *Lancet* 2023; **401**: 173-175 [*RCA*] [PMID: 36563697 DOI: 10.1016/S0140-6736(22)02584-3] [FullText]

91 **Adams SJ**, Stone E, Baldwin DR, Vliegenthart R, Lee P, Fintelmann FJ. Lung cancer screening. *Lancet* 2023; **401**: 390-408 [*RCA*] [PMID: 36563698 DOI: 10.1016/S0140-6736(22)01694-4] [FullText]

92 **Abbasi J**. Artificial Intelligence in COVID-19 Imaging Mismatched to the Clinic. *JAMA* 2021; **326**: 124 [*RCA*] [PMID: 34255021 DOI: 10.1001/jama.2021.10888] [FullText]

93 **Bi WL**, Hosny A, Schabath MB, Giger ML, Birkbak NJ, Mehrtash A, Allison T, Arnaout O, Abbosh C, Dunn IF, Mak RH, Tamimi RM, Tempany CM, Swanton C, Hoffmann U, Schwartz LH, Gillies RJ, Huang RY, Aerts HJWL. Artificial intelligence in cancer imaging: Clinical challenges and applications. *CA Cancer J Clin* 2019; **69**: 127-157 [*RCA*] [PMID: 30720861 DOI: 10.3322/caac.21552] [FullText] [Full Text (PDF)]

94 **Ghassemi M**, Oakden-Rayner L, Beam AL. The false hope of current approaches to explainable artificial intelligence in health care. *Lancet Digit Health* 2021; **3**: e745-e750 [*RCA*] [PMID: 34711379 DOI: 10.1016/S2589-7500(21)00208-9] [FullText]

95 **Nagaraju RM**, Gurushankar G, Bhimarao, Kadakola B. Efficacy of High Frequency Ultrasound in Localization and Characterization of Orbital Lesions. *J Clin Diagn Res* 2015; **9**: TC01-TC06 [*RCA*] [PMID: 26500977 DOI: 10.7860/JCDR/2015/13021.6428] [FullText]

96 **Silverman RH**. High-resolution ultrasound imaging of the eye - a review. *Clin Exp Ophthalmol* 2009; **37**: 54-67 [*RCA*] [PMID: 19138310 DOI: 10.1111/j.1442-9071.2008.01892.x] [FullText] [Full Text(PDF)]

World Journal of Radiology

Submit a Manuscript: https://www.f6publishing.com

World J Radiol 2025 November 28; 17(11): 113012

DOI: 10.4329/wjr.v17.i11.113012

ISSN 1949-8470 (online)

MINIREVIEWS

Point-of-care ultrasonography for detecting raised intracranial pressure through optic nerve sheath diameter in non-traumatic headache patients

Yehya Tlaiss, Alaa Tarchichi, Katherine Atallah, Ehab Al Mashtoub, Issa Zalzali, Zeinab Chokor, Issam Fassih, Najah Harb, Jane Kassas, Hussein Hamze

Specialty type: Radiology, nuclear medicine and medical imaging

Provenance and peer review: Invited article; Externally peer reviewed.

Peer-review model: Single blind

Peer-review report's classification

Scientific Quality: Grade C

Novelty: Grade B

Creativity or Innovation: Grade C

Scientific Significance: Grade D

P-Reviewer: Singh B, MD, United States

Received: August 13, 2025

Revised: August 27, 2025

Accepted: November 4, 2025

Published online: November 28, 2025

Processing time: 106 Days and 18.6 Hours

Yehya Tlaiss, Alaa Tarchichi, Ehab Al Mashtoub, Department of Ophthalmology, University of Balamand, Beirut 1100, Lebanon

Katherine Atallah, Zeinab Chokor, Issam Fassih, Jane Kassas, Hussein Hamze, Department of Radiology, University of Balamand, Beirut 1100, Lebanon

Issa Zalzali, Najah Harb, Department of Internal Medicine, University of Balamand, Beirut 1100, Lebanon

Corresponding author: Yehya Tlaiss, MD, Department of Ophthalmology, University of Balamand, Hazmieh, Beirut 1100, Lebanon. yehyatlaiss@hotmail.com

Abstract

Non-traumatic headache is a common presentation in both emergency and outpatient settings, where timely identification of raised intracranial pressure (ICP) is crucial to prevent severe neurological complications. Conventional diagnostic methods such as computed tomography and lumbar puncture have important limitations, including invasiveness, delayed availability, and limited sensitivity in certain contexts. Point-of-care ultrasound measurement of the optic nerve sheath diameter (ONSD) has emerged as a rapid, non-invasive tool for detecting elevated ICP at the bedside. The technique is based on the anatomical continuity between the intracranial subarachnoid space and the optic nerve sheath, which expands in response to increased ICP. Evidence from multiple studies and meta-analyses indicates that ONSD measurements above 5.0-5.7 mm in adults strongly correlate with elevated ICP, showing pooled sensitivities and specificities approaching 90%. This modality enables immediate triage, guides urgency of neuroimaging, reduces unnecessary radiation exposure, and can be applied in outpatient and low-resource settings. Despite these advantages, ONSD assessment is subject to operator dependency, variability in threshold values, and reduced accuracy in patients with certain ocular or systemic conditions. Advances in artificial intelligence–assisted measurement, coupled with standardized training protocols, have the potential to improve reproducibility and broaden adoption. Overall, point-of-care ultrasound-based ONSD measurement represents a valuable adjunct in the early evaluation of patients with non-traumatic headache, facilitating faster diagnosis, better resource utilization, and improved patient

outcomes.

Key Words: Point-of-care ultrasound; Optic nerve sheath diameter; Intracranial pressure; Headache; Non-traumatic

©The Author(s) 2025. Published by Baishideng Publishing Group Inc. All rights reserved.

Core Tip: Non-traumatic headache can be the first sign of raised intracranial pressure, requiring rapid recognition to prevent neurological deterioration. Conventional diagnostics such as computed tomography and lumbar puncture have limitations. Point-of-care ultrasound measurement of optic nerve sheath diameter is a fast, non-invasive method with high sensitivity and specificity for detecting elevated intracranial pressure. Its use can expedite diagnosis, guide urgent management, and reduce unnecessary imaging, especially in outpatient and resource-limited settings. Standardized training and emerging artificial intelligence-assisted measurement promise to enhance its reliability and broaden its clinical impact.

Citation: Tlaiss Y, Tarchichi A, Atallah K, Al Mashtoub E, Zalzali I, Chokor Z, Fassih I, Harb N, Kassas J, Hamze H. Point-of-care ultrasonography for detecting raised intracranial pressure through optic nerve sheath diameter in non-traumatic headache patients. *World J Radiol* 2025; 17(11): 113012
URL: https://www.wjgnet.com/1949-8470/full/v17/i11/113012.htm
DOI: https://dx.doi.org/10.4329/wjr.v17.i11.113012

INTRODUCTION

Headache is one of the most frequent neurological complaints in both emergency departments and outpatient clinics. Non-traumatic headaches account for approximately 2%-4% of all emergency visits, making it a common yet challenging presentation[1]. While the majority of headaches are benign primary disorders (*e.g.* migraine or tension-type), clinicians must remain vigilant for secondary causes. In particular, even in the absence of trauma, a headache can be the first sign of elevated intracranial pressure (ICP) due to an underlying pathology that may be life-threatening. Early identification of an ICP-related headache is crucial, as delayed recognition of raised ICP can lead to catastrophic neurological outcomes[2]. Elevated ICP may precipitate cerebral ischemia, brain herniation, or even death if not promptly managed[2]. Evidence from multiple studies and meta-analyses indicates that optic nerve sheath diameter (ONSD) measurements above 5.0-5.7 mm in adults strongly correlate with elevated ICP, showing pooled sensitivities and specificities approaching 90%. Therefore, timely recognition and intervention are essential to prevent catastrophic outcomes. Therefore, distinguishing high-risk headaches suggestive of intracranial hypertension from benign causes is a critical priority for emergency physicians, neurologists, and ophthalmologists.

Conventional diagnostic approaches for suspected increased ICP each have significant limitations. Neuroimaging such as computed tomography (CT) of the head is often the first step to evaluate secondary headaches, but a normal CT does not rule out elevated ICP and only reveals specific causes (*e.g.* mass lesions or hemorrhage) when present. Furthermore, CT involves radiation exposure and may not be immediately accessible in all settings. Direct measurement of cerebrospinal fluid pressure *via* lumbar puncture (LP) remains the diagnostic gold standard for confirming intracranial hypertension, but LP is invasive, time-consuming, and contraindicated if elevated ICP is strongly suspected due to the risk of precipitating herniation. These logistical and safety limitations of CT and LP can delay diagnosis in an acute headache scenario[3]. In the emergency setting, there is a pressing need for a rapid, bedside technique to screen for raised ICP that avoids the delays and risks of conventional tests[3].

Point-of-care ultrasonography (POCUS) measurement of the ONSD has emerged as a promising solution to this diagnostic gap. The optic nerve sheath is contiguous with the intracranial subarachnoid space, and it expands when ICP rises. Bedside ocular ultrasound allows clinicians to directly visualize this sheath distension. Ultrasound-based ONSD assessment is non-invasive, repeatable, and can be performed in seconds at the patient's bedside, making it ideal for urgent evaluation. It eliminates the need to transport unstable patients for radiographic studies and avoids the radiation and procedural risks associated with CT or LP[3]. In recent years, multiple studies and meta-analyses have demonstrated that an enlarged ONSD on ultrasound correlates strongly with raised ICP, with high sensitivity and specificity reported for detecting intracranial hypertension[4]. In practice, a normal ONSD measurement has a high negative predictive value, helping clinicians confidently rule out significant ICP elevation in many cases[5]. As a result, ONSD POCUS is being increasingly adopted as a fast screening tool for elevated ICP in emergency and critical care settings.

Clinical scenarios where ONSD ultrasonography is particularly indicated include patients presenting with acute severe headache accompanied by red-flag features such as visual disturbances, altered mental status, or focal neurological deficits. It is also useful in suspected idiopathic intracranial hypertension (IIH), meningitis or intracranial infection, and in patients where CT is delayed or unavailable, or LP is contraindicated. In these situations, bedside POCUS offers a rapid and non-invasive alternative to guide urgent management decisions.

In summary, timely detection of elevated ICP in patients with headache (even without trauma) is of great clinical importance to prevent neurological deterioration. Unfortunately, traditional modalities like CT and LP have practical drawbacks in the acute setting. ONSD measurement by POCUS offers a rapid, non-invasive approach to bridge this gap.

This paper explores the utility of POCUS-measured ONSD for early identification of raised ICP in non-traumatic headache patients, aiming to guide clinicians in integrating this technique into early headache evaluation for better patient outcomes.

LITERATURE REVIEW

Anatomy and technique

The optic nerve sheath is a continuation of the dura mater, the outermost membrane of the meninges that envelops the brain. Similar to the brain, the nerve is surrounded by the arachnoid and pia mater, with cerebrospinal fluid (CSF) filling the subarachnoid space in between[6].

Due to this anatomy, alterations in ICP are transmitted to the optic nerve sheath *via* the subarachnoid space, leading to its dilation as ICP rises. Due to this physiological connection, the ONSD can be used as a non-invasive substitute biomarker for elevated ICP[7]. Ultrasonographic evaluation of the ONSD has proven to be safe, rapid, and portable across diverse settings such as emergency and critical care units. This technique visualizes optic nerve sheath enlargement resulting from increased CSF pressure in the subarachnoid space as ICP rises.

The technique requires the patient to be positioned supine and the eye in a neutral gaze. A high-frequency linear transducer (typically 7.5-15 MHz) is placed over the closed upper eyelid. To prevent any pressure on the eye, which might lead to inaccurate readings, a small amount of ultrasonic gel is utilized[8].

The ONSD is measured 3 mm posterior to the retina, along a line perpendicular to the optic nerve's long axis, to provide the most reliable values[9]. Typically, assessments are conducted on both eyes, and an average is calculated. Several systematic reviews and studies tried to give a threshold value for abnormal ONSD. It was found that a common cutoff for elevated ICP is an ONSD measurement exceeding 5.0 mm in adults (or as high as 5.7 mm according to certain studies). However, the cutoff can differ with population, pathology, and measurement method[10]. For example, a cutoff of 5.9 mm was reported in pediatric intensive care studies[11]. A sensitivity of 90% and a specificity of 85% for detecting increased ICP by ONSD were reported in a meta-analysis[12]. Nevertheless, accuracy can be affected by patient's position, probe orientation, and measurement site. Therefore, to ensure consistency and minimize variability between observers, this technique requires attention to probe placement, angle, and site of measurement[12]. Although ONSD ultrasound cannot replace direct ICP monitoring in critical care and neurosurgical settings, it serves as a valuable bedside instrument, especially in circumstances where invasive monitoring is either unfeasible or not recommended.

The optic nerve sheath expands in response to increased ICP due to its continuity with the intracranial subarachnoid space, which is filled with CSF. This anatomical relationship is the basis for using ONSD measurement as a surrogate marker for raised ICP (Figure 1). The technique is illustrated in Figure 2A, which shows probe positioning over the closed eyelid, and Figure 2B, which demonstrates a typical sonographic appearance of the ONSD with calipers.

Evidence and diagnostic accuracy

Because of the anatomical continuity between the intracranial subarachnoid space and the optic nerve sheath, elevations in ICP lead to measurable sheath distension. Numerous studies have validated this correlation and assessed the diagnostic performance of ONSD ultrasonography in detecting raised ICP[13]. Research has shown that patients with elevated ICP tend to have significantly larger ONSD values compared to those with normal ICP. Analysis of 22 studies conducted over 17 years revealed that patients with elevated ICP had a mean ONSD of 5.82 mm [95% confidence interval (CI): 5.58-6.06 mm], which closely matches magnetic resonance imaging-based measurements. A subset of 15 studies found that patients with elevated ICP had an ONSD of 5.6 mm, compared to 4.1 mm in those without elevated ICP, which further supports its diagnostic utility[14].

ONSD ultrasonography demonstrates robust diagnostic performance. A study found that sonographic ONSD had a 93.2% sensitivity and 91.1% specificity in detecting raised ICP when compared to CT imaging, with an overall accuracy of 92%[15]. A practical threshold of 5.0 mm has been identified in multiple studies, yielding both high negative and positive predictive values. An ONSD cutoff of 5.0 mm yielded a sensitivity of 88% and a specificity of 93%[16]. Another study at the same threshold reported 100% sensitivity and 95% specificity[17]. An optimal cutoff of at least 4.8 mm was shown to detect ICP ≥ 20 mmHg with 96% sensitivity and 94% specificity[18].

Other studies have proposed higher cut-off values. Research has shown that a cutoff of 6.1 mm yields 100% sensitivity and 83% specificity for ICP above 20 cmH_2O[19]. An optimal cutoff of 5.68 mm was reported[20] while 5.7 mm was identified as the most accurate value[21].

A recent meta-analysis revealed that the pooled sensitivity was 0.90 (95%CI: 0.85-0.93) and the pooled specificity was 0.87 (95%CI: 0.80-0.91)[22]. Studies with higher cutoffs, ranging from 5.6 mm to 6.3 mm, demonstrated greater specificity (0.93) compared to 0.78, without affecting sensitivity, implying that this range may have more practical clinical applications[22].

A systematic review of 12 studies found that ONSD values below 5 mm typically indicate normal ICP, whereas values above 6 mm suggest elevated ICP exceeding 20 mmHg, with a sensitivity of nearly 90% and a specificity of around 85%. The diagnostic accuracy was highest when ONSD values were 5.85 mm or greater, particularly beyond 6 mm[23].

Reported sensitivity and specificity values vary depending on the population studied and the measurement cut-off used, with most adult thresholds ranging from 5.0 mm to 5.7 mm. A summary of key studies, including their diagnostic performance and cut-off values, is provided in Figure 3.

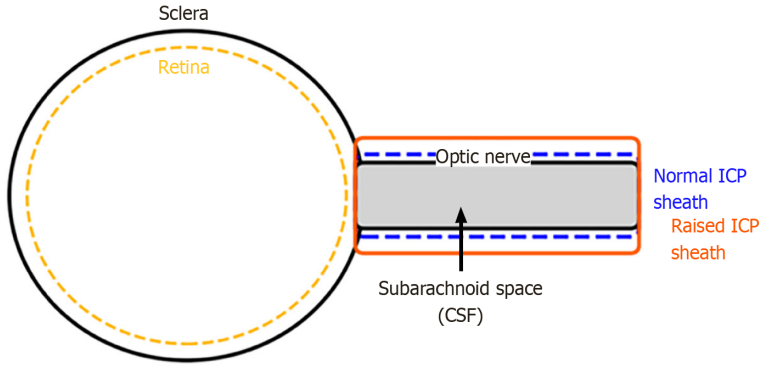


Figure 1 Anatomical relationship of the optic nerve sheath to the intracranial subarachnoid space, illustrating sheath expansion in raised intracranial pressure. ICP: Intracranial pressure; CSF: Cerebrospinal fluid.

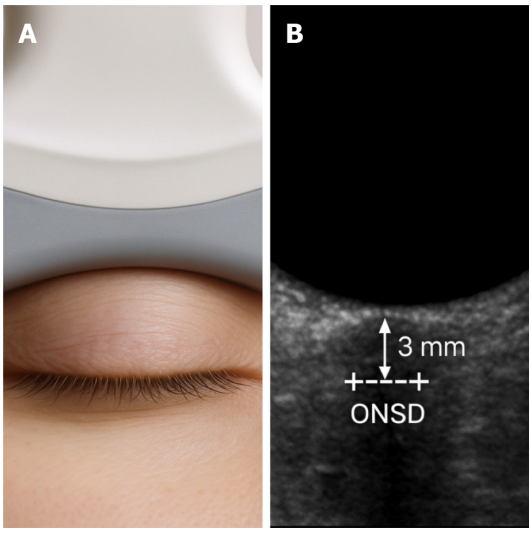


Figure 2 Ultrasonographic technique for measuring optic nerve sheath diameter using point-of-care ultrasound. A: Proper ultrasound probe placement over the closed eyelid for optic nerve sheath diameter measurement; B: Sonographic image of the optic nerve sheath diameter with calipers placed 3 mm posterior to the retina. ONSD: Optic nerve sheath diameter.

There is no consensus in the literature on a definitive ONSD threshold, with reported cutoffs varying from 4.1 mm to 7.2 mm. The high sensitivity of ONSD ultrasonography, despite its variability, makes it a valuable tool for screening and ruling out elevated ICP, and for guiding decisions on further invasive testing[22]. The need for standardizing ultrasound measurement techniques and cutoffs in future studies is highlighted by these findings[23].

CLINICAL USE AND INTEGRATION OF POCUS ONSD IN HEADACHE MANAGEMENT

POCUS for red-flag headaches in emergency settings

POCUS measurement of ONSD has become a critical bedside tool in emergency departments, particularly for patients presenting with "red flag" headaches that may indicate elevated ICP. It is particularly valuable for rapid assessment of patients who present to the ED with headaches associated with symptoms that indicate increased ICP such as visual disturbances, altered level of consciousness, or neurological deficits. Rapid identification of raised ICP allows clinicians to make immediate clinical decisions, often prior to definitive imaging.

Patients with serious intracranial disorders reported increasing headaches typically demonstrate much larger ONSD measurements with the average ONSD around 6.2 mm, while the average ONSD in patients with benign headaches is about 4.5 mm. An ONSD cut-off of approximately 5.2 mm is found to accurately distinguish patients that require urgent evaluation and intervention with those with benign headaches with sensitivity near 98% and specificity at 100%[24]. In another systematic review, they concluded that ultrasound was reliable as a diagnostic tool for the detection of elevated ICP, with a pooled sensitivity of 92% and specificity of 86%[25].

Clinicians practicing in the ED use ocular ultrasound to screen patients with severe or concerning headaches rapidly. If they see an enlarged ONSD, they escalate imaging or clinical intervention. If they see a normal ONSD, they can reassure the patient while then guiding their clinical thought process towards other possible diagnosis. Ocular ultrasound in this

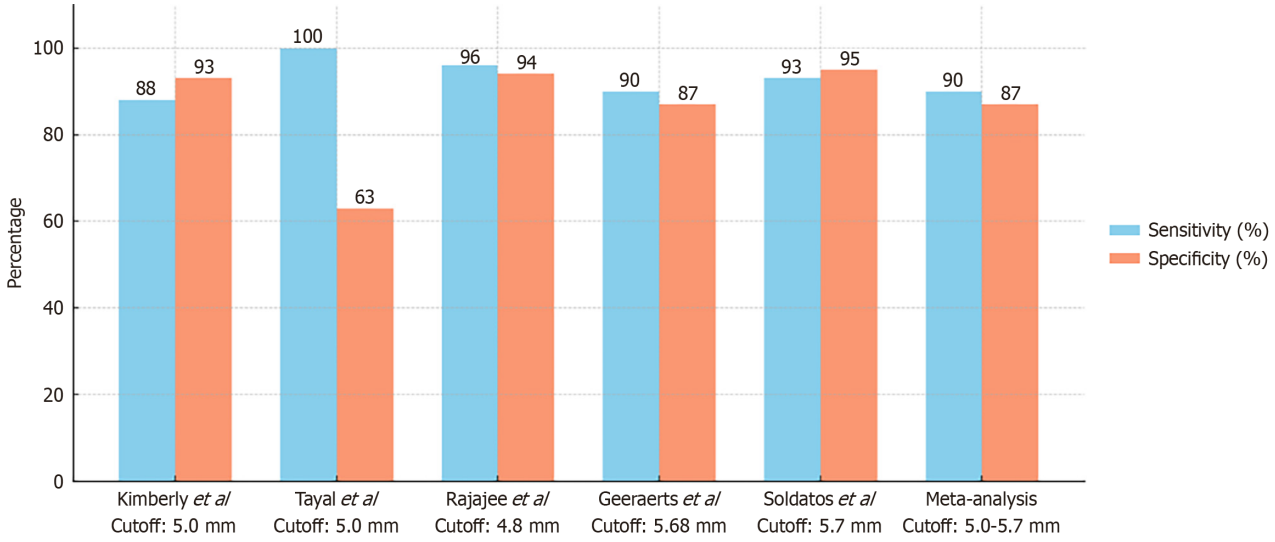


Figure 3 Diagnostic accuracy of point-of-care ultrasound–measured optic nerve sheath diameter for detecting raised intracranial pressure, showing sensitivity, specificity, and cut-off values from key studies.

scenario is easier and more effective than traditional fundoscopy because of the accessible, fast, and non-invasive nature of ultrasound. Fundoscopy can be highly subjective but may also alter the patient experience dramatically (and cause discomfort) in cases of urgency[26].

A good example of the potential value of POCUS is a patient with an acute neurological decline. At the bedside, ONSD ultrasound demonstrated extremely high ICP, leading to potentially lifesaving interventions such as intubation and neurosurgery before obtaining advanced imaging[27]. These examples document how bedside ultrasound can change patient care quickly by allowing pivotal time-sensitive interventions to occur.

Impact on diagnosis, treatment speed, and patient outcomes

Use of ocular POCUS in the initial evaluation of headache patients in urgent-care or emergency settings greatly impacts the speed at which the diagnosis is made and treatment initiated. A scan will facilitate the immediate evaluation of elevated ICP, allowing a clinical workup to be directed towards the most urgent imaging and management decisions for the patient. Conversely, if ONSD is normal, an immediate management decision may delay imaging and the need for invasive procedures, which would be useful in low-resource settings, emergency departments, urgent care centers, and specialist consultations where waiting for advanced imaging is a reality.

In outpatient care, POCUS can also assist to expedite patient management decisions. A recent outpatient case of a chronic headache required a very prompt ultrasound assessment. The ultrasound performed while the patient was at the bedside found an ONSD of 6 mm which was stretched out considerably; enough to facilitate a clinical referral and a subsequent definitive diagnosis of IIH and to avoid potentially unnecessary visits to the emergency department and advanced imaging[28]. This incorporation of ultrasound in outpatient care will accelerate and simplify patient management.

Serial ONSD measurements in critical care allow dynamic real time assessments and monitoring of ICP. One perioperative patient suffering from acute neurological deterioration underwent a timely ultrasound evaluation which revealed marked elevation in the ONSD allowing for timely medical interventions such as osmotic therapy[29]. Thus, a series of ultrasound assessment allows for monitoring patients' treatment response, while identifying worsening progression necessitating intervention.

Additionally, ultrasound assessments provide opportunities to eliminate unnecessary imaging and procedures. Patients with primary benign headaches demonstrated normal ONSD measurements, nearby safely ruling out the need of urgent neuroimaging and thus decrease overall costs and the threat of radiation[25]. Therefore, this type of selective approach is highly beneficial in outpatient or resource limited environments.

Outpatient and follow-up applications

POCUS is also important outside of acute care and still works great in outpatient neurology and ophthalmology clinics. Patients suffering with chronic headaches or symptoms suggestive of IIH can be evaluated very fast with ultrasound, allowing for quick confirmation or exclusion of any high ICP.

Ocular ultrasound is recommended in the routine outpatient evaluation of patients with suspected IIH and gives reliable diagnostic information even before traditional signs (such as papilledema) are apparent[30]. Depending on patient's treatment and the resolution or exacerbation of symptoms, serial ultrasound measurements provide objective indications for clinician to justify treatment effectiveness instead of relying on repeated invasive measures.

In primary care, ultrasound provides a hybrid step between their first suspicion and a definitive diagnosis, supporting their ultimate decision of whether to urgently refer or order additional tests. This reduces wasted time and resources, while also helping ensure their patients receive appropriate and timely care.

Benefits in low-resource and rural settings

POCUS is particularly important in rural and resource-limited settings, especially because many of the higher-end imaging modalities are not available. Studies evaluating optic nerve ultrasound have shown a reasonable correlation with CT scan findings in rural clinical environments, and a cutoff of 5.2 mm for ONSD was found to be a reasonable predictor of ICP[31]. This simple diagnostic modality allows urgent transfer of patients or a quick local intervention allowing clinicians in remote areas to quickly identify the need for further intervention.

Because ultrasonography is highly portable and easy to use, particularly relevant to the practice of rural healthcare, it allows clinicians to almost immediately identify candidates for urgent neurological intervention from a substantial distance from an acute care site[3]. In particular, if rural clinicians encounter any patient with headache or with new-onset alertness-reducing neurologic issue such as suspected meningitis; they can quickly perform ultrasound without waiting for other imaging thus allowing for immediate decisions about transfer or management. A resolution of "normal" on ultrasound means these providers can confidently locally manage the patient and prevent unnecessary transfers - saving precious resources and time.

In conclusion, ocular ultrasound is a simple and effective addition to the clinical workflow of a range of healthcare providers which can improve the accuracy of diagnosis, the speed of patient management, and efficiency of resource use in an array of settings from urban emergency departments to remote rural clinics.

Limitations of ONSD POCUS

Despite its benefits, ONSD measurement using POCUS presents several limitations that must be acknowledged when interpreting its results. One of the primary challenges is the variability in measurements between different operators. The technique requires precise anatomical visualization and probe positioning, and without sufficient training, there is a significant risk of inter- and intra-operator variability[32]. This variability can influence diagnostic accuracy, particularly when small differences in sheath diameter may have clinical significance. In addition, a newly introduced automated frame selection method achieved an intraclass correlation coefficient of only 0.782 compared to expert clinicians, reflecting substantial operator related differences in manually selecting optimal images[33].

Proper training and continued practice are essential for clinicians to obtain reliable measurements. Nevertheless, many emergency and critical care providers lack formal training in ocular ultrasonography. A study found that even after a brief instructional session, novice users displayed considerable variation in ONSD measurements[34], emphasizing the importance of hands-on experience and quality assurance mechanisms. In a recent study, after a brief 4 hours theoretical and hands on training session, intensive care unit residents and medical students achieved measurement agreement within a 0.5 mm of expert values on Bland Altman analysis, while nursing students exhibited the highest error rates[35].

Patient-specific factors can also affect the accuracy of ONSD assessment. Chronic optic nerve conditions like glaucoma or optic neuritis can change the structure of the optic nerve sheath, making ONSD measurements less reliable. For example, patients with normal tension glaucoma have been shown to have smaller sheath diameters despite normal ICP [36]. Additionally, acquiring a clear image of the optic nerve sheath in patients with periorbital edema or obesity can be technically challenging due to increased tissue depth and poor acoustic windows[18].

Technical aspects of ultrasound imaging can significantly influence the accuracy of ONSD measurements. Factors such as gain, frequency settings, dynamic range, and common imaging artifacts (like acoustic shadowing, speckle, and beam refraction) can distort the results if not appropriately adjusted or accounted for during scanning[37]. Importantly, ONSD cutoff selection involves a sensitivity–specificity balance: Lower thresholds improve detection rates but may increase false positives. For instance, a pediatric emergency care study found that an ONSD cutoff of 4.9 mm had a sensitivity of 90% but specificity as low as 47%, leading to potential overdiagnosis[38]. Variations in equipment further complicate measurement consistency. High-frequency linear transducers are generally recommended, but variations in image resolution, presets, and device quality can lead to inconsistent results. Mean error rates in ONSD measurements differed significantly across three ultrasound systems[39], suggesting that "device choice alone can materially impact diagnostic performance".

Contraindications to ONSD ultrasonography are limited but important to consider. Absolute contraindication includes suspected or confirmed open globe injury, where probe pressure could cause extrusion of ocular contents. Relative contraindications include recent ocular surgery, significant orbital trauma, or severe eye infections, where manipulation of the eyelid may worsen the condition. In these cases, alternative methods for ICP evaluation should be used.

FUTURE APPLICATIONS AND IMPROVEMENTS IN POCUS-ONSD

POCUS assessment of the ONSD continues to evolve with new technologies and protocols that enhance its role in ICP monitoring. Ongoing research is exploring artificial intelligence (AI)-assisted interpretation and automated measurement tools. Advanced image-analysis algorithms have been developed to automatically measure ONSD on ultrasound images with high precision comparable to expert clinicians, reducing operator-dependent variability[18,40]. These AI-driven systems may enable reliable ONSD assessment even by less experienced users and in austere settings, by providing consistent measurements and identifying optimal images for analysis.

Comprehensive training programs and standardized protocols are essential to ensure safe and reliable use. Proper operator training and uniform technique are critical, as measurement inconsistencies have historically limited ONSD's reliability. An international consensus in 2024 introduced a standardized ONSD ultrasound quality criteria checklist to improve consistency in image acquisition and measurement[37]. Studies also demonstrate that with brief dedicated training, even non-physician providers (*e.g.* nurses or medical students) can learn to obtain accurate ONSD mea-

surements, approaching expert-level agreement[35]. Implementing formal training curricula and adherence to consensus protocols will help minimize inter-operator variation and improve the safety of widespread ONSD use.

Future studies should aim to validate ONSD measurement in broader non-traumatic headache populations. To date, ONSD ultrasound is well-established for detecting raised ICP in traumatic brain injury - it has even been incorporated into some traumatic brain injury management guidelines[41]. However, evidence in non-traumatic neurologic conditions (such as spontaneous intracerebral hemorrhage, stroke, meningitis, or IIH) is less extensive and sometimes inconsistent [42]. Recent reviews indicate ONSD can be a useful adjunct for identifying elevated ICP in acute stroke, intracranial bleeding, and intracranial infections, but call for further research to refine diagnostic cutoffs and validate its prognostic value in these diverse, non-trauma patient groups[42]. Expanding research to headache patients without trauma (to distinguish benign *vs* dangerous causes) will be important for broader clinical adoption.

Integrating POCUS ONSD into clinical guidelines could improve care efficiency. Incorporating ONSD measurement into emergency and critical care algorithms may streamline the evaluation of suspected intracranial hypertension. For example, using ONSD ultrasound at the bedside could help triage which headache patients require urgent neuroimaging, thereby reducing unnecessary radiation and delays. Formal guideline endorsements and inclusion in protocols (*e.g.* for emergency headache workups or intensive care unit monitoring) would standardize its use and magnify its impact on care delivery. Integrating ONSD into routine practice may enable clinicians to make faster, more informed decisions in time-sensitive neurological emergencies.

Ultimately, POCUS-based ONSD measurement represents a promising tool for early ICP detection that warrants broader adoption and further study. It is a rapid, noninvasive, and repeatable bedside technique with growing evidence of diagnostic accuracy for raised ICP in both traumatic and non-traumatic contexts[43,44]. ONSD ultrasound is considered safe and low-cost, with the potential to screen patients who may need confirmatory neuroimaging or invasive monitoring[43]. Key next steps include leveraging innovations like AI to assist interpretation, ensuring practitioners are well-trained, and conducting large multicenter trials in varied patient populations. With these improvements, ONSD POCUS may be more widely adopted as an efficient early-warning tool for intracranial hypertension, improving patient triage and outcomes.

Recently, an international expert consensus introduced the ONSD POCUS Quality Criteria Checklist (ONSD POCUS QCC), providing standardized guidance for image acquisition and measurement in clinical and research settings[45].

CONCLUSION

POCUS measurement of the ONSD is a rapid, non-invasive, and reliable method for detecting raised ICP in patients presenting with non-traumatic headache. Given its high diagnostic accuracy, ease of bedside application, and utility across emergency, outpatient, and resource-limited settings, it serves as a valuable adjunct to traditional neuroimaging and invasive monitoring. While operator dependency and variability in cut-off values remain limitations, advances in standardized training and AI-assisted measurement are likely to enhance consistency. Wider adoption and further validation in diverse patient populations could significantly improve early diagnosis, triage efficiency, and patient outcomes.

FOOTNOTES

Author contributions: Tlaiss Y handled conceptualization, methodology, and supervision; Tarchichi A managed data curation and investigation; Tlaiss Y, Tarchichi A, and Kassas J were responsible for writing the original draft; Tlaiss Y and Fassih I managed supervision; Atallah K conducted literature review and formal analysis; Zalzali I managed resources and project administration; Chokor Z did literature search and validation; Fassih I conducted formal analysis and critical revision; Harb N handled data curation and resources; Kassas J took charge of investigation; Hamze H oversaw methodology and validation; Tlaiss Y, Atallah K, Zalzali I, Chokor Z, Harb N, and Hamze H oversaw writing review and editing; Mashtoub EA, Chokor Z, and Hamze H were responsible for validation; Mashtoub EA additionally collected data and did visualization; Atallah K and Fassih I handled formal analysis; Tarchichi A and Harb N managed data curation; Zalzali I and Harb N oversaw resources; Tlaiss Y and Hamze H handled methodology; and all authors thoroughly reviewed and endorsed the final manuscript.

Conflict-of-interest statement: All the authors report no relevant conflicts of interest for this article.

Open Access: This article is an open-access article that was selected by an in-house editor and fully peer-reviewed by external reviewers. It is distributed in accordance with the Creative Commons Attribution NonCommercial (CC BY-NC 4.0) license, which permits others to distribute, remix, adapt, build upon this work non-commercially, and license their derivative works on different terms, provided the original work is properly cited and the use is non-commercial. See: https://creativecommons.org/Licenses/by-nc/4.0/

Country of origin: Lebanon

ORCID number: Yehya Tlaiss 0009-0003-5266-3690; Alaa Tarchichi 0009-0003-4165-9936.

S-Editor: Bai Y
L-Editor: A
P-Editor: Lei YY

REFERENCES

1 **Munoz-Ceron J**, Marin-Careaga V, Peña L, Mutis J, Ortiz G. Headache at the emergency room: Etiologies, diagnostic usefulness of the ICHD 3 criteria, red and green flags. *PLoS One* 2019; **14**: e0208728 [*RCA*] [PMID: 30615622 DOI: 10.1371/journal.pone.0208728] [FullText] [Full Text(PDF)]

2 **Patel S**, Maria-Rios J, Parikh A, Okorie ON. Diagnosis and management of elevated intracranial pressure in the emergency department. *Int J Emerg Med* 2023; **16**: 72 [*RCA*] [PMID: 37833652 DOI: 10.1186/s12245-023-00540-x] [FullText] [Full Text(PDF)]

3 **Lau T**, Ahn JS, Manji R, Kim DJ. A Narrative Review of Point of Care Ultrasound Assessment of the Optic Nerve in Emergency Medicine. *Life (Basel)* 2023; **13**: 531 [*RCA*] [PMID: 36836888 DOI: 10.3390/life13020531] [FullText]

4 **Lin JJ**, Chen AE, Lin EE, Hsia SH, Chiang MC, Lin KL. Point-of-care ultrasound of optic nerve sheath diameter to detect intracranial pressure in neurocritically ill children - A narrative review. *Biomed J* 2020; **43**: 231-239 [*RCA*] [PMID: 32335329 DOI: 10.1016/j.bj.2020.04.006] [Full Text] [Full Text(PDF)]

5 **Koziarz A**, Sne N, Kegel F, Nath S, Badhiwala JH, Nassiri F, Mansouri A, Yang K, Zhou Q, Rice T, Faidi S, Passos E, Healey A, Banfield L, Mensour M, Kirkpatrick AW, Nassar A, Fehlings MG, Hawryluk GWJ, Almenawer SA. Bedside Optic Nerve Ultrasonography for Diagnosing Increased Intracranial Pressure: A Systematic Review and Meta-analysis. *Ann Intern Med* 2019; **171**: 896-905 [*RCA*] [PMID: 31739316 DOI: 10.7326/M19-0812] [FullText]

6 **Bartsch AJ**, Homola G, Biller A, Smith SM, Weijers HG, Wiesbeck GA, Jenkinson M, De Stefano N, Solymosi L, Bendszus M. Manifestations of early brain recovery associated with abstinence from alcoholism. *Brain* 2007; **130**: 36-47 [*RCA*] [PMID: 17178742 DOI: 10.1093/brain/awl303] [FullText]

7 **Boysen SR**, Pang JM, Mikler JR, Knight CG, Semple HA, Caulkett NA. Comparison of tranexamic acid plasma concentrations when administered *via* intraosseous and intravenous routes. *Am J Emerg Med* 2017; **35**: 227-233 [*RCA*] [PMID: 27816438 DOI: 10.1016/j.ajem.2016.10.054] [FullText]

8 **Robba C**, Santori G, Czosnyka M, Corradi F, Bragazzi N, Padayachy L, Taccone FS, Citerio G. Optic nerve sheath diameter measured sonographically as non-invasive estimator of intracranial pressure: a systematic review and meta-analysis. *Intensive Care Med* 2018; **44**: 1284-1294 [*RCA*] [PMID: 30019201 DOI: 10.1007/s00134-018-5305-7] [FullText]

9 **Sekhon MS**, Griesdale DE, Robba C, McGlashan N, Needham E, Walland K, Shook AC, Smielewski P, Czosnyka M, Gupta AK, Menon DK. Erratum to: Optic nerve sheath diameter on computed tomography is correlated with simultaneously measured intracranial pressure in patients with severe traumatic brain injury. *Intensive Care Med* 2015; **41**: 177 [*RCA*] [PMID: 25403757 DOI: 10.1007/s00134-014-3560-9] [FullText]

10 **Liu D**, Li Z, Zhang X, Zhao L, Jia J, Sun F, Wang Y, Ma D, Wei W. Assessment of intracranial pressure with ultrasonographic retrobulbar optic nerve sheath diameter measurement. *BMC Neurol* 2017; **17**: 188 [*RCA*] [PMID: 28962603 DOI: 10.1186/s12883-017-0964-5] [FullText] [Full Text(PDF)]

11 **Aslan N**, Yıldızdaş D, Horoz ÖÖ, Özsoy M, Yöntem A, Çetinalp E, Mert GG. Evaluation of ultrasonographic optic nerve sheath diameter and central retinal artery Doppler indices by point-of-care ultrasound in pediatric patients with increased intracranial pressure. *Turk J Pediatr* 2021; **63**: 300-306 [*RCA*] [PMID: 33929120 DOI: 10.24953/turkjped.2021.02.014] [FullText]

12 **Robba C**, Ball L, Battaglini D, Iannuzzi F, Brunetti I, Fiaschi P, Zona G, Taccone FS, Messina A, Mongodi S, Pelosi P. Effects of positive end-expiratory pressure on lung ultrasound patterns and their correlation with intracranial pressure in mechanically ventilated brain injured patients. *Crit Care* 2022; **26**: 31 [*RCA*] [PMID: 35090525 DOI: 10.1186/s13054-022-03903-7] [FullText] [Full Text(PDF)]

13 **Getachew M**, Abdulahi M, Muluberehan N, Hussen Z, Alemayehu A, Abebe T, Hussein A, Hutchinson P, Kolias A, Semework M, Tirsit A, Laeke T, Tadela A, Hassen GW. Optic nerve sheath diameter measurement using point-of-care ultrasound to assess intracranial pressure of adult patients with traumatic brain injury in resource-limited setting. *Interdiscip Neurosurg* 2023; **34**: 101847 [DOI: 10.1016/j.inat.2023.101847] [FullText]

14 **Montorfano L**, Yu Q, Bordes SJ, Sivanushanthan S, Rosenthal RJ, Montorfano M. Mean value of B-mode optic nerve sheath diameter as an indicator of increased intracranial pressure: a systematic review and meta-analysis. *Ultrasound J* 2021; **13**: 35 [*RCA*] [PMID: 34215966 DOI: 10.1186/s13089-021-00235-5] [FullText] [Full Text(PDF)]

15 **Incecik F**, Ozcan N, Ozcanyuz DG, Mert GG. Acetazolamide-Induced Agranulocytosis in a Patient with Pseudotumor Cerebri. *Ann Indian Acad Neurol* 2020; **23**: 732-733 [*RCA*] [PMID: 33623291 DOI: 10.4103/aian.AIAN_58_19] [FullText] [Full Text(PDF)]

16 **Kimberly HH**, Shah S, Marill K, Noble V. Correlation of optic nerve sheath diameter with direct measurement of intracranial pressure. *Acad Emerg Med* 2008; **15**: 201-204 [*RCA*] [PMID: 18275454 DOI: 10.1111/j.1553-2712.2007.00031.x] [FullText]

17 **Tayal VS**, Neulander M, Norton HJ, Foster T, Saunders T, Blaivas M. Emergency department sonographic measurement of optic nerve sheath diameter to detect findings of increased intracranial pressure in adult head injury patients. *Ann Emerg Med* 2007; **49**: 508-514 [*RCA*] [PMID: 16997419 DOI: 10.1016/j.annemergmed.2006.06.040] [FullText]

18 **Rajajee V**, Vanaman M, Fletcher JJ, Jacobs TL. Optic nerve ultrasound for the detection of raised intracranial pressure. *Neurocrit Care* 2011; **15**: 506-515 [*RCA*] [PMID: 21769456 DOI: 10.1007/s12028-011-9606-8] [FullText]

19 **Širanović M**, Turković TM, Gopčević A, Kelečić M, Kovač N, Kovač J, Rode B, Vučić M. Comparison of ultrasonographic measurement of optic nerve sheath diameter (ONSD) versus direct measurement of intracranial pressure (ICP) in traumatic brain injury patients. *Signa Vitae* 2011; **6**: 33-35 [*RCA*] [DOI: 10.22514/SV61.042011.5] [FullText]

20 **Geeraerts T**, Launey Y, Martin L, Pottecher J, Vigué B, Duranteau J, Benhamou D. Ultrasonography of the optic nerve sheath may be useful for detecting raised intracranial pressure after severe brain injury. *Intensive Care Med* 2007; **33**: 1704-1711 [*RCA*] [PMID: 17668184 DOI: 10.1007/s00134-007-0797-6] [FullText]

21 **Soldatos T**, Chatzimichail K, Papathanasiou M, Gouliamos A. Optic nerve sonography: a new window for the non-invasive evaluation of intracranial pressure in brain injury. *Emerg Med J* 2009; **26**: 630-634 [*RCA*] [PMID: 19700575 DOI: 10.1136/emj.2008.058453] [FullText]

22 **Berhanu D**, Ferreira JC, Abegão Pinto L, Aguiar de Sousa D, Lucas Neto L, Tavares Ferreira J. The role of optic nerve sheath ultrasonography in increased intracranial pressure: A systematic review and meta analysis. *J Neurol Sci* 2023; **454**: 120853 [*RCA*] [PMID: 37925899 DOI: 10.1016/j.jns.2023.120853] [FullText]

23 **Martínez-Palacios K**, Vásquez-García S, Fariyike OA, Robba C, Rubiano AM; noninvasive ICP monitoring international consensus group. Using Optic Nerve Sheath Diameter for Intracranial Pressure (ICP) Monitoring in Traumatic Brain Injury: A Scoping Review. *Neurocrit Care* 2024; **40**: 1193-1212 [*RCA*] [PMID: 38114797 DOI: 10.1007/s12028-023-01884-1] [FullText] [Full Text(PDF)]

24 **Bastani Viarsagh S**, Agar A, Lawlor M, Fraser C, Golzan M. Non-invasive assessment of intracranial pressure through the eyes: current

developments, limitations, and future directions. *Front Neurol* 2024; **15**: 1442821 [*RCA*] [PMID: 39524910 DOI: 10.3389/fneur.2024.1442821] [FullText]

25 **İşlek Yüksel A**, Selvi F, Yüksel S, Avcı M, Çalışkan Günay G, Kozacı N. The Role of Optic Nerve Sheath Diameter in Differential Diagnosis in Patients with Headache, A Prospective, Randomized Controlled Study. *Glob Emerg Crit Care* 2025; **4**: 23-19 [DOI: 10.4274/globecc.galenos.2024.91300] [FullText]

26 **Wilson CL**, Leaman SM, O'Brien C, Savage D, Hart L, Jehle D. Novice emergency physician ultrasonography of optic nerve sheath diameter compared to ophthalmologist fundoscopic evaluation for papilledema. *J Am Coll Emerg Physicians Open* 2021; **2**: e12355 [*RCA*] [PMID: 33532756 DOI: 10.1002/emp2.12355] [FullText] [Full Text(PDF)]

27 **Amin D**, McCormick T, Mailhot T. Elevated Intracranial Pressure Diagnosis with Emergency Department Bedside Ocular Ultrasound. *Case Rep Emerg Med* 2015; **2015**: 385970 [*RCA*] [PMID: 26587297 DOI: 10.1155/2015/385970] [FullText] [Full Text(PDF)]

28 **Gupta A**, Nagaraju SP, Bhojaraja MV, Swaminathan SM, Mohan PB. Hypertension in Chronic Kidney Disease: An Update on Diagnosis and Management. *South Med J* 2023; **116**: 237-244 [*RCA*] [PMID: 36724542 DOI: 10.14423/SMJ.0000000000001516] [FullText]

29 **Naik SS**, Krishnakumar M, Sundaram M, Goyal A. Saved by the bell: Point of care ocular ultrasound in raised intracranial pressure. *J Neurosci Rural Pract* 2022; **13**: 806-807 [*RCA*] [PMID: 36743771 DOI: 10.25259/JNRP-2022-7-10] [FullText]

30 **De Bernardo M**, Vitiello L, De Pascale I, Capasso L, Cornetta P, Rosa N. Optic Nerve Ultrasound Evaluation in Idiopathic Intracranial Hypertension. *Front Med (Lausanne)* 2022; **9**: 845554 [*RCA*] [PMID: 35299843 DOI: 10.3389/fmed.2022.845554] [FullText] [Full Text (PDF)]

31 **Sujan MU**, Rao MR, Kisan R, Abhishekh HA, Nalini A, Raju TR, Sathyaprabha TN. Influence of hydrotherapy on clinical and cardiac autonomic function in migraine patients. *J Neurosci Rural Pract* 2016; **7**: 109-113 [*RCA*] [PMID: 26933356 DOI: 10.4103/0976-3147.165389] [FullText]

32 **Dubourg J**, Javouhey E, Geeraerts T, Messerer M, Kassai B. Ultrasonography of optic nerve sheath diameter for detection of raised intracranial pressure: a systematic review and meta-analysis. *Intensive Care Med* 2011; **37**: 1059-1068 [*RCA*] [PMID: 21505900 DOI: 10.1007/s00134-011-2224-2] [FullText]

33 **Li R**, Tang W, Li P, Huang Q, She J, Li S, Xu H, Wan Y, Liu J, Fu H, Li X, Chen J. Automated measurement of optic nerve sheath diameter using ocular ultrasound video. *Med Biol Eng Comput* 2025 [*RCA*] [PMID: 41087787 DOI: 10.1007/s11517-025-03442-7] [FullText]

34 **Maude RR**, Hossain MA, Hassan MU, Osbourne S, Sayeed KL, Karim MR, Samad R, Borooah S, Dhillon B, Day NP, Dondorp AM, Maude RJ. Transorbital sonographic evaluation of normal optic nerve sheath diameter in healthy volunteers in Bangladesh. *PLoS One* 2013; **8**: e81013 [*RCA*] [PMID: 24312515 DOI: 10.1371/journal.pone.0081013] [FullText] [Full Text(PDF)]

35 **Garofalo E**, Neri G, Bosco V, Caroleo Z, Virdò F, Mastrangelo H, Guzzi G, Cammarota G, Robba C, Longhini F, Bruni A; ONSD study group. Efficacy of a theoretical-practical course for the ultrasound measurement of the optic nerve diameter in different healthcare operators. *Ultrasound J* 2025; **17**: 28 [*RCA*] [PMID: 40522589 DOI: 10.1186/s13089-025-00431-7] [FullText]

36 **Lee SH**, Kim TW, Lee EJ, Kil H. Association between Optic Nerve Sheath Diameter and Lamina Cribrosa Morphology in Normal-Tension Glaucoma. *J Clin Med* 2023; **12**: 360 [*RCA*] [PMID: 36615160 DOI: 10.3390/jcm12010360] [FullText]

37 **Hirzallah MI**, Sarwal A, Dentinger AM, Robba C, Valaikienė J, Lochner P, Schlachetzki F, Mills DM, Ertl M, Hakimi R, Bhise S, Pansell J. Ultrasonographic Optic Nerve Sheath Diameter Technical Pitfalls and Imaging Artifacts. *J Ultrasound Med* 2025; **44**: 1103-1120 [*RCA*] [PMID: 39931745 DOI: 10.1002/jum.16655] [FullText]

38 **Nagpal V**, Batra P, Bhaskar V, Gupta P, Bhatt S, Sahu P. Optic Nerve Sheath Diameter by Point of Care Ultrasound to Detect Raised Intracranial Pressure in Children. *Pediatr Emerg Care* 2025; **41**: 847-853 [*RCA*] [PMID: 40725989 DOI: 10.1097/PEC.0000000000003447] [FullText]

39 **Johnson GGRJ**, Jelic T, Derksen A, Unger B, Zeiler FA, Ziesmann MT, Gillman LM. Accuracy of Optic Nerve Sheath Diameter Measurements in Pocket-Sized Ultrasound Devices in a Simulation Model. *Front Med (Lausanne)* 2022; **9**: 831778 [*RCA*] [PMID: 35308521 DOI: 10.3389/fmed.2022.831778] [FullText] [Full Text(PDF)]

40 **Meiburger KM**, Naldi A, Michielli N, Coppo L, Fassbender K, Molinari F, Lochner P. Automatic Optic Nerve Measurement: A New Tool to Standardize Optic Nerve Assessment in Ultrasound B-Mode Images. *Ultrasound Med Biol* 2020; **46**: 1533-1544 [*RCA*] [PMID: 32147099 DOI: 10.1016/j.ultrasmedbio.2020.01.034] [FullText]

41 **Carney N**, Totten AM, O'Reilly C, Ullman JS, Hawryluk GW, Bell MJ, Bratton SL, Chesnut R, Harris OA, Kissoon N, Rubiano AM, Shutter L, Tasker RC, Vavilala MS, Wilberger J, Wright DW, Ghajar J. Guidelines for the Management of Severe Traumatic Brain Injury, Fourth Edition. *Neurosurgery* 2017; **80**: 6-15 [*RCA*] [PMID: 27654000 DOI: 10.1227/NEU.0000000000001432] [FullText]

42 **Bhide M**, Juneja D, Singh O, Mohanty S. Optic nerve sheath diameters in nontraumatic brain injury: A scoping review and role in the intensive care unit. *World J Crit Care Med* 2024; **13**: 97205 [*RCA*] [PMID: 39253313 DOI: 10.5492/wjccm.v13.i3.97205] [FullText] [Full Text(PDF)]

43 **Lochner P**, Czosnyka M, Naldi A, Lyros E, Pelosi P, Mathur S, Fassbender K, Robba C. Optic nerve sheath diameter: present and future perspectives for neurologists and critical care physicians. *Neurol Sci* 2019; **40**: 2447-2457 [*RCA*] [PMID: 31367861 DOI: 10.1007/s10072-019-04015-x] [FullText]

44 **Aletreby W**, Alharthy A, Brindley PG, Kutsogiannis DJ, Faqihi F, Alzayer W, Balhahmar A, Soliman I, Hamido H, Alqahtani SA, Karakitsos D, Blaivas M. Optic Nerve Sheath Diameter Ultrasound for Raised Intracranial Pressure: A Literature Review and Meta-analysis of its Diagnostic Accuracy. *J Ultrasound Med* 2022; **41**: 585-595 [*RCA*] [PMID: 33893746 DOI: 10.1002/jum.15732] [FullText]

45 **Hirzallah MI**, Lochner P, Hafeez MU, Lee AG, Krogias C, Dongarwar D, Hartman ND, Ertl M, Robba C, Malojcic B, Valaikiene J, Sarwal A, Hakimi R, Schlachetzki F; Optic Nerve Sheath Diameter Point-of-Care Ultrasonography Quality Criteria Checklist (ONSD POCUS QCC) Expert Panelists. Optic Nerve Sheath Diameter Point-of-Care Ultrasonography Quality Criteria Checklist: An International Consensus Statement on Optic Nerve Sheath Diameter Imaging and Measurement. *Crit Care Med* 2024; **52**: 1543-1556 [*RCA*] [PMID: 38836697 DOI: 10.1097/CCM.0000000000006345] [FullText]

World Journal of Radiology

Submit a Manuscript: https://www.f6publishing.com

World J Radiol 2025 November 28; 17(11): 113701

DOI: 10.4329/wjr.v17.i11.113701

ISSN 1949-8470 (online)

MINIREVIEWS

Neuroimaging with photon-counting computed tomography: A review of clinical applications

Arosh S Perera Molligoda Arachchige, Gabriel Amorim Moreira Alves, Daniil Fedorov, Gaia Ressa, Luca Cappellini, Riccardo Levi, Giovanni Savini, Federica Catapano, Marco Francone, Letterio S Politi

Specialty type: Radiology, nuclear medicine and medical imaging

Provenance and peer review: Invited article; Externally peer reviewed.

Peer-review model: Single blind

Peer-review report's classification

Scientific Quality: Grade B, Grade B

Novelty: Grade B, Grade B

Creativity or Innovation: Grade B, Grade C

Scientific Significance: Grade B, Grade B

P-Reviewer: Liu K, Chief Physician, China; Masood Z, PhD, PharmD, Professor, Pakistan

Received: September 1, 2025

Revised: October 11, 2025

Accepted: October 28, 2025

Published online: November 28, 2025

Processing time: 87 Days and 10.8 Hours

Arosh S Perera Molligoda Arachchige, Gabriel Amorim Moreira Alves, Daniil Fedorov, Luca Cappellini, Federica Catapano, Marco Francone, Letterio S Politi, Department of Biomedical Sciences, Humanitas University, Pieve Emanuele 20072, Milan, Italy

Gaia Ressa, Riccardo Levi, Giovanni Savini, Marco Francone, Department of Radiology, IRCCS Humanitas Research Hospital, Rozzano 20089, Lombardy, Italy

Letterio S Politi, Department of Neuroradiology, IRCCS Humanitas Research Hospital, Rozzano 20089, Lombardy, Italy

Corresponding author: Arosh S Perera Molligoda Arachchige, MD, Department of Biomedical Sciences, Humanitas University, Via Rita Levi Montalcini, Pieve Emanuele 20072, Milan, Italy. aroshshavinda.pereramolligodaarachchige@st.hunimed.eu

Abstract

Photon-counting computed tomography (PCCT) represents a transformative advancement in neuroimaging, offering superior spatial resolution, spectral imaging capabilities, reduced radiation dose, and enhanced contrast-to-noise ratios. This review explores the technical foundations of PCCT, its advantages over conventional CT, and its growing applications in neuroimaging. PCCT has shown promise in improving neurovascular imaging, detecting small vessels, and reducing artifacts near metallic implants. It also enhances the visualization of spontaneous intracranial hypotension and cerebrospinal fluid leaks and provides superior diagnostic accuracy in acute ischemic stroke imaging. However, current limitations, including protocol complexity, high data volume, and the absence of integrated artificial intelligence noise reduction algorithms, pose challenges to widespread adoption. Future research should address these limitations and refine PCCT's applications to unlock its full clinical potential.

Key Words: Computed tomography; Photon-counting; Head; Neuroimaging; Neurovascular

©The Author(s) 2025. Published by Baishideng Publishing Group Inc. All rights reserved.

Core Tip: Photon-counting computed tomography offers unprecedented spatial and spectral resolution in neuroimaging, enabling improved detection of subtle pathologies such as small vessels, cerebrospinal fluid leaks, and early ischemic changes, while reducing artifacts and radiation dose. Despite current challenges in protocol standardization, data handling, and integration of artificial intelligence-based noise reduction, photon-counting computed tomography holds strong potential to become a new standard in clinical neuroimaging.

Citation: Perera Molligoda Arachchige AS, Alves GAM, Fedorov D, Ressa G, Cappellini L, Levi R, Savini G, Catapano F, Francone M, Politi LS. Neuroimaging with photon-counting computed tomography: A review of clinical applications. *World J Radiol* 2025; 17(11): 113701
URL: https://www.wjgnet.com/1949-8470/full/v17/i11/113701.htm
DOI: https://dx.doi.org/10.4329/wjr.v17.i11.113701

INTRODUCTION

Computed tomography (CT) has become essential in diagnosing and evaluating numerous neurological conditions. Since its development in the 1970s, CT technology has advanced substantially, evolving from basic single-source systems to sophisticated scanners with larger detectors, faster helical scans, and multi-energy capabilities. In the 1990s, we witnessed the introduction of spiral CT, wide detector CT in 2004, dual-source CT in 2005, and dual-layer CT detectors in 2013. In the last two decades, dual-source CT systems have become widely used in clinical settings, especially in emergency neuroimaging[1,2]. The most recent innovation in CT technology is photon-counting detectors (PCDs). On September 29, 2021, the United States Food and Drug Administration approved the first photon-counting CT (PCCT) for clinical use, which has mainly been tested on models and adult patients. Other manufacturers are currently developing their system, but there is only scant information available on system design, capabilities, and, to our best knowledge, no use in humans [1,3,4]. Several manufacturers have now developed PCCT systems, including Siemens Healthineers (NAEOTOM Alpha), GE HealthCare (Revolution Aspire), Canon Medical (Aquilion PC CT), and United Imaging (uMI PCCT). While the core principle of direct photon conversion remains similar, these systems differ in detector materials (*e.g.*, cadmium telluride *vs* cadmium zinc telluride), energy threshold design, count rate capability, and noise correction algorithms. Such variations lead to differences in achievable spatial resolution, spectral separation, and reconstruction efficiency, which can influence both image quality and dose performance across vendors. This review will explore PCCT based on our experience, outlining its technical foundations, highlighting its advantages over traditional CT, and discussing its established and potential applications in neuroimaging.

DETECTOR TECHNOLOGY

Energy-integrating detectors (EIDs) use a two-step process to convert X-ray photons into electronic signals. Incoming X-rays are first converted into visible light by a scintillator (*e.g.*, gadolinium oxysulfide or cadmium tungstate), which emits light when exposed to ionizing radiation. This light is then absorbed by photodiodes, generating an electrical signal. EIDs output a signal proportional to the total X-ray energy deposited but lack the ability to distinguish photon energy levels, limiting their spectral information. Reflective components like septa are used to capture dispersing light photons but reduce geometric dose efficiency and spatial resolution[5,6]. In contrast, PCDs directly convert X-ray photons into electrical signals using semiconductors such as cadmium telluride, cadmium zinc telluride, or gallium arsenide. When photons interact with the semiconductor, they generate electron-hole pairs that are directed toward a pixelated anode under an applied voltage, creating an electrical pulse. Application-specific integrated circuits process these pulses, categorizing photons into 2-8 predefined energy levels. This allows PCDs to provide energy spectra for each photon, enhancing tissue characterization, electronic noise reduction, spatial resolution, and dose efficiency[5,6].

Furthermore, PCDs have the unique ability to register low-energy photons that are often discarded in EIDs due to electronic noise or inefficiencies in light conversion. This capability significantly enhances soft tissue contrast, enabling improved visualization of structures with subtle density differences, such as vessels or lesions in adipose tissue. Additionally, capturing low-energy photons contributes to dose efficiency by ensuring that a broader range of the X-ray spectrum contributes to image formation, thereby reducing unnecessary radiation exposure to the patient[5,6]. Unlike EIDs, PCDs eliminate the need for septa, enabling smaller pixel sizes and higher spatial resolution. However, technical challenges like charge sharing and pulse pile-up can occur. PCCT systems achieve improved image quality by enhancing the contrast-to-noise ratio (CNR) and offering advanced spectral imaging capabilities akin to color photography, where energy levels provide depth rather than relying solely on intensity[5,6] (Table 1; Figure 1).

Table 1 Comparison of energy integrating *vs* photon counting detector systems used in computed tomography

	Energy integrating detectors	Photon counting detectors
Principle of operation	Measures the total energy deposited by all incoming photons, without distinguishing their individual energies	Detects and counts individual photons, measuring their energy levels to differentiate photon spectra
Energy conversion	X-rays, light energy, and electrical energy	X-rays, electrical energy
Detector material	Typically uses scintillators (*e.g.*, cesium iodide) coupled with photodiodes	Utilizes semiconductors (*e.g.*, cadmium telluride or silicon)
Energy resolution	Poor - cannot differentiate photon energies, resulting in a loss of spectral information	High - excellent energy resolution, enabling spectral imaging and material decomposition
Dose efficiency	Lower - loses information due to electronic noise and scatter	Higher - better noise performance and higher signal-to-noise ratio, enabling lower radiation dose
Spatial resolution	Moderate - limited by the size of the scintillator and optical coupling	High - smaller pixel sizes and direct detection improve spatial resolution
Spectral imaging capability	Limited - no ability to differentiate or quantify materials based on photon energy	Superior - enables spectral imaging by separating photons into energy bins for material characterization
Contrast Resolution	Limited - relies on iodine contrast enhancement but lacks the ability to differentiate materials based on energy spectra	High - can improve contrast resolution by distinguishing between materials using energy-specific information
Detector efficiency	Lower - efficiency decreases at higher photon energies due to scattering and light loss in the scintillator	Higher - direct photon-to-electron conversion results in greater efficiency across a wide energy range
Scatter sensitivity	Higher - more susceptible to scatter artifacts, reducing image quality	Lower - better scatter rejection due to energy discrimination
Temporal resolution	Limited - relies on integration over a specific time interval, which may result in temporal blurring	High - fast photon counting allows better temporal resolution for dynamic imaging
Artifacts	Susceptible to beam hardening and metal artifacts due to a lack of spectral differentiation	Reduces beam hardening and metal artifacts by using spectral information
Cost	Lower - widely used and cheaper due to mature technology and simpler design	Higher - emerging technology with more complex manufacturing processes and semiconductor materials
Power consumption	Lower - simpler electronics and integration processes result in reduced power needs	Higher - photon counting electronics and energy discrimination require more power
Longevity and robustness	High - well-established and reliable for routine use	Moderate - sensitive semiconductor materials may be prone to degradation over time or under high doses

APPLICATIONS

Vascular imaging

PCCT can offer enhanced visualization of stents and reduced blooming artifacts in head and neck angiographies. PCCT angiography provides precise lumen visualization and depiction of metallic stent meshes with higher accuracy than EID-CT angiography (CTA). PCCT reduces artifacts from metallic implants, such as intracranial clips and coils, by leveraging high-energy bins that suppress beam-hardening and electronic noise[7-9]. The reduced lateral spreading of secondary quanta in PCDs also relaxes the need for inter-pixel septa and enables the use of a much smaller pixel size (*e.g.*, 0.1 mm) without sacrificing geometry efficiency. The inherent equal weighting of high and low energy photons in PCDs offers an improvement in the CNR of iodinated vessels. The energy resolving capability can also be used to generate virtual monoenergetic CT images that, upon optimization of the keV level, can improve the CNR of iodinated objects such as blood vessels[8]. Enhanced visualization with lower noise, superior signal-to-noise ratio (SNR), and reduced artifacts improves the evaluation of vascular anatomy, small arterial structures, tiny intracranial vessels, and diminutive vessels, and helps distinguish intracranial aneurysms from infundibula[7]. Blooming artifact reduction, through decreased voxel size and high-energy virtual monoenergetic imaging, reduces artifactual stenoses in calcified plaques and facilitates the characterization of structures near surgical clips[7]. PCCT allows improved evaluation of vascular stents, enabling better visualization of individual stent struts, enhanced evaluation of in-stent stenoses in small arteries, and improved assessment of aneurysms treated with occlusion systems like the Woven EndoBridge device[7].

Reduced beam hardening artifact benefits include better assessment of arterial segments near the skull base and cervical vertebrae, as well as superior evaluation of the petrous segment of the internal carotid artery, which is often obscured by beam hardening artifacts on EID-CT[10]. Spinal photon-counting CTA can be used for the characterization of spinal vascular malformations, including spinal dural arteriovenous fistulas, with high spatial resolution, helping to identify tiny vessels. Multi-energy acquisition allows for a virtual monoenergetic image to enhance iodine contrast, facilitating better vessel visualization with smaller or equal contrast doses[7].

While digital subtraction angiography remains the clinical gold standard for cerebrovascular evaluation, CTA is widely accepted as a non-invasive diagnostic alternative for imaging large cerebral arteries and veins. An important challenge that currently remains for CTA is its limited performance in imaging small perforating arteries with diameters below 0.5

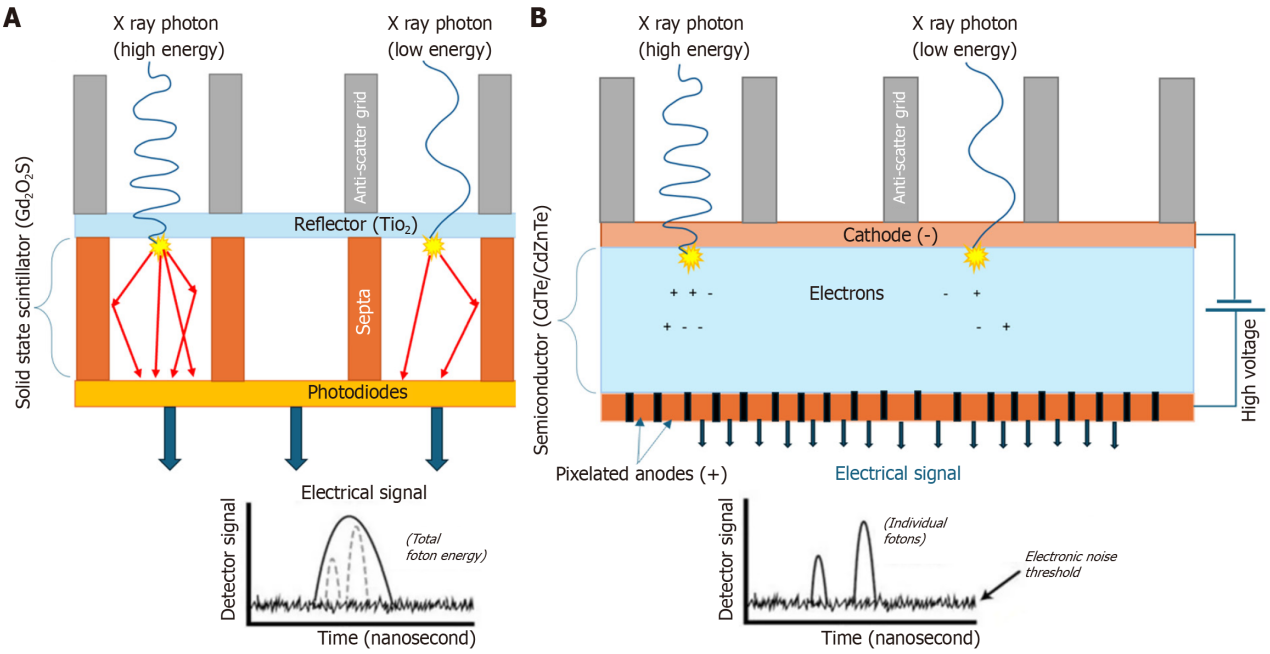


Figure 1 A comparison of traditional energy integrating *vs* photon-counting detector systems. A: Energy integrating; B: Photon-counting detector.

mm[8]. PCCT can effectively improve the image quality of CTA maximum intensity projection (MIP) images, benefiting the visualization of perforating or small vessels for a given radiation exposure level, as evidenced by its ability to unveil structures not seen before, such as short and long posterior ciliary arteries. A recent work by Harvey *et al*[8] studied the potential benefits of using PCCT to improve the performance of CTA in imaging these small arteries. In particular, the study focused on an important component of the CTA image package known as the MIP image. PCDs lead to improved vessel SNR in MIP images since the SNR of PCCT MIP was found to be 5.8 ± 1.3 for PCCT, compared with 4.4 ± 0.9 for MDCT ($P < 0.01$)[8]. Further, the enhanced spatial resolution helps in identifying the arteriovenous malformation nidus and its reduction upon gamma-knife treatment.

SIH and CSF venous fistulas

Cerebrospinal fluid (CSF)-venous fistulas (CVFs), first identified in 2014, are a significant cause of spontaneous intracranial hypotension (SIH). Detecting CVFs using standard anatomical imaging can be difficult because, unlike other spinal CSF leaks, they do not typically result in fluid pooling in the epidural space, and the imaging signs are often subtle. To aid in CVF detection, specialized myelographic techniques have been developed[11]. Recently, PCCT myelography (PC-CTM) has been introduced as an effective method for identifying CSF-venous fistulas, demonstrating its potential for early diagnosis and targeted treatment of SIH. PC-CTM is likely to offer advantages in localizing dural tears, a different type of spontaneous spinal CSF leak that requires distinct myelographic techniques for accurate identification[7]. The high spatial resolution of PCCT allows for precise anatomical identification of leak sites with high sensitivity, without significant loss of specificity (Figure 2). This technique is capable of localizing subtle leaks and characterizing small osseous spicules. Additionally, it enables the creation of virtual monoenergetic images without dual-energy techniques and improves the visibility of nerve root sleeves, enhancing the detection and assessment of CVF leaks[12].

The Bern score, which is based on brain magnetic resonance imaging findings in patients with suspected SIH, categorizes patients into high, intermediate, or low probabilities of having a spinal CSF leak or CVF, aiding in the selection of further investigations like digital subtraction myelography (DSM) or CT myelography[13-15]. These procedures, while necessary, are invasive, time-intensive, and involve significant radiation exposure. PCCT has shown potential for reducing radiation doses compared to EID-CT, making PC-CTM an appealing first-line imaging choice, particularly for younger patients. PC-CTM also offers enhanced visualization of venous abnormalities, including arteriovenous malformations and vascular shunts[13-15]. Works of Madhavan *et al*[16] found that decubitus PC-CTM for patients with intermediate and high Bern scores achieved diagnostic yields comparable to those reported for decubitus DSM and EID-CTM. Notably, PC-CTM showed higher yields in patients with low-probability Bern scores than other methods. However, the retrospective nature of this study calls for future prospective research to compare the sensitivity of PC-CTM with other modalities[17]. Another study by the same group confirmed the superiority of PC-CTM over DSM and EID-CTM for detecting CVFs, though limited by a small sample size, highlighting the need for studies involving larger patient groups[18]. PC-CTM offers further benefits, such as thinner axial section thicknesses (0.2-0.4 mm compared to 0.6 mm in EID-CT) for clearer visualization of small veins and improved temporal resolution. Faster scan speeds (average of 5.0 seconds) reduce motion artifacts and enable multiple time-point sampling within short intervals[18].

Acute ischemic stroke

PCCT images have 12.8%-20.6% less image noise and a 19%-20% higher signal-to-noise ratio than EID-CT for both grey



Figure 2 Cerebrospinal fluid-venous fistulas are challenging to detect using conventional computed tomography imaging. NAEOTOM Alpha makes Cerebrospinal fluid-venous fistulas visible (orange coloured arrow). Copyright ©Siemens Healthineers AG 2024. The authors have obtained the permission (Supplementary material).

and white matter, resulting in improved image quality and enhanced grey-white matter contrast, being about 15.7% higher compared to EID-CT[19,20]. As a result, it has the potential to significantly aid in the early detection and diagnosis of brain pathologies, including acute strokes, intracranial hemorrhage, and other soft-tissue abnormalities, by identifying subtle attenuation differences such as grey matter hypoattenuation changes, the insular ribbon sign, and other early ischemic changes[19,20]. In acute ischemic stroke patients, distinguishing between contrast pooling and hemorrhages (subarachnoid or parenchymal) is crucial for post-mechanical thrombectomy management. PCCT can accurately differentiate between hemorrhage and contrast media, preventing misdiagnosis and ensuring appropriate treatment decisions [19-21]. PCCT can potentially streamline acute stroke protocols by enabling multi-contrast imaging in a single scan, reducing time delays and improving diagnostic accuracy[22].

Imaging of atherosclerotic plaques

While traditional CT is commonly used for identifying calcium in atheromatous plaques, plaque rupture risk is influenced by several other factors beyond just calcium, such as intraplaque hemorrhage and lipid content. PCCT has the potential to go beyond calcium detection, making it highly valuable for evaluating the broader composition of atherosclerotic plaques. This could enhance our understanding of rupture-prone plaques, improving diagnosis, risk assessment, and the monitoring of treatments or preventive measures[23]. A recent study conducted using five carotid plaques from donations of patients with carotid stenosis undergoing endarterectomy showed that PCCT can distinguish several rupture-prone plaque features: Calcium and thrombus were shown to be distinguishable from intraplaque hemorrhage, fibrosis, fibrous cap, lipids, and necrosis. PCCT has the potential to detect photons in separate energy bins, reducing energy overlap and improving spectral separation. At high resolution, PCCT reduces calcium overestimation by minimizing blooming artifacts, a limitation of conventional CT. The study was, however, limited by the small number of carotid plaques and was conducted *ex vivo* without the use of contrast agents. The use of contrast agents would likely improve differentiation of plaque features[24].

Spectral PCCT faces technical challenges, including charge sharing, K-fluorescence escape, and photon count rate limitations, which affect spatial and energy resolution. Mitigations to these challenges include techniques like Charge summing, pixel masking, per-pixel calibration, and protocol optimizations, with anticipated future improvements as the technology evolves. Once adapted clinically, spectral PCCT could enable precise diagnosis and treatment planning, giving clinicians a detailed view of atheroma within arteries for better surgical intervention outcomes[25]. Experimental studies with apolipoprotein E knockout mice showed spectral PCCT's ability to differentiate materials like gold, iodine, and bone, revealing macrophage accumulation in atherosclerotic models[26,27].

Post-treatment follow-up of treated aneurysms and intracranial stents

PCCT angiography can serve as an alternative to selective angiography, providing a less invasive and lower-radiation option for patients. This is especially valuable in cranial and spinal imaging, though detailed hemodynamic studies may still require conventional cerebral angiography[28]. PCCT angiography offers high precision in visualizing metallic stent structures, supporting its use in both stent and vascular imaging. Known for its enhanced spatial resolution, cone-beam CT with diluted contrast media is widely used for postoperative evaluations, particularly to assess stent adhesion and detect in-stent thrombosis. Given that PCCT angiography achieves comparable image quality to cone-beam CT, it presents a promising, less invasive alternative for detailed postoperative vascular assessments, allowing for effective monitoring of stent apposition, in-stent thrombosis (Figure 3), and intimal hyperplasia[28,29]. The PCCT angiography images captured the stent's structure, and comparison of three-dimensional images from EID-CTA and PCCT angiography demonstrated that PCCT angiography offered superior resolution for evaluating stent shape and apposition. High

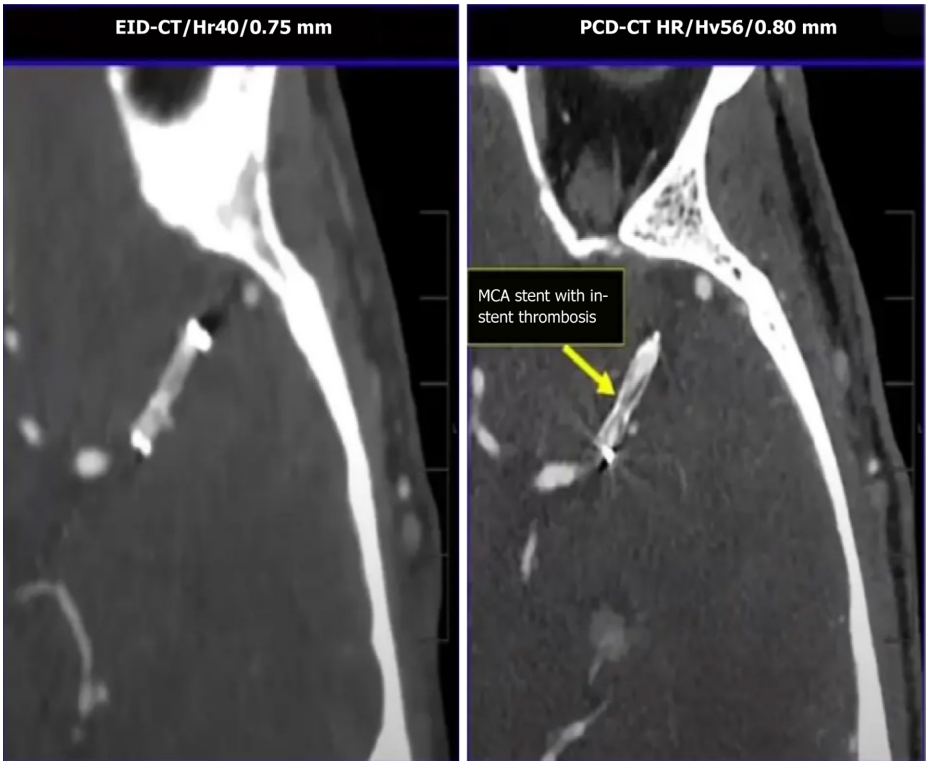


Figure 3 Image showing a conventional image of a head computed tomography angiogram (on the left) and its corresponding photon-counting computed tomography version (on the right), which clearly shows a middle cerebral artery stent with in-stent thrombosis. EID-CT: Energy-integrating detector-computed tomography; PCD-CT: Photon-counting detector-computed tomography; MCA: Middle cerebral artery. Image courtesy of Professor Cynthia H McCollough, Mayo Clinic, Rochester, MN, United States.

kernels in PCCT enable detailed visualization of stent mesh and lumen, allowing clinicians to assess the stent's integration with the vessel wall and detect issues like partial attachment ("fish-mouthing"). However, further research is needed to optimize kernel settings for evaluating in-stent intimal growth[29].

Assessment of DBS electrodes

Directional deep-brain stimulation (DBS) electrodes are increasingly used, but conventional CT is unable to directly image segmented contacts owing to physics-based resolution constraints. PCDs are a relatively novel technology that enables high-resolution imaging while addressing several limitations intrinsic to conventional CT[30] (Figure 4). Post-operative electrode segment orientation assessment is necessary because of the possibility of significant deviation during or immediately after insertion. PCCT can enable clear *in vivo* imaging of DBS electrodes, including segmented contacts and markers for all major lead manufacturers[31] (Figure 5). Manfield *et al*[30] describe postoperative imaging and reconstruction protocols developed to enable optimal lead visualization. High-fidelity images were obtained for 15 patients, clearly indicating the segmented contacts and directional markers both on CT alone and when fused to magnetic resonance imaging[30,32]. The highest resolution offered by PCCT is now 0.11 mm, some two to four times finer than that of contemporary conventional CT[33]. PCCT, including high-resolution lead tip imaging, delivered a statistically significant 13% dose reduction compared with their previously used combination of standard head CT plus fluoroscopy [30]. For most leads, the directly imaged lead orientations and depths corresponded closely to those predicted by CT artifact-based reconstructions. Indeed, conventional CT artifact-based methods can have a 180° error in orientation assessment, whereas PCCT provides direct and accurate imaging of lead orientation[30].

PCCT scans offer clearer imaging of electrode contacts and internal structures, which can aid in identifying faults in cases of suspected lead fractures. Variations in lead construction among manufacturers influence the ability to resolve internal structures[34-36]. PCCT can easily capture the directional segmentation of DBS electrodes for all major commercial systems, while also reducing radiation exposure compared to traditional imaging techniques. Its capability to discern fine details, such as the individual wires in certain DBS leads, provides valuable insights for diagnosing potential issues like lead fractures. Postoperative PCCT imaging is already a routine practice in many DBS centers for confirming target accuracy and excluding hematomas[30]. Using PCCT for DBS electrode imaging enables anatomically guided programming, which may streamline device setup and reduce time and complexity. Conventional methods, such as rotational fluoroscopy and CT artifact analysis, have limitations, including the need for orthogonal views and the potential for miscalculations in lead orientation[30].

Middle ear and internal ear

PCCT offers superior in-plane resolution and thinner section thickness compared to EID-CT. This enhanced resolution

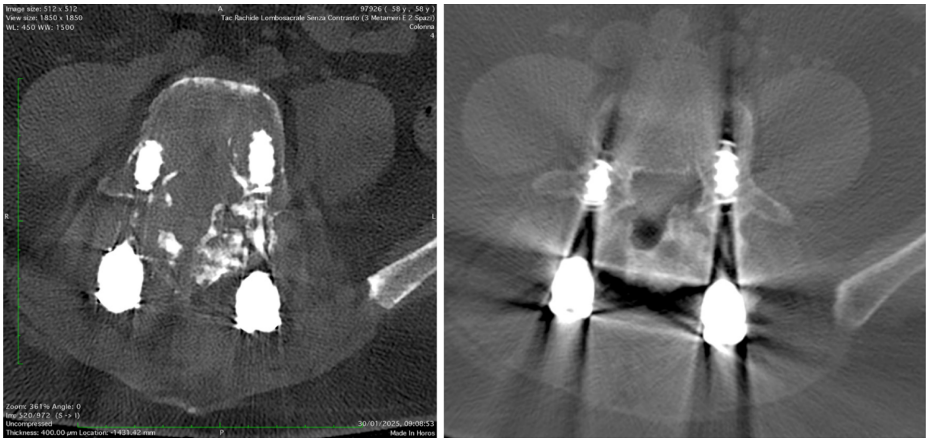


Figure 4 On the lumbar spine images acquired on the photon-counting computed tomography (on the left), the metallic artifacts are less evident when compared with conventional computed tomography (on the right).

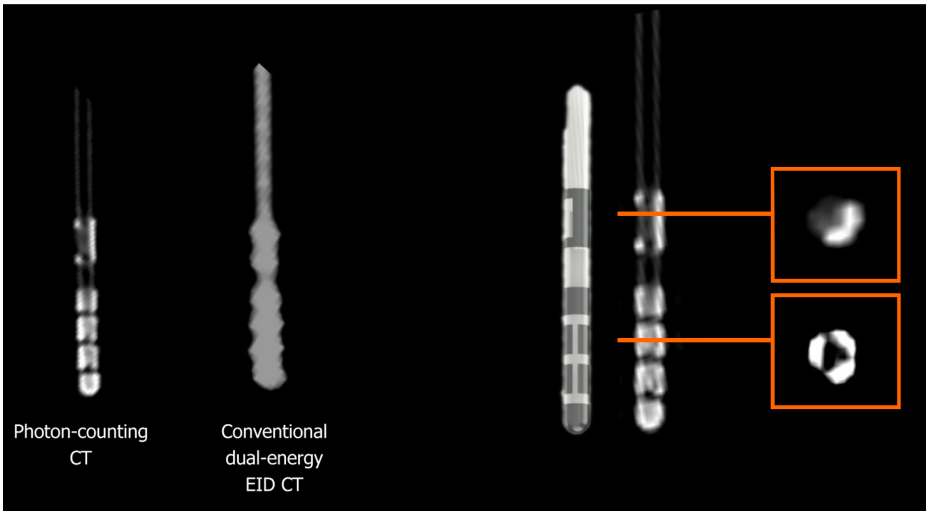


Figure 5 Direct visualization of the DBS electrode with photon-counting computed tomography without having to rely on streak artifacts that overlap each other with multiple electrodes. CT: Computed tomography; EID-CT: Energy-integrating detector-computed tomography. Image courtesy of Professor Erik H Middlebrooks, Mayo Clinic, Jacksonville, FL, United States.

produces sharper images that consistently reveal fine details. Specifically, the microarchitecture of the ossicles, ossicular ligaments, tendons, and bony protuberances, which are crucial for accurate interpretation, is much more clearly visualized with PCCT. PCCT images offer detailed visualization of the complex anatomy of the epitympanum and hypotympanum, which are essential for diagnosing middle ear pathologies[37]. This enhanced clarity is especially relevant for assessing ossicular chain anomalies, including discontinuities, fibrous unions, congenital fusions, and fixations such as otosclerosis (Figure 6) and tympanosclerosis, thereby potentially improving clinical outcomes in ear pathology diagnostics[38]. Although ossicular chain dislocation is uncommon and often related to temporal bone trauma, its exact prevalence is not well defined. Approximately 50% of temporal bone fractures involve ossicular damage, but dislocations can occur even in the absence of fractures. Conventional imaging often struggles to detect dislocations, particularly in the incudomalleolar joint, whereas PCCT excels in identifying even minor dislocations with higher precision. The three-dimensional reconstruction capability further enhances the assessment of incudomalleolar and incudostapedial joints from various perspectives, improving diagnostic accuracy[37-39].

A study evaluating PCCT highlighted its potential for enhanced postoperative cochlear implantation imaging, which was shown by the fact that PCCT achieved higher interelectrode wire visibility (81.5%) compared to EID CT (EID-CT, 67.9%; $P < 0.001$)[40]. Additionally, PCCT provided more accurate measurements of electrode contact diameters, closer to the gold standard. No significant differences were observed in halo artifact diameters between the two modalities. While promising, the study's small sample size and use of cadaveric specimens necessitate further research to validate these findings and optimize imaging settings[40].

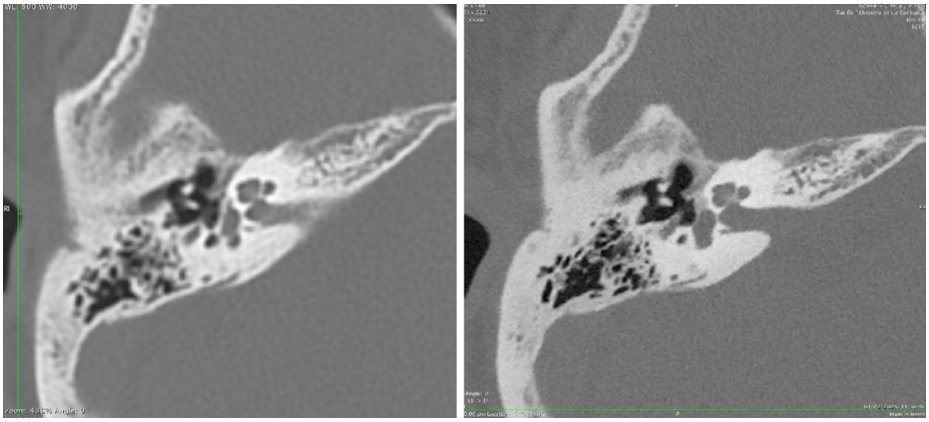


Figure 6 Axial high-resolution computed tomography image of the right temporal bone. On the photon-counting computed tomography image on the right is clearly evident a focus of otospongiosis that cannot be clearly identified on the traditional computed tomography image on the left. Visualized in the form of a hypodense demineralized otosclerotic plaque is noted in the fissula ante fenestram.

TECHNICAL CHALLENGES

PCCT in neuroimaging faces several limitations that impact its clinical utility. Protocol optimization remains a challenge, as PCCT systems introduce additional complexity with adjustable bin thresholds, increasing the risk of errors that may necessitate rescans[41]. Unlike conventional CT, PCCT lacks integrated artificial intelligence-based noise reduction algorithms, which are critical for achieving both high resolution and low dose imaging[42]. Furthermore, PCCT generates significantly larger data volumes - estimated at 2-35 times higher than conventional CT - complicating storage, interpretation, and workflow management[3,43]. The quality of monoenergetic reformats in commercially available PCCT systems is inferior to dual-energy CT in key image quality parameters, and persistent artifacts below the calvarium and in the posterior fossa further diminish diagnostic reliability[44]. Additionally, PCCT systems currently offer fewer spectral outputs (four) compared to spectral CT systems (ten), limiting their analytical potential in applications such as proton therapy planning[3]. These challenges underscore the need for technological advancements to fully realize PCCT's potential in neuroimaging.

FUTURE DIRECTIONS AND CLINICAL OUTLOOK

PCCT's primary advantages - namely ultra-high spatial resolution, spectral quantification, and reduced radiation exposure - position it as a transformative modality for neurological imaging. Future development will likely focus on integrating artificial intelligence for noise suppression and automated spectral decomposition, expanding applications in perfusion and functional neuroimaging, and enhancing vendor interoperability. The next phase of PCCT adoption will depend on protocol standardization, cross-vendor calibration, and outcome-based validation in large patient cohorts.

CONCLUSION

PCCT marks a significant step forward in neuroimaging, delivering superior image quality, advanced spectral imaging, and reduced artifacts compared to traditional CT modalities. Its potential to improve the diagnosis of complex neurological conditions such as vascular abnormalities, CSF leaks, and acute ischemic strokes is evident from emerging studies (Table 2). Despite these advancements, technical challenges such as protocol optimization, data management, and noise reduction must be addressed to enable widespread clinical implementation. Future developments, including the integration of artificial intelligence algorithms and enhanced hardware designs, will be critical to overcoming current limitations. With continued innovation, PCCT is poised to become a cornerstone of neuroimaging, offering unparalleled diagnostic insights and patient care.

Table 2 Summary of established clinical neuroimaging applications of photon-counting computed tomography, along with the key properties of photon-counting computed tomography that provide benefits over conventional computed tomography

Clinical application	Key properties of PCCT	Advantages in neurology
Neurovascular imaging	High spatial resolution, reduction of blooming artifacts, enhanced visualization of stents and metallic implants	Improved evaluation of tiny intracranial vessels, arterial stenoses, and vascular stents; reduced artifacts near the skull

		base
Acute ischemic stroke	Superior signal-to-noise ratio, enhanced grey-white matter contrast	Early detection of ischemic changes, differentiation of hemorrhage from contrast media
Spinal CSF leaks and fistulas	Enhanced resolution, virtual monoenergetic imaging	Precise detection of CSF leaks and venous fistulas, reduced radiation exposure
Deep brain stimulation electrode imaging	Ultra-high resolution, reduced noise, clear visualization of segmented contacts	Accurate postoperative assessment of electrode placement and orientation
Middle and internal ear pathologies	Superior in-plane resolution, thinner section thickness	Enhanced visualization of ossicular chains, dislocations, and cochlear implant positioning
Atherosclerotic plaque characterization	Material differentiation through spectral imaging	Improved detection of rupture-prone plaques and assessment of intraplaque hemorrhage and lipid content
Post-treatment monitoring (Aneurysms and stents)	High-resolution imaging, reduced blooming artifacts	Detailed visualization of stent apposition, in-stent stenoses, and aneurysm occlusion devices
Cranial and spinal tumors	Enhanced contrast-to-noise ratio, soft-tissue resolution	Better delineation of tumor margins and detection of smaller lesions

PCCT: Photon-counting computed tomography; CSF: Cerebrospinal fluid.

FOOTNOTES

Author contributions: Perera Molligoda Arachchige AS conceived, designed, and planned the review; Politi LS and Perera Molligoda Arachchige AS prepared and curated the figures; all authors contributed equally to the literature review, critical discussion, and revision of the manuscript draft written by Perera Molligoda Arachchige AS. All authors read and approved the final version of the manuscript.

Conflict-of-interest statement: All the authors report no relevant conflicts of interest for this article.

Open Access: This article is an open-access article that was selected by an in-house editor and fully peer-reviewed by external reviewers. It is distributed in accordance with the Creative Commons Attribution NonCommercial (CC BY-NC 4.0) license, which permits others to distribute, remix, adapt, build upon this work non-commercially, and license their derivative works on different terms, provided the original work is properly cited and the use is non-commercial. See: https://creativecommons.org/Licenses/by-nc/4.0/

Country of origin: Italy

ORCID number: Arosh S Perera Molligoda Arachchige 0000-0002-3875-0267; Gabriel Amorim Moreira Alves 0009-0003-0148-6401; Letterio S Politi 0000-0002-6190-6688.

S-Editor: Bai SR
L-Editor: A
P-Editor: Zhang YL

REFERENCES

1 Understanding the technology behind photon-counting CT. [cited 31 March 2025]. Available from: https://www.siemens-healthineers.com/en-us/computed-tomography/technologies-and-innovations/photon-counting-ct
2 **Wang A**, Cunningham I, Danielsson M, Fahrig R, Flohr T, Hoeschen C, Noo F, Sabol JM, Siewerdsen JH, Tingberg A, Yorkston J, Zhao W, Samei E. Science and practice of imaging physics through 50 years of SPIE Medical Imaging conferences. *J Med Imaging (Bellingham)* 2022; **9**: 012205 [*RCA*] [PMID: 35309720 DOI: 10.1117/1.JMI.9.S1.012205] [FullText]
3 **Potter CA**, Sodickson AD. Dual-Energy CT in Emergency Neuroimaging: Added Value and Novel Applications. *Radiographics* 2016; **36**: 2186-2198 [*RCA*] [PMID: 27831844 DOI: 10.1148/rg.2016160069] [FullText]
4 FDA Clears First Major Imaging Device Advancement for Computed Tomography in Nearly a Decade. [cited 31 March 2025]. Available from: https://www.fda.gov/news-events/press-announcements/fda-clears-first-major-imaging-device-advancement-computed-tomography-nearly-decade
5 **Esquivel A**, Ferrero A, Mileto A, Baffour F, Horst K, Rajiah PS, Inoue A, Leng S, McCollough C, Fletcher JG. Photon-Counting Detector CT: Key Points Radiologists Should Know. *Korean J Radiol* 2022; **23**: 854-865 [*RCA*] [PMID: 36047540 DOI: 10.3348/kjr.2022.0377] [FullText] [Full Text(PDF)]
6 **Kreisler B**. Photon counting Detectors: Concept, technical Challenges, and clinical outlook. *Eur J Radiol* 2022; **149**: 110229 [*RCA*] [PMID: 35278927 DOI: 10.1016/j.ejrad.2022.110229] [FullText]
7 **Madhavan AA**, Bathla G, Benson JC, Diehn FE, Nagelschneider AA, Lehman VT. High yield clinical applications for photon counting CT in neurovascular imaging. *Br J Radiol* 2024; **97**: 894-901 [*RCA*] [PMID: 38460543 DOI: 10.1093/bjr/tqae058] [FullText]
8 **Harvey EC**, Feng M, Ji X, Zhang R, Li Y, Chen GH, Li K. Impacts of photon counting CT to maximum intensity projection (MIP) images of cerebral CT angiography: theoretical and experimental studies. *Phys Med Biol* 2019; **64**: 185015 [*RCA*] [PMID: 31315093 DOI: 10.1088/1361-6560/ab32fe] [FullText]

9 **Perera Molligoda Arachchige AS**, Verma Y. Role of photon-counting computed tomography in pediatric cardiovascular imaging. *World J Clin Pediatr* 2025; **14**: 99288 [*RCA*] [PMID: 40059896 DOI: 10.5409/wjcp.v14.i1.99288] [FullText] [Full Text(PDF)]

10 **Meloni A**, Cau R, Saba L, Positano V, De Gori C, Occhipinti M, Celi S, Bossone E, Bertacchi J, Punzo B, Mantini C, Cavaliere C, Maffei E, Cademartiri F. Photon-Counting Computed Tomography Angiography of Carotid Arteries: A Topical Narrative Review with Case Examples. *Diagnostics (Basel)* 2024; **14**: 2012 [*RCA*] [PMID: 39335691 DOI: 10.3390/diagnostics14182012] [FullText]

11 **Kranz PG**, Gray L, Malinzak MD, Houk JL, Kim DK, Amrhein TJ. CSF-Venous Fistulas: Anatomy and Diagnostic Imaging. *AJR Am J Roentgenol* 2021; **217**: 1418-1429 [*RCA*] [PMID: 34191547 DOI: 10.2214/AJR.21.26182] [FullText]

12 **Schwartz FR**, Kranz PG, Malinzak MD, Cox DN, Ria F, McCabe C, Harrawood B, Leithe LG, Samei E, Amrhein TJ. Myelography Using Energy-Integrating Detector CT Versus Photon-Counting Detector CT for Detection of CSF-Venous Fistulas in Patients With Spontaneous Intracranial Hypotension. *AJR Am J Roentgenol* 2024; **222**: e2330673 [*RCA*] [PMID: 38294163 DOI: 10.2214/AJR.23.30673] [FullText] [Full Text(PDF)]

13 **Dobrocky T**, Grunder L, Breiding PS, Branca M, Limacher A, Mosimann PJ, Mordasini P, Zibold F, Haeni L, Jesse CM, Fung C, Raabe A, Ulrich CT, Gralla J, Beck J, Piechowiak EI. Assessing Spinal Cerebrospinal Fluid Leaks in Spontaneous Intracranial Hypotension With a Scoring System Based on Brain Magnetic Resonance Imaging Findings. *JAMA Neurol* 2019; **76**: 580-587 [*RCA*] [PMID: 30776059 DOI: 10.1001/jamaneurol.2018.4921] [FullText]

14 **Callen AL**, Pattee J, Thaker AA, Timpone VM, Zander DA, Turner R, Birlea M, Wilhour D, O'Brien C, Evan J, Grassia F, Carroll IR. Relationship of Bern Score, Spinal Elastance, and Opening Pressure in Patients With Spontaneous Intracranial Hypotension. *Neurology* 2023; **100**: e2237-e2246 [*RCA*] [PMID: 37015821 DOI: 10.1212/WNL.0000000000207267] [FullText]

15 **Huynh TJ**, Parizadeh D, Ahmed AK, Gandia CT, Davison HC, Murray JV, Mark IT, Madhavan AA, Shlapak D, Rozen TD, Brinjikji W, Vibhute P, Gupta V, Brewer K, Fermo O. Lateral Decubitus Dynamic CT Myelography with Real-Time Bolus Tracking (dCTM-BT) for Evaluation of CSF-Venous Fistulas: Diagnostic Yield Stratified by Brain Imaging Findings. *AJNR Am J Neuroradiol* 2023; **45**: 105-112 [*RCA*] [PMID: 38164531 DOI: 10.3174/ajnr.A8082] [FullText]

16 **Madhavan AA**, Cutsforth-Gregory JK, Brinjikji W, Bathla G, Benson JC, Diehn FE, Eckel LJ, Mark IT, Morris PP, Payne MA, Verdoorn JT, Weber NM, Yu L, Baffour F, Fletcher JG, McCollough CH. Diagnostic Performance of Decubitus Photon-Counting Detector CT Myelography for the Detection of CSF-Venous Fistulas. *AJNR Am J Neuroradiol* 2023; **44**: 1445-1450 [*RCA*] [PMID: 37945523 DOI: 10.3174/ajnr.A8040] [FullText]

17 **Madhavan AA**, Cutsforth-Gregory JK, Brinjikji W, Benson JC, Johnson-Tesch BA, Liebo GB, Mark IT, Oien MP, Shlapak DP, Yu L, Verdoorn JT. Benefits of Photon-Counting CT Myelography for Localization of Dural Tears in Spontaneous Intracranial Hypotension. *AJNR Am J Neuroradiol* 2024; **45**: 668-671 [*RCA*] [PMID: 38485199 DOI: 10.3174/ajnr.A8179] [FullText]

18 **Madhavan AA**, Yu L, Brinjikji W, Cutsforth-Gregory JK, Schwartz FR, Mark IT, Benson JC, Amrhein TJ. Utility of Photon-Counting Detector CT Myelography for the Detection of CSF-Venous Fistulas. *AJNR Am J Neuroradiol* 2023; **44**: 740-744 [*RCA*] [PMID: 37202116 DOI: 10.3174/ajnr.A7887] [FullText]

19 **Pourmorteza A**, Symons R, Reich DS, Bagheri M, Cork TE, Kappler S, Ulzheimer S, Bluemke DA. Photon-Counting CT of the Brain: In Vivo Human Results and Image-Quality Assessment. *AJNR Am J Neuroradiol* 2017; **38**: 2257-2263 [*RCA*] [PMID: 28982793 DOI: 10.3174/ajnr.A5402] [FullText]

20 **Risch F**, Berlis A, Kroencke T, Schwarz F, Maurer CJ. Discrimination of Hemorrhage and Contrast Media in a Head Phantom on Photon-Counting Detector CT Data. *AJNR Am J Neuroradiol* 2024; **45**: 183-187 [*RCA*] [PMID: 38164551 DOI: 10.3174/ajnr.A8093] [FullText]

21 **Jarunnarumol N**, Kamalian S, Lev MH, Gupta R. Neuroradiology Applications of Dual and Multi-energy Computed Tomography. *Radiol Clin North Am* 2023; **61**: 973-985 [*RCA*] [PMID: 37758364 DOI: 10.1016/j.rcl.2023.05.009] [FullText]

22 **Abel F**, Schubert T, Winklhofer S. Advanced Neuroimaging With Photon-Counting Detector CT. *Invest Radiol* 2023; **58**: 472-481 [*RCA*] [PMID: 37158466 DOI: 10.1097/RLI.0000000000000984] [FullText]

23 **Shami A**, Sun J, Gialeli C, Markstad H, Edsfeldt A, Aurumskjöld ML, Gonçalves I. Atherosclerotic plaque features relevant to rupture-risk detected by clinical photon-counting CT ex vivo: a proof-of-concept study. *Eur Radiol Exp* 2024; **8**: 14 [*RCA*] [PMID: 38286959 DOI: 10.1186/s41747-023-00410-4] [FullText]

24 **Healy J**, Searle E, Panta RK, Chernoglazov A, Roake J, Butler P, Butler A, Gieseg SP; MARS collaboration. Ex-vivo atherosclerotic plaque characterization using spectral photon-counting CT: Comparing material quantification to histology. *Atherosclerosis* 2023; **378**: 117160 [*RCA*] [PMID: 37495488 DOI: 10.1016/j.atherosclerosis.2023.06.007] [FullText]

25 **Wang AS**, Pelc NJ. Spectral Photon Counting CT: Imaging Algorithms and Performance Assessment. *IEEE Trans Radiat Plasma Med Sci* 2021; **5**: 453-464 [*RCA*] [PMID: 35419500 DOI: 10.1109/trpms.2020.3007380] [FullText]

26 **Cormode DP**, Roessl E, Thran A, Skajaa T, Gordon RE, Schlomka JP, Fuster V, Fisher EA, Mulder WJ, Proksa R, Fayad ZA. Atherosclerotic plaque composition: analysis with multicolor CT and targeted gold nanoparticles. *Radiology* 2010; **256**: 774-82. [*RCA*] [PMID: 20668118 DOI: 10.1148/radiol.10092473] [FullText] [Full Text(PDF)]

27 **Cormode DP**, Si-Mohamed S, Bar-Ness D, Sigovan M, Naha PC, Balegamire J, Lavenne F, Coulon P, Roessl E, Bartels M, Rokni M, Blevis I, Boussel L, Douek P. Multicolor spectral photon-counting computed tomography: in vivo dual contrast imaging with a high count rate scanner. *Sci Rep* 2017; **7**: 4784 [*RCA*] [PMID: 28684756 DOI: 10.1038/s41598-017-04659-9] [FullText] [Full Text(PDF)]

28 **Higaki F**, Hiramatsu M, Yasuhara T, Sasada S, Otani Y, Haruma J, Inoue T, Morimitsu Y, Akagi N, Matsui Y, Iguchi T, Hiraki T. Cranial and spinal computed tomography (CT) angiography with photon-counting detector CT: comparison with angiographic and operative findings. *Jpn J Radiol* 2025; **43**: 143-151 [*RCA*] [PMID: 39283532 DOI: 10.1007/s11604-024-01661-w] [FullText]

29 **Funama Y**, Oda S, Teramoto F, Aoki Y, Takahashi I, Kojima S, Goto T, Tanaka K, Kidoh M, Nagayama Y, Nakaura T, Hirai T. Improving Visualization of In-stent Lumen Using Prototype Photon-counting Detector Computed Tomography with High-resolution Plaque Kernel. *J Med Phys* 2024; **49**: 127-132 [*RCA*] [PMID: 38828063 DOI: 10.4103/jmp.jmp_163_23] [FullText] [Full Text(PDF)]

30 **Manfield J**, Thomas S, Bogdanovic M, Sarangmat N, Antoniades C, Green AL, FitzGerald JJ. Seeing Is Believing: Photon Counting Computed Tomography Clearly Images Directional Deep Brain Stimulation Lead Segments and Markers After Implantation. *Neuromodulation* 2024; **27**: 557-564 [*RCA*] [PMID: 37921733 DOI: 10.1016/j.neurom.2023.09.003] [FullText]

31 **Egger K**, Rau A, Urbach H, Reisert M, Reinacher PC. 3D X-ray based visualization of directional deep brain stimulation lead orientation. *J Neuroradiol* 2022; **49**: 293-297 [*RCA*] [PMID: 33984378 DOI: 10.1016/j.neurad.2021.05.002] [FullText]

32 **Almahariq F**, Sedmak G, Vuletić V, Dlaka D, Orešković D, Marčinković P, Raguž M, Chudy D. The Accuracy of Direct Targeting Using Fusion of MR and CT Imaging for Deep Brain Stimulation of the Subthalamic Nucleus in Patients with Parkinson's Disease. *J Neurol Surg A*

Cent Eur Neurosurg 2021; **82**: 518-525 [*RCA*] [PMID: 33618414 DOI: 10.1055/s-0040-1715826] [FullText]

33 **Mergen V**, Sartoretti T, Baer-Beck M, Schmidt B, Petersilka M, Wildberger JE, Euler A, Eberhard M, Alkadhi H. Ultra-High-Resolution Coronary CT Angiography With Photon-Counting Detector CT: Feasibility and Image Characterization. *Invest Radiol* 2022; **57**: 780-788 [*RCA*] [PMID: 35640019 DOI: 10.1097/RLI.0000000000000897] [FullText] [Full Text(PDF)]

34 **Krauss JK**, Lipsman N, Aziz T, Boutet A, Brown P, Chang JW, Davidson B, Grill WM, Hariz MI, Horn A, Schulder M, Mammis A, Tass PA, Volkmann J, Lozano AM. Technology of deep brain stimulation: current status and future directions. *Nat Rev Neurol* 2021; **17**: 75-87 [*RCA*] [PMID: 33244188 DOI: 10.1038/s41582-020-00426-z] [FullText]

35 **Hart MG**, Posa M, Buttery PC, Morris RC. Increased variance in second electrode accuracy during deep brain stimulation and its relationship to pneumocephalus, brain shift, and clinical outcomes: A retrospective cohort study. *Brain Spine* 2022; **2**: 100893 [*RCA*] [PMID: 36248097 DOI: 10.1016/j.bas.2022.100893] [FullText] [Full Text(PDF)]

36 **Henry KR**, Miulli MM, Nuzov NB, Nolt MJ, Rosenow JM, Elahi B, Pilitsis J, Golestanirad L. Variations in Determining Actual Orientations of Segmented Deep Brain Stimulation Leads Using the DiODe Algorithm: A Retrospective Study Across Different Lead Designs and Medical Institutions. *Stereotact Funct Neurosurg* 2023; **101**: 338-347 [*RCA*] [PMID: 37717576 DOI: 10.1159/000531644] [FullText] [Full Text(PDF)]

37 **Rao D**, Murray JV, Agarwal AK, Sandhu SJ, Rhyner PA. Comprehensive Review of External and Middle Ear Anatomy on Photon-Counting CT. *AJNR Am J Neuroradiol* 2024; **45**: 1857-1864 [*RCA*] [PMID: 38806238 DOI: 10.3174/ajnr.A8359] [FullText]

38 **Takahashi Y**, Higaki F, Sugaya A, Asano Y, Kojima K, Morimitsu Y, Akagi N, Itoh T, Matsui Y, Hiraki T. Evaluation of the ear ossicles with photon-counting detector CT. *Jpn J Radiol* 2024; **42**: 158-164 [*RCA*] [PMID: 37633874 DOI: 10.1007/s11604-023-01485-0] [FullText] [Full Text(PDF)]

39 **Zhou W**, Lane JI, Carlson ML, Bruesewitz MR, Witte RJ, Koeller KK, Eckel LJ, Carter RE, McCollough CH, Leng S. Comparison of a Photon-Counting-Detector CT with an Energy-Integrating-Detector CT for Temporal Bone Imaging: A Cadaveric Study. *AJNR Am J Neuroradiol* 2018; **39**: 1733-1738 [*RCA*] [PMID: 30093479 DOI: 10.3174/ajnr.A5768] [FullText]

40 **Waldeck S**, Overhoff D, Alizadeh L, Becker BV, Port M, Froelich MF, Brockmann MA, Schumann S, Vogl TJ, Schoenberg SO, Schmidt S. Photon-Counting Detector CT Virtual Monoengergetic Images for Cochlear Implant Visualization-A Head to Head Comparison to Energy-Integrating Detector CT. *Tomography* 2022; **8**: 1642-1648 [*RCA*] [PMID: 35894001 DOI: 10.3390/tomography8040136] [FullText] [Full Text (PDF)]

41 **Yao Y**, Li L, Chen Z. Dynamic-dual-energy spectral CT for improving multi-material decomposition in image-domain. *Phys Med Biol* 2019; **64**: 135006 [*RCA*] [PMID: 30986774 DOI: 10.1088/1361-6560/ab196d] [FullText]

42 **Baffour FI**, Huber NR, Ferrero A, Rajendran K, Glazebrook KN, Larson NB, Kumar S, Cook JM, Leng S, Shanblatt ER, McCollough CH, Fletcher JG. Photon-counting Detector CT with Deep Learning Noise Reduction to Detect Multiple Myeloma. *Radiology* 2023; **306**: 229-236 [*RCA*] [PMID: 36066364 DOI: 10.1148/radiol.220311] [FullText]

43 **van der Bie J**, van Straten M, Booij R, Bos D, Dijkshoorn ML, Hirsch A, Sharma SP, Oei EHG, Budde RPJ. Photon-counting CT: Review of initial clinical results. *Eur J Radiol* 2023; **163**: 110829 [*RCA*] [PMID: 37080060 DOI: 10.1016/j.ejrad.2023.110829] [FullText]

44 **Michael AE**, Boriesosdick J, Schoenbeck D, Woeltjen MM, Saeed S, Kroeger JR, Horstmeier S, Lennartz S, Borggrefe J, Niehoff JH. Image-Quality Assessment of Polyenergetic and Virtual Monoenergetic Reconstructions of Unenhanced CT Scans of the Head: Initial Experiences with the First Photon-Counting CT Approved for Clinical Use. *Diagnostics (Basel)* 2022; **12**: 265 [*RCA*] [PMID: 35204356 DOI: 10.3390/diagnostics12020265] [FullText] [Full Text(PDF)]

World Journal of Radiology

Submit a Manuscript: https://www.f6publishing.com

World J Radiol 2025 November 28; 17(11): 113153

DOI: 10.4329/wjr.v17.i11.113153

ISSN 1949-8470 (online)

ORIGINAL ARTICLE

Retrospective Study

Variations in the spatial relationship between the hyoid bone and the carotid arteries and their clinical significance

Nektaria Karangeli, George Triantafyllou, Panagiotis Papadopoulos-Manolarakis, Nikolaos-Achilleas Arkoudis, Georgios Velonakis, Alexandros Samolis, Maria Piagkou

Specialty type: Radiology, nuclear medicine and medical imaging

Provenance and peer review: Invited article; Externally peer reviewed.

Peer-review model: Single blind

Peer-review report's classification

Scientific Quality: Grade A, Grade B, Grade B, Grade B, Grade C, Grade C

Novelty: Grade A, Grade B, Grade B, Grade B, Grade B, Grade C

Creativity or Innovation: Grade A, Grade B, Grade B, Grade B, Grade B, Grade C

Scientific Significance: Grade A, Grade B, Grade B, Grade B, Grade B, Grade C

P-Reviewer: Papadopoulos VP, MD, PhD, Assistant Professor, Associate Chief Physician, Greece; Shi YC, PhD, China; Zharikov YO, MD, PhD, Associate Professor, Russia

Received: August 18, 2025

Revised: September 3, 2025

Accepted: November 7, 2025

Published online: November 28, 2025

Processing time: 102 Days and 10.4 Hours

Nektaria Karangeli, George Triantafyllou, Panagiotis Papadopoulos-Manolarakis, Alexandros Samolis, Maria Piagkou, Department of Anatomy, School of Medicine, Faculty of Health Sciences, National and Kapodistrian University of Athens, Athens 11527, Attikí, Greece

George Triantafyllou, Maria Piagkou, "VARIANTIS" Research Laboratory, Department of Clinical Anatomy, Mazovian Academy in Płock, Płock 09-402, Poland

Panagiotis Papadopoulos-Manolarakis, Department of Neurosurgery, General Hospital of Nikaia-Piraeus, Athens 18454, Attikí, Greece

Nikolaos-Achilleas Arkoudis, Georgios Velonakis, Research Unit of Radiology and Medical Imaging, National and Kapodistrian University of Athens, Athens 11528, Greece

Nikolaos-Achilleas Arkoudis, Georgios Velonakis, Second Department of Radiology, General University Hospital "Attikon", National and Kapodistrian University of Athens, Athens 12462, Chaidari, Greece

Co-corresponding authors: George Triantafyllou and Nikolaos-Achilleas Arkoudis.

Corresponding author: Nikolaos-Achilleas Arkoudis, MD, PhD, Research Unit of Radiology and Medical Imaging, National and Kapodistrian University of Athens, 19 Papadiamantopoulou, Athens 11528, Greece. nick.arkoudis@gmail.com

Abstract

BACKGROUND

The topography between the common carotid artery (CA), internal CA, and external CA (ECA) with the greater horn of the hyoid bone (GHHB) is of particular importance for anatomists, radiologists and neck surgeons.

AIM

To investigate these topographical relationships emphasizing anatomical classification, sexual dimorphism, and clinical significance.

METHODS

A retrospective study was performed on 224 computed tomography angiographies from a cohort comprising 161 male and 63 female patients, with a mean age of 63.2 years. Multiplanar and three-dimensional reconstructions were

executed utilizing Horos software. The spatial relationships between the CA and hyoid bone were categorized based on the 12-type classification system delineated by Manta *et al* in 2023. The data were subsequently stratified by sex and laterality.

RESULTS

Type 0 (no arterial contact with the GHHB) was the most common configuration (46.9%), followed by type VI (ECA lateral to GHHB, 23.9%) and type VIII (internal CA and ECA lateral to GHHB, 13.2%). Bilateral symmetry was present in 54.02% of cases, mainly in males. Statistically significant sex-based differences were found (P = 0.012), while laterality was not significant (P = 0.779).

CONCLUSION

Carotid–hyoid topography displays significant anatomical variation with clinically essential patterns. Non-null variants, such as types VI and VIII, may increase the risk of dynamic carotid compression, especially in younger patients with cryptogenic cerebrovascular symptoms. Recognizing these variants during preoperative imaging is crucial to minimize surgical risk and inform patient care.

Key Words: External carotid artery; Internal carotid artery; Hyoid bone; Topography; Variation

©The Author(s) 2025. Published by Baishideng Publishing Group Inc. All rights reserved.

Core Tip: The spatial relationship between the hyoid bone and carotid arteries is highly variable and may predispose patients to vascular compression, stroke, or surgical complications. This retrospective computed tomography angiography-based study of 224 patients highlights common topographical variants, their sex-related distribution, and clinical implications. Recognition of these carotid-hyoid configurations in pre-operative imaging can aid in preventing iatrogenic injury, improving diagnosis in cryptogenic cerebrovascular events, and guiding safer surgical planning.

Citation: Karangeli N, Triantafyllou G, Papadopoulos-Manolarakis P, Arkoudis NA, Velonakis G, Samolis A, Piagkou M. Variations in the spatial relationship between the hyoid bone and the carotid arteries and their clinical significance. *World J Radiol* 2025; 17(11): 113153
URL: https://www.wjgnet.com/1949-8470/full/v17/i11/113153.htm
DOI: https://dx.doi.org/10.4329/wjr.v17.i11.113153

INTRODUCTION

A complex interplay of muscular, skeletal, and neurovascular elements defines the anatomy of the head and neck. Among these, the vascular structures exhibit considerable morphological and topographical variability, often with critical implications during diagnostic assessments and surgical interventions[1-6].

The common carotid artery (CCA) bifurcates into the internal carotid artery (ICA) and the external carotid artery (ECA), typically around the C3-C5 vertebral levels. However, this variation can be significant across individuals[7]. The ECA supplies the extracranial tissues of the head and neck, whereas the ICA predominantly serves intracranial structures, including cerebral circulation[8].

During their cervical course, the ICA and ECA exhibit distinct spatial relationships with bony landmarks, including the hyoid bone (HB), styloid process, and mandible. These relationships are not merely anatomical curiosities - they carry potential clinical consequences. Positional anomalies can contribute to vascular compression, altered hemodynamics, or surgical hazards during procedures in the parapharyngeal, retropharyngeal, or suprahyoid spaces[2,9-11]. However, the current literature lacks anatomical classifications and clear linking to clinical symptoms.

Our previous study, based on 100 computed tomography angiography cases, demonstrated that while HB often lies close to carotid arteries (CAs), its morphometric parameters (*e.g.*, horn length or angle) did not significantly influence arterial positioning[12]. However, given the increasing reports of functional carotid compression

by the HB in cases of transient ischemic attack (TIA) or unexplained cerebrovascular symptoms[13-15], further investigation in a larger cohort is warranted.

The objective of this radioanatomical study was to examine the topographical relationship between the CAs and the HB in a significantly larger dataset, with a focus on variant classification, sex differences, and potential clinical relevance.

MATERIALS AND METHODS

This retrospective study analyzed 224 computed tomography angiography scans archived at the General Hospital of Nikaia-Piraeus, following approval by the institutional ethics committee, approval No. 56485. The sample consisted of 224 patients (161 males and 63 females), aged 20 years to 89 years (mean age, 63.2 years). All scans were acquired using a 128-slice SOMATOM go. Top scanner (Siemens Healthineers), with patients positioned supine and the head in a neutral alignment. A 30% iodine-based contrast medium (60 mL) was administered intravenously at a rate of 4.0-4.5 mL/second. Inclusion criteria were excellent quality of the scan, without pathological processes distorting the anatomy of the area. Scans exhibiting inadequate image quality or anatomical distortion due to pathology (*e.g.*, tumor, trauma, congenital malformations) were excluded, as per the exclusion criteria defined in previous studies[9]. Image processing and analysis were performed using Horos software (Horos Project). Each dataset was reviewed in axial, coronal, and sagittal planes, with additional three-dimensional reconstructions generated for enhanced anatomical assessment.

The carotid bifurcation (CB) was first classified as either suprahyoid or infrahyoid, based on its vertical relation to the greater horn of the HB (GHHB) observed in sagittal views. Subsequently, the topographical relationships between the Cas - CCA, ICA, and ECA - and the GHHB were assessed in axial and 3D views. These spatial configurations were categorized using the twelve-type classification system introduced by Manta *et al*[2]. This system includes types 0 through XII, describing whether arteries pass medial, lateral, or posterior to the GHHB, or have no contact (null Type 0). Each type reflects distinct topographical variants that may influence clinical outcomes and surgical planning.

Demographic and anatomical data were stratified by side (left *vs* right) and sex (male *vs* female). Categorical variables were analyzed using the χ^2 test for unpaired comparisons and McNemar's test for paired variables. All statistical analyses were conducted using IBM SPSS Statistics for macOS, Version 29 (IBM Corp., Armonk, NY, United States), with a P value < 0.05 considered statistically significant.

RESULTS

Among the 448 heminecks evaluated (224 patients), 46.9% demonstrated no direct spatial relationship between the CAs and the HB (type 0). All the observed relationships are presented in Figures 1, 2, 3, 4, 5, 6, and 7. The most common non-null configuration was type VI, in which the ECA was lateral to the GHHB, observed in 23.9% of sides (Figure 3). This was followed by type VIII (both ICA and ECA lateral to the GHHB) in 13.2% (Figure 5), and type IX (ICA medial to the GHHB) in 10% (Figure 6). Less frequent configurations included type X (CB lateral to GHHB, 3.6%) (Figure 7), type XI (ECA lateral, ICA medial, 1.1%) (Figure 2), type I (ECA medial, 0.4%) (Figure 1), type XII (ECA medial, ICA lateral, 0.4%) (Figure 4), and type IV (CCA medial, 0.2%) (Figure 2). Types II, III, V, and VII were not observed in this cohort (Table 1).

Sex- and side-specific distributions depicted the following results: No significant association was found with side laterality (McNemar's test, $P = 0.779$); however, sex-based differences were significant (χ^2 test, $P = 0.012$). Males showed higher frequencies of types I, VI, and VIII, whereas females were more likely to present with types 0, IV, and IX through XII.

Analysis of bilateral symmetry revealed that 121 patients (54.02%) exhibited symmetrical carotid-hyoid topography. The most frequent symmetric configuration was bilateral type 0 (70 cases), followed by type VI (31 cases), type VIII (10 cases), type IX (9 cases), and type X (1 case). No bilateral cases were observed for the other configurations.

Bilateral symmetry was notably more common among males. Of the 70 bilateral null-type cases, 46 were male. Similarly, 25 of 31 type VI, 9 of 10 type VIII, and 7 of 9 type IX symmetric cases occurred in male patients. The single bilateral type X case was also male. No bilateral instances of types I, IV, XI, or XII were identified.

DISCUSSION

When comparing our findings with those reported by Manta *et al*[2], several notable differences and similarities become apparent. The proportion of null cases in our sample was lower (46.9%) compared to that reported by Manta *et al*[2] (57.14%), indicating possible variations in population anatomy, imaging protocols, or classification criteria. Both studies identified type VI as the most common anatomical pattern. However, differences emerged, such as the higher frequency of type VIII in our cohort *vs* its lower ranking in Manta *et al*[2] dataset. Conversely, types II, III, and V - found in Manta *et al*[2] study - were not observed in our analysis (Figure 8). These differences may be due to ethnic, geographical, or methodological factors and deserve further investigation across multiple centers (Table 2).

Sexual dimorphism became a significant factor. Our data revealed statistical differences between male and female distributions, which partially align with Manta *et al*'s report[2]. The female predominance in types IV, X, and XI, and male dominance in types I, VI, and VIII, support the idea that sex influences vascular topography. However, these sex-related results should be taken into careful consideration due to the sex imbalance of our sample. These patterns suggest

Table 1 The topographical types are categorized by sides and sexes, *n* (%)

Topographical types	Total	Left	Right	*P* value	Female	Male	*P* value
Type 0	210 (46.9)	107	103	0.779	69	141	0.012[a]
Type I	2 (0.4)	0	2		0	2	
Type II	0 (0)	0	0		0	0	
Type III	0 (0)	0	0		0	0	
Type IV	1 (0.2)	0	1		1	0	
Type V	0 (0)	0	0		0	0	
Type VI	107 (23.9)	50	57		29	78	
Type VII	1 (0.2)	0	1		0	1	
Type VIII	59 (13.2)	28	31		12	47	
Type IX	45 (10)	24	21		7	38	
Type X	16 (3.6)	10	6		4	12	
Type XI	5 (1.1)	3	2		3	2	
Type XII	2 (0.4)	2	0		1	1	

[a]*P* value < 0.05, statistically significant result.

The topographical types, as classified by Manta *et al*[2], are categorized by sides and sexes.

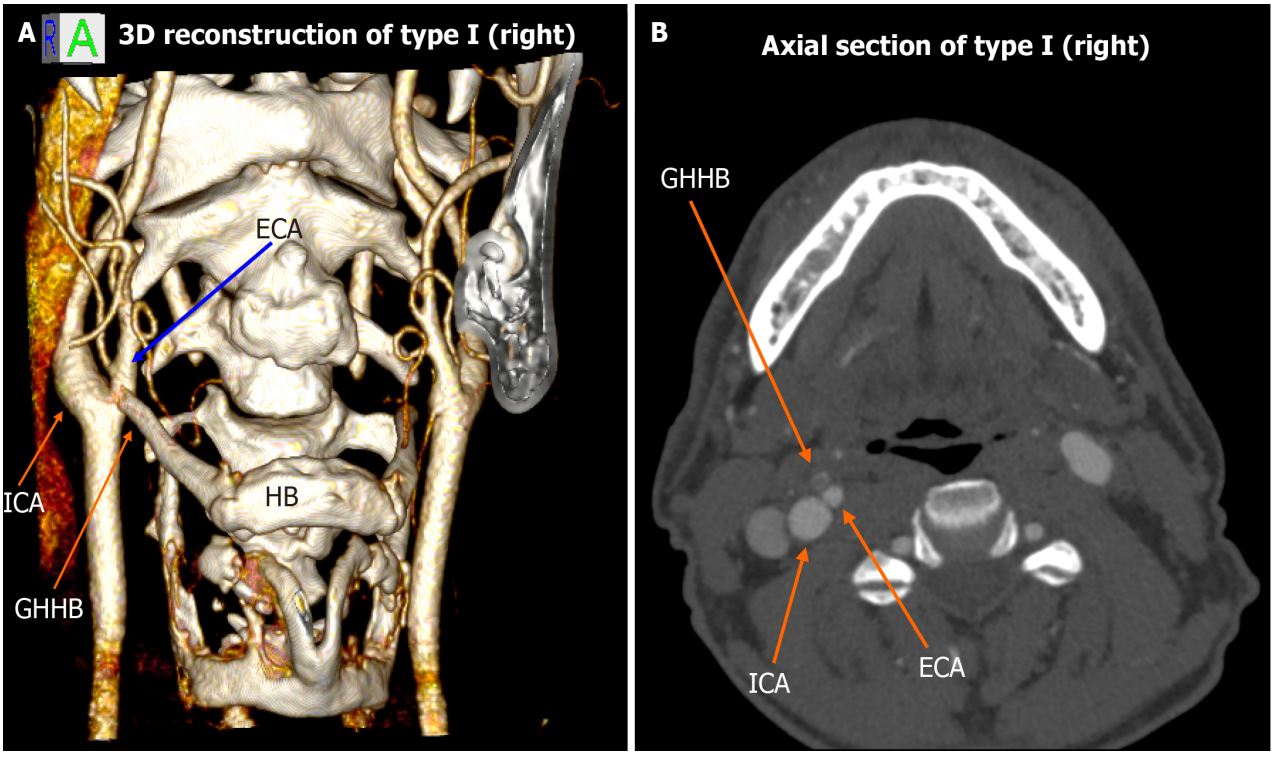


Figure 1 Type I spatial configuration (right-sided). A: 3D volume rendering shows the external carotid artery medial to the greater horn of the hyoid bone, while the internal carotid artery remains lateral; B: Corresponding axial computed tomography angiography slice confirming the same relationship. ECA: External carotid artery; GHHB: Greater horn of the hyoid bone; HB: Hyoid bone; ICA: Internal carotid artery.

hormonal, developmental, or biomechanical effects and require further targeted biomechanical and morphometric research.

We reviewed the current literature for clinical references to carotid-hyoid relationships (Table 2). Several case reports within the existing literature have described a spectrum of carotid-hyoid topographical variants, underscoring both the anatomical intricacy and the potential clinical ramifications of these configurations. Within the reviewed bibliography, documented clinical cases have included two instances of type II, two of type IV, six of type VIII, one of type IX, two of

Table 2 A summary of the observed types, classification, comparison with the previous study and comments about the clinical significance

Topographical types	Anatomical relationship	Current study	Manta *et al*[2]	Comments
Type 0	Carotid arteries posterior to the tip of the GHHB	46.9%	57.14%	Null type
Type I	ECA medial to GHHB	0.4%	0.34%	Low clinical penetrance, hemodynamically not significant carotid artery compression
Type II	ICA medial to GHHB	0%	0.34%	Low clinical penetrance, associated with reported cases of TIAs in systemic prothrombotic conditions or repetitive mechanical neck stress situations
Type III	Both ICA and ECA medial to GHHB	0%	1.02%	Low clinical penetrance, hemodynamically not significant carotid artery compression
Type IV	CCA medial to GHHB	0.2%	1.02%	Low clinical penetrance, associated with neurological deficits contralateral to the affected vessel in elderly patients
Type V	CB medial to GHHB	0%	0.34%	Low clinical penetrance, hemodynamically not significant carotid artery compression
Type VI	ECA lateral to GHHB	23.9%	20.41%	High anatomical prevalence, not implicated in any reported cases of TIA or stroke
Type VII	ICA lateral to GHHB	0.2%	0%	Low clinical penetrance, hemodynamically not significant carotid artery compression
Type VIII	Both ICA and ECA lateral to GHHB	13.2%	3.74%	High clinical penetrance, associated with significant neurological symptomatology, including hemiparesis, hemiplegia, aphasia, cervical pain, and loss of somatosensory function
Type IX	CCA lateral to GHHB	10%	8.5%	Low clinical penetrance, associated with the formation of a carotid pseudoaneurysm
Type X	CB lateral to GHHB	3.6%	6.46%	Low clinical penetrance, associated with the dissection of a carotid pseudoaneurysm
Type XI	ICA medial and ECA lateral to GHHB	1.1%	0.34%	High clinical penetrance, involving cases of cryptogenic strokes or unexplained TIAs in younger patients
Type XII	ECA medial and ICA lateral to GHHB	0.4%	0.34%	Low clinical penetrance, associated with neurological deficits contralateral to the affected vessel in elderly patients

ECA: External carotid artery; ICA: Internal carotid artery; CCA: Common carotid artery; GHHB: Greater horn of the hyoid bone; CB: Carotid bifurcation; TIAs: Transient ischemic attack.

type X, eight of type XI, and one of type XII, as per the classification system[13,14,16-33]. Strikingly, the majority of these cases involved young patients who presented with TIA in the absence of traditional cardiovascular or systemic risk factors, thereby prompting detailed vascular imaging and subsequent identification of atypical carotid-hyoid spatial relationships as potential etiological contributors. The reported TIA symptomatology commonly included hemiparesis affecting the ipsilateral upper and lower limbs, leading clinicians to consider mechanical or dynamic extrinsic arterial compromise in the differential diagnosis[24,31].

Notably, types I, III, V, VI, and VII have not been documented in any clinical case reports to date. This absence may be indicative of low clinical penetrance, or may alternatively reflect a diminished propensity of these configurations to induce hemodynamically significant CA compression. However, the possibility of subclinical or context-dependent risk cannot be excluded, and warrants further investigation - particularly under dynamic conditions such as cervical rotation, swallowing, or phonation.

Of particular interest is type VI, which emerged as the most frequently encountered non-null configuration in both our dataset and that of Manta *et al*[2]. Despite its high anatomical prevalence, type VI has not been implicated in any reported cases of TIA or stroke, suggesting that this configuration may be inherently benign with respect to cerebrovascular compromise. One possible explanation for the clinical silence of type VI is that the lateral positioning of the ECA relative to the HB places it at lower risk of compression during swallowing or cervical motion, compared to medial or combined medial-lateral configurations. This apparent paradox between anatomical frequency and clinical silence raises important considerations regarding the threshold at which spatial proximity translates into pathological interaction, and highlights the need for functional imaging studies and longitudinal clinical correlation to distinguish anatomical variants of no consequence from those with latent pathogenic potential[2].

In the context of type II carotid-hyoid configurations, where the ICA lies medial to the GHHB, both published case reports to date involve young female patients, highlighting a possible sex- and age-related anatomical susceptibility[16,17]. Tokunaga *et al*[17] reported a patient with transient left hemiparesis and ipsilateral sensory disturbance, in the setting of underlying Sjögren's syndrome. Dynamic carotid ultrasonography revealed positional displacement of the right ICA, with significant shifts observed during head rotation and deglutition, implicating a mechanical interaction between the

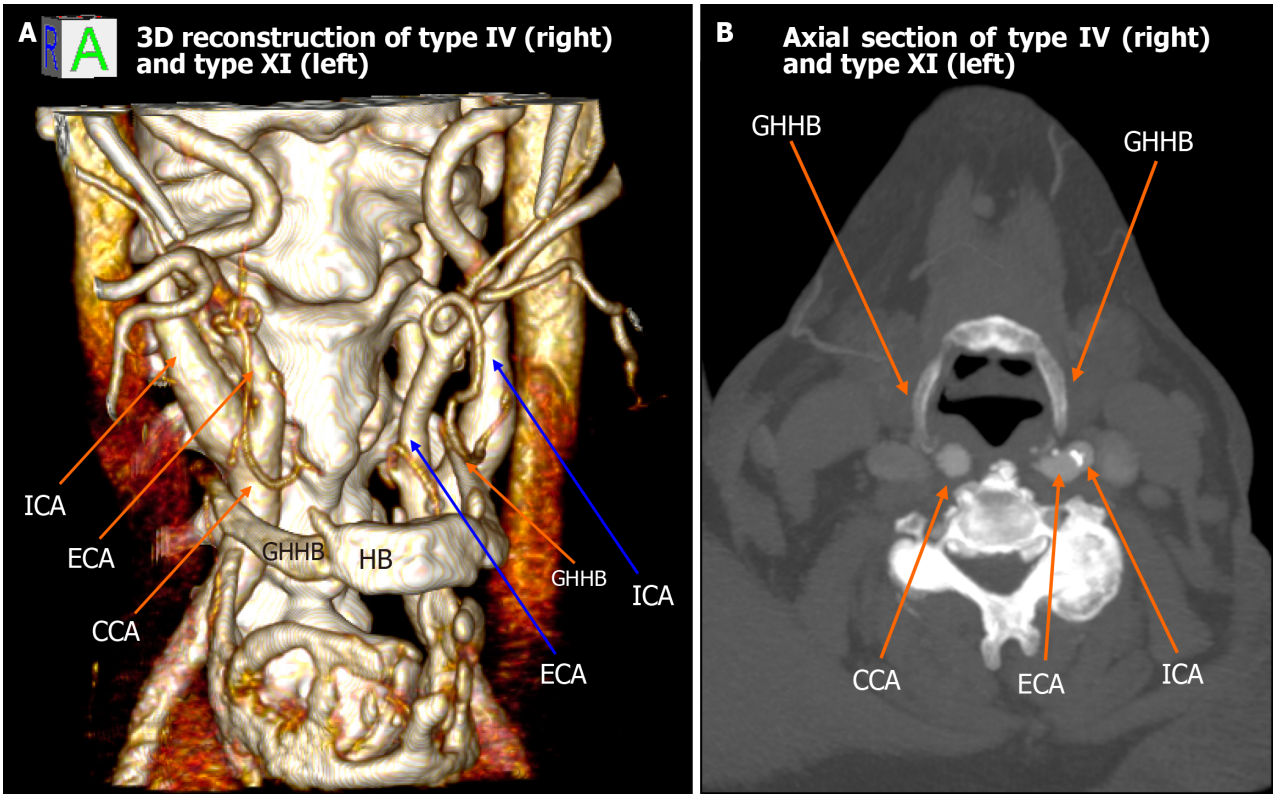


Figure 2 Type IV (right) and type XI (left) configuration. A: 3D reconstruction shows the right common carotid artery positioned medial to the greater horn of hyoid bone (type IV) and the left external carotid artery lateral with internal carotid artery medial to greater horn of hyoid bone (type XI); B: Axial computed tomography images confirm the asymmetric carotid-hyoid relationships. ICA: Internal carotid artery; ECA: External carotid artery; CCA: Common carotid artery; GHHB: Greater horn of hyoid bone; HB: Hyoid bone.

HB and the CA. In a separate report, Kho *et al*[16] described a young female patient who, in addition to transient hemiparesis and sensory deficits, exhibited dysphagia. Following vascular imaging, the aberrant medial positioning of the ICA relative to the HB was identified. Notably, symptom onset was temporally associated with a behavioral habit of frequent, rapid side-to-side cervical movements described as "neck clicking". This repetitive mechanical motion likely exacerbated dynamic ICA compression, resulting in neurological symptoms attributable to transient arterial insufficiency or microembolism. Together, these cases underscore the clinical relevance of type II configurations, particularly when compounded by systemic prothrombotic conditions or repetitive mechanical neck stress, and suggest that even anatomically rare variants may have significant cerebrovascular implications under specific dynamic or behavioral circumstances.

In cases of type IV carotid-hyoid configuration, wherein the CCA is positioned medially to the GHHB, the literature documents two clinically significant cases, both involving 70-year-old individuals who presented with neurological deficits contralateral to the affected vessel, and in both instances, pathology was localized to the right CCA[13,18]. In the first case, the patient exhibited mild left-sided hemiparesis with preserved sensory function but demonstrated disorientation to place, attributed to a 90% stenosis of the right CCA[18]. In the second report, the patient presented with left-sided hemiplegia accompanied by motor aphasia. Imaging revealed an unstable atherosclerotic plaque within the right CCA, presumed to be the source of embolic eve. These cases suggest that the type IV anatomical configuration may predispose the CCA to mechanical stress or compression, potentially contributing to plaque instability and subsequent cerebrovascular ischemia. Although direct causality remains speculative, the medial displacement of the CCA relative to the hyoid apparatus may represent a contributory factor in cases of otherwise unexplained common carotid pathology, particularly in elderly patients[13,18].

In the context of type VIII carotid-hyoid configuration, where both the external and internal CAs (ECA and ICA, respectively) are positioned lateral to the GHHB, multiple case reports have documented significant neurological symptomatology, including hemiparesis, hemiplegia, aphasia, cervical pain, and loss of somatosensory function. These events are frequently attributed to TIAs, potentially precipitated by dynamic vascular compression during cervical movement or elevated intrathoracic pressure[19,23]. Behavioral and lifestyle factors appear to play a contributory role in some of these cases. Notably, activities such as heavy weightlifting and golfing - which involve abrupt or repetitive cervical rotation and strain - have been associated with the onset of TIA symptoms in patients exhibiting type VIII anatomy[20,22]. In one case, the ICA entrapment observed in conjunction with type VIII was exacerbated by both an elongated GHHB and a coexisting elongated styloid process, although the styloid-hyoid complex appeared to be the principal mechanical factor in arterial compromise[20]. In our study, type VIII was observed in 13.2% of cases, making it one of the most prevalent non-null configurations. Given both its relatively high frequency in the general population and its documented association with symptomatic cases in the literature, this variant should raise clinical caution, especially in patients

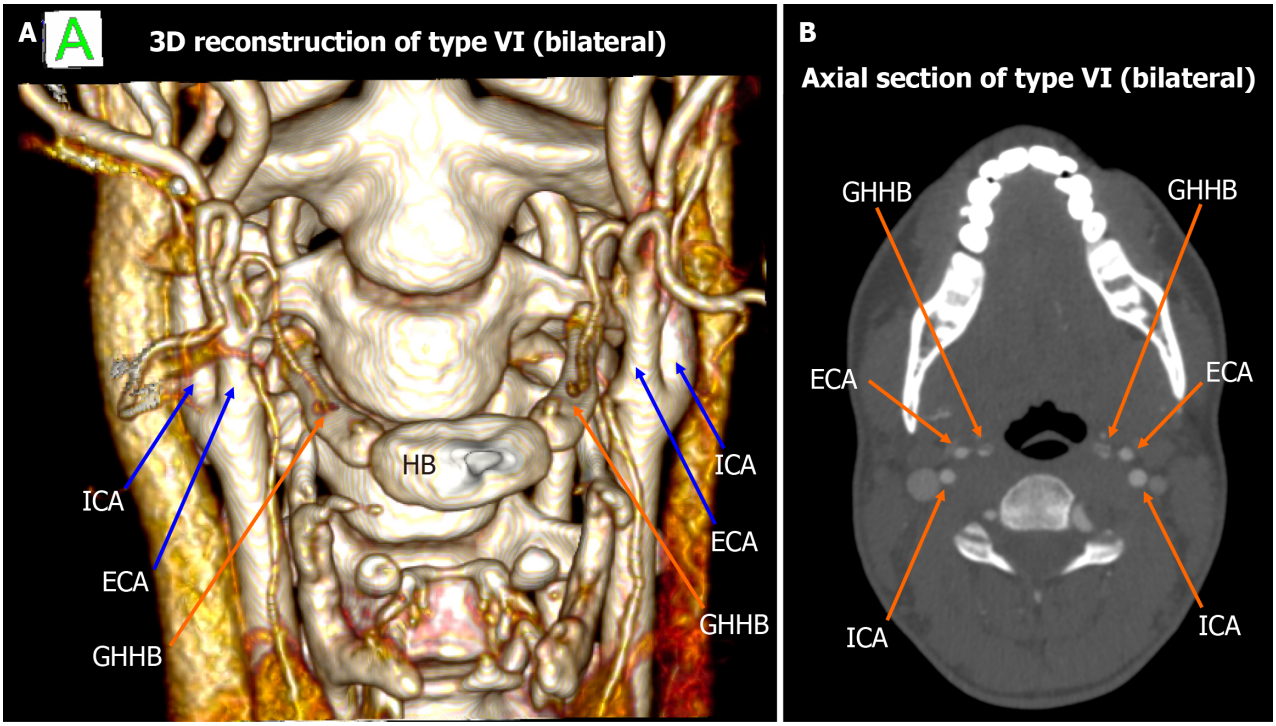


Figure 3 Type VI bilateral configuration. A: 3D reconstruction shows the external carotid arteries bilaterally lateral to the greater horn of hyoid bone; B: The axial view demonstrates the symmetry of this type VI pattern. ICA: Internal carotid artery; ECA: External carotid artery; GHHB: Greater horn of hyoid bone; HB: Hyoid bone.

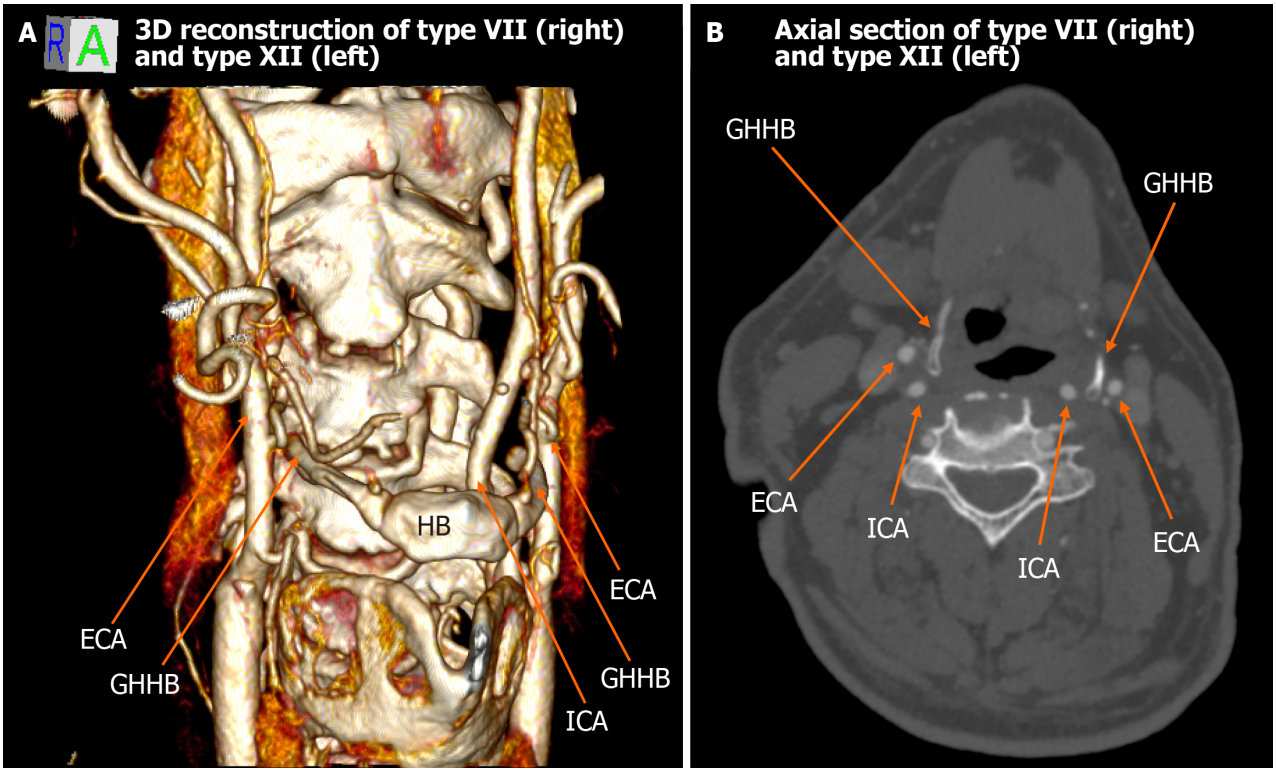


Figure 4 Type VII (right) and type XII (left). A: The 3D rendering reveals that the right external carotid artery and internal carotid artery are both located lateral to the greater horn of hyoid bone (type VII), whereas on the left, the external carotid artery is medial, and the internal carotid artery is lateral to the greater horn of hyoid bone (type XII); B: Axial computed tomography confirms the described relationships. ICA: Internal carotid artery; ECA: External carotid artery; GHHB: Greater horn of hyoid bone; HB: Hyoid bone.

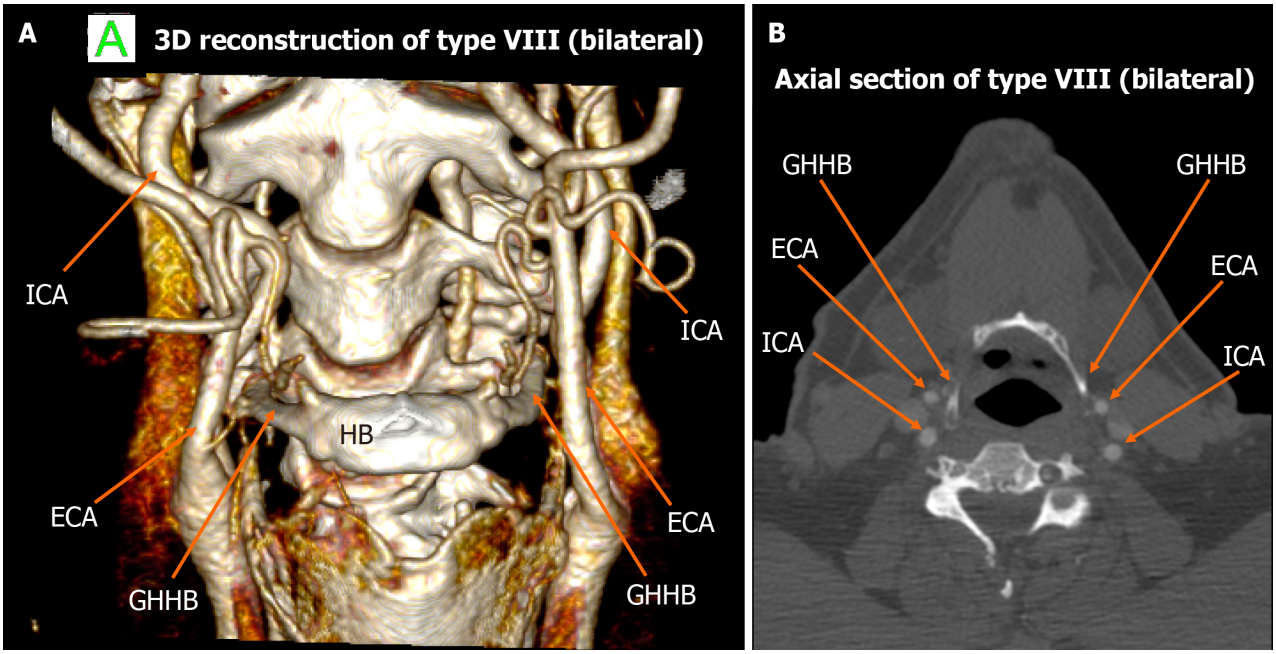


Figure 5 Type VIII bilateral configuration. A: 3D volume-rendered image depicts both internal carotid artery and external carotid artery lateral to the greater horn of hyoid bone bilaterally; B: Axial computed tomography angiography confirms this symmetric type VIII presentation. ICA: Internal carotid artery; ECA: External carotid artery; GHHB: Greater horn of hyoid bone; HB: Hyoid bone.

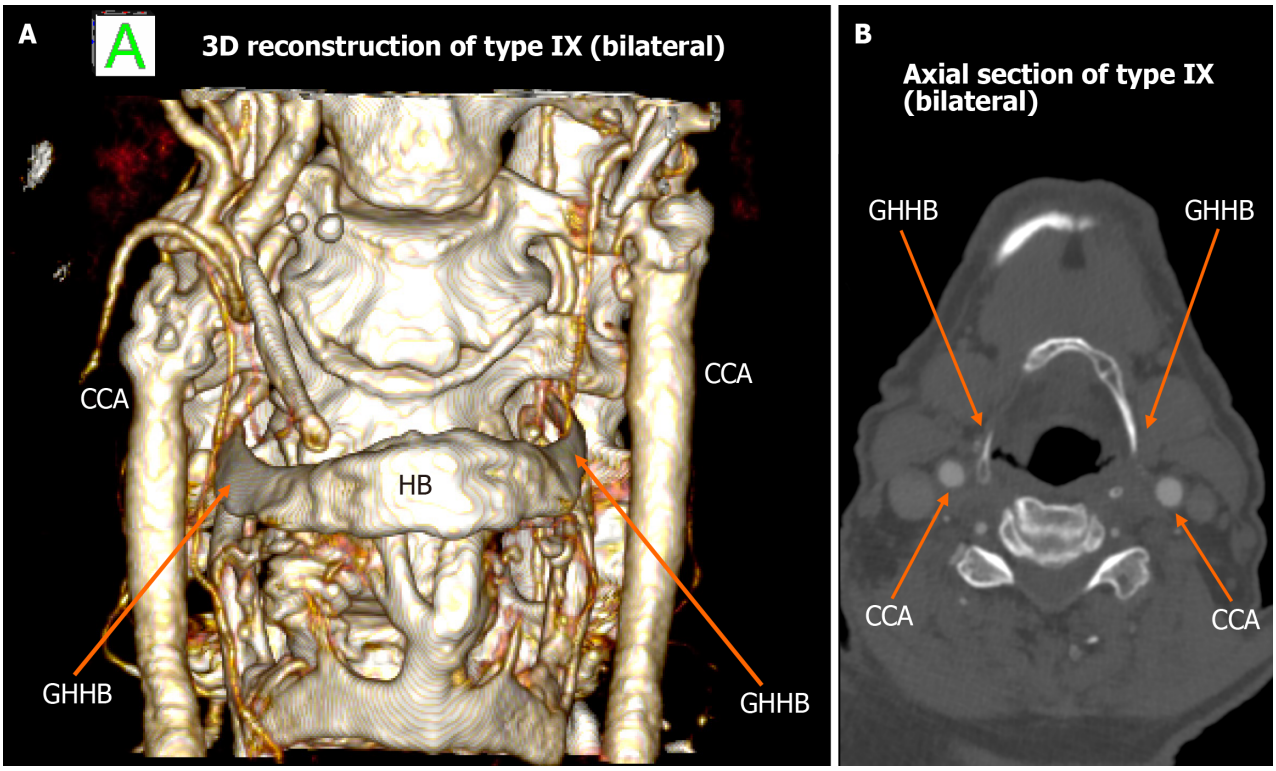


Figure 6 Type IX bilateral configuration. A: 3D reconstruction shows the internal carotid artery positioned medially to the greater horn of hyoid bone on both sides; B: Axial computed tomography angiography illustrates bilateral type IX anatomy. ICA: Internal carotid artery; GHHB: Greater horn of hyoid bone; HB: Hyoid bone; CCA: Common carotid artery.

presenting with unexplained cerebrovascular symptoms.

Schneider *et al*[25] reported a case of carotid pseudoaneurysm formation associated with a type IX carotid-hyoid configuration, characterized by lateral displacement of the CCA relative to the GHHB. The patient was asymptomatic but presented with a palpable cervical mass, prompting further vascular imaging. The investigation revealed that the chronic mechanical irritation of the arterial wall - due to its close spatial relationship with the GHHB - had likely contributed to

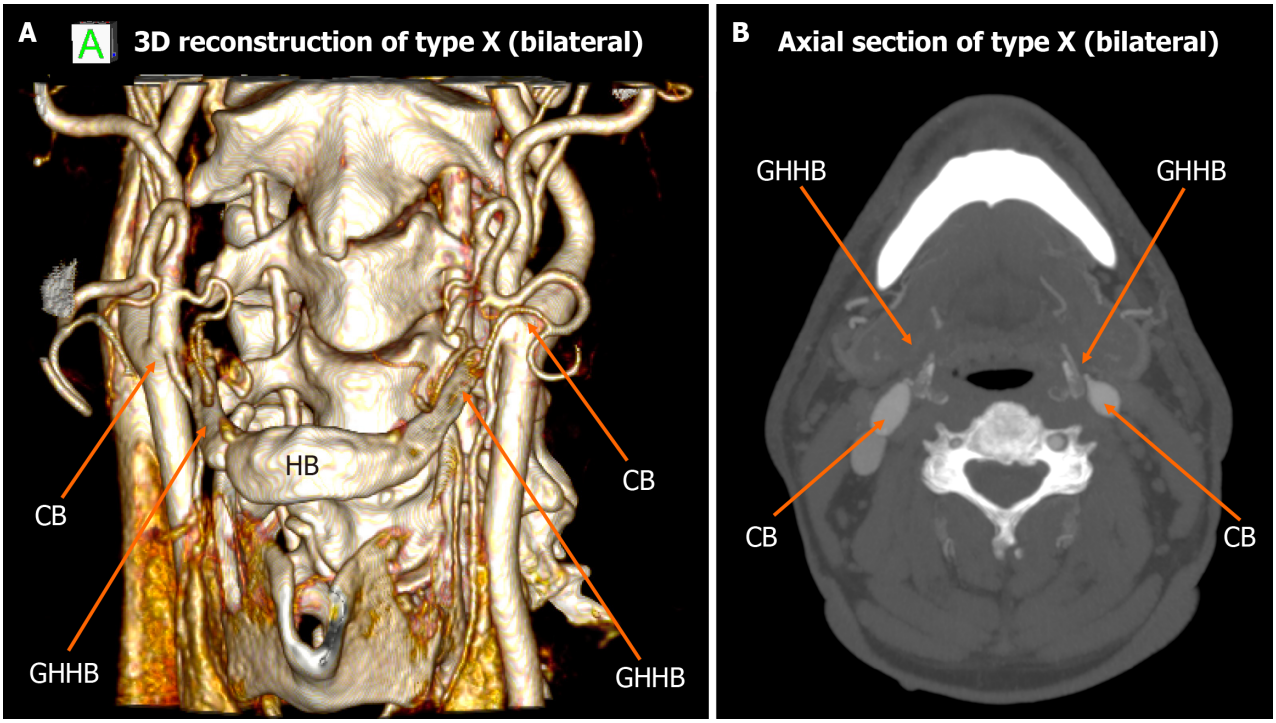


Figure 7 Type X bilateral configuration. A: 3D reconstruction demonstrating the carotid bifurcation located lateral to the greater horn of hyoid bone on both sides; B: Axial view highlights bilateral type X relationship. CB: Carotid bifurcation; GHHB: Greater horn of hyoid bone; HB: Hyoid bone.

localized inflammation and subsequent pseudoaneurysm development. The patient's history of heavy weightlifting was identified as a potential exacerbating factor, amplifying repetitive microtrauma at the site of arterial-bony contact.

Type X carotid-hyoid configurations, in which the CB is positioned laterally to the GHHB, have been implicated in clinically relevant vascular pathology. Ye *et al*[27] described a case involving a patient who presented with right-sided hemiparesis, in whom imaging revealed two cystic lesions with internal calcifications and a pronounced spatial proximity between the GHHB and the ICA. A dissecting aneurysm of the ICA was identified, which the authors attributed to mechanical stress and chronic irritation associated with an elongated HB abutting the arterial wall[2].

Type XI carotid-hyoid configurations, characterized by the ECA positioned laterally and the ICA medially to the GHHB, appear to be the most frequently represented anatomical variant in the published clinical literature concerning TIAs. All reported cases have presented with classic focal neurological deficits[14,26,28-32]. Importantly, these cases span a wide age range, with several involving young adults lacking conventional cardiovascular risk factors, thereby contributing to the broader diagnostic framework of embolic stroke of undetermined source. One particularly illustrative case involved a patient who, in addition to transient neurological symptoms, reported a chronic ipsilateral otalgia lasting over two years, highlighting the possibility of atypical and prolonged prodromal symptoms in carotid-hyoid pathology.

Notably, in the majority of these reports, the CB was found to be situated lower than its typical anatomical location - often at the C3-C4 vertebral level or below. Given both the frequency of type XI in symptomatic individuals and the potential for recurrent or unexplained cerebrovascular events, this configuration warrants heightened clinical attention, particularly in cases of cryptogenic stroke or unexplained TIAs in younger patients[14,31]. Keshelava *et al*[32] documented a case of type XII (ECA medial, ICA lateral) carotid-hyoid configuration, involving a 70-year-old female patient who presented with left-sided hemiparesis. Management in this case consisted exclusively of anticoagulant therapy, without surgical intervention.

A nuanced understanding of the medial *vs* lateral displacement of the CAs relative to the GHHB is essential for preoperative planning and intraoperative navigation, especially in anatomically complex or constrained surgical fields. Variants classified as types I-V, where the CAs are positioned medial to the GHHB, are intimately related to the parapharyngeal space. In such configurations, the ICA may lie immediately subjacent to the pharyngeal mucosa, dramatically increasing the risk of iatrogenic vascular injury during procedures such as transoral biopsies, abscess drainage, or resection of pharyngeal tumors - notably in anatomically sensitive regions like the pyriform[1-6]. Furthermore, in otolaryngological surgeries such as tonsillectomy, adenoidectomy, and soft palate repair, patients with medially displaced carotid anatomy may be at elevated risk for catastrophic hemorrhage, pseudoaneurysm formation, or even airway compromise if arterial injury occurs[1,34].

In contrast, types VI-X, characterized by lateral displacement of the carotid vessels, present a different set of challenges. The close spatial relationship between the arteries and the sternocleidomastoid muscle, as well as deeper structures like the posterior belly of the digastric and stylopharyngeus muscles, may lead to increased arterial compression during dynamic head and neck motion and can complicate transcervical surgical approaches to parapharyngeal or retropharyngeal tumors[1,34]. In procedures such as deep lobe parotidectomy or lateral pharyngeal wall access, these variants necessitate heightened intraoperative caution to avoid unintentional vascular compromise. Types XI and XII are distin-

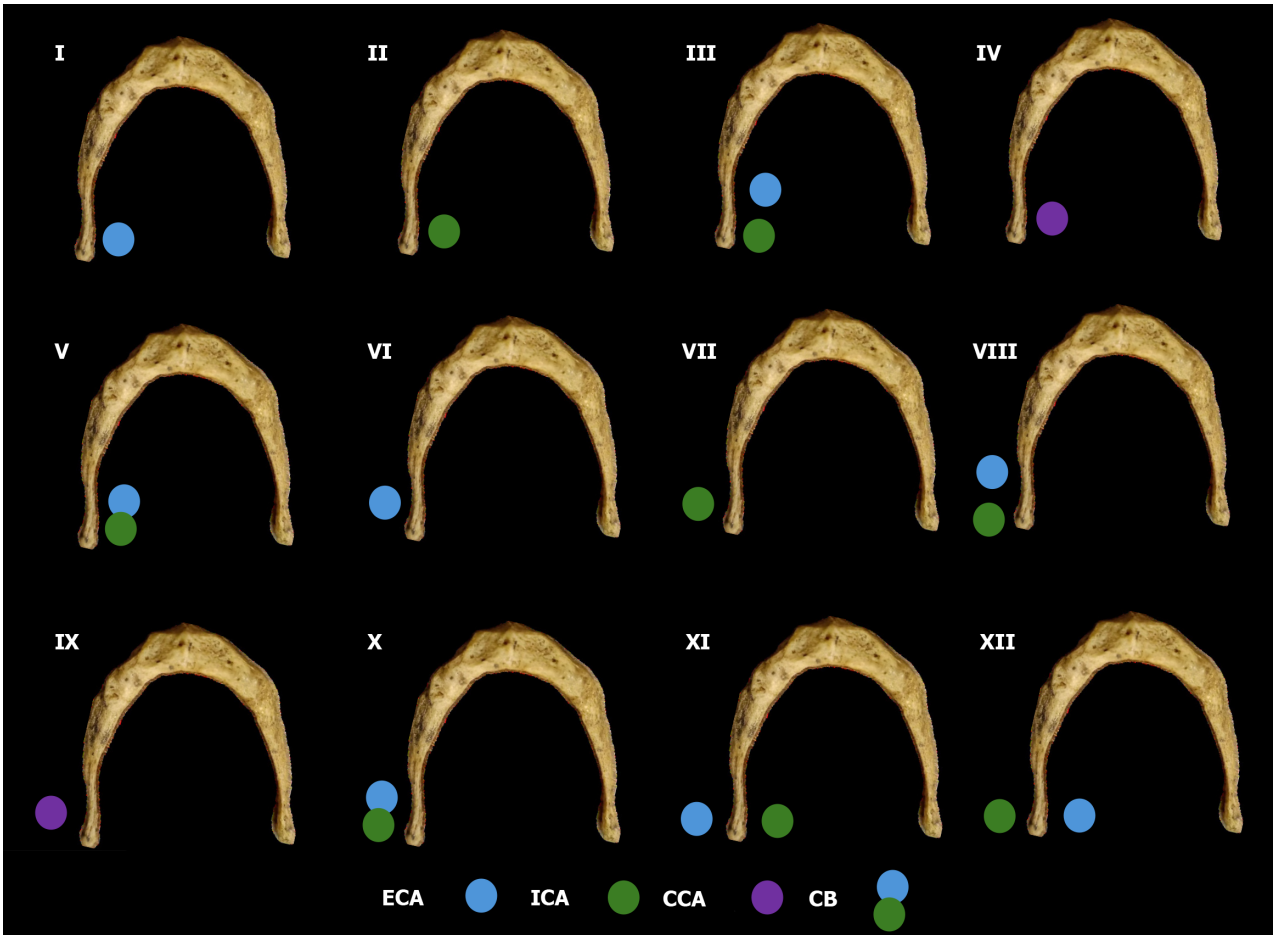


Figure 8 Schematic representation of all topographical patterns between the external carotid artery, internal carotid artery or common carotid artery with the hyoid bone. ICA: Internal carotid artery; ECA: External carotid artery; CCA: Common carotid artery; CB: Carotid bifurcation.

guished by the presence of arterial structures positioned both laterally and medially, thereby subjecting these variants to a dual spectrum of associated vascular risks.

Finally, aberrant courses of the CAs should always be included in the differential diagnosis of submucosal oropharyngeal masses and atypical pharyngeal presentations, particularly when imaging reveals unexpected vascular contours or displacements. A comprehensive preoperative assessment, ideally including contrast-enhanced CT or MR angiography, is essential in mitigating risks and optimizing outcomes in this anatomically vulnerable region[2,35].

The current study is limited by its moderate sample size and sex imbalance. Additionally, our findings are based on a single-center cohort and may not apply universally. The sex imbalance could have affected our sample and the statistically significant difference identified between female and male patients. Due to the retrospective and anatomical nature of the present study, the patients' medical history was unknown. Future research should include larger, multicenter, and demographically diverse groups. Incorporating dynamic imaging, functional testing, and long-term clinical follow-up would help better define the accurate risk profile of each topographical variant, while biomechanical and genetic studies will enhance our knowledge for sex- and nationality-based differences.

CONCLUSION

This study highlights the significant diversity of carotid-hyoid relationships and identifies specific spatial patterns with clear clinical implications. Using the classification system of Manta *et al*[2], we confirmed that type VI is the most common non-null variant; however, its apparent clinical silence contrasts with the pathological potential of less frequent configurations, such as types VIII and XI, which have been linked to TIA s and other vascular complications. Our findings also demonstrate pronounced sexual dimorphism and lateral asymmetry, highlighting the importance of personalized anatomical assessment evaluation. Carotid variants that are displaced medially increase surgical risk, especially in transoral and pharyngeal procedures, while lateralized types may lead to dynamic arterial compression or complicate cervical access routes. Including carotid-hyoid topographical assessment in routine preoperative imaging and clinical decision-making can help prevent iatrogenic injury, improve diagnostic accuracy in cryptogenic stroke, and enhance surgical planning.

FOOTNOTES

Author contributions: Karangeli N was responsible for project development, data collection and management; Triantafyllou G contributed to conceptualization; Karangeli N, Triantafyllou G, Papadopoulos-Manolarakis P, Arkoudis NA, Velonakis G, Samolis A, and Piagkou M contributed to data analysis and manuscript writing; Maria Piagkou oversaw the project (supervision); Triantafyllou G and Arkoudis NA they contributed equally to this article, they are the co-corresponding authors of this manuscript; and all authors thoroughly reviewed and endorsed the final manuscript.

Institutional review board statement: This study was approved by the Medical Ethics Committee of General Hospital of Nikaia-Piraeus, approval No. 56485.

Informed consent statement: Informed consent was obtained from the patients enrolled in the current study.

Conflict-of-interest statement: All the authors report no relevant conflicts of interest for this article.

Data sharing statement: All the data are available upon reasonable request to the authors.

Open Access: This article is an open-access article that was selected by an in-house editor and fully peer-reviewed by external reviewers. It is distributed in accordance with the Creative Commons Attribution NonCommercial (CC BY-NC 4.0) license, which permits others to distribute, remix, adapt, build upon this work non-commercially, and license their derivative works on different terms, provided the original work is properly cited and the use is non-commercial. See: https://creativecommons.org/Licenses/by-nc/4.0/

Country of origin: Greece

ORCID number: Nektaria Karangeli 0009-0009-3251-2434; George Triantafyllou 0009-0001-0122-2436; Panagiotis Papadopoulos-Manolarakis 0009-0008-5662-8354; Nikolaos-Achilleas Arkoudis 0000-0002-0783-5700; Georgios Velonakis 0000-0002-0050-284X; Maria Piagkou 0000-0002-4831-8005.

S-Editor: Bai Y
L-Editor: A
P-Editor: Xu J

REFERENCES

1 **Paulsen F**, Tillmann B, Christofides C, Richter W, Koebke J. Curving and looping of the internal carotid artery in relation to the pharynx: frequency, embryology and clinical implications. *J Anat* 2000; **197** Pt 3: 373-381 [*RCA*] [PMID: 11117624 DOI: 10.1046/j.1469-7580.2000.19730373.x] [FullText]

2 **Manta MD**, Rusu MC, Hostiuc S, Vrapciu AD, Manta BA, Jianu AM. The Carotid-Hyoid Topography Is Variable. *Medicina (Kaunas)* 2023; **59**: 1494 [*RCA*] [PMID: 37629784 DOI: 10.3390/medicina59081494] [FullText] [Full Text(PDF)]

3 **Rusu MC**, Tudose RC, Vrapciu AD, Popescu ŞA. Lowered hyoid bone overlapping the thyroid cartilage in CT angiograms. *Surg Radiol Anat* 2024; **46**: 333-339 [*RCA*] [PMID: 38315210 DOI: 10.1007/s00276-024-03300-5] [FullText]

4 **Dumitru CC**, Vrapciu AD, Jianu AM, Hostiuc S, Rusu MC. The retromandibular loop of the external carotid artery. *Ann Anat* 2024; **253**: 152226 [*RCA*] [PMID: 38331006 DOI: 10.1016/j.aanat.2024.152226] [FullText]

5 **Triantafyllou G**, Paschopoulos I, Duparc F, Tsakotos G, Tsiouris C, Olewnik Ł, Georgiev G, Zielinska N, Piagkou M. The superior thyroid artery origin pattern: A systematic review with meta-analysis 2024 Preprint. Available from: bioRxiv: 10.21203/rs.3.rs-4557932/v1 [DOI: 10.21203/rs.3.rs-4557932/v1] [FullText]

6 **Triantafyllou G**, Vassiou K, Duparc F, Vlychou M, Paschopoulos I, Tsakotos G, Tudose RC, Rusu MC, Piagkou M. The lingual and facial arteries' common origin: a systematic review with meta-analysis and a computed tomography angiography study. *Surg Radiol Anat* 2024; **46**: 1937-1947 [*RCA*] [PMID: 39331140 DOI: 10.1007/s00276-024-03490-y] [FullText]

7 **Manta MD**, Rusu MC, Hostiuc S, Tudose RC, Manta BA, Jianu AM. The vertical topography of the carotid bifurcation - original study and review. *Surg Radiol Anat* 2024; **46**: 1253-1263 [*RCA*] [PMID: 38847826 DOI: 10.1007/s00276-024-03404-y] [FullText] [Full Text(PDF)]

8 **Standring S**, Anand N, Birch R, Collins P, Crossman A, Gleeson M, Jawaheer G, Smith A, Spratt J, Stringer M, Tubbs S, Tunstall R, Wein A, Wigley C. Gray's Anatomy: the anatomical basis of clinical practice. 41st ed. London: Elsevier, 2015

9 **Karangeli N**, Triantafyllou G, Duparc F, Vassiou K, Vlychou M, Tsakotos G, Piagkou M. Retrostyloid and retromandibular courses of the external carotid artery. *Surg Radiol Anat* 2024; **47**: 23 [*RCA*] [PMID: 39652124 DOI: 10.1007/s00276-024-03546-z] [FullText]

10 **Triantafyllou G**, Botis G, Vassiou K, Vlychou M, Tsakotos G, Kalamatianos T, Matsopoulos G, Piagkou M. The styloid process length and the stylohyoid chain ossification affect its relationship with the carotid arteries. *Ann Anat* 2025; **257**: 152342 [*RCA*] [PMID: 39341465 DOI: 10.1016/j.aanat.2024.152342] [FullText]

11 **Triantafyllou G**, Papadopoulos-Manolarakis P, Vassiou K, Vlychou M, Karangeli N, Papanagiotou P, Tsakotos G, Piagkou M. The impact of the styloid process angulation on the carotid arteries. *Ann Anat* 2025; **258**: 152378 [*RCA*] [PMID: 39818238 DOI: 10.1016/j.aanat.2025.152378] [FullText]

12 **Karangeli N**, Triantafyllou G, Papadopoulos-Manolarakis P, Tsakotos G, Vassiou K, Vlychou M, Papanagiotou P, Piagkou M. The Anatomical Relationship Between the Hyoid Bone and the Carotid Arteries. *Diagnostics (Basel)* 2025; **15**: 1485 [*RCA*] [PMID: 40564806 DOI: 10.3390/diagnostics15121485] [FullText] [Full Text(PDF)]

13 **Suematsu T**, Kawabata S, Nishikawa Y, Hirai N, Nakamura M, Terada E, Kajikawa R, Tsuzuki T. Mechanical compression of the carotid artery by the pharynx in the retropharyngeal space during swallowing and the induction of stenosis and embolic stroke: illustrative case. *J Neurosurg Case Lessons* 2024; **8**: CASE2483 [*RCA*] [PMID: 39102751 DOI: 10.3171/CASE2483] [FullText]

14 **Mutimer CA**, Campbell BCV. Thromboembolism From Hyoid Bone-Related Direct Carotid Artery Compression. *Stroke* 2024; **55**: e157-e158 [*RCA*] [PMID: 38629306 DOI: 10.1161/STROKEAHA.124.047098] [FullText]

15 **Bouille F**, De Malherbe M, Pico F. Ischemic Stroke Due to Compression of a Wandering Internal Carotid Artery by the Hyoid Bone. *JAMA Neurol* 2025; **82**: 303-304 [*RCA*] [PMID: 39899308 DOI: 10.1001/jamaneurol.2024.5028] [FullText]

16 **Kho LK**, Bates TR, Thompson A, Dharsono F, Prentice D. Cerebral embolism and carotid-hyoid impingement syndrome. *J Clin Neurosci* 2019; **64**: 27-29 [*RCA*] [PMID: 30987808 DOI: 10.1016/j.jocn.2019.03.040] [FullText]

17 **Tokunaga K**, Uehara T, Kanamaru H, Kataoka H, Saito K, Ishibashi-Ueda H, Shobatake R, Yamamoto Y, Toyoda K. Repetitive Artery-to-Artery Embolism Caused by Dynamic Movement of the Internal Carotid Artery and Mechanical Stimulation by the Hyoid Bone. *Circulation* 2015; **132**: 217-219 [*RCA*] [PMID: 26195490 DOI: 10.1161/CIRCULATIONAHA.114.015144] [FullText]

18 **Abdelaziz OS**, Ogilvy CS, Lev M. Is there a potential role for hyoid bone compression in pathogenesis of carotid artery stenosis? *Surg Neurol* 1999; **51**: 650-653 [*RCA*] [PMID: 10369234 DOI: 10.1016/s0090-3019(99)00022-1] [FullText]

19 **Mori M**, Yamamoto H, Koga M, Okatsu H, Shono Y, Toyoda K, Fukuda K, Iihara K, Yamada N, Minematsu K. Hyoid bone compression-induced repetitive occlusion and recanalization of the internal carotid artery in a patient with ipsilateral brain and retinal ischemia. *Arch Neurol* 2011; **68**: 258-259 [*RCA*] [PMID: 21320995 DOI: 10.1001/archneurol.2010.371] [FullText]

20 **Renard D**, Freitag C. Hyoid-related internal carotid artery dissection. *J Neurol* 2012; **259**: 2501-2502 [*RCA*] [PMID: 22843137 DOI: 10.1007/s00415-012-6621-4] [FullText]

21 **Renard D**, Rougier M, Aichoun I, Labauge P. Hyoid bone-related focal carotid vasculopathy. *J Neurol* 2011; **258**: 1540-1541 [*RCA*] [PMID: 21327849 DOI: 10.1007/s00415-011-5940-1] [FullText]

22 **Hong JM**, Kim TJ, Lee JS, Lee JS. Neurological picture. Repetitive internal carotid artery compression of the hyoid: a new mechanism of golfer's stroke? *J Neurol Neurosurg Psychiatry* 2011; **82**: 233-234 [*RCA*] [PMID: 20587482 DOI: 10.1136/jnnp.2010.213777] [FullText]

23 **Yukawa S**, Yamamoto S, Hara H. Carotid artery dissection associated with an elongated hyoid bone. *J Stroke Cerebrovasc Dis* 2014; **23**: e411-e412 [*RCA*] [PMID: 25126696 DOI: 10.1016/j.jstrokecerebrovasdis.2014.04.006] [FullText]

24 **González Villaman CM**, Domínguez Quiñónez R, Castillo Espinal L. Internal carotid artery dissection associated with an elongated hyoid bone in a patient with vascular Ehlers-Danlos syndrome. *BMJ Case Rep* 2024; **17**: e260764 [*RCA*] [PMID: 39153759 DOI: 10.1136/bcr-2024-260764] [FullText]

25 **Schneider CG**, Kortmann H. Pseudoaneurysm of the common carotid artery due to ongoing trauma from the hyoid bone. *J Vasc Surg* 2007; **45**: 186-187 [*RCA*] [PMID: 17210407 DOI: 10.1016/j.jvs.2006.08.075] [FullText]

26 **Liu S**, Nezami N, Dardik A, Nassiri N. Hyoid bone impingement contributing to symptomatic atherosclerosis of the carotid bifurcation. *J Vasc Surg Cases Innov Tech* 2020; **6**: 89-92 [*RCA*] [PMID: 32095663 DOI: 10.1016/j.jvscit.2020.01.001] [FullText] [Full Text(PDF)]

27 **Ye Q**, Liu Y, Tang H, Zhou Q, Zhang H, Liu H. Hyoid bone compressioninduced carotid dissecting aneurysm: A case report. *Exp Ther Med* 2023; **26**: 551 [*RCA*] [PMID: 37928507 DOI: 10.3892/etm.2023.12249] [FullText] [Full Text(PDF)]

28 **Kölbel T**, Holst J, Lindh M, Mätzsch T. Carotid artery entrapment by the hyoid bone. *J Vasc Surg* 2008; **48**: 1022-1024 [*RCA*] [PMID: 18992420 DOI: 10.1016/j.jvs.2008.04.062] [FullText]

29 **Martinelli O**, Fresilli M, Jabbour J, Di Girolamo A, Irace L. Internal Carotid Stenosis Associated with Compression by Hyoid Bone. *Ann Vasc Surg* 2019; **58**: 379.e1-379.e3 [*RCA*] [PMID: 30684622 DOI: 10.1016/j.avsg.2018.09.043] [FullText]

30 **Plotkin A**, Bartley MG, Bowser KE, Yi JA, Magee GA. Carotid Artery Entrapment by the Hyoid Bone-A Rare Cause of Recurrent Strokes in a Young Patient. *Ann Vasc Surg* 2019; **57**: 48.e7-48.e11 [*RCA*] [PMID: 30218829 DOI: 10.1016/j.avsg.2018.09.001] [FullText]

31 **Bicevska K**, Skrastina S, Kupcs K, Raita A, Balodis A. Functional Compression of the Right Internal Carotid Artery by the Hyoid Bone in a Patient with Moyamoya Syndrome and Low Internal Carotid Artery Bifurcation: A Case Report. *Vasc Health Risk Manag* 2025; **21**: 383-389 [*RCA*] [PMID: 40395490 DOI: 10.2147/VHRM.S520022] [FullText] [Full Text(PDF)]

32 **Keshelava G**, Robakidze Z. Internal Carotid Artery Stenosis and Entrapment by the Hyoid Bone. *Eur J Vasc Endovasc Surg* 2024; **68**: 422 [*RCA*] [PMID: 38583739 DOI: 10.1016/j.ejvs.2024.03.043] [FullText]

33 **Keshelava G**, Robakidze Z, Tsiklauri D. External Carotid Artery Entrapment by the Hyoid Bone Associated with an Atherosclerotic Stenosis of the Internal Carotid Artery. *Diseases* 2024; **12**: 258 [*RCA*] [PMID: 39452501 DOI: 10.3390/diseases12100258] [FullText]

34 **Bernardes MND**, Cascudo NCM, El Cheikh MR, Gonçalves VF, Lamounier P, Ramos HVL, Costa CC. Aberrant common and internal carotid arteries and their surgical implications: a case report. *Braz J Otorhinolaryngol* 2021; **87**: 366-369 [*RCA*] [PMID: 33303416 DOI: 10.1016/j.bjorl.2020.10.008] [FullText] [Full Text(PDF)]

35 **Baba A**, Kurokawa R, Kayama R, Tsuneoka Y, Kurokawa M, Ota Y, Suzuki T, Yamauchi H, Matsushima S, Ojiri H. A rare case of positional changes of carotid artery depicted within a single MR study and a wandering carotid artery depicted on a serial MR studies. *Radiol Case Rep* 2022; **17**: 50-53 [*RCA*] [PMID: 34765059 DOI: 10.1016/j.radcr.2021.09.071] [FullText] [Full Text(PDF)]

World Journal of Radiology

Submit a Manuscript: https://www.f6publishing.com

World J Radiol 2025 November 28; 17(11): 111651

DOI: 10.4329/wjr.v17.i11.111651

ISSN 1949-8470 (online)

ORIGINAL ARTICLE

Observational Study

Shear wave elastography in healthy patients: Pancreatic stiffness is less reliable than liver and spleen measurements

Nicholas Viceconti, Mattia Paratore, Fabio Del Zompo, Maria Assunta Zocco, Maria Elena Ainora, Giorgio Esposto, Antonio Gasbarrini, Maurizio Pompili, Laura Riccardi, Matteo Garcovich

Specialty type: Radiology, nuclear medicine and medical imaging

Provenance and peer review: Invited article; Externally peer reviewed.

Peer-review model: Single blind

Peer-review report's classification

Scientific Quality: Grade B, Grade B

Novelty: Grade B, Grade C

Creativity or Innovation: Grade A, Grade B

Scientific Significance: Grade C, Grade D

P-Reviewer: Hassan AH, PharmD, PhD, Assistant Professor, Chief Pharmacist, Lecturer, Senior Researcher, Egypt

Received: July 8, 2025

Revised: September 15, 2025

Accepted: November 6, 2025

Published online: November 28, 2025

Processing time: 142 Days and 11.3 Hours

Nicholas Viceconti, Mattia Paratore, Laura Riccardi, Matteo Garcovich, Diagnostic and Interventional Ultrasound Unit, CEMAD Digestive Disease Center, Fondazione Policlinico Universitario Agostino Gemelli IRCCS, Rome 00168, Italy

Fabio Del Zompo, Maria Assunta Zocco, Maria Elena Ainora, Giorgio Esposto, Antonio Gasbarrini, Internal Medicine and Gastroenterology Unit, CEMAD Digestive Disease Center, Fondazione Policlinico Universitario Gemelli IRCCS, Rome 00168, Italy

Maria Assunta Zocco, Antonio Gasbarrini, Maurizio Pompili, Translational Medicine and Surgery Department, Catholic University of the Sacred Heart, Fondazione Policlinico Universitario Gemelli IRCCS, Rome 00168, Italy

Maurizio Pompili, Internal Medicine and Liver Transplantation Unit, Fondazione Policlinico Universitario Gemelli IRCCS, Rome 00168, Italy

Corresponding author: Mattia Paratore, MD, Diagnostic and Interventional Ultrasound Unit, CEMAD Digestive Disease Center, Fondazione Policlinico Universitario Agostino Gemelli IRCCS, Largo Agostino Gemelli, 8, Rome 00168, Italy.
mattia.paratore@guest.policlinicogemelli.it

Abstract

BACKGROUND

Shear wave elastography (SWE) is a non-invasive ultrasound-based technique used to assess tissue stiffness, which reflects underlying pathological changes. While SWE has been widely applied for liver fibrosis evaluation, its application to other abdominal organs, such as the spleen and pancreas, is gaining interest. However, normal stiffness values and inter-system agreement remain poorly defined.

AIM

To assess the feasibility and agreement of liver, spleen, and pancreas stiffness using three SWE methods.

METHODS

This single-center observational study enrolled 50 healthy adult volunteers. Liver, spleen, and pancreas stiffness were assessed using three SWE methods: Point-SWE (p-QElaXto) and 2-Dimensional-SWE (2D-QElaXto) with Esaote MyLab 9,

and 2D-SWE with SuperSonic Imagine. Feasibility, inter-operator reproducibility, and concordance among systems were evaluated. Stiffness was expressed as median kPa values, and technical reliability was assessed using the interquartile range/median ratio and stability index thresholds.

RESULTS

Liver and spleen stiffness assessment was feasible in > 98% of patients, while pancreas stiffness was measurable in 84%-88% depending on the SWE technique. Mean liver stiffness ranged between 3.9-4.7 kPa across techniques, spleen stiffness ranged from 19.4-23.0 kPa, and pancreas stiffness from 5.2-7.6 kPa. Inter-operator agreement was excellent for liver (intraclass correlation coefficient > 0.90) and good to moderate for spleen and pancreas (intraclass correlation coefficient from 0.43 to 0.90). Bland-Altman analysis confirmed good correlation but also systematic differences among devices, especially in pancreas measurements.

CONCLUSION

This is the first study to establish normal liver, spleen, and pancreas stiffness using MyLab 9 SWE integrated methods as compared to SuperSonic Imagine, with acceptable inter-technique agreement. Liver and spleen values matched existing guidelines; pancreas SWE showed more variability and reduced reproducibility.

Key Words: Shear wave elastography; Stiffness; Liver; Spleen; Pancreas; Healthy patients; Ultrasound; Elastography

©The Author(s) 2025. Published by Baishideng Publishing Group Inc. All rights reserved.

Core Tip: In the literature, normal stiffness values for liver, spleen, and pancreas in healthy individuals are not well established. This is partly due to differences in equipment and cut-off values used, and partly due to inter-operator variability. In this study, we evaluated these parameters in 50 healthy individuals using three different methods (two of which were integrated into the same scan) to assess their correlation with clinical and technical features.

Citation: Viceconti N, Paratore M, Del Zompo F, Zocco MA, Ainora ME, Esposto G, Gasbarrini A, Pompili M, Riccardi L, Garcovich M. Shear wave elastography in healthy patients: Pancreatic stiffness is less reliable than liver and spleen measurements. *World J Radiol* 2025; 17(11): 111651

URL: https://www.wjgnet.com/1949-8470/full/v17/i11/111651.htm

DOI: https://dx.doi.org/10.4329/wjr.v17.i11.111651

INTRODUCTION

Shear wave elastography (SWE) is a non-invasive ultrasound (US) technique that quantifies tissue stiffness and is increasingly applied to abdominal organs[1,2]. Establishing reference values in healthy individuals is crucial, since abnormal stiffness is associated with clinically relevant conditions such as liver fibrosis, portal hypertension, and pancreatic disease. In chronic liver disease, SWE-derived liver stiffness strongly correlates with fibrosis stage and disease progression[3-5]. Spleen stiffness has also emerged as a promising surrogate marker of portal hypertension[2,6,7]. However, reliable cut-offs still require robust normal ranges in healthy subjects and reproducible measurements across different systems. In the literature, liver and spleen normal stiffness values are not well established. There is a great variability of normal stiffness values, partly due to the availability of different equipment and the different cut-off employed, partly due to inter-operator variability. Liver stiffness normal values disagreement was reviewed and summarized in a range from 2.6 kPa to 7.5 kPa[8]. Spleen stiffness normal values were investigated in several studies, and their values ranged from 16.6 ± 2.5 kPa[1] to 18.14 ± 3.08 kPa[9].

The use of SWE is steadily increasing, also engaging other organs such as the pancreas. In fact, pancreatic stiffness has been linked to steatosis, metabolic syndrome, acute and chronic pancreatitis, and post-surgical outcomes[10]. Nevertheless, normal reference values remain poorly defined, and data are inconsistent across studies, with studies reporting normal values ranging from 0.52 m/second to 4.60 m/second[11,12]. A major limitation of SWE is the variability among US platforms and even across software versions of the same manufacturer. Recent consensus guidelines[13] have underlined the need for harmonization and for studies assessing inter-system reproducibility before stiffness thresholds can be widely adopted in practice.

Esaote MyLab 9 is one of the latest equipment introduced in 2017 by Esaote (Genova, Italy), and it is embedded with point-SWE (p-QElaXto) and 2-Dimensional-SWE (2D-QElaXto). To date, no published studies have established normal reference values for abdominal organs using this platform to the best of our knowledge. The aim of the present study was to assess the feasibility and agreement of liver, spleen, and pancreas stiffness measurements obtained with p-QElaXto and 2D-QElaXto on Esaote MyLab 9, compared with 2D-SWE on the SuperSonic Imagine Aixplorer (SSI). We sought to define normal stiffness ranges in healthy individuals and to evaluate their relationship with clinical and technical factors. Additionally, we examined inter-operator variability across the different SWE modalities.

MATERIALS AND METHODS

Study design

The study was designed as an observational single-center study according to the principles of the Declaration of Helsinki and the ethical standards of the local institutional research committee (Comitato Etico, Fondazione Policlinico Universitario Agostino Gemelli IRCCS). All subjects were made aware of the purpose of the study and agreed by signing the informed consent before taking part in the examination. We enrolled 50 healthy adult subjects (27 men and 23 women), primarily from hospital employees, residents, and students with no history of chronic diseases or other pathological conditions, in a period from January 2021 to June 2021.

The inclusion criteria were: (1) Age ≥ 18 years; no history of focal and/or diffuse disease of the analyzed organs; (2) No hematological disorders or other pathological conditions; (3) Negative viral serology for hepatitis B, hepatitis C and human immunodeficiency virus; (4) Laboratory tests within the normal range (in the previous 6 months), alcohol consumption not exceeding 30 g/daily for men and 20 g/daily for women; and (5) Suitable visualization and normal morphology of examined organs in US imaging. The exclusion criteria were: (1) Body mass index (BMI) > 30 kg/m^2; (2) Moderate/severe steatosis at standard B-mode; and (3) Ongoing or previous infections, recent or past injury, important recent or past bleeding, immune system disorders, and pregnant or breastfeeding women. Subjects with mild hepatic steatosis or slightly overweight were retained, as low-grade steatosis is common in the general population and does not substantially affect shear-wave elastography. Moreover, standard B-mode US reliably detects moderate-to-severe, but not necessarily mild steatosis[14].

Equipment and technical approach

The examination consisted of stiffness evaluation through p-QElaXto, 2D-QElaXto, and SSI by an experienced operator (> 5 years of experience with different elastography techniques). A standardized protocol was used to minimize pre-compression, enforce breath-hold at end-expiration, and ensure uniform region of interest (ROI) placement. Moreover, to test the reproducibility of the SWE techniques, the first 10 patients enrolled in the study underwent additional elastography examination performed by a second operator, and median organ stiffness values were compared. To minimize measurement bias, operators performed SWE examinations independently and were blinded to prior results and to each other's measurements when assessing interobserver reproducibility.

Liver, spleen, and pancreas stiffness were measured with the patient in the supine position and during breath-hold in neutral respiration, using standardized acoustic windows for each organ. For liver and spleen, intercostal approaches were used; for pancreas, the best available window (head, body, or tail) was selected according to individual anatomy. For each organ, up to 10 valid measurements were obtained in accordance with the European Federation of Societies for Ultrasound in Medicine and Biology and the World Federation for Ultrasound in Medicine and Biology (WFUMB recommendations, which indicate that a minimum of 5-10 acquisitions improves measurement reliability and reproducibility, especially in liver elastography. Full details of probe placement and acquisition protocols are provided in the Supplementary material.

SWE with Esaote was performed with a MyLab 9 equipment with convex broadband abdominal probe C1-8 MHz, obtaining up to 10 valid measurements with p-QElaXto and 5 valid measurements with 2D-QElaXto for every organ, considering median values in kPa and the ratio between interquartile range (IQR) and the median value (M) (directly provided by the software) for the analysis (Figure 1A-F, respectively). To further investigate whether a reduced number of acquisitions could still provide reliable results for p-QElaXto, we compared the mean values obtained from 10 measurements with those derived from the first 5 acquisitions. 2D-SSI was performed with Mach 30 Aixplorer (Aix-en-Provence, France) with a convex probe XC6-1 MHz, obtaining 5 valid measurements for every organ, recording median values in kPa and stability index (SI) (Figure 1G-I). For 2D-SWE systems, liver stiffness was measured in an ROI of 10 mm and 15 mm in a central area of the colorimetric map showing the best signal homogeneity. Moreover, for pancreas stiffness measurement, the ROI dimension was adjusted according to organ anatomy when using 2D-SWE techniques. All the SWE measurements for every single patient lasted no longer than 10 minutes for both elastography techniques.

Technical feasibility was calculated after the exclusion of technical failures and unreliable measurements. Based on current literature, "technical failures" were defined as no successful measurement after 10 attempts for p-QElaXto and as the inability to measure stiffness in a homogeneous ROI of at least 10 mm for 2D-SWE techniques. "Unreliable measurements" were defined by an IQR/M ratio > 0.30 and SI < 80% for QElaxto and SSI techniques, respectively[15,16]. The remaining were considered "technically feasible".

Statistical analysis

Individual patient measurements derived from multiple samples (*e.g.*, liver stiffness derived from five or ten measurements) were expressed as medians. IQR for liver stiffness measurements and IQR/M were calculated at the individual patient level and were considered as an indicator for measurement quality. Pearson correlation was used to assess univariate relationships between continuous variables after verification of data normality with the Shapiro-Wilk test. Pearson's correlation coefficients were classified as follows: 0-0.19, very weak correlation; 0.20-0.39, weak; 0.40-0.59, moderate; 0.60-0.79, strong; and 0.80-1.00, very strong. Interobserver reproducibility was estimated with a single-measure two-way mixed intraclass correlation coefficient (ICC) test for absolute agreement in a subgroup of patients. Based on the 95% confidence interval (CI) of the ICC estimate, values less than 0.5, between 0.5 and 0.75, between 0.75 and 0.9, and greater than 0.90 were considered indicative of poor, moderate, good, and excellent reliability, respectively[17]. In addition to the ICC used to assess inter-operator reproducibility, we also calculated the concordance correlation coefficient (CCC) and the coefficient of variation (CV%) to evaluate inter-technique agreement between the three SWE

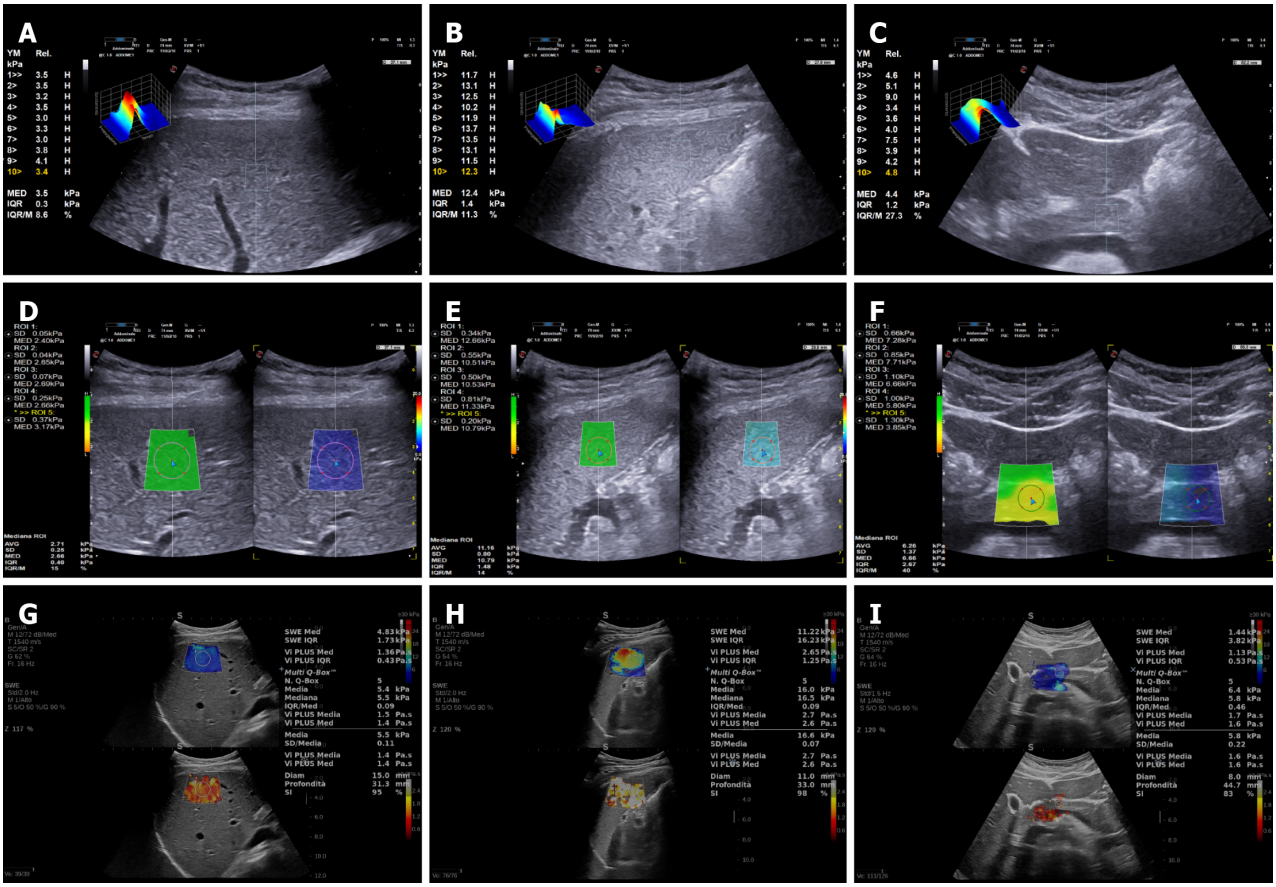


Figure 1 Shear wave elastography in healthy patients. A-C: Point-shear wave elastography of liver (A), spleen (B), and pancreas (C); D-F: 2-dimensional-shear wave elastography of liver (D), spleen (E), and pancreas (F); G-I: 2-dimensional-SuperSonic Imagine Aixplorer of liver (G), spleen (H), and pancreas (I).

methods (2D-QElaXto, p-QElaXto, and SSI). The CCC was computed according to Lin's method, combining measures of precision and accuracy, while the CV was calculated as the ratio between the standard deviation of paired differences and their mean value, expressed as a percentage. All comparisons were considered exploratory, and no adjustment for multiple testing was applied. Statistical analysis was performed by using the Statistical Package for the Social Sciences (SPSS 22.0; SPSS Inc., Chicago, IL, United States).

RESULTS

Study population

We enrolled a total of 50 patients in the study period. Organ stiffness measurements were obtained by the three different SWE techniques (2D-QElaXto, p-QElaXto, and SSI). Descriptive statistics of the "healthy" study population are reported in Table 1. Among the whole cohort, the mean BMI was 23 kg/m^2, with only two subjects showing a hyperechoic liver (both with mild liver steatosis and BMI > 25 kg/m^2) and one subject with a hyperechoic pancreas (mild fatty infiltration) on US scanning. In two other patients, pancreas visualization on US was suboptimal due to intestinal gas, and therefore, pancreatic stiffness was not performed.

Feasibility and reproducibility of organ stiffness measurements

The feasibility of the three SWE techniques was excellent, and successful measurements were obtained in all 50 subjects for liver and spleen stiffness assessment. In only one patient, IQR/M ratio was > 30% when performing liver stiffness with 2D-QElaXto with a ROI of 10 mm (but not with a ROI of 15 mm). In another single subject, spleen stiffness measurements were unreliable (IQR/M ratio > 30% or SI < 80%) with all three techniques. These unreliable measurements were probably due to the reduced spleen width (< 2.5 cm) found in this lean female volunteer (BMI 19 kg/m^2). Moreover, in six other patients, spleen stiffness assessment with p-QElaXto was unreliable when performing only 5 measurements, but not when completing the evaluation with 10 measurements. In four of the aforementioned patients, spleen stiffness was also unreliable with 2D-QElaXto by using an ROI of 10 mm, but not with a ROI of 15 mm. To summarize, the feasibility and reliability for liver and spleen stiffness assessment were 100% if 10 measurements were performed with p-QElaXto and a ROI of 15 mm was selected when using the 2D-SWE technique.

Table 1 Descriptive statistics of the "healthy" study population

Variables	Total	Males	Females
Age (years)	37 ± 10	39 ± 11	35 ± 9
BMI (kg/m^2)	23 ± 3	24 ± 2	21 ± 2
Spleen bipolar diam (cm)	10.8 ± 1.3	11.6 ± 0.9	9.8 ± 1.0
Spleen area (cm^2)	33.3 ± 8.6	37 ± 8	29 ± 7
Pancreas body thick (cm)	1.1 ± 0.3	1.2 ± 0.3	1.1 ± 0.2

BMI: Body mass index.

When performing SWE of the pancreas, the feasibility was not quite as excellent as for the liver and spleen. Specifically, in six subjects undergoing pancreas evaluation with 2D-QElaXto, measurements were either unreliable or showed inhomogeneous filling of the colorimetric map (Figure 2). Assessment with p-QElaXto was unreliable in ten patients when only the first 5 measurements were considered, but if the other five measurements were added, IQR/M ratio was > 30% only in four patients. Pancreas stiffness with SSI was not feasible in four patients due to SI < 80% (three patients) or inhomogeneous filling of the colorimetric map (one patient). Eventually, if the two failed visualizations of the organ are included, the overall feasibility of pancreas stiffness was 84%, 88% and 88% for 2D-QElaXto, p-QElaxto with 10 measurements, and SSI, respectively.

The ICC for liver stiffness measurement evaluated on 10 subjects was excellent for all three SWE techniques: 0.963 (95%CI: 0.850.99) for 2D-QElaXto (with a ROI of 15 mm), 0.906 (95%CI: 0.62-0.98) for p-QElaXto (10 measurements), and 0.928 (95%CI: 0.70-0.98) for SSI (with a ROI of 15 mm). Interoperator agreement was also very good for spleen stiffness measurements, but only for p-QElaXto and SSI, with a reliability of 0.929 (95%CI: 0.56-0.98) and 0.835 (95%CI: 0.38-0.96), respectively. 2D-QElaXto showed only a moderate agreement with an agreement of 0.519 (95%CI: -0.85 to 0.87). A similar trend was also observed for pancreas stiffness interobserver reproducibility: 0.831 (95%CI: 0.28-0.96) for p-QElaXto, 0.844 (95%CI: 0.41-0.96) for SSI, but only 0.434 (95%CI: -1.00 to 0.86) for 2D-QElaXto.

Liver stiffness measurement and concordance between SWE devices

The overall values of the median liver stiffness in the 50 healthy subjects ranged from 2.4 kPa to 8.1 kPa across the different SWE techniques (Table 2). Specifically, considering the whole study group, the mean liver stiffness value for 2D-QElaXto was 3.9 kPa regardless of whether a 10 mm or 15 mm ROI was used. For p-QElaX the mean liver stiffness values were 4.4 kPa for both 5 and 10 measurements. Mean liver stiffness obtained with SSI was 4.6 kPa and 4.7 kPa using a 10 mm and 15 mm ROI, respectively.

Bland-Altman analysis showed that 2D-QElaXto average values were 0.8 kPa (CI: -1.9 kPa to 0.4 kPa) lower than those obtained with SSI, even in the presence of a significant correlation (r = 0.75; P < 0.001). A similar trend was observed for mean p-QElaXto values, which were only 0.3 kPa (CI: -1.6 kPa to 1.0 kPa) lower than those obtained with SSI (r = 0.71; P < 0.001) (Supplementary material). For the liver stiffness measurements, concordance was good (CCC = 0.67-0.80; CV < 12%), confirming the robustness of measurements across systems.

Spleen stiffness measurement and concordance between SWE devices

The mean value of spleen bipolar diameter was 10.8 ± 1.3 cm, while the splenic area and spleen width mean values were 33.3 ± 8.6 cm^2 and 3.5 ± 0.6 cm, respectively. The overall values of the median spleen stiffness in the whole group ranged from 9.8 kPa to 46.9 kPa for the various SWE techniques (Table 3). Specifically, the mean spleen stiffness value for 2D-QElaXto was 19.4 kPa with an ROI of 10 mm and 20.0 kPa with an ROI of 15 mm. For p-QElaX, the mean spleen stiffness values were 23.0 kPa and 22.9 kPa when performing 5 or 10 measurements, respectively. Mean spleen stiffness values obtained with SSI were 21.9 kPa using a 10 mm ROI and 21.7 kPa with a 15 mm ROI.

Bland-Altman analysis showed that 2D-QElaXto average values were 1.7 kPa (CI: -7.4 kPa to 3.9 kPa) lower than those obtained with SSI, even in the presence of a significant good correlation (r = 0.79; P < 0.001). Regarding p-QElaXto, mean values were 1.2 kPa (CI: -6.4 kPa to 8.8 kPa) higher than those obtained with SSI (r = 0.68; P < 0.001) (Supplementary material). For the spleen stiffness measurements, CCC ranged from 0.61 to 0.73 (CV < 13%), consistent with moderate-to-good agreement.

Pancreas stiffness and variability between SWE devices

Pancreas stiffness evaluation was strongly influenced by organ visualization in every single subject. Consequently, a complete US assessment of the pancreas - including head, body, and tail - was achieved only in 23 subjects (46% of the whole population). SWE was therefore performed in the organ section with the best acoustic window. For 2D-SWE techniques (2D-QElaXto and SSI), the ROI dimension was adjusted according to organ anatomy (mean ROI size was 8.0 mm). The median pancreas stiffness in the whole group ranged from 2.7 kPa to 18.0 kPa for the various SWE techniques (Table 4). Particularly, the mean pancreas stiffness value for 2D-QElaXto was 5.2 kPa, while the mean values for p-QElaXto were 5.9 kPa and 6.1 kPa when performing 5 or 10 measurements, respectively. The mean pancreas stiffness value for SSI was 7.6 kPa.

Table 2 Median liver stiffness values

SWE technique	2D-QElaXto (10 mm ROI)	2D-QElaXto (15 mm ROI)	p-QElaXto (5 meas)	p-QElaXto (10 meas)	SSI (10 mm ROI)	SSI (15 mm ROI)
Mean liver stiffness (kPa)	3.9	3.9	4.4	4.4	4.6	4.7
Range (kPa)	2.4-6.5	2.7-6.8	3-0-8.1	3.0-8.0	3.5-7.3	3.5-7.1
SD	0.8	0.8	0.9	0.9	0.9	0.9
95%CI	3.66-4.11	3.69-4.15	4.13-4.66	4.12-4.65	4.41-4.89	4.44-4.93

2D-QElaXto: 2-dimensional-shear wave elastography; p-QElaXto: Point-shear wave elastography; SSI: SuperSonic Imagine; ROI: Region of interest; CI: Confidence interval.

Table 3 Median spleen stiffness values

SWE technique	2D-QElaXto (10 mm ROI)	2D-QElaXto (15 mm ROI)	p-QElaXto (5 meas)	p-QElaXto (10 meas)	SSI (10 mm ROI)	SSI (15 mm ROI)
Mean spleen stiffness (kPa)	19.4	20.0	23.0	22.9	21.9	21.7
Range (kPa)	9.8-26.7	11.7-32.6	13.5-46.9	13.1-36.1	13.4-35.9	13.5-33.8
SD	3.9	4.3	6.1	5.0	4.8	4.6
95%CI	18.27-20.60	18.72-21.20	21.10-24.86	21.45-24.34	20.57-23.33	20.37-23.04

2D-QElaXto: 2-dimensional-shear wave elastography; p-QElaXto: Point-shear wave elastography; SSI: SuperSonic Imagine; ROI: Region of interest; CI: Confidence interval.

Table 4 Median pancreas stiffness values

SWE technique	2D-QElaXto	p-QElaXto (5 meas)	p-QElaXto (10 meas)	SSI
Mean pancreas stiffness (kPa)	5.2	5.9	6.1	7.6
Range (kPa)	2.9-15.0	2.8-17.4	3.1-18.0	2.7-17.2
SD	1.9	2.5	2.4	2.6
95%CI	4.63-5.80	5.03-6.70	5.40-6.83	6.86-8.41

2D-QElaXto: 2-dimensional-shear wave elastography; p-QElaXto: Point-shear wave elastography; SSI: SuperSonic Imagine; CI: Confidence interval.

Bland-Altman analysis showed that 2D-QElaXto average values were 2.2 kPa (CI: -6.3 kPa to 1.9 kPa) lower than those obtained with SSI, with only a moderate correlation (r = 0.56; P < 0.001). A similar trend was observed for mean p-QElaXto values, which were 1.5 kPa (CI: -6.4 kPa to 3.4 kPa) lower than those obtained with SSI (r = 0.49; P = 0.01) (Supplementary material). However, the correlation was stronger when comparing 2D-QElaXto with p-QElaXto average values (r = 0.75; P < 0.05). As opposed to liver and spleen, pancreatic stiffness measurements showed lower concordance (CCC = 0.35-0.66; CV 22%-32%), in line with the higher variability already observed in the Bland-Altman analysis.

DISCUSSION

Over recent years, ultrasonography and elastography techniques have garnered growing interest due to their capability for both qualitative and quantitative analysis of tissue stiffness, offering additional data compared to traditional semeiological examination. This heightened interest has led to the development of a wide array of US commercial devices, equipped with their own dedicated SWE technique. Our study aimed to assess the feasibility and agreement among three different SWE techniques (2D-QElaXto, p-QElaXto, and 2D-SWE SSI) to establish normal stiffness values for the liver, spleen, and pancreas, considering the substantial inter-system variability.

The different SWE techniques demonstrated excellent feasibility for the assessment of liver and spleen stiffness, whereas the feasibility for pancreatic evaluation was moderately lower. This limitation is primarily attributable to various anatomical and functional factors. Assessing pancreatic stiffness remains a technically demanding and clinically intriguing challenge. The retroperitoneal location increases depth and bowel-gas interposition, often limiting ROI size and

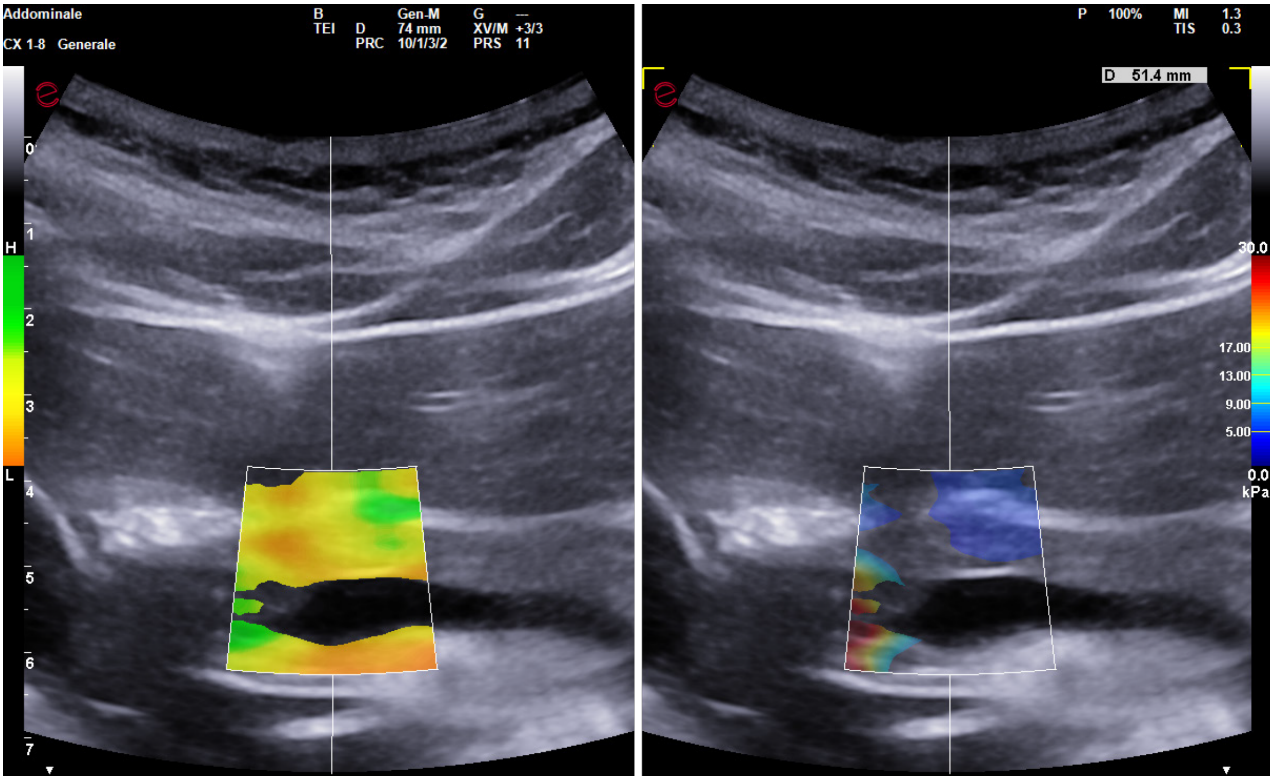


Figure 2 2-dimensional-shear wave elastography of pancreas: Inhomogeneous filling of the colorimetric map suggests an unreliable measurement.

reducing map homogeneity[18]. Proximity to the aorta may introduce pulsation-related artifacts[19]. Measurements are also sensitive to respiratory phase, with deep inspiration yielding higher values than free breathing[20]. Beyond acquisition constraints, variability is influenced by anthropometric factors such as BMI and gland depth[18,21]. Age and sex also play a role, affecting measured stiffness and inter-observer agreement[22]. In our study, a complete US evaluation of the pancreas was feasible in only 23 subjects, and, during 2D-SWE acquisitions, the ROI size was adapted to the specific anatomy of each patient. Simethicone-water-rotation protocols have been proposed to enhance pancreatic visibility[23]. However, their adoption in routine clinical settings is limited, and adequate pancreatic imaging remains challenging. In addition, both inter- and intra-operator variability were significantly higher for pancreatic stiffness assessment compared to liver and spleen, further confirming the technical challenges associated with evaluating the pancreatic gland. Bland-Altman analysis confirmed that for liver and spleen, the mean inter-device differences were small (< 2 kPa) and unlikely to affect interpretation in healthy subjects, whereas pancreatic measurements showed wider limits of agreement (up to ± 6 kPa), indicating lower reproducibility. Because of the limited sample size and the homogeneous demographic profile of our study population, no formal multivariate regression analysis could be reliably performed to identify predictors of pancreatic measurement unreliability. Future multicenter studies with larger and more heterogeneous cohorts may be helpful to quantitatively assess how anthropometric and technical parameters contribute to pancreatic SWE variability.

Concerning stiffness measurements, our findings aligned with the well-established reference values for liver elastography, while contributing novel data on spleen and pancreatic elastography, along with relevant technical considerations. In our study, liver stiffness values in healthy subjects measured with 2D-QElaXto and p-QElaXto were 3.9 kPa and 4.4 kPa, respectively, showing a good agreement with 2D-SWE SSI. These values agree with the Society of Radiologists in the US's Consensus[24] and subsequent WFUMB Guidelines[13] "rule of four", which states that the liver with a stiffness value equal to or less than 5 kPa (1.3 m/second) has a high probability of being normal. Furthermore, liver stiffness evaluation using different sizes of ROI for 2D-SWE techniques, 10 mm and 15 mm, showed no significant variation with similar values to other studies[8,9,25]. These findings support the robustness of the "rule of four" as a universal reference threshold that can be reliably applied across different elastographic equipment to exclude the presence of significant liver fibrosis.

Regarding the spleen stiffness, values ranged from 19.4 kPa (2D-QElaXto, 10 mm ROI) to 23.0 kPa (p-QElaXto, 5 measurements). Few studies have investigated spleen stiffness in healthy adults, and their reported values are consistent with our results[1,9,26]. For example, Leung *et al*[26] reported a mean spleen stiffness value of 17.3 ± 2.6 kPa in a cohort of healthy volunteers, with no statistically significant difference observed between male and female subjects. In recent years, efforts have focused on defining universal cut-off values for spleen elastography. Similar to liver elastography, these thresholds aim to rule out clinically significant portal hypertension (CSPH) or high-risk esophageal varices in patients with compensated advanced chronic liver disease (cACLD)[7,27,28]. Recently, the role of spleen stiffness in identifying or ruling out CSPH in cACLD patients was clarified by the 2024 WFUMB guidelines[13], which introduced a "Baveno

VII−SSM dual-cutoff model"[13,29]. This model incorporates LSM, SSM and platelet count to improve diagnostic accuracy, establishing 21 kPa as the upper SSM threshold for excluding CSPH - slightly lower than the threshold proposed in Baveno VII[13]. It should be noted, however, that these thresholds refer to values obtained by transient elastography in cACLD patients, and no guideline-based cut-offs are currently available for SWE. The spleen stiffness values obtained in our cohort, together with the high reproducibility of liver and spleen measurements, support the clinical use of SWE for non-invasive assessment of liver fibrosis and for spleen-based evaluation of portal hypertension. Future studies should clarify whether spleen stiffness values in healthy individuals overlap with those of cACLD patients without CSPH.

Lastly, regarding pancreatic elastography, the mean stiffness values in healthy subjects in our cohort ranged from 5.2 kPa with 2D-QElaX to 6.1 kPa with SSI. These findings are in line with previously reported normal ranges. For example, Kaya *et al*[20] found median values around 4-5 kPa during free breathing, while Nosakova *et al*[21] reported a mean of approximately 6.1 kPa using 2D-SWE. Similarly, Gallotti *et al*[12] described mean velocities of 1.40 m/second (approximately 6 kPa) with ARFI in healthy volunteers, and Choudhury *et al*[30] reported mean values of 8.7-9.0 kPa in an Indian cohort, highlighting possible variability related to population and methodology. Other studies confirmed normal pancreas stiffness around 6-7 kPa in controls[31], whereas markedly higher values (23.8 ± 6.7 kPa) were reported by Durmaz *et al*[32]. Taken together, our data fall within the lower-to-mid portion of the spectrum of published reference values, supporting their reliability while underlining the considerable heterogeneity observed across studies depending on technique, respiratory phase, and anthropometric factors.

Although inter-system variability currently limits routine pancreatic SWE, emerging evidence indicates that stiffness measurements may provide additional value in detecting pancreatic steatosis, in correlation with metabolic syndrome and cardiovascular risk stratification[33,34], and in the evaluation of inflammatory changes in acute and chronic pancreatitis[11,33]. Latest evidence reports also a significant correlation between concomitant increase of pancreatic and splenic stiffness in patients with portal hypertension[35]. We acknowledge some potential limitations of our study. Firstly, the limited number of participants in our study may have affected the statistical power, potentially increasing the margin of error. Also, the recruitment of hospital staff and medical students may introduce a selection bias, as this group is relatively homogeneous in terms of age, health status, and BMI. To strengthen the validity of our findings, future multicenter studies should include a more demographically diverse cohort to improve generalizability. Secondly, it is important to note that our investigation was conducted within a single institution. Thirdly, measurements in our study were performed using a generation-specific device, and the normal values generated may be representative of this model and generation. However, it would be advisable to verify the concordance between different models and generations of the same manufacturer because the lack of harmonization across US platforms restricts comparability of SWE values, highlighting the importance of multicenter studies and standardized acquisition protocols for clinical adoption.

CONCLUSION

Our study provides preliminary reference stiffness values in healthy adults using three SWE techniques, with robust liver and spleen reproducibility that supports integration of SWE into multiparametric US assessment of chronic liver disease and portal hypertension. In contrast, pancreatic stiffness measurements remain more variable, highlighting the need for optimized acquisition protocols and standardization before SWE can be reliably applied in pancreatic routine clinical practice. Future multicenter studies with larger cohorts should focus on harmonizing reference values and technical parameters across different systems and manufacturers, enabling SWE to evolve into a truly reproducible, quantitative, and cross-platform non-invasive tool for abdominal organ evaluation.

ACKNOWLEDGEMENTS

Thanks to Fondazione Roma for its commitment to support our research.

FOOTNOTES

Author contributions: Viceconti N, Garcovich M, Del Zompo F, Riccardi L, and Garcovich M contributed to conceptualization, investigation, and editing; Viceconti N and Garcovich M contributed to study design, supervision, writing the first draft, and review; Paratore M, Riccardi L, and Garcovich M contributed to acquisition, analysis, and interpretation of data; all authors revised the manuscript critically for intellectual content and approved the final version.

Institutional review board statement: This study was reviewed and approved by the Comitato Etico, Fondazione Policlinico Universitario Agostino Gemelli IRCCS, No. 3584.

Informed consent statement: Each patient agreed to participate in the study by written informed consent.

Conflict-of-interest statement: All the authors report no relevant conflicts of interest for this article.

Data sharing statement: All participants' personal data were anonymized before analysis, and data handling fully complied with the

General Data Protection Regulation (EU) 2016/679 (GDPR) and applicable national privacy laws. The authors can provide datasets upon reasonable request.

STROBE statement: The authors have read the STROBE Statement-checklist of items, and the manuscript was prepared and revised according to the STROBE Statement-checklist of items.

Open Access: This article is an open-access article that was selected by an in-house editor and fully peer-reviewed by external reviewers. It is distributed in accordance with the Creative Commons Attribution NonCommercial (CC BY-NC 4.0) license, which permits others to distribute, remix, adapt, build upon this work non-commercially, and license their derivative works on different terms, provided the original work is properly cited and the use is non-commercial. See: https://creativecommons.org/Licenses/by-nc/4.0/

Country of origin: Italy

ORCID number: Nicholas Viceconti 0009-0007-4084-9999; Mattia Paratore 0000-0002-7546-8041; Fabio Del Zompo 0000-0003-3905-9627; Maria Assunta Zocco 0000-0002-0814-9542; Maria Elena Ainora 0000-0001-5847-1065; Giorgio Esposto 0009-0007-8296-168X; Antonio Gasbarrini 0000-0003-4863-6924; Maurizio Pompili 0000-0001-6699-7980; Laura Riccardi 0000-0001-6249-0314; Matteo Garcovich 0000-0002-5805-7953.

Corresponding Author's Membership in Professional Societies: United European Gastroenterology, .

S-Editor: Bai SR
L-Editor: A
P-Editor: Xu J

REFERENCES

1 **Pawluś A**, Inglot MS, Szymańska K, Kaczorowski K, Markiewicz BD, Kaczorowska A, Gąsiorowski J, Szymczak A, Inglot M, Bladowska J, Zaleska-Dorobisz U. Shear wave elastography of the spleen: evaluation of spleen stiffness in healthy volunteers. *Abdom Radiol (NY)* 2016; **41**: 2169-2174 [*RCA*] [PMID: 27389244 DOI: 10.1007/s00261-016-0834-4] [FullText] [Full Text(PDF)]

2 **Ferraioli G**, Tinelli C, Lissandrin R, Zicchetti M, Bernuzzi S, Salvaneschi L, Filice C; Elastography Study Group. Ultrasound point shear wave elastography assessment of liver and spleen stiffness: effect of training on repeatability of measurements. *Eur Radiol* 2014; **24**: 1283-1289 [*RCA*] [PMID: 24643497 DOI: 10.1007/s00330-014-3140-y] [FullText]

3 **European Association for the Study of the Liver**. EASL Clinical Practice Guidelines on non-invasive tests for evaluation of liver disease severity and prognosis - 2021 update. *J Hepatol* 2021; **75**: 659-689 [*RCA*] [PMID: 34166721 DOI: 10.1016/j.jhep.2021.05.025] [FullText]

4 **Wu M**, Wu L, Jin J, Wang J, Li S, Zeng J, Guo H, Zheng J, Chen S, Zheng R. Liver Stiffness Measured with Two-dimensional Shear-Wave Elastography Is Predictive of Liver-related Events in Patients with Chronic Liver Disease Due to Hepatis B Viral Infection. *Radiology* 2020; **295**: 353-360 [*RCA*] [PMID: 32125254 DOI: 10.1148/radiol.2020191481] [FullText]

5 **Ferraioli G**, Wong VW, Castera L, Berzigotti A, Sporea I, Dietrich CF, Choi BI, Wilson SR, Kudo M, Barr RG. Liver Ultrasound Elastography: An Update to the World Federation for Ultrasound in Medicine and Biology Guidelines and Recommendations. *Ultrasound Med Biol* 2018; **44**: 2419-2440 [*RCA*] [PMID: 30209008 DOI: 10.1016/j.ultrasmedbio.2018.07.008] [FullText]

6 **Gibiino G**, Garcovich M, Ainora ME, Zocco MA. Spleen ultrasound elastography: state of the art and future directions - a systematic review. *Eur Rev Med Pharmacol Sci* 2019; **23**: 4368-4381 [*RCA*] [PMID: 31173311 DOI: 10.26355/eurrev_201905_17944] [FullText]

7 **Reiberger T**. The Value of Liver and Spleen Stiffness for Evaluation of Portal Hypertension in Compensated Cirrhosis. *Hepatol Commun* 2022; **6**: 950-964 [*RCA*] [PMID: 34904404 DOI: 10.1002/hep4.1855] [FullText] [Full Text(PDF)]

8 **Dong Y**, Sirli R, Ferraioli G, Sporea I, Chiorean L, Cui X, Fan M, Wang WP, Gilja OH, Sidhu PS, Dietrich CF. Shear wave elastography of the liver - review on normal values. *Z Gastroenterol* 2017; **55**: 153-166 [*RCA*] [PMID: 28192849 DOI: 10.1055/s-0042-117226] [FullText]

9 **Giuffrè M**, Macor D, Masutti F, Abazia C, Tinè F, Patti R, Buonocore MR, Colombo A, Visintin A, Campigotto M, Crocè LS. Evaluation of spleen stiffness in healthy volunteers using point shear wave elastography. *Ann Hepatol* 2019; **18**: 736-741 [*RCA*] [PMID: 31054978 DOI: 10.1016/j.aohep.2019.03.004] [FullText]

10 **Sezgin O**, Yaraş S, Özdoğan O. Pancreatic Steatosis Is Associated with Both Metabolic Syndrome and Pancreatic Stiffness Detected by Ultrasound Elastography. *Dig Dis Sci* 2022; **67**: 293-304 [*RCA*] [PMID: 33651254 DOI: 10.1007/s10620-021-06844-3] [FullText]

11 **Dietrich CF**, Hocke M. Elastography of the Pancreas, Current View. *Clin Endosc* 2019; **52**: 533-540 [*RCA*] [PMID: 31311914 DOI: 10.5946/ce.2018.156] [FullText] [Full Text(PDF)]

12 **Gallotti A**, D'Onofrio M, Pozzi Mucelli R. Acoustic Radiation Force Impulse (ARFI) technique in ultrasound with Virtual Touch tissue quantification of the upper abdomen. *Radiol Med* 2010; **115**: 889-897 [*RCA*] [PMID: 20082227 DOI: 10.1007/s11547-010-0504-5] [FullText]

13 **Ferraioli G**, Barr RG, Berzigotti A, Sporea I, Wong VW, Reiberger T, Karlas T, Thiele M, Cardoso AC, Ayonrinde OT, Castera L, Dietrich CF, Iijima H, Lee DH, Kemp W, Oliveira CP, Sarin SK. WFUMB Guideline/Guidance on Liver Multiparametric Ultrasound: Part 1. Update to 2018 Guidelines on Liver Ultrasound Elastography. *Ultrasound Med Biol* 2024; **50**: 1071-1087 [*RCA*] [PMID: 38762390 DOI: 10.1016/j.ultrasmedbio.2024.03.013] [FullText]

14 **Hernaez R**, Lazo M, Bonekamp S, Kamel I, Brancati FL, Guallar E, Clark JM. Diagnostic accuracy and reliability of ultrasonography for the detection of fatty liver: a meta-analysis. *Hepatology* 2011; **54**: 1082-1090 [*RCA*] [PMID: 21618575 DOI: 10.1002/hep.24452] [FullText]

15 **Dietrich CF**, Bamber J, Berzigotti A, Bota S, Cantisani V, Castera L, Cosgrove D, Ferraioli G, Friedrich-Rust M, Gilja OH, Goertz RS, Karlas T, de Knegt R, de Ledinghen V, Piscaglia F, Procopet B, Saftoiu A, Sidhu PS, Sporea I, Thiele M. EFSUMB Guidelines and Recommendations on the Clinical Use of Liver Ultrasound Elastography, Update 2017 (Long Version). *Ultraschall Med* 2017; **38**: e16-e47 [*RCA*] [PMID: 28407655 DOI: 10.1055/s-0043-103952] [FullText]

16 **Dietrich CF**, Abramowicz JS, Chammas MC, Chou YH, Condous G, Kim SH, Nolsøe CP, Vinayak S, Jenssen C. World Federation for

Ultrasound in Medicine and Biology (WFUMB) Policy Document Development Strategy - Clinical Practice Guidelines, Position Statements and Technological Reviews (on behalf of the WFUMB publication committee and Executive Bureau). *Ultrasound Med Biol* 2021; **47**: 2779-2781 [*RCA*] [PMID: 34119356 DOI: 10.1016/j.ultrasmedbio.2021.04.017] [FullText]

17 **Bartko JJ**. Measures of agreement: a single procedure. *Stat Med* 1994; **13**: 737-745 [*RCA*] [PMID: 8023046 DOI: 10.1002/sim.4780130534] [FullText]

18 **Huang J**, Peng J, Long H, Ruan S, Yao L, Xie X, Lin M, Zhang X. Feasibility and Measurement Value of Pancreatic 2-D Shear Wave Elastography in Healthy Adults: Evaluation, Influencing Factors, Reference Range, Measurement Stability and Reproducibility. *Ultrasound Med Biol* 2024; **50**: 184-190 [*RCA*] [PMID: 37880058 DOI: 10.1016/j.ultrasmedbio.2023.09.015] [FullText]

19 **Marasco G**, Ricci C, Grasso V, Alvisi M, Serra C, Ravaioli F, Casadei R, Colecchia A. Pancreatic ultrasound elastography is not useful to predict the risk of pancreatic fistulas after pancreatic resection. *Updates Surg* 2020; **72**: 1081-1087 [*RCA*] [PMID: 32248425 DOI: 10.1007/s13304-020-00748-z] [FullText]

20 **Kaya M**, Gürün E. Do deep inspiration breath-holds and free-breathing affect pancreatic tissue stiffness in shear wave elastography? *Abdom Radiol (NY)* 2022; **47**: 2390-2396 [*RCA*] [PMID: 35507067 DOI: 10.1007/s00261-022-03535-z] [FullText]

21 **Nosakova L**, Uhrik P, Pindura M, Vojtko M, Hoferica J, Cmarkova K, Miklusica J, Banovcin P. Pancreatic stiffness and anthropometric parameters in healthy volunteers. *Bratisl Lek Listy* 2024; **125**: 172-175 [*RCA*] [PMID: 38385543 DOI: 10.4149/BLL_2024_27] [FullText]

22 **Stumpf S**, Jaeger H, Graeter T, Oeztuerk S, Schmidberger J, Haenle MM, Kratzer W; Elasto-Study Group Ulm. Influence of age, sex, body mass index, alcohol, and smoking on shear wave velocity (p-SWE) of the pancreas. *Abdom Radiol (NY)* 2016; **41**: 1310-1316 [*RCA*] [PMID: 26880176 DOI: 10.1007/s00261-016-0661-7] [FullText] [Full Text(PDF)]

23 **Abu-Yousef MM**, El-Zein Y. Improved US visualization of the pancreatic tail with simethicone, water, and patient rotation. *Radiology* 2000; **217**: 780-785 [*RCA*] [PMID: 11110943 DOI: 10.1148/radiology.217.3.r00dc37780] [FullText]

24 **Barr RG**, Wilson SR, Rubens D, Garcia-Tsao G, Ferraioli G. Update to the Society of Radiologists in Ultrasound Liver Elastography Consensus Statement. *Radiology* 2020; **296**: 263-274 [*RCA*] [PMID: 32515681 DOI: 10.1148/radiol.2020192437] [FullText]

25 **Mulabecirovic A**, Mjelle AB, Gilja OH, Vesterhus M, Havre RF. Liver elasticity in healthy individuals by two novel shear-wave elastography systems-Comparison by age, gender, BMI and number of measurements. *PLoS One* 2018; **13**: e0203486 [*RCA*] [PMID: 30216377 DOI: 10.1371/journal.pone.0203486] [FullText] [Full Text(PDF)]

26 **Leung VY**, Shen J, Wong VW, Abrigo J, Wong GL, Chim AM, Chu SH, Chan AW, Choi PC, Ahuja AT, Chan HL, Chu WC. Quantitative elastography of liver fibrosis and spleen stiffness in chronic hepatitis B carriers: comparison of shear-wave elastography and transient elastography with liver biopsy correlation. *Radiology* 2013; **269**: 910-918 [*RCA*] [PMID: 23912619 DOI: 10.1148/radiol.13130128] [FullText]

27 **Ginès P**, Krag A, Abraldes JG, Solà E, Fabrellas N, Kamath PS. Liver cirrhosis. *Lancet* 2021; **398**: 1359-1376 [*RCA*] [PMID: 34543610 DOI: 10.1016/S0140-6736(21)01374-X] [FullText]

28 **Song J**, Huang J, Huang H, Liu S, Luo Y. Performance of spleen stiffness measurement in prediction of clinical significant portal hypertension: A meta-analysis. *Clin Res Hepatol Gastroenterol* 2018; **42**: 216-226 [*RCA*] [PMID: 29223365 DOI: 10.1016/j.clinre.2017.11.002] [FullText]

29 **de Franchis R**, Bosch J, Garcia-Tsao G, Reiberger T, Ripoll C; Baveno VII Faculty. Baveno VII - Renewing consensus in portal hypertension. *J Hepatol* 2022; **76**: 959-974 [*RCA*] [PMID: 35120736 DOI: 10.1016/j.jhep.2021.12.022] [FullText]

30 **Choudhury SR**, Verma M, Gupta P, Singh H, Sharma V, Kochhar R. Ultrasound Shear Wave Elastography of Normal Pancreas in Adult Subjects. *J Gastrointestinal Abdominal Radiol* 2023; **06**: 148-153 [*RCA*] [DOI: 10.1055/s-0042-1758126] [FullText]

31 **Suzuki H**, Ishikawa T, Ohno E, Iida T, Uetsuki K, Yashika J, Yamada K, Yoshikawa M, Furukawa K, Nakamura M, Honda T, Ishigami M, Kawashima H, Fujishiro M. An initial trial of quantitative evaluation of autoimmune pancreatitis using shear wave elastography and shear wave dispersion in transabdominal ultrasound. *Pancreatology* 2021; **21**: 682-687 [*RCA*] [PMID: 33648879 DOI: 10.1016/j.pan.2021.02.014] [FullText]

32 **Durmaz MS**, Arslan S, Özbakır B, Güngör G, Tolu İ, Arslan FZ, Sivri M, Koplay M. Effectiveness of Shear Wave Elastography in the diagnosis of acute pancreatitis on admission. *Med Ultrason* 2018; **20**: 278-284 [*RCA*] [PMID: 30167579 DOI: 10.11152/mu-1398] [FullText]

33 **Paratore M**, Garcovich M, Ainora ME, Del Vecchio LE, Cuccia G, Riccardi L, Pompili M, Gasbarrini A, Zocco MA. The Role of Transabdominal Ultrasound Elastography in Gastrointestinal Non-Liver Diseases: Current Application and Future Prospectives. *Diagnostics (Basel)* 2023; **13**: 2266 [*RCA*] [PMID: 37443663 DOI: 10.3390/diagnostics13132266] [FullText] [Full Text(PDF)]

34 **Zhang Y**, Liu Y, Petrov MS. Relationship of fat in the pancreas with cardiovascular disease: A systematic review and meta-analysis. *Obes Rev* 2025; **26**: e13914 [*RCA*] [PMID: 40015555 DOI: 10.1111/obr.13914] [FullText] [Full Text(PDF)]

35 **Wekerle M**, Murillo K, vonBoscamp M, Hauber V, Ebert MP, Antoni C, Hirth M. Point-shear wave elastography generated by acoustic radiation force impulse in chronic pancreatitis. *United European Gastroenterol J* 2024; **12**: 667-677 [*RCA*] [PMID: 38363191 DOI: 10.1002/ueg2.12543] [FullText]

World Journal of Radiology

Submit a Manuscript: https://www.f6publishing.com

World J Radiol 2025 November 28; 17(11): 114193

DOI: 10.4329/wjr.v17.i11.114193

ISSN 1949-8470 (online)

LETTER TO THE EDITOR

Value of radiomics models in precision diagnosis of dual-phenotype hepatocellular carcinoma and intrahepatic cholangiocarcinoma

Xu Qi, Fei-Yu Zhao

Specialty type: Radiology, nuclear medicine and medical imaging

Provenance and peer review: Invited article; Externally peer reviewed.

Peer-review model: Single blind

Peer-review report's classification

Scientific Quality: Grade B, Grade B, Grade B, Grade D

Novelty: Grade B, Grade B, Grade C, Grade D

Creativity or Innovation: Grade B, Grade B, Grade C, Grade C

Scientific Significance: Grade B, Grade B, Grade B, Grade D

P-Reviewer: Dubey V, Researcher, India; Yang L, MD, Professor, China

Received: September 17, 2025

Revised: October 3, 2025

Accepted: November 4, 2025

Published online: November 28, 2025

Processing time: 74 Days and 23.7 Hours

Xu Qi, Department of Radiology, Peking Union Medical College Hospital, Beijing 100730, China

Fei-Yu Zhao, Department of Radiation Oncology, The Fifth Medical Center of Chinese PLA General Hospital, Beijing 100071, China

Corresponding author: Fei-Yu Zhao, PhD, Department of Radiation Oncology, The Fifth Medical Center of Chinese PLA General Hospital, No. 8 East Main Street, Fengtai District, Beijing 100071, China. 1029279130@qq.com

Abstract

In the clinical diagnosis and treatment of liver tumors, the differential diagnosis between dual-phenotype hepatocellular carcinoma and intrahepatic cholangiocarcinoma has long been a challenging problem for clinicians. These two types of tumors not only exhibit overlapping pathological features but also have significantly different treatment strategies and prognoses. Misdiagnosis can directly affect patients' quality of life. Recently, a study published by Zhang *et al* has brought groundbreaking insights into this dilemma. Radiomics technology has demonstrated remarkable value in the differential diagnosis of these two diseases, opening up a new path for the precise diagnosis and treatment of liver tumors.

Key Words: Dual-phenotype hepatocellular carcinoma; Intrahepatic cholangiocarcinoma; Radiomics; Differential diagnosis; Machine learning

©The Author(s) 2025. Published by Baishideng Publishing Group Inc. All rights reserved.

Core Tip: A recent study published by Zhang *et al* focuses on exploring the practical value of radiomics in ahcieving the differential diagnosis between dual-phenotype hepatocellular carcinoma and intrahepatic cholangiocarcinoma. Its constructed combined model, with an area under the receiver operating characteristic curve of 0.892, can effectively boost diagnostic accuracy and provide significant assistance to less-experienced radiologists in clinical practice. However, the study still faces limitations of single-center data and small sample size, and future research thus needs to carry out multi-center studies and promote multi-omics fusion to address these issues.

Citation: Qi X, Zhao FY. Value of radiomics models in precision diagnosis of dual-phenotype hepatocellular carcinoma and intrahepatic cholangiocarcinoma. *World J Radiol* 2025; 17(11): 114193
URL: https://www.wjgnet.com/1949-8470/full/v17/i11/114193.htm
DOI: https://dx.doi.org/10.4329/wjr.v17.i11.114193

TO THE EDITOR

Dual-phenotype hepatocellular carcinoma (DPHCC) and intrahepatic cholangiocarcinoma (ICC) are two clinically important subtypes of primary liver cancer, but their differential diagnosis has long plagued clinicians due to overlapping pathological and imaging features[1,2]. DPHCC is a rare special subtype of hepatocellular carcinoma, characterized by simultaneous differentiation of hepatocyte and cholangiocyte lineages; it has stronger biological aggressiveness, higher rates of microvascular invasion, and poorer sensitivity to radiotherapy and chemotherapy than conventional HCC, leading to significantly worse prognosis[3]. In contrast, ICC originates from intrahepatic bile duct epithelial cells, spreads mainly through lymph node metastasis, and its standard treatment relies on surgical resection combined with postoperative adjuvant chemotherapy[4]. Misdiagnosis between DPHCC and ICC directly leads to inappropriate treatment selection: For example, treating DPHCC with ICC-oriented adjuvant chemotherapy may result in ineffective therapy and missed opportunities for targeted intervention, while misclassifying ICC as DPHCC may lead to unnecessary aggressive surgical approaches and increased postoperative complications[2,5]. Traditional imaging diagnosis (such as computed tomography and magnetic resonance imaging) relies on qualitative description of tumor morphology, vascular enhancement patterns, and peritumoral changes. In this context, radiomics, which extracts quantitative features from medical images and constructs diagnostic models *via* machine learning, has emerged as a promising tool to address this diagnostic dilemma[6].

Study design and clinical significance

A study recently published by Zhang *et al* has brought groundbreaking insights into this dilemma. This study constructed a clinical sign model, a radiomics model, and a combined model, and conducted an in-depth analysis of the imaging data from 53 DPHCC patients and 124 ICC patients. The results showed that the area under the curve of the combined model in the test set reached 0.892, significantly superior to that of the single clinical model. More notably, with the assistance of the model, the diagnostic area under the curve of less experienced radiologists (with 5 years of experience) increased from 0.698 to 0.946, confirming the unique role of radiomics in bridging the gap in diagnostic experience. This finding not only validates the clinical applicability of radiomics but also reveals its great potential as a "digital biopsy" tool. The core value of radiomics lies in converting texture features in medical images that are difficult to capture with the naked eye into quantitative data and uncovering the essence of diseases through machine learning algorithms[7]. Compared with traditional imaging diagnosis, this study adopted whole-tumor slice-by-slice delineation of regions of interest, avoiding the limitations of single-slice analysis and comprehensively capturing tumor heterogeneity, which reflects the imaging manifestations of molecular-level differences between DPHCC and ICC. The 28 radiomic features screened in the study may represent the "imaging fingerprints" of the biological behaviors of these two tumors, such as cell proliferation and angiogenesis.

Zhang *et al*'s work has some notable innovations compared with earlier studies on DPHCC-ICC differential diagnosis [1]: (1) Whole-tumor regions of interest delineation: Unlike Gu *et al*[8] (who focused on tumor parenchyma only), Zhang *et al*[1] adopted slice-by-slice delineation of the entire tumor, including the tumor margin and peritumoral tissues. This approach comprehensively captures tumor heterogeneity, which better reflects the molecular-level differences between DPHCC (with hepatocyte-cholangiocyte dual differentiation) and ICC (with bile duct epithelial differentiation); and (2) feature interpretability clues: The 28 screened radiomic features included 12 texture features (*e.g.*, gray-level co-occurrence matrix entropy) and 8 shape features (*e.g.*, tumor sphericity), which may correspond to biological behaviors such as cell proliferation (reflected by texture irregularity) and angiogenesis (reflected by enhancement heterogeneity) in DPHCC and ICC. This provides a basis for linking radiomic features to pathological mechanisms, whereas Gu *et al*'s study (focused on magnetic resonance imaging qualitative features) lacked such quantitative-pathological correlation analysis[8].

From a practical clinical perspective, radiomics models are particularly valuable for physicians at different experience levels. For experienced doctors, the model can serve as a reference to help reduce subjective bias in diagnosis; for young, less experienced doctors, radiomics models can help them quickly improve their diagnostic capabilities. Currently, the diagnosis and treatment of liver tumors are moving towards precision and personalization[9]. As a special subtype of HCC, DPHCC has characteristics of both hepatocyte and cholangiocyte differentiation, with stronger microvascular invasion ability and higher resistance to radiotherapy and chemotherapy[7]. In contrast, ICC primarily spreads through lymph node metastasis, and adjuvant chemotherapy after surgery is the standard treatment[10]. Precise differentiation between the two directly determines the choice of surgical approach and adjuvant treatment strategies. The introduction of radiomics models not only improves the accuracy of preoperative diagnosis but also provides objective quantitative evidence for clinical decision-making, promoting the shift from "experience-based medicine" to "data-driven medicine".

Existing challenges and future directions

However, Zhang *et al*'s study also highlights common challenges in the clinical translation of radiomics. The single-center retrospective design may introduce selection bias, the limited sample size may affect the generalization ability of the

model, and the integration of imaging data with multi-omics information remains to be further explored. In the future, multi-center large-sample studies, cross-modal data fusion (such as integration with genomics and proteomics), and the development of interpretable artificial intelligence algorithms will be crucial for overcoming these bottlenecks. Model interpretability can be improved by integrating SHapley Additive exPlanations into radiomics models, an approach that quantifies the contribution of each feature to the diagnostic result[11]. As medical imaging evolves from "qualitative description" to "quantitative analysis" and artificial intelligence transitions from the laboratory to the clinical frontline, radiomics is reshaping the diagnostic paradigm for liver tumors. This study not only provides a practical tool for the differential diagnosis of DPHCC and ICC but also heralds the advent of a new era where "imaging serves as a biomarker". With the continuous iteration of technology and the innovation of concepts, radiomics is bound to play an even more significant role in tumor early screening, treatment efficacy assessment, prognosis prediction, and other fields.

FOOTNOTES

Author contributions: Qi X and Zhao FY contributed to manuscript writing, provided ideas for the draft, and revised the article.

Conflict-of-interest statement: All the authors report no relevant conflicts of interest for this article.

Open Access: This article is an open-access article that was selected by an in-house editor and fully peer-reviewed by external reviewers. It is distributed in accordance with the Creative Commons Attribution NonCommercial (CC BY-NC 4.0) license, which permits others to distribute, remix, adapt, build upon this work non-commercially, and license their derivative works on different terms, provided the original work is properly cited and the use is non-commercial. See: https://creativecommons.org/Licenses/by-nc/4.0/

Country of origin: China

ORCID number: Fei-Yu Zhao 0009-0001-4466-5018.

S-Editor: Bai SR
L-Editor: Wang TQ
P-Editor: Lei YY

REFERENCES

1 **Zhang CC**, Lu D, Yang J, Zhang L, Zeng XF, Fang XM, Fan CG. Clinical value and applicability of radiomics in differential diagnosis of dual-phenotype hepatocellular carcinoma and intrahepatic cholangiocarcinoma. *World J Radiol* 2025; **17**: 108247 [*RCA*] [PMID: 40606043 DOI: 10.4329/wjr.v17.i6.108247] [FullText] [Full Text(PDF)]

2 **Wang Y**, Wang X, Huang X, Zhang J, Hu J, Qi Y, Xiang B, Wang Q. Integrated Genomic and Transcriptomic Analysis reveals key genes for predicting dual-phenotype Hepatocellular Carcinoma Prognosis. *J Cancer* 2021; **12**: 2993-3010 [*RCA*] [PMID: 33854600 DOI: 10.7150/jca.56005] [FullText] [Full Text(PDF)]

3 **Wu Q**, Zhang T, Xu F, Cao L, Gu W, Zhu W, Fan Y, Wang X, Hu C, Yu Y. MRI-based deep learning radiomics to differentiate dual-phenotype hepatocellular carcinoma from HCC and intrahepatic cholangiocarcinoma: a multicenter study. *Insights Imaging* 2025; **16**: 27 [*RCA*] [PMID: 39881111 DOI: 10.1186/s13244-025-01904-y] [FullText] [Full Text(PDF)]

4 **Moris D**, Palta M, Kim C, Allen PJ, Morse MA, Lidsky ME. Advances in the treatment of intrahepatic cholangiocarcinoma: An overview of the current and future therapeutic landscape for clinicians. *CA Cancer J Clin* 2023; **73**: 198-222 [*RCA*] [PMID: 36260350 DOI: 10.3322/caac.21759] [FullText]

5 **Yu ZC**, Fang ZK, Yu Y, Liu SY, Wang KD, Shi ZJ, Jin LM, Huang XK, Lu Y, Shen GL, Liu JW, Huang DS, Zhang CW, Liang L. The Clinical Characteristics, Patterns of Recurrence, and Long-Term Survival Outcomes of Dual-Phenotype Hepatocellular Carcinoma After Curative Liver Resection. *J Hepatocell Carcinoma* 2025; **12**: 183-192 [*RCA*] [PMID: 39902378 DOI: 10.2147/JHC.S493094] [FullText] [Full Text(PDF)]

6 **Cianflone F**, Lazarevic D, Palmisano A, Fallara G, Larcher A, Freschi M, Dell'Antonio G, Scotti GM, Morelli MJ, Ferrara AM, Trevisani F, Cinque A, Esposito A, Briganti A, Tacchetti C, Doglioni C, Del Maschio A, de Cobelli F, Bertini R, Salonia A, Montorsi F, Tonon G, Capitanio U. Radiomic and gEnomic approaches for the enhanced DIagnosis of clear cell REnal Cancer (REDIRECt): a translational pilot methodological study. *Transl Androl Urol* 2022; **11**: 149-158 [*RCA*] [PMID: 35280651 DOI: 10.21037/tau-21-713] [FullText] [Full Text (PDF)]

7 **Gillies RJ**, Kinahan PE, Hricak H. Radiomics: Images Are More than Pictures, They Are Data. *Radiology* 2016; **278**: 563-577 [*RCA*] [PMID: 26579733 DOI: 10.1148/radiol.2015151169] [FullText] [Full Text(PDF)]

8 **Gu HX**, Huang XS, Xu JX, Zhu P, Xu JF, Fan SF. Diagnostic Value of MRI Features in Dual-phenotype Hepatocellular Carcinoma: A Preliminary Study. *J Digit Imaging* 2023; **36**: 2554-2566 [*RCA*] [PMID: 37578576 DOI: 10.1007/s10278-023-00888-9] [FullText]

9 **Peng MH**, Zhang KL, Guan SW, Lin Q, Yu HB. Advances and challenges in pathomics for liver cancer: From diagnosis to prognostic stratification. *World J Clin Oncol* 2025; **16**: 107646 [*RCA*] [PMID: 40585839 DOI: 10.5306/wjco.v16.i6.107646] [FullText] [Full Text(PDF)]

10 **Li XH**, Zhou EL, Zhao CY, Cui BK, Dong XY, Du H, Lin XJ. Adjuvant chemotherapy combined with immunotherapy in patients with cholangiocarcinoma after radical resection. *Cancer Med* 2023; **12**: 21742-21750 [*RCA*] [PMID: 38059559 DOI: 10.1002/cam4.6738] [Full Text]

11 **Ponce-Bobadilla AV**, Schmitt V, Maier CS, Mensing S, Stodtmann S. Practical guide to SHAP analysis: Explaining supervised machine learning model predictions in drug development. *Clin Transl Sci* 2024; **17**: e70056 [*RCA*] [PMID: 39463176 DOI: 10.1111/cts.70056] [Full

Text] [Full Text(PDF)]

World Journal of Radiology

Submit a Manuscript: https://www.f6publishing.com

World J Radiol 2025 November 28; 17(11): 114451

DOI: 10.4329/wjr.v17.i11.114451

ISSN 1949-8470 (online)

LETTER TO THE EDITOR

Magnetic resonance tractography of the cervical spine: Toward routine clinical use

Arosh S Perera Molligoda Arachchige

Specialty type: Radiology, nuclear medicine and medical imaging

Provenance and peer review: Invited article; Externally peer reviewed.

Peer-review model: Single blind

Peer-review report's classification
Scientific Quality: Grade B
Novelty: Grade B
Creativity or Innovation: Grade C
Scientific Significance: Grade B

P-Reviewer: Xia L, MD, China

Received: September 19, 2025
Revised: October 21, 2025
Accepted: October 29, 2025
Published online: November 28, 2025
Processing time: 69 Days and 3.9 Hours

Arosh S Perera Molligoda Arachchige, Faculty of Medicine, Humanitas University, Pieve Emanuele 20072, Lombardy, Italy

Corresponding author: Arosh S Perera Molligoda Arachchige, MD, Faculty of Medicine, Humanitas University, Via Rita Levi Montalcini 4, Pieve Emanuele 20072, Lombardy, Italy. aroshperera@outlook.it

Abstract

Spinal cord injury and non-traumatic myelopathies are major causes of lifelong disability, yet conventional magnetic resonance imaging (MRI) can underestimate microstructural damage. Diffusion tensor imaging (DTI) and tractography map white-matter integrity by measuring fractional anisotropy (FA) and mean diffusivity (MD), but their adoption in spine imaging has been limited by long scan times and complex post-processing. Supsupin *et al* report a two-minute cervical DTI sequence integrated into routine MRI and applied to four representative pathologies – spinal cord contusion, metastatic compression, degenerative myelopathy, and multiple sclerosis – compared with five controls. Each lesion showed distinctive tractographic and quantitative patterns: For example, reduced FA with preserved MD in contusion and combined FA decrease and MD elevation in metastatic compression. These findings highlight the potential of tractography to improve diagnosis, guide surgical planning, and monitor treatment, while maintaining clinical feasibility. Remaining challenges include limited angular resolution, motion artifacts, and the need for multicenter validation and advanced reconstruction methods. This manuscript places the study in the context of current spinal diffusion imaging and outlines future directions toward routine, precision care.

Key Words: Magnetic resonance imaging; Tractography; Cervical; Spine; Diffusion tensor imaging

©The Author(s) 2025. Published by Baishideng Publishing Group Inc. All rights reserved.

Core Tip: A rapid two-minute diffusion tensor imaging sequence enables cervical spinal cord tractography during routine magnetic resonance imaging (MRI). Supsupin *et al* demonstrate that distinct fractional anisotropy and mean diffusivity patterns reveal microstructural injury in contusion, metastasis, degenerative myelopathy, and multiple sclerosis – lesions that may appear less conspicuous on conventional MRI. Their work shows how tractography can support diagnosis, surgical planning, and longitudinal follow-up.

Citation: Perera Molligoda Arachchige AS. Magnetic resonance tractography of the cervical spine: Toward routine clinical use. *World J Radiol* 2025; 17(11): 114451
URL: https://www.wjgnet.com/1949-8470/full/v17/i11/114451.htm
DOI: https://dx.doi.org/10.4329/wjr.v17.i11.114451

TO THE EDITOR

Spinal cord disorders including trauma, degenerative myelopathy, metastatic disease, and demyelinating disorders are major causes of lifelong disability and reduced quality of life. Globally, hundreds of thousands of people sustain spinal cord injury each year, and many more live with chronic compressive or inflammatory conditions. Early detection of microstructural cord damage is critical for prognosis, surgical planning, and monitoring therapeutic response[1]. Conventional magnetic resonance imaging (MRI), while indispensable for depicting gross cord morphology and signal changes, often fails to reveal subtle axonal injury or the precise extent of fiber disruption.

Diffusion tensor imaging (DTI) and tractography, which reconstruct the three-dimensional organization of white matter fibers, provide a window into these otherwise invisible changes. By measuring the directionality of water diffusion, DTI quantifies fractional anisotropy (FA) and mean diffusivity (MD), surrogate markers of axonal integrity and extracellular edema. Tractography then integrates these data to render a virtual map of cord tracts, offering the possibility of more accurate diagnosis and individualized management[2-4]. Despite this promise, spinal applications of tractography have lagged behind cranial uses because of long acquisition times, motion artifacts, and the need for specialized post-processing.

STUDY HIGHLIGHTS

In this issue of *World Journal of Radiology*, Supsupin *et al*[5] demonstrate that these barriers can be substantially lowered. They incorporated a 2-minute cervical spine DTI sequence into routine MRI and used deterministic tractography with automated topology-informed pruning to evaluate four representative pathologies – cord contusion, metastatic compression, degenerative myelopathy, and multiple sclerosis – against five healthy controls.

Distinct tractographic signatures emerged. In the cord contusion case, FA was reduced at the lesion with preserved MD, consistent with axonal disorganization without widespread necrosis or edema. Metastatic compression produced both decreased FA and elevated MD, reflecting tract disruption and tissue infiltration. Degenerative myelopathy demonstrated visual tract interruption despite relatively preserved FA, illustrating how selective fiber loss or partial-volume effects can mask scalar abnormalities[6]. Finally, demyelinating disease revealed moderate FA reduction with only mild MD elevation, a pattern compatible with localized myelin loss.

These quantitative and qualitative findings provide a more nuanced picture than conventional MRI alone and illustrate how tractography can inform surgical or medical decision-making when conventional images underestimate the severity of fiber injury[7].

CLINICAL SIGNIFICANCE

The clinical implications are substantial. First, the authors' ultra-short acquisition, about two minutes added to the MRI exam, addresses one of the main impediments to routine spinal tractography[5]. Second, the combination of rapid acquisition and straightforward deterministic reconstruction supports integration into standard clinical workflows, including preoperative planning for tumor resection or decompressive surgery, and serial follow-up in demyelinating disease. Third, FA and MD measurements derived from the lesion core and adjacent segments may help predict neurological outcomes and guide rehabilitation, paralleling similar applications of brain tractography in stroke and trauma[4,8].

These strengths align with the growing emphasis on precision medicine. Reliable early identification of microstructural injury may allow targeted interventions to prevent secondary degeneration, optimize timing of surgery, and monitor therapeutic efficacy.

TECHNICAL CONTEXT AND CHALLENGES

Spinal tractography presents unique technical hurdles. The cervical cord's small cross-section, surrounding cerebrospinal fluid, and frequent patient motion create geometric distortions and lower signal-to-noise ratios. Supsupin *et al*[5] used a six-direction acquisition, a pragmatic choice for minimizing scan time but one that limits angular resolution and sensitivity to complex fiber crossings[9]. Higher-direction acquisitions – typically at least 17 directions – yield more accurate tractography but at the cost of longer imaging times and greater motion sensitivity.

Another challenge is the fundamental limitation of the DTI model, which assumes a single dominant fiber orientation per voxel. This can obscure crossing, merging, or branching fibers. Advanced reconstruction methods such as generalized q-sampling imaging can resolve multiple orientations and may improve anatomic fidelity, though at the price of longer acquisitions and more complex post-processing[10]. Distortion-correction strategies, including reverse phase-encoding and cardiac gating, could further enhance data quality[8].

BROADER PERSPECTIVE

The work by Supsupin *et al*[5] dovetails with a growing literature that seeks to translate tractography from research to everyday clinical care. Several groups have shown that FA correlates with neurological impairment and outcome in cervical myelopathy[6] and that diffusion changes can signal disease activity in demyelinating conditions[4]. In neurosurgical planning, tractography has already improved the safety of tumor resection and deep brain stimulation[8]. By applying similar principles to the spinal cord in a rapid, clinically feasible manner, the current study advances the field toward true bedside applicability.

Looking ahead, multi-institutional studies with larger, pathologically diverse cohorts will be essential to validate diagnostic accuracy and prognostic value. Integration with surgical navigation systems, machine-learning-based segmentation, and quantitative outcome measures could further enhance clinical impact. Importantly, reproducibility across different scanners and institutions must be established if the method is to inform treatment guidelines and reimbursement decisions.

CONCLUSION

By showing that robust cervical spinal cord tractography can be performed with minimal additional scan time, Supsupin *et al*[5] provide a practical framework for incorporating diffusion imaging into daily radiological practice. Their rapid DTI protocol delivers actionable insights into microstructural integrity across a spectrum of diseases, bringing us closer to an era where spinal tractography complements conventional MRI as a standard component of precision spinal care.

FOOTNOTES

Author contributions: Perera Molligoda Arachchige AS read and approved the final version of the manuscript to be published.

Conflict-of-interest statement: The author has no conflicts of interest to declare.

Open Access: This article is an open-access article that was selected by an in-house editor and fully peer-reviewed by external reviewers. It is distributed in accordance with the Creative Commons Attribution NonCommercial (CC BY-NC 4.0) license, which permits others to distribute, remix, adapt, build upon this work non-commercially, and license their derivative works on different terms, provided the original work is properly cited and the use is non-commercial. See: https://creativecommons.org/Licenses/by-nc/4.0/

Country of origin: Italy

ORCID number: Arosh S Perera Molligoda Arachchige 0000-0002-3875-0267.

S-Editor: Luo ML
L-Editor: A
P-Editor: Zhang YL

REFERENCES

1 **Lu Y**, Shang Z, Zhang W, Pang M, Hu X, Dai Y, Shen R, Wu Y, Liu C, Luo T, Wang X, Liu B, Zhang L, Rong L. Global incidence and characteristics of spinal cord injury since 2000-2021: a systematic review and meta-analysis. *BMC Med* 2024; **22**: 285 [*RCA*] [PMID: 38972971 DOI: 10.1186/s12916-024-03514-9] [FullText] [Full Text(PDF)]

2 **Yamada K**, Sakai K, Akazawa K, Yuen S, Nishimura T. MR tractography: a review of its clinical applications. *Magn Reson Med Sci* 2009; **8**: 165-174 [*RCA*] [PMID: 20035125 DOI: 10.2463/mrms.8.165] [FullText]

3 **Wu BW**, Barr S. Applications of Whole Brain Tractography and Implications for Clinical Practice. *Cureus* 2017; **9**: e1753 [*RCA*] [PMID: 29226043 DOI: 10.7759/cureus.1753] [FullText] [Full Text(PDF)]

4 **Costanzo R**, Brunasso L, Paolini F, Benigno UE, Porzio M, Giammalva GR, Gerardi RM, Umana GE, di Bonaventura R, Sturiale CL, Visocchi M, Iacopino DG, Maugeri R. Spinal Tractography as a Potential Prognostic Tool in Spinal Cord Injury: A Systematic Review. *World Neurosurg* 2022; **164**: 25-32 [*RCA*] [PMID: 35500874 DOI: 10.1016/j.wneu.2022.04.103] [FullText]

5 **Supsupin EP**, Serrano A, Louviere C, Pearson L, Hernandez M, Sekar V, Amer A, Cikla U, Virarkar M, Gumus KZ. Magnetic resonance tractography of the cervical spine: A rapid diffusion tensor imaging protocol to serve as a clinical evaluation tool. *World J Radiol* 2025; **17**: 110267 [*RCA*] [PMID: 41025056 DOI: 10.4329/wjr.v17.i9.110267] [FullText] [Full Text(PDF)]

6 **Ellingson BM**, Salamon N, Hardy AJ, Holly LT. Prediction of Neurological Impairment in Cervical Spondylotic Myelopathy using a Combination of Diffusion MRI and Proton MR Spectroscopy. *PLoS One* 2015; **10**: e0139451 [*RCA*] [PMID: 26431174 DOI: 10.1371/journal.pone.0139451] [FullText] [Full Text(PDF)]

7 **Farquharson S**, Tournier JD, Calamante F, Fabinyi G, Schneider-Kolsky M, Jackson GD, Connelly A. White matter fiber tractography: why we need to move beyond DTI. *J Neurosurg* 2013; **118**: 1367-1377 [*RCA*] [PMID: 23540269 DOI: 10.3171/2013.2.JNS121294] [FullText]

8 **Yang JY**, Yeh CH, Poupon C, Calamante F. Diffusion MRI tractography for neurosurgery: the basics, current state, technical reliability and challenges. *Phys Med Biol* 2021; **66** [*RCA*] [PMID: 34157706 DOI: 10.1088/1361-6560/ac0d90] [FullText]

9 **Jin Z**, Bao Y, Wang Y, Li Z, Zheng X, Long S, Wang Y. Differences between generalized Q-sampling imaging and diffusion tensor imaging in visualization of crossing neural fibers in the brain. *Surg Radiol Anat* 2019; **41**: 1019-1028 [*RCA*] [PMID: 31144009 DOI: 10.1007/s00276-019-02264-1] [FullText] [Full Text(PDF)]

10 **Dauleac C**, Frindel C, Mertens P, Jacquesson T, Cotton F. Overcoming challenges of the human spinal cord tractography for routine clinical use: a review. *Neuroradiology* 2020; **62**: 1079-1094 [*RCA*] [PMID: 32363485 DOI: 10.1007/s00234-020-02442-8] [FullText]

Published by **Baishideng Publishing Group Inc**
7041 Koll Center Parkway, Suite 160, Pleasanton, CA 94566, USA
Telephone: +1-925-3991568
E-mail: office@baishideng.com
Help Desk: https://www.f6publishing.com/helpdesk
https://www.wjgnet.com

© 2025 Baishideng Publishing Group Inc. All rights reserved.